



HAL
open science

Structured catalytic supports based on functionalized polyurethane foams: applications in photocatalysis and semi-hydrogenation of alkynes

Han Peng

► **To cite this version:**

Han Peng. Structured catalytic supports based on functionalized polyurethane foams: applications in photocatalysis and semi-hydrogenation of alkynes. Other. Université de Strasbourg, 2023. English. NNT: 2023STRAF007 . tel-04480490

HAL Id: tel-04480490

<https://theses.hal.science/tel-04480490>

Submitted on 27 Feb 2024

HAL is a multi-disciplinary open access archive for the deposit and dissemination of scientific research documents, whether they are published or not. The documents may come from teaching and research institutions in France or abroad, or from public or private research centers.

L'archive ouverte pluridisciplinaire **HAL**, est destinée au dépôt et à la diffusion de documents scientifiques de niveau recherche, publiés ou non, émanant des établissements d'enseignement et de recherche français ou étrangers, des laboratoires publics ou privés.

ÉCOLE DOCTORALE DES SCIENCES CHIMIQUES**LIMA -UMR 7042****THÈSE** présentée par :**Han PENG**soutenue le : **30 janvier 2023**pour obtenir le grade de : **Docteur de l'université de Strasbourg**

Discipline/ Spécialité : Chimie

Supports catalytiques structurés à base de mousses de polyuréthane fonctionnalisées : applications en photocatalyse et en semi-hydrogénation d'alcynes

THÈSE dirigée par :**M. RITLENG Vincent**

Professeur, Université de Strasbourg

RAPPORTEURS :**Mme. DE OLIVEIRA VIGIER Karine**

Professeur, Université de Poitiers

Mme. OUALI Armelle

Chargé de Recherches CNRS, Ecole Nationale Supérieure de Chimie de Montpellier

AUTRES MEMBRES DU JURY :**M. JIERRY Loïc**

Professeur, Université de Strasbourg

M. EDOUARD David

Maître de Conférences, Université de Lyon 1

Acknowledgments

My study at the ECPM (Ecole européenne de Chimie, Polymères et Matériaux) will soon come to the end. Dedicated to my PhD thesis, I wish to express my sincere appreciation to all those who have assisted, supported and guided me during these three years of my PhD at University of Strasbourg.

First of all, I would like to take this opportunity to express my genuine gratitude to my supervisor, Prof. Vincent RITLENG, for giving me this PhD position at University of Strasbourg. Besides, I feel so appreciated for his experimental and literary guidance during these three years. He aided me in building a rigorous attitude to scientific research which could become a great fortune in my future career. Finally, without his meticulous corrections of my thesis, my research work would not have been narrated and illustrated precisely and vividly.

Secondly, I should thank all the members of our COA (Chimie Organométallique Appliquée) group, Prof. Michael CHETCUTI, Dr. Christophe MICHON, Dr. Ahmed AIT KHOUYA, Dr. Marta GARCIA-AVELLO MENDEZ for all the support I have received during my three years. I should also thank all the members of ICPEES (Institute of Chemistry and Processes for Energy, Environment and Health) group, especially Dr. Cuong PHAM-HUU for his experimental suggestions and his PhD student Xiong ZHANG for his solicitude in living and studying. I want also to acknowledge all the staff that's has provided their help and expertise for the characterization analyses displayed in this thesis: Mr. Thierry ROMERO (SEM, SEM-EDX), Dr. Vasiliki PAPAETHIMIOU (XPS), Dr. Philippe BERTANI (CP-MAS NMR), Dr. Emeric WASIELEWSKI (NMR), Mr. Matthieu CHESSE (GC).

I would also like to thank Pr. Karine DE OLIVEIRA VIGIER (Université de Poitiers), Dr. Armelle OUALI (Ecole Nationale Supérieure de Chimie de Montpellier), Pr. Loïc JIERRY (Université de Strasbourg) and Dr. David EDOUARD (Université de Lyon I) for accepting to be the jury member of my thesis and to evaluate this work.

I thank all the consideration and support from my family and they have inspired me greatly no matter in life or in study through these years. I also owe my sincere gratitude to my friends who have made my life so fruitful in Strasbourg.

Finally, I deeply appreciate the financial support provided by IdEx Unistra 2019 which gave me an opportunity to study abroad and gain insight in France.

Abbreviations

Abbreviations

AC : active carbon

CNT : carbon nanotubes

SCS: structured catalytic support

OCPUF: open cell polyurethane foam

PDA: polydopamine

MOF: metal organic framework

TRIS: 2-amino-2-hydroxymethyl-propane-1,3-diol

APTES: 3-(triethoxysilyl)propan-1-amine

EDC: 3-[(ethylimino)methylidene]amino-N,N-dimethylpropan-1-amine

NHS: N-hydroxysuccinimide

DCC: dicyclohexylcarbodiimide

DMAP: 4-(dimethylamino)pyridine

PET-RAFT: photoinduced electron/energy transfer-reversible addition-fragmentation chain transfer

CPDTC: 2-cyano-2-propyl dodecyl trithiocarbonate

GW: glass wool

DMA: 9,10-dimethylantracene

COMU: (1-cyano-2-ethoxy-2-oxoethylideneaminoxy)dimethylamino-morpholino-carbenium hexafluorophosphate

PEI: poly(ethylenimine)

NSs : nanosheets

NPs: nanoparticles

TGA: thermogravimetric analysis

XRD: X-ray powder diffraction

PA: phenylacetylene

ST: styrene

EB: ethylbenzene

CA: contact angle

XPS: X-ray photoelectron spectrometry

EDX: energy dispersive X-ray spectrometry

ICP-AES: inductively coupled plasma atomic emission spectroscopy

Conv.: conversion

DMF: dimethylformamide

PEG: polyethylene glycol

TBME: *tert*-butylmethyl ether
Cat.: catalyst
SEM: scanning Electron Microscope
TEM: transmission electron microscope
TOF: turn-over frequency
TON: Turn-over number
m-: meta-
o-: ortho-
p-: para-
Ph: phenyl
Py: pyridine
Bpy: 2,2'-bipyridine
s: singlet
d: doublet
t: triplet
q: quartet
m: multiplet
NMR: nuclear magnetic resonance spectroscopy
CP-MAS: cross-polarization magic angle spinning
r.t.: room temperature
rpm: round per minute
THF: tetrahydrofurane
GC: gas chromatography
equiv.: equivalent

Résumé

Introduction

Les supports catalytiques structurés (SCS) sont très largement étudiés pour des applications dans des procédés continus dans l'industrie. Ces derniers présentent, en effet, généralement un rapport surface/volume élevé, et permettent des transferts de masse efficaces avec une faible perte de charge. En outre, leur structure ouverte ainsi que leur forme macroscopique permettent un mélange intime des réactifs et une grande accessibilité aux sites actifs, tout en évitant la séparation fastidieuse des produits du catalyseur.¹ Parmi la variété de SCS, les mousses à cellules ouvertes sont des candidats de choix. De structure céramique ou métallique, ces architectures hôtes sont des supports idéaux pour les nanoparticules (NPs) métalliques actives en catalyse pour des procédés s'effectuant à haute température.² Cependant, ces mousses rigides sont préparées à partir de mousses polymères via des étapes longues et énergivores.³ En outre, ces structures présentent plusieurs inconvénients inhérents à leur nature : (i) leur grande rigidité génère des microfissures et les rend fragiles, (ii) la présence de nombreuses cellules fermées réparties de manière aléatoire réduit la reproductibilité des réactions, et (iii) de nombreux traitements chimiques dans des milieux hautement corrosifs sont souvent nécessaires pour récupérer le catalyseur adsorbé sur la mousse avant son élimination.⁴

Le développement actuel d'une production chimique s'effectuant à plus basse température et dans des conditions moins corrosives permet d'envisager l'utilisation de mousses polymères à cellules ouvertes telles que les mousses de polyuréthane. Ces matériaux sont peu onéreux, souples, légers et possèdent les mêmes caractéristiques morphologiques que les mousses rigides.⁵ Cependant, du fait de l'absence de microporosité et de la relative inertie chimique du polyuréthane, une modification adéquate de la surface de ces mousses doit être réalisée pour permettre l'accroche de catalyseurs en surface sans modifier ni leurs propriétés de transport, ni leurs propriétés mécaniques. Dans cette optique, notre attention s'est portée vers une approche éco-compatible et économiquement viable, inspirée du principe d'adhésion des moules à la surface de tous types de matériaux.⁶ Ainsi, notre équipe a récemment décrit (i) le revêtement de mousses à cellules ouvertes de polyuréthane (PUF) avec une couche adhésive de polydopamine (PDA) par simple immersion dans une solution aqueuse tamponnée de dopamine,⁷ (ii) leur fonctionnalisation ultérieure, tant avec des (nano)particules⁸ qu'avec composés moléculaires possédant un bras alcoxysilane,⁹ et

(iii) l'application des matériaux résultant en catalyse organique⁹ ou pour la dégradation de colorants.⁸ La grande polyvalence de la PDA, qui peut interagir avec pratiquement tous types de surfaces et peut être facilement fonctionnalisée, constitue le point clé du succès de cette approche. Les fonctions catéchols et amines de la PDA confèrent, en effet, à la fois de fortes propriétés d'adhésion et la possibilité de modifier la surface au moyen de différentes interactions chimiques incluant les liaisons hydrogène, les empilements π , les liaisons de coordination, et les additions de type Michael (via la formation de groupes imine lors de la polymérisation).¹⁰ Ces propriétés permettent un ancrage robuste des catalyseurs, qui a conduit à une activité et une stabilité élevée des matériaux catalytiques synthétisés jusqu'ici⁷⁻⁹ ainsi qu'à l'absence de lixiviation de la phase active dans le milieu réactionnel.

Lors de la dernière décennie, la catalyse photoredox sous lumière visible a émergé comme un puissant outil en synthèse organique.¹¹ Des limitations importantes demeurent cependant. Elles proviennent principalement (i) du coût souvent important du photocatalyseur (PC) qui est fréquemment à base de Ru ou d'Ir, et (ii) du coefficient d'extinction molaire souvent important du PC qui entrave la pénétration de la lumière dans la solution et engendre ainsi des vitesses de réaction fortement réduites lors du passage à grande échelle dans des réacteurs batch en raison du faible rapport surface sur volume de ces derniers.¹² Des réponses possibles à ces limitations passent par l'immobilisation du PC sur un support solide, afin de développer des PCs hétérogènes aisément récupérables et réutilisables, et/ou l'utilisation de réacteurs en flux continu. Dans ce contexte, **un premier axe de recherche** a concerné l'immobilisation de PCs fonctionnant sous lumière visible sur des mousses à cellules ouvertes de polyuréthane enrobées de polydopamine (PDA@PUF) pour développer des PCs recyclables pouvant potentiellement être utilisés en flux continu du fait des propriétés de transport des mousses à cellules ouvertes et de leurs larges pores qui laissent aisément passer la lumière (**Figure 1**).¹³



Figure 1. Réaction en flux sous lumière visible avec un PC@PDA@PUF.

L'hydrogénation sélective d'alcynes en alcènes est une réaction d'importance tant en synthèse organique qu'au niveau industriel.¹⁴ Cependant, la production d'oléfines à partir d'alcynes nécessite des catalyseurs capables, à la fois d'hydrogéner la triple liaison et d'entraver la sur-hydrogénation vers la formation d'alcanes. En outre, ces catalyseurs doivent limiter le phénomène d'isomérisation des alcènes.¹⁵ Les catalyseurs supportés contenant des nanoparticules (NPs) de Pd sont des catalyseurs de choix en termes d'activité, mais souffrent souvent d'une sélectivité modérée. Une approche classique pour augmenter leur chimiosélectivité repose sur la modification des NPs par l'addition de ligands azotés, phosphorés ou soufrés, ou le co-dopage avec un métal moins actif.¹⁶ Un exemple typique dans ce domaine est le catalyseur de Lindlar dans lequel Pd/CaCO₃ est partiellement « empoisonné » par l'addition de Pb et de quinoline. La présence de Pb constitue cependant une limitation environnementale sérieuse. Une autre approche repose sur la stratégie d'isolement des sites actifs visant au développement des catalyseurs à « atomes uniques ».¹⁶ Ces deux stratégies requièrent cependant des solutions synthétiques complexes et onéreuses qui compromettent à la fois leur durabilité et leur développement à grande échelle. Dans ce contexte, **un second axe de recherche** visait au développement de catalyseurs de semi-hydrogénation d'alcènes qui soient faciles à préparer (i.e. : sans ligands ou co-catalyseur), hautement efficaces et sélectifs sous pression modérée de H₂, et aisément réutilisables.

Résultats et discussions

Axe I. Mousses de polyuréthane enrobées de polydopamine comme support structuré pour le développement de photocatalyseurs hétérogènes aisément réutilisables

Photocatalyseur hétérogène à base de [Ru(bpy)₃]²⁺

[Ru(bpy)₃]Cl₂ occupe une place de choix parmi les photocatalyseurs. Il a donc naturellement été choisi afin d'établir une preuve de concept. La stratégie retenue pour son immobilisation à la surface des mousses de polyuréthane enrobées de polydopamine (PDA@PUF) repose sur la faisabilité de greffage covalent d'un catalyseur moléculaire comportant un bras alcoxysilane précédemment établie au laboratoire par condensation des groupements alcoxysilane avec les groupements catéchols présent en surface de la PDA.⁹

Ainsi après enrobage d'un échantillon cubique de PUF par une fine couche de PDA par simple immersion dans une solution aqueuse de dopamine à température ambiante, tamponnée à un pH de 8,5, typique d'un environnement marin, suivie de lavages à l'eau,⁷⁻⁹ le matériau PDA@PUF a ensuite été fonctionnalisé avec Ru(bpy)₃²⁺ via un procédé de silanisation avec la 3-(triéthoxysilyl)propan-1-amine (APTES), suivi du couplage de l'acide [2,2'-bipyridine]-4-carboxylique avec la mousse aminée résultante en présence d'EDC, et enfin de la complexation du ruthénium à la bipyridine greffée par réaction avec [Ru(bpy)₂Cl₂] (**Figure 2**).

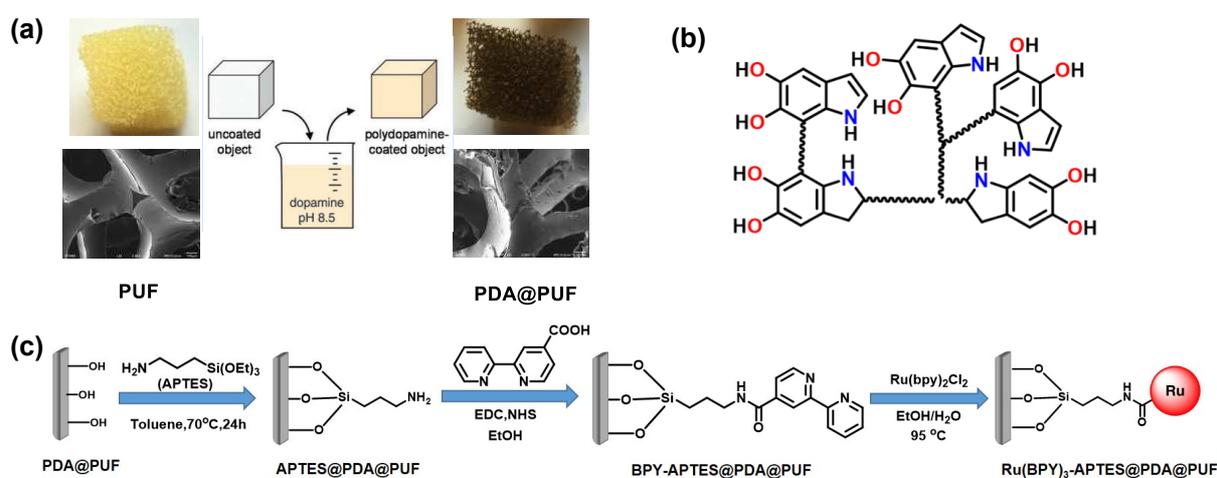


Figure 2. (a) Enrobage de PUF avec de la PDA (b) Structure de la PDA (c) Stratégie de fonctionnalisation pour l'immobilisation de Ru(bpy)₃²⁺ sur PDA@PUF.

Le succès du greffage covalent de l'APTES sur la PDA a été démontré par RMN CP-MAS ²⁹Si et celui de la fonctionnalisation ultérieure avec Ru(bpy)₃²⁺ par analyses ICP-AES, spectroscopie XPS, et cartographie des éléments par MEB-EDX. Ainsi, le spectre RMN CP-MAS ²⁹Si de APTES@PDA@PUF a révélé des signaux à -64,3, -56,4, -53,4 et -42,0 ppm (**Figure 3A**), démontrant la présence de structures T₁ et T₂, ainsi que de structures réticulées T₃+T₃' et T₄+T₄'¹⁷ similaires à celles observées avec l'APTES ancrée de manière covalente sur une matrice de silice.¹⁸ L'analyse élémentaire par ICP-AES a permis de déterminer des teneurs moyennes en Si et en Ru de 1,564± 0,020 et 2,024± 0,027 g/kg pour du Ru(bpy)₃-APTES@PDA@PUF fraîchement préparé. Les images de microscopie électronique à balayage (MEB) de Ru(bpy)₃-APTES@PDA@PUF révèlent une surface rugueuse typique des mousses enrobées de PDA (**Figure 3B**), et les micrographies combinées à la spectroscopie EDX une distribution élémentaire homogène en surface, sans agrégats ou

ségrégations évidents (Fig. 3C). Enfin, la spectroscopie XPS a confirmé la présence en surface des éléments O, N, C, Si et Ru. La valeur du pic de Ru3d_{5/2} n'a cependant pas pu être déterminée avec précision en raison du faible rapport signal sur bruit, rendant difficile l'attribution à une espèce spécifique de ruthénium.

L'activité catalytique d'échantillons de Ru(bpy)₃-APTES@PDA@PUF de 1.5 cm × 1.5 cm × 3 cm a ensuite été étudiée de manière approfondie dans des réactions d'homocouplages oxydatifs d'amines benzyliques¹⁹ (0.9 mol% Ru) et de couplages croisés déshydrogénants de type aza-Henry²⁰ (4.5 mol% Ru) sous lumière visible (LED bleu, 18 W) et oxygène moléculaire comme oxydant vert (**Figure 4A**). Après des expériences d'optimisation conduites avec des substrats modèles ayant permis d'établir un rôle primordial du solvant dans les deux réactions, le matériau catalytique macroscopique s'est révélé efficace dans l'acétonitrile à 30-35 °C pour les homocouplages d'amines et dans le méthanol à la même température pour les couplages croisés déshydrogénants. Une bonne tolérance fonctionnelle a ainsi été établie, ainsi qu'une excellente stabilité ; ces études ayant été conduites avec une seule mousse pour chaque réaction.

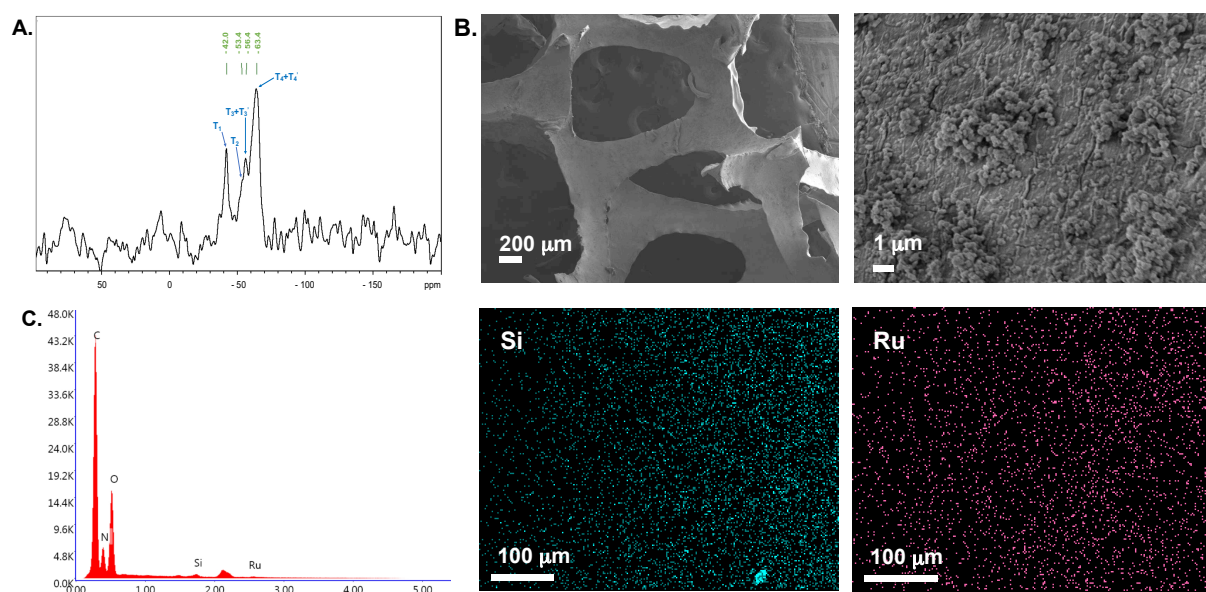


Figure 3. (A) Spectre RMN CP-MAS ²⁹Si de APTES@PDA@PUF. (B) Images MEB à fort et faible grossissements de Ru(bpy)₃-APTES@PDA@PUF tel que synthétisé. (C) Spectre EDX et cartographie élémentaire de Ru(bpy)₃-APTES@PDA@PUF.

Afin de mettre cette stabilité en exergue, des tests de recyclage de Ru(bpy)₃-APTES@PDA@PUF ont été réalisés pour chacune des réactions. Pour se faire, la

mousse était simplement retirée du milieu en fin de réaction, lavée dans un bain à ultrason, séchée sous vide, puis réutilisée. L'activité s'est révélée excellente pour au moins 6 cycles dans les 2 cas, avec une amélioration notable des rendements observées lors des cycles 1 à 3 pour l'homocouplage de la benzylamine (**Figure 4B**) et lors des cycles 1 à 6 pour la nitrométhylation de la N-phényl-tétrahydroisoquinoléine (**Figure 4C**).

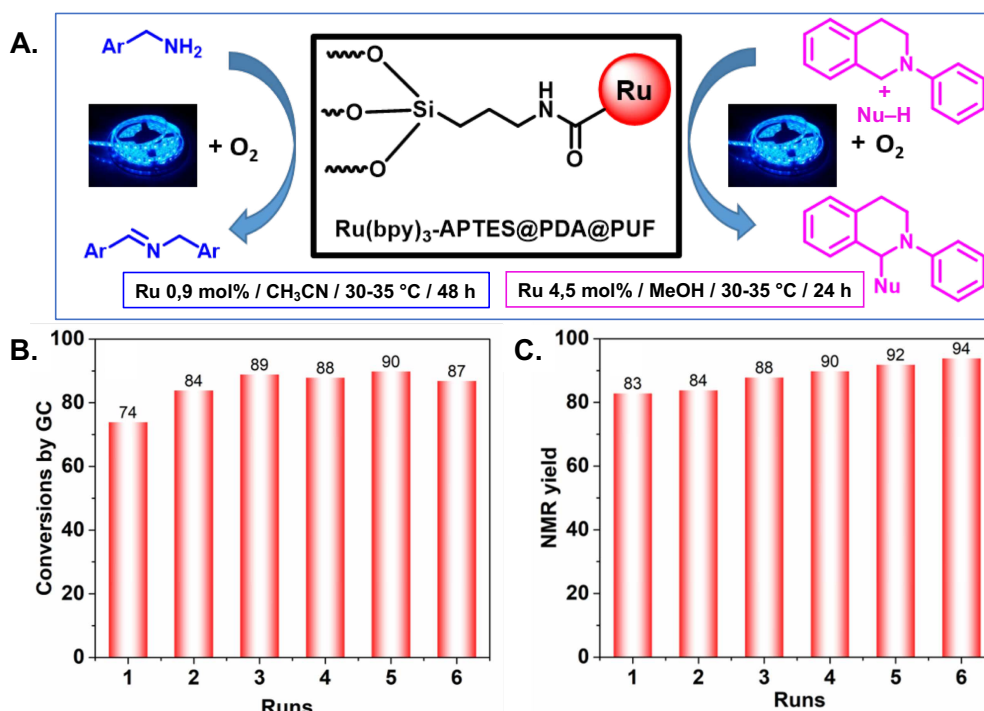


Figure 4. (A) Homocouplage oxydatif de benzylamines et couplages croisés déshydrogénants de type aza-Henry photocatalysés par Ru(bpy)₃-APTES@PDA@PUF sous lumière bleue (LED, 18W) (B) Recyclage de Ru(bpy)₃-APTES@PDA@PUF pour l'homocouplage de la benzylamine (C) et la nitrométhylation de la N-phényl-tétrahydroisoquinoléine.

Cette amélioration progressive de l'activité catalytique semble résulter de la modification de la couche supérieure de la PDA, marquée par un changement progressif de la couleur de la mousse du brun-noir vers le brun-rouge voire l'orange (suivant la réaction considérée), suggérant une meilleure accessibilité du catalyseur. Ce changement de couleur des mousses s'accompagne d'un polissage de leur surface révélé par des images MEB d'une mousse usagée après six cycles catalytiques (**Figure 5**). De façon notable, d'après la cartographie établie par MEB-EDX, la distribution des éléments sur la surface de la mousse ne semble pas affectée par ce polissage de la surface. Toutefois, lorsqu'on compare les spectres XPS à haute

résolution de la mousse fraîchement synthétisée à ceux de la mousse usagée, il apparaît une diminution relative en surface de la proportion de noyaux Ru3d_{5/2} et une augmentation de celle de Si2p (**Figure 5**). Ces résultats sont en accord avec les analyses ICP-AES de la mousse usagée après 6 cycles catalytiques qui montrent une diminution de la teneur en Ru de l'ordre de 30% alors que celle de Si ne varie pas de façon significative. Tout ceci suggère que la liaison catéchol–silicium, qu'elle soit linéaire ou réticulée, est suffisamment stable pour résister à des conditions réactionnelles corrosives, ce qui est en accord avec nos observations précédentes avec des catalyseurs moléculaires immobilisés sur PDA@PUF par condensation d'un bras alcoxysilane avec les catéchols de la PDA.⁹ Néanmoins, le fait que malgré la stabilité de cette liaison de la lixiviation de Ru ait été observée, suggère soit que du [Ru(bpy)₂Cl₂] était simplement adsorbé en surface soit, plus probablement, que la liaison amide entre l'ancrage siloxytriéthylamino et le bipyridine n'était pas stable dans les conditions opérationnelles utilisées. Il conviendra donc à l'avenir de réexaminer l'ancrage covalent de [Ru(bpy)₃]²⁺ sur PDA@PUF en évitant un lien amide.²¹

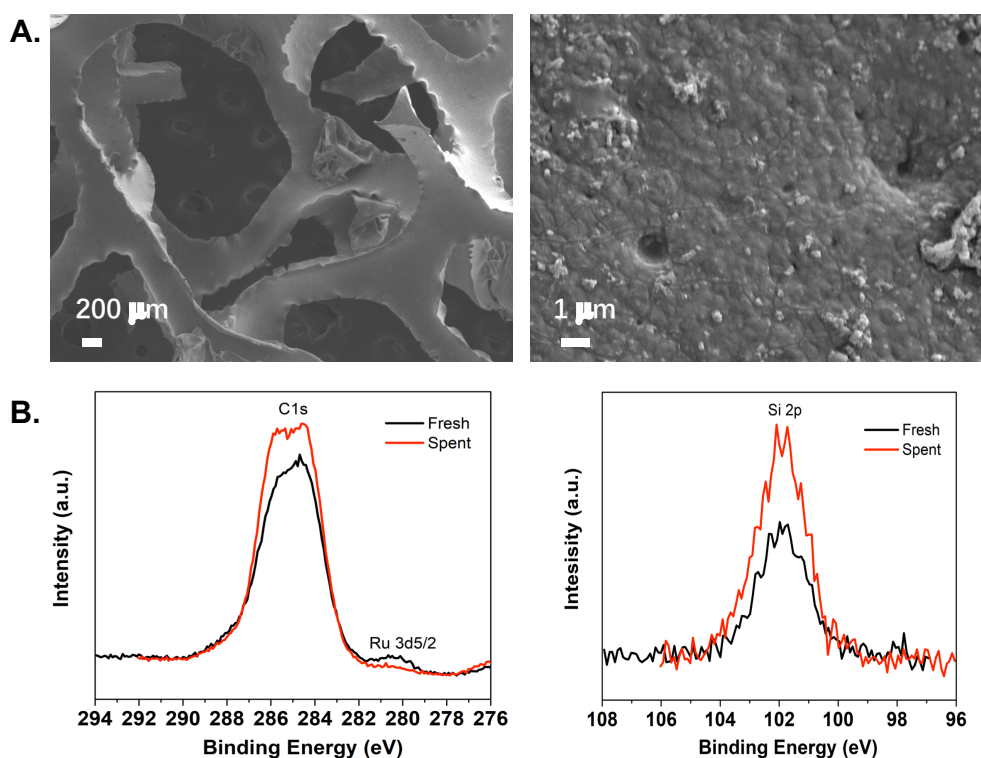


Figure 5. (A) Images MEB à fort et faible grossissements de Ru(bpy)₃-APT@PDA@PUF après 6 cycles catalytiques. (B) Spectres XPS à haute résolution des régions des noyaux C1s, Ru3d_{5/2} et Si2p de Ru(bpy)₃-APT@PDA@PUF tel que synthétisé (noir) et après 6 cycles catalytiques (rouge).

Photocatalyseur hétérogène à base d'éosine Y

Parallèlement à l'étude de l'immobilisation de $[\text{Ru}(\text{bpy})_3]^{2+}$ sur PDA@PUF , l'hétérogénéisation de l'éosine Y, un PC organique courant pouvant servir d'alternative à l'emploi de PCs à base de métaux nobles chers et toxiques,²² a également été étudiée. Pour se faire, une stratégie d'ancrage similaire à celle utilisée pour $[\text{Ru}(\text{bpy})_3]^{2+}$ a été adoptée. Ainsi, un échantillon cubique d'une mousse PDA@PUF a été traité avec de l'APTES dans le toluène à 70 °C, et la mousse amino-fonctionnalisée résultante APTES@PDA@PUF couplée avec l'éosine Y en présence d'EDC (**Figure 6**).

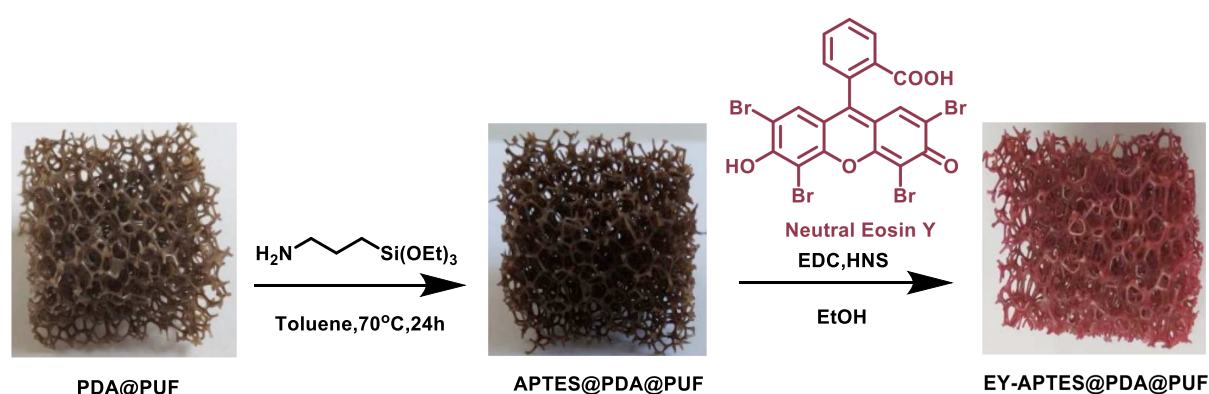


Figure 6. Stratégie de fonctionnalisation de PDA@PUF pour l'immobilisation d'éosine Y.

L'analyse élémentaire par ICP-AES de EY-APTES@PDA@PUF fraîchement préparé a révélé des teneurs moyennes en Si et en Br de $2,544 \pm 0,077$ et $1,051 \pm 0,029$ g/kg, et le spectre RMN CP-MAS ^{29}Si des signaux à -65,1, -59,9, -50,3 et -42,5 ppm (**Figure 7A**) de façon similaire à ce qui a été observé avec APTES@PDA@PUF (voir plus haut), ce qui suggère la préservation des structures T_1 et T_2 , ainsi que de structures réticulées $\text{T}_3+\text{T}_3'$ et $\text{T}_4+\text{T}_4'$ après le couplage en présence d'EDC, et met en exergue la robustesse des liaisons silicium-catéchol formées lors de la première étape de la stratégie de post-fonctionnalisation. Enfin, les images MEB de EY-APTES@PDA@PUF révèlent une surface rugueuse typique des mousses enrobées de PDA (**Figure 7B**) et la spectroscopie EDX confirme la présence de Si et Br (**Figure 7C**).

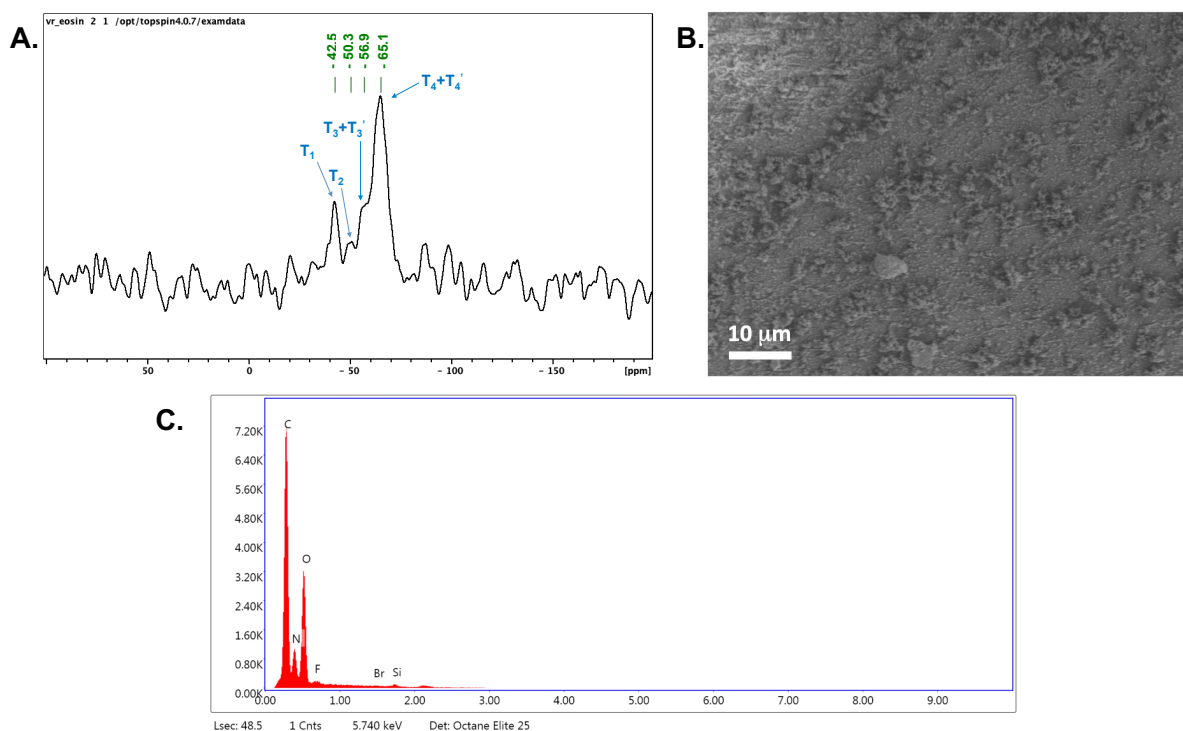


Figure 7. Spectre RMN CP-MAS ^{29}Si (A), image MEB à fort grossissement (B) et spectre EDX (C) de EY-APTES@PDA@PUF.

L'activité catalytique du PC hétérogène résultant, EY-APTES@PDA@PUF (8 cm^3 , 0,46 mol% EY) a d'abord été étudié pour la photo-oxydation de sels de *N*-alkylpyridinium en quinolones and isoquinolones, en particulier pour l'oxydation de l'iodure de 2-méthyl-5-nitroisoquinolin-2-ium sous lumière blanche (LED, 24W) dans l'acétonitrile en présence de Cs_2CO_3 à 30-35 $^\circ\text{C}$.²³ De façon satisfaisante, 69 % de rendement a été obtenu après 18 h de réaction et la mousse a pu être utilisée six fois sans perte apparente d'activité (**Figure 8**). Il est notable toutefois que le milieu réactionnel était légèrement teinté en orange après chaque réaction, suggérant une certaine lixiviation de l'éosine. En accord avec cela, la mousse est devenue brunâtre après six cycles catalytiques et l'analyse ICP-AES indique une perte de Si de l'ordre de 22%. Il est à signaler aussi qu'une réaction de fond est observable dans les mêmes conditions mais sans catalyseur, avec 44% de rendement, ce qui peut expliquer l'absence de perte apparente d'activité malgré la lixiviation de l'éosine.

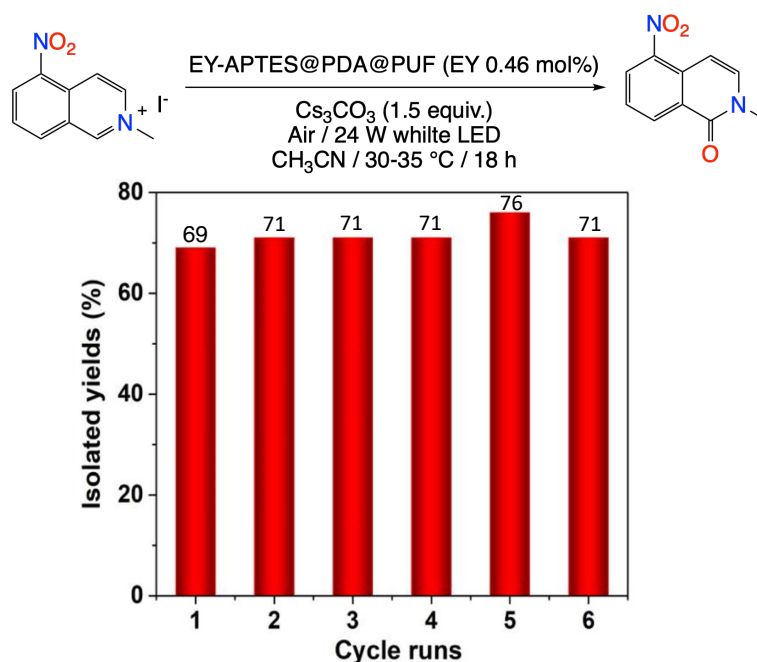


Figure 8. Oxydation de l'iodure 2-méthyl-5-nitroisoquinolin-2-ium photocatalysée par EY-APT@PDA@PUF sous lumière blanche (LED, 24W), rendements obtenus pendant 6 cycles consécutifs.

Afin d'en savoir davantage sur la modification de la surface de la mousse, la mousse usagée a été analysée par MEB et spectroscopie EDX. Comme pour Ru(bpy)₃-APTE@PDA@PUF, les images MEB à haute résolution ont révélé un polissage. La spectroscopie EDX, quant à elle, a confirmé la présence des éléments C, N, O et Si sur la surface mais n'a plus permis de détecter du Br. Du Cs provenant de la base utilisée a été détecté en revanche.

Afin de mieux appréhender l'influence de la lixiviation de l'éosine sur l'activité catalytique de EY-APT@PDA@PUF, une réaction totalement silencieuse en absence de photocatalyseur a ensuite été étudiée : la photo-oxydation de sulfures en sulfoxydes.²⁴ Dans un mélange CH₃CN/H₂O (4:1) à 30-35 °C sous lumière blanche (LED, 24 W), le *p*-tolyl-méthyl sulfure a été oxydé à 98% après 48 h de réaction en présence de EY-APT@PDA@PUF (8 cm³, 0,18 mol% EY) (TON 544, TOF 11.3 h⁻¹). Dans ce cas cependant, une diminution graduelle de l'activité a été observé au fil des cycles, de 98% dans le premier cycle à 59% dans le cinquième (**Figure 9**). En accord avec cette observation, des analyses ICP-AES de la mousse usagée ont révélé une perte d'éosine de l'ordre de 34%, avec une teneur en Br de 0,691 ± 0,019 g/kg contre 1,051 ± 0,029 g/kg dans une mousse fraîchement préparée. En outre, une

expérience de contrôle de type « stop & go » a montré la poursuite de la progression de la réaction lorsque la mousse est retirée du milieu, ce qui a confirmé sans ambiguïté la lixiviation de l'éosine.

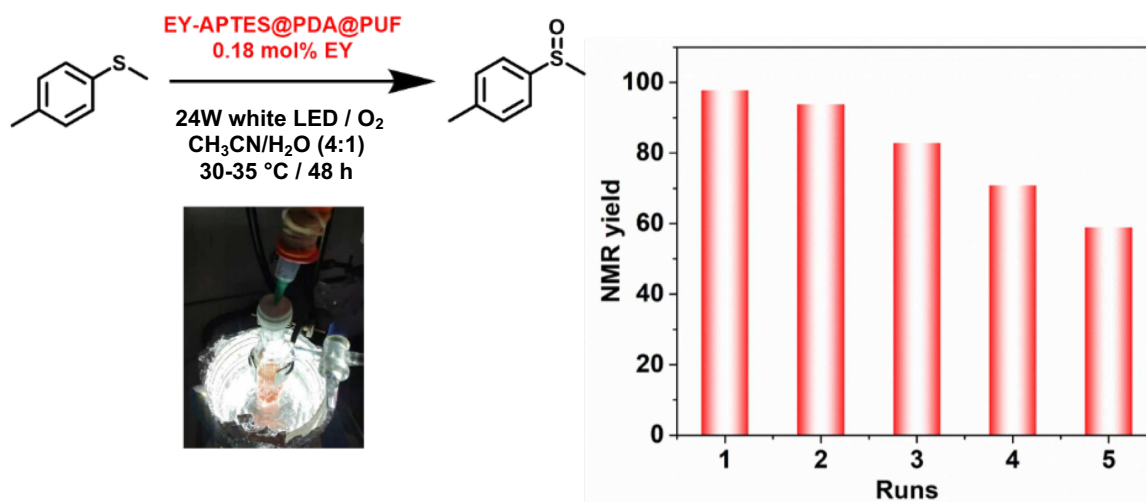


Figure 9. Oxydation du sulfure de méthyle *p*-tolyle photocatalysée par EY-APTES@PDA@PUF (8 cm³, 0,18 mol% EY), rendements obtenus pendant 5 cycles consécutifs.

Une forte adsorption de l'éosine sur la PDA et une faible efficacité du couplage médié par EDC étant suspectée être à l'origine de ce phénomène, de nouvelles stratégies de préparation du photocatalyseur supporté ont été envisagées. Dans une première tentative, l'éosine Y a été couplée à l'APTES en présence de COMU au lieu d'EDC, et ce avant la procédure d'ancrage covalent à PDA@PUF afin d'essayer de minimiser la simple adsorption de l'éosine sur la PDA (**Figure 10**). Une importante lixiviation a cependant de nouveau été observée lors des tests catalytiques.

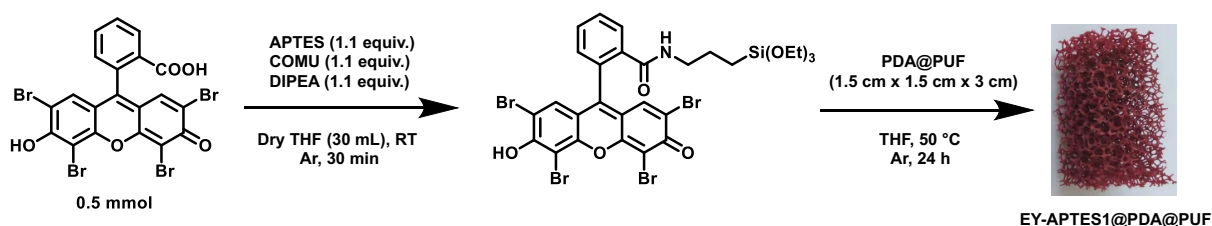


Figure 10. Couplage éosine Y-APTES médié par COMU et condensation APTES-PDA en un pot pour l'ancrage de EY-APTES sur PDA@PUF.

Une stratégie totalement différente a alors été envisagée. Après une réaction de couplage de l'éosine Y avec la dopamine en présence d'un large excès de cette dernière, le mélange résultant a été placé dans les conditions d'auto-polymérisation de la dopamine, afin de générer un revêtement hybride PDA-EY qui a été utilisé pour

enrober un échantillon cubique de PUF et fournir un matériau PDA-EY@PUF sans APTES (**Figure 11**). Une fois encore cependant, une importante lixiviation a été observée lors des tests catalytiques.

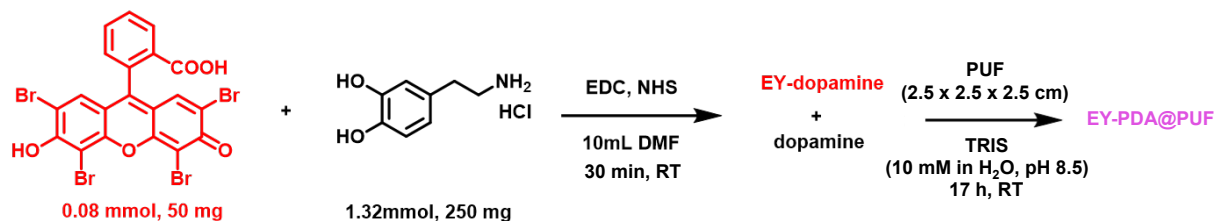


Figure 11. Revêtement de PUF avec un hydride EY-PDA.

La combinaison d'éosine Y et de PDA ne semble donc pas appropriée pour immobiliser l'éosine Y de façon robuste sur des PUFs et des stratégies alternatives devront être envisagées.

Axe II. Mousse de polyuréthane enrobée de polydopamine et fonctionnalisée au Pd comme catalyseur structuré facile à préparer et réutiliser pour la semi-hydrogénation sélective d'alcynes

Dans cette partie de la thèse visant à développer un catalyseur de semi-hydrogénation d'alcynes qui soit facile à préparer et aisément réutilisable, un sel de Pd(II) a été immobilisé sur un échantillon cubique de mousse de polyuréthane enrobée de polydopamine, PDA@PUF, par simple immersion de ce dernier dans une solution hydro-alcoolique de $[Pd(NH_3)_4]Cl_2$ pendant 19 h à température ambiante (**Figure 12**).

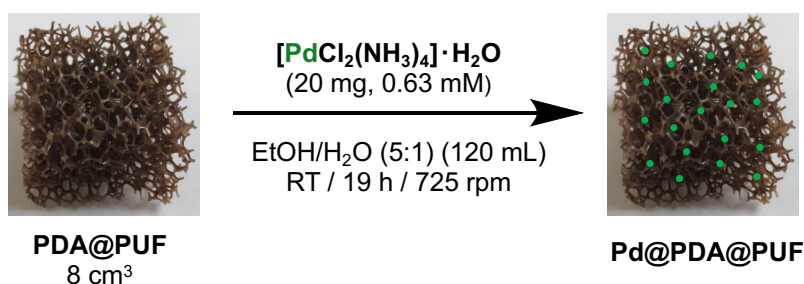


Figure 12. Immobilisation en une étape d'un sel de Pd(II) sur PDA@PUF

Des mesures ICP-AES réalisées sur plusieurs échantillons de Pd@PDA@PUF ont établi une charge moyenne de Pd de $2,437 \pm 0,323$ g/kg (soit $0,244 \pm 0,032$ % en masse). Les images MEB à haute résolution (HR-MEB) ont révélé une surface

rugueuse typique des mousses enrobées de PDA sans présence détectable de particules de Pd (**Figure 13A-B**), et les micrographies MEB combinées à la spectroscopie EDX une distribution quasi-uniforme du Pd sur la surface de la mousse (**Figure 13C-D**), sans zone apparente d'agrégats ou de ségrégations, assurant une relativement bonne homogénéité du matériau. La spectroscopie XPS, quant à elle, a montré une absence initiale de réduction du Pd(II) en Pd(0) malgré les propriétés redox de la PDA (+0.3 V/NHE vs. +0.99 V/NHE pour le couple Pd²⁺/Pd⁰). L'ensemble de ces données suggèrent une dispersion uniforme d'ions de Pd(II) coordonnés par les groupements catéchols de la PDA, résultant ainsi en une dispersion de la phase active de type « atome unique » qui serait à l'origine de la très haute sélectivité observée en semi-hydrogénation des alcynes (*vide infra*).

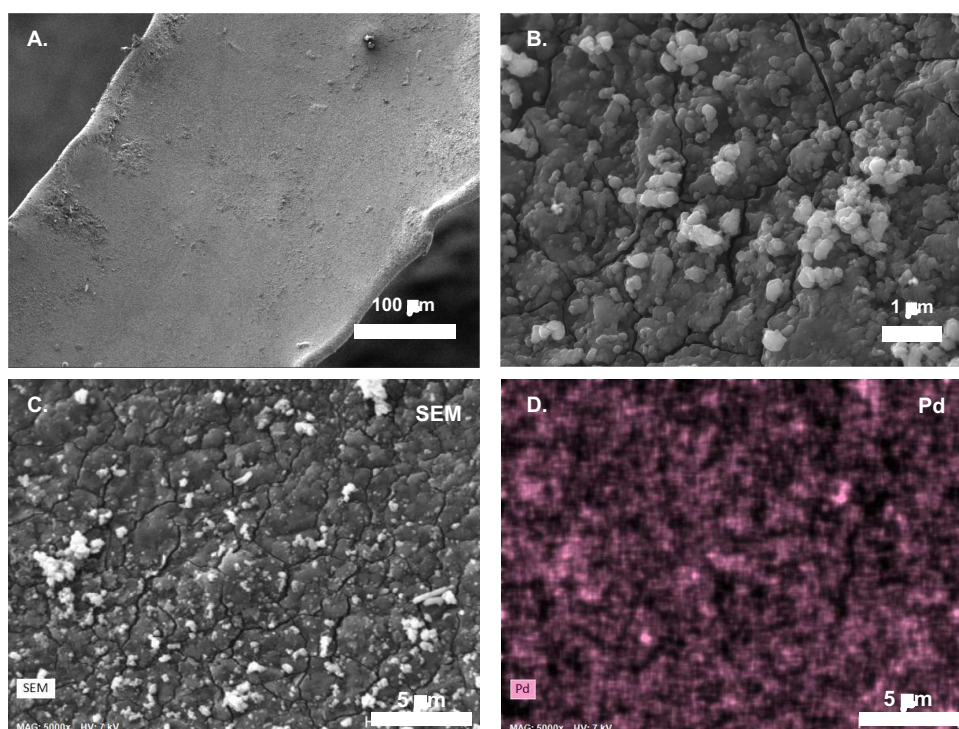


Figure 13. (A-B) Images HR-SEM avec différents grossissements de Pd@PDA@PUF. (C-D) Cartographie du Pd sur Pd@PDA@PUF obtenue par SEM-EDX.

Ainsi, avec une charge catalytique de 0,12 mol% en Pd, une concentration en substrat de 0,3 M dans l'éthanol à température ambiante, et sous un flux de H₂ de 13 mL/min, Pd@PDA@PUF a permis l'hydrogénation du phénylacétylène en styrène avec une sélectivité de 95% à 98% de conversion. Ce n'est qu'une fois tout le phénylacétylène consommé que la sur-hydrogénation en éthylbenzène a été observée de façon notable (**Figure 14A**). Une sélectivité du même ordre a été observée avec

tous les alcynes vrais étudiés (1-heptyne, 4-phényl-1-butyne et 2-méthylbut-3-yn-2-ol), les réactions de sur-hydrogénation ou d'isomérisation d'alcène n'intervenant qu'une fois tout l'alcyne de départ intégralement consommé. Avec les alcynes internes comme le 3-hexyne ou le 4-octyne, la sélectivité observée s'est révélée encore meilleure puisque quasiment aucune sur-hydrogénation ou isomérisation d'alcène n'a été observée, même plusieurs heures après que tout l'alcyne a été consommé (**Figure 14B**).

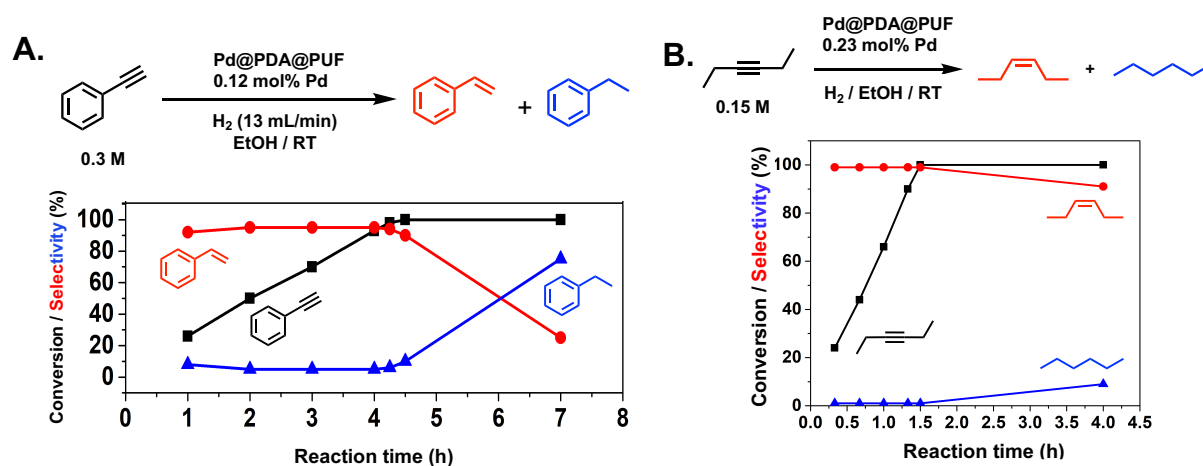


Figure 14. (A) Hydrogénation du phénylacétylène. (B) Hydrogénation du 3-hexyne. Carrés noirs : conversion de l'alcyne, cercles rouges : sélectivité en alcène, triangles bleus : sélectivité en alcane

De façon remarquable, aucune lixiviation du Pd n'a été observée par analyses ICP-AES et Pd@PDA@PUF (0.23 à 1.4 mol%) s'est montré également efficace en catalyse de Suzuki permettant le couplage de divers bromures d'aryle avec l'acide phénylboronique avec des rendements variant entre 83 et 97 % en conditions aérobies dans un mélange éthanol/eau (1 :1) à 65 °C en présence de K₃PO₄ (1,5 équiv.) comme base (**Figure 15**).

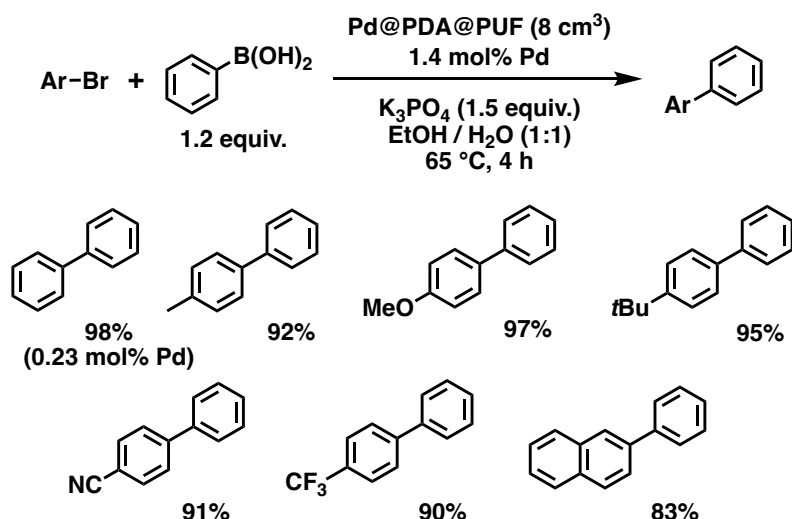


Figure 15. Couplage de Suzuki catalysé par Pd@PDA@PUF.

Afin de mettre en exergue la stabilité et la polyvalence de Pd@PDA@PUF, 15 cycles catalytiques consécutifs ont été réalisés avec un seul échantillon cubique de Pd@PDA@PUF (8 cm³, Pd : 0,23 mol%), consistant en 5 cycles de semi-hydrogénation du phénylacétylène, suivis de 5 cycles de couplage Suzuki du bromobenzène avec l'acide phénylboronique, puis à nouveau de 5 cycles de semi-hydrogénation du phénylacétylène (**Figure 16**). De façon satisfaisante, aucune baisse d'activité ou de sélectivité n'a été observée lors de ces 15 cycles, quelques soit la réaction considérée. Une amélioration progressive des performances a même été observée lors des 5 premiers cycles de semi-hydrogénation.

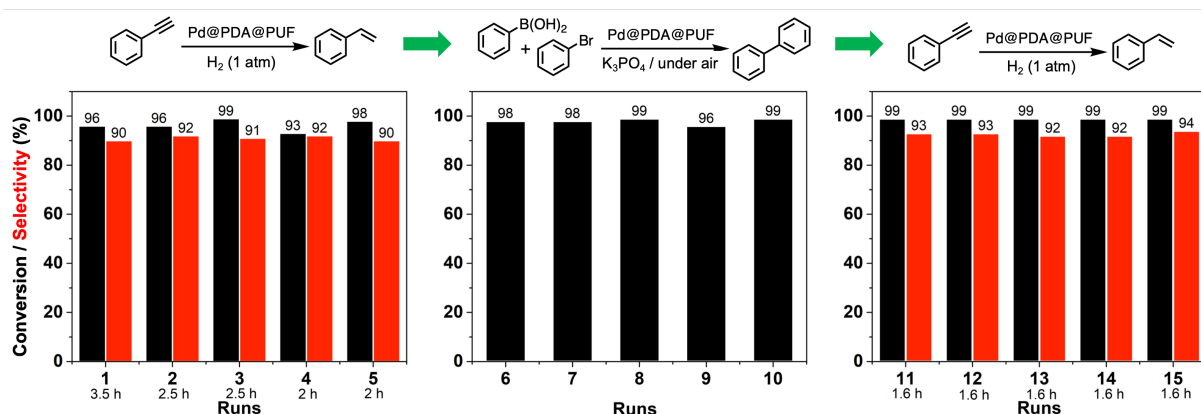


Figure 16. Conversion et sélectivité mesurées sur les 15 cycles successifs de semi-hydrogénation du phénylacétylène (cycles 1 à 5 et 11 à 15) et de couplage Suzuki du bromobenzène avec l'acide phénylboronique (cycles 6 à 10) catalysés par un seul échantillon cubique de Pd@PDA@PUF (8 cm³, Pd : 0.23 % molaire)

Des études XPS réalisées à l'issue des 15 cycles catalytiques ainsi qu'à l'issue d'expériences de contrôle, permettent d'expliquer ce phénomène par une réduction progressive des espèces immobilisées de Pd(II) en Pd(0) dans les conditions réactionnelles (**Figure 17**). En outre, l'analyse de la mousse Pd@PDA@PUF après les 15 cyclages catalytiques par HR-SEM et SEM-EDX révèle une remarquable stabilité de la surface avec une absence de modification apparente et une absence de mobilité du Pd qui est toujours distribué de façon très homogène (**Figure 18**), suggérant ainsi une réduction des ions de Pd(II) coordonnées au catéchols de la PDA en « atomes isolés » de Pd(0). Cette dispersion de la phase active est certainement à l'origine de la très haute sélectivité observée en semi-hydrogénation des alcynes. Enfin, il est notable que la forte interaction entre le Pd(0) et la couche adhésive non-innocente de PDA, en plus d'empêcher la lixiviation de ce dernier dans le milieu, empêche également sa réoxydation lorsque la mousse est exposée à l'air, même de façon prolongée, ce qui est absolument remarquable.

Ces résultats remarquables rendent a priori possible des semi-hydrogénations extrêmement sélectives en conditions de flux. Ceci est actuellement à l'étude en collaboration avec l'équipe du Dr. David Edouard de CP2M à l'Université de Lyon I dans un réacteur à lit dynamique, et les premiers résultats sont très prometteurs.

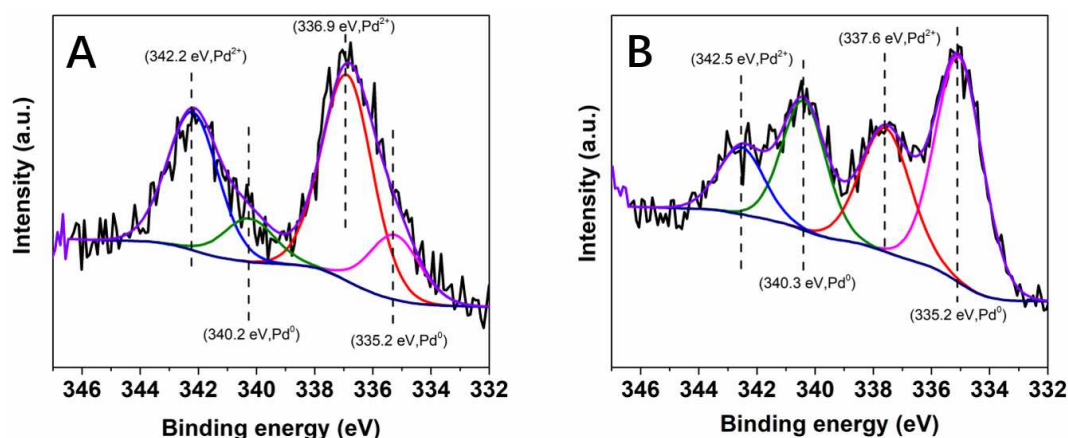


Figure 17. Spectres XPS à haute résolution de la région du noyau Pd3d de Pd@PDA@PUF. (A) Après un cycle de semi-hydrogénation du phénylacétylène. (B) Après un cycle de couplage de Suzuki du bromobenzène et de l'acide phénylboronique.

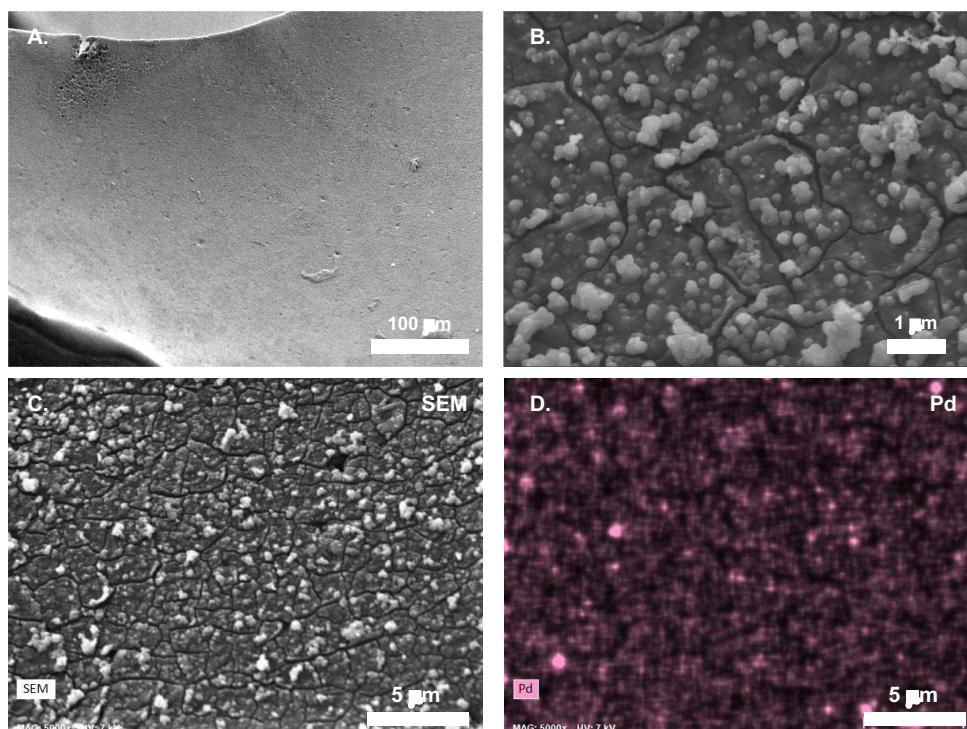


Figure 18. (A-B) Images HR-SEM avec différents grossissements de Pd@PDA@PUF après 15 cyclages catalytiques. (C-D) Cartographie du Pd sur Pd@PDA@PUF après 15 cyclages catalytiques obtenue par SEM-EDX.

3) Conclusion générale

Lors de cette thèse centrée sur le développement de mousses de polyuréthane enrobées d'une couche adhésive de polydopamine aisément fonctionnalisable comme supports catalytiques structurés, deux axes ont été étudiés.

Dans le premier axe, des mousses photocatalytiques Ru(bpy)₃-APTES@PDA@PUF et EY-APTES@PDA@PUF ont été préparées selon une méthode de fonctionnalisation covalente de PDA@PUF impliquant une étape de silanisation. Pour le premier, une très bonne efficacité a été observée sous lumière bleue dans des réactions d'homocouplages oxydatifs d'amines benzyliques et dans des réactions de couplages croisés déshydrogénants de type aza-Henry en présence d'oxygène moléculaire comme oxydant « vert ». Ru(bpy)₃-APTES@PDA@PUF a montré un champ réactionnel relativement étendu dans les deux réactions, ainsi qu'une excellente réutilisabilité puisqu'il a pu être utilisé jusqu'à 6 fois sans perte d'activité. Malgré le fait qu'environ 30% de lixiviation du ruthénium a été observée après 6 cycles catalytiques – ce qui résulte probablement de la sensibilité du lien amide et non de celle de l'ancrage catéchol-silicium, comme suggéré par les analyses ICP-

AES – une amélioration des performances catalytiques a même été observée au cours des tests de recyclages pour les deux types de réactions. Comme suggéré par l'évolution de la couleur des mousses, des analyses SEM et XPS, cette amélioration des propriétés catalytiques résulte probablement d'une modification de la couche supérieure de la polydopamine qui ferait migrer le $[\text{Ru}(\text{bpy})_3]^{2+}$ restant en surface et le rendrait donc plus accessible. Cette stratégie d'ancrage s'est cependant révélée non universelle puisque dans le cas de EY-APTES@PDA@PUF, une importante lixiviation a été observée lors des tests catalytiques pour la photo-oxydation de sulfures en sulfoxydes sous lumière blanche. En conséquence, d'autres approches ont été envisagées, toutes sans succès, soulevant la question d'une éventuelle incompatibilité entre la PDA et l'éosine Y sous conditions de photocatalyse.

Dans le second axe, des mousses Pd@PDA@PUF pouvant servir de catalyseur hétérogène polyvalent et hautement fiable pour diverses transformations organiques sans procédure préalable de réduction du Pd ont été aisément préparées via une simple procédure de trempage d'une mousse PDA@PUF dans une solution hydro-alcoolique de $[\text{Pd}(\text{NH}_3)_4]\text{Cl}_2$ à température ambiante. Ces mousses agissent comme un catalyseur efficace et réutilisable pour la semi-hydrogénation d'alcyne sous 1 atm de H_2 à température ambiante, donnant des sélectivités pouvant aller jusqu'à 99% à plus de 99% de conversion, et pour le couplage de Suzuki de bromures d'aryle en conditions aérobies. De façon remarquable, Pd@PDA@PUF est extrêmement stable et n'a montré aucune diminution de son activité ou de sa sélectivité lorsqu'une mousse a été utilisée pendant 15 cycles successifs d'hydrogénation et de couplage croisé. Le catalyseur a même montré une amélioration progressive de ses performances lors des 5 premiers cycles, due (i) à la réduction progressive des espèces de Pd(II) immobilisées en Pd(0), comme démontré par XPS, et (ii) à l'existence de fortes interactions entre le Pd et la couche adhésive, redox non-innocente, de PDA qui préviennent la réoxydation de la phase active de Pd lors d'une exposition à l'air ainsi que sa lixiviation dans le milieu réactionnel. En outre, la très petite taille des espèces de Pd, comme montré par HR-MEB et MEB-EDX, suggère une simple coordination des ions de Pd(II) par les groupements catéchols de la PDA. La dispersion résultante de type « atome unique » de la phase active et l'absence d'agrégation du Pd réduit au cours du temps est vraisemblablement à l'origine de la très haute sélectivité observée en hydrogénation sélective d'alcyne en alcène, faisant de ce catalyseur un exemple

rare, sinon unique, de catalyseur sélectif de semi-hydrogénation d'alcynes dont le mode de préparation va à l'encontre de la tendance actuelle qui est de développer des approches de plus en plus sophistiquées pour contrôler la taille et la forme de la phase active. Enfin, la modulation aisée de la taille et de la forme des mousses de Pd@PDA@PUF, ainsi que leurs propriétés de transport, permettent d'envisager avec confiance une adaptation à un processus en flux.

Références

1. Bakker, J. J. W.; Groendijk, W. J.; de Lathouder, K. M.; Kapteijn, F.; Moulijn, J. A.; Kreutzer, M. T.; Wallin, S. A. *Ind. Eng. Chem. Res.* **2007**, *46* (25), 8574-8583
2. (a) Giani, L.; Groppi, G.; Tronconi, E. *Ind. Eng. Chem. Res.* **2005**, *44* (14), 4993-5002. (b) Lacroix, M.; Dreibine, L.; de Tymowski, B.; Vigneron, F.; Edouard, D.; Bégin, D.; Nguyen, P.; Pham, C.; Savin-Poncet, S.; Luck, F.; Ledoux, M.-J.; Pham-Huu, C. *Appl. Catal. A* **2011**, *397* (1), 62-72. (c) Lacroix, M.; Nguyen, P.; Schweich, D.; Pham-Huu, C.; Savin-Poncet, S.; Edouard, D. *Chem. Eng. Sci.* **2007**, *62* (12), 3259-3267.
3. Richardson, J. T.; Peng, Y.; Remue, D. *Appl. Catal. A*, **2000**, *204*, 19.
4. Lacroix, M.; Dreibine, L.; de Tymowski, B.; Vigneron, F.; Edouard, D.; Bégin, D.; Nguyen, P.; Pham, C.; Savin-Poncet, S.; Luck, F.; Ledoux, M.-J.; Pham-Huu, C. *Appl. Catal. A*, **2011**, *397*, 62
5. Engels, H.-W.; Pirkl, H.-G.; Albers, R.; Albach, R. W.; Krause, J.; Hoffmann, A.; Casselmann, H.; Dormish, J. *Angew. Chem. Int. Ed.* **2013**, *52* (36), 9422-9441.
6. Lee, H.; Dellatore, S. M.; Miller, W. M.; Messersmith, P. B. *Science* **2007**, *318* (5849), 426-430.
7. Edouard, D.; Ritleng, V.; Jierry, L.; Chau-Dalencón, N. T. T. WO 2016012689A2, 2016.
8. Pardieu, E.; Chau, N. T. T.; Dintzer, T.; Romero, T.; Favier, D.; Roland, T.; Edouard, D.; Jierry, L.; Ritleng, V. *Chem. Commun.* **2016**, *52* (25), 4691-4693
9. Ait Khouya, A.; Mendez Martinez, M. L.; Bertani, P.; Romero, T.; Favier, D.; Roland, T.; Guidal, V.; Bellière-Baca, V.; Edouard, D.; Jierry, L.; Ritleng, V. *Chem. Commun.* **2019**, *55* (79), 11960-11963.
10. Saiz-Poseu, J.; Mancebo-Aracil, J.; Nador, F.; Busqué, F.; Ruiz-Molina, D. *Angew. Chem. Int. Ed.*, **2019**, *58*, 696-714.
11. Prier, C. K.; Rankic, D. A.; MacMillan, D. W. C. *Chem. Rev.* **2013**, *113* (7), 5322-5363.
12. Douglas, J. J.; Sevrin, M. J.; Stephenson, C. R. *J. Org. Proc. Res. Dev.* **2016**, *20* (7), 1134-1147.
13. Ponzio, F.; Kelber, J.; Birba, L.; Rekab, K.; Ritleng, V.; Jierry, L.; Edouard, D. *Environ.*

Technol. Innov. **2021**, *23*, 101618.

14. Blaser, H. U.; Schnyder, A.; Steiner, H.; Rössler, F.; Baumeister, P. *Selective hydrogenation of functionalized hydrocarbons*. in: Ertl G.; Knözinger, H.; Schüth, F.; Weitkamp (Eds), J., *Handbook of Heterogeneous Catalysis*, Wiley-VCH, Weinheim, 2008, pp. 3284-3308.
15. Oger, C.; Balas, L.; Durand, T.; Galano, J.-M. *Chem. Rev.* **2013**, *113* (3), 1313-1350.
16. Zhang, L.; Zhou, M.; Wang, A.; Zhang, T. *Chem. Rev.* **2020**, *120* (2), 683-733.
17. Albert, K.; Pfeleiderer, B.; Bayer, E.; Schnabel, R., *J. Colloid Interf. Sci.* **1991**, *142* (1), 35-40
18. Vejayakumaran, P.; Rahman, I. A.; Sipaut, C. S.; Ismail, J.; Chee, C. K., *J. Colloid Interface Sci.* **2008**, *328* (1), 81-91
19. (a) Xu, C.; Liu, H.; Li, D.; Su, J.-H.; Jiang, H.-L. *Chem. Sci.* **2018**, *9* (12), 3152-3158. (b) Han, A.; Sun, J.; Zhang, H.; Chuah, G.-K.; Jaenicke, S. *ChemCatChem* **2019**, *11* (24), 6425-6430.
20. (a) Condie, A. G.; González-Gómez, J. C.; Stephenson, C. R. J., Visible-Light Photoredox Catalysis: Aza-Henry Reactions via C-H Functionalization. *J. Am. Chem. Soc.* **2010**, *132* (5), 1464-1465. (b) Zhi, Y.; Ma, S.; Xia, H.; Zhang, Y.; Shi, Z.; Mu, Y.; Liu, X. *Appl. Catal. B* **2019**, *244*, 36-44.
21. Yakushev, A. A.; Abel, A. S.; Averin, A. D.; Beletskaya, I. P.; Cheprakov, A. V.; Ziankou, I. S.; Bonneviot, L.; Bessmertnykh-Lemeune, A., Visible-light photocatalysis promoted by solid- and liquid-phase immobilized transition metal complexes in organic synthesis. *Coord. Chem. Rev.* **2022**, *458*, 214331.
22. Herbrink, F.; Camarero González, P.; Krstic, M.; Puglisi, A.; Benaglia, M.; Sanz, M. A.; Rossi, S. *Appl. Sci.* **2020**, *10* (16), 5596.
23. Jin, Y.; Ou, L.; Yang, H.; Fu, H., *J. Am. Chem. Soc.* **2017**, *139* (40), 14237-14243.
24. (a) Sridhar, A.; Rangasamy, R.; Selvaraj, M. *New J. Chem.* **2019**, *43* (46), 17974-17979. (b) Chu, Y.; Huang, Z.; Liu, R.; Boyer, C.; Xu, J. *ChemPhotoChem* **2020**, *4* (10), 5201-5208.

Introduction

Introduction

Table of contents

I) Introduction.....	28
I-1) Catalyst support.....	28
I-1-1) Carbon materials	29
I-1-2) Oxides	30
I-1-3) Polymers.....	32
I-2) Macroscopically structured catalytic supports	32
I-3) Polyurethane foams	34
I-4) Properties of open cell polyurethane foams	36
I-5) Polydopamine and marine organisms	38
I-6) Origin of the adhesive properties of polydopamine and mechanism of formation	39
I-7) PDA as catalyst and catalytic support	41
I-8) Coating of open cell polyurethane foams (PUF) by PDA	42
I-9) Functionalization of PDA@PUF for catalytic and adsorption applications.....	44
I-9-1) Covalent functionalization of PDA@PUF	44
I-9-2) Functionalization of PDA@PUF with sodium borohydride.....	46
I-9-3) Functionalization of PUF@PDA with metal (nano)particles.....	47
I-9-4) Functionalization of PDA@PUF with metal oxide nanoparticles.....	49
I-9-5) Functionalization of PDA@PUF with carbon materials.....	50
I-9-6) Functionalization of PDA@PUF with metal-organic frameworks	51
II) Conclusion.....	53

I) Introduction

1-1) Catalyst supports – a short overview

A catalyst is a substance that can accelerate reactions without changing the standard Gibbs energy.¹ The process where the catalyst plays its part is called catalysis. Catalysts are both reactants and products in the reaction. When the catalyst and reactants are in the same phase, catalysis is referred as homogeneous, whereas when they are in separated phases, catalysis is referred as heterogeneous. As homogeneous catalysts are usually well-defined molecules, they have the advantage of having unique active sites that can be finely tuned to the targeted reaction. This usually results in excellent selectivity. However, the contribution of homogeneous catalytic processes in the chemical industry is significantly lower than that of heterogeneous catalytic processes. This is because these catalysts are often only stable under relatively mild conditions, which limits their applicability, and because they are dispersed in the same phase as the reactants, products and solvents, which renders their separation at the end of the reaction difficult and costly, even impossible.²⁻

4

In heterogeneous catalysis, most often catalysts are solids, and the reactants gases or liquids, which facilitates the separation of the reaction products from the catalyst at the end of the reaction, and is a clear advantage over homogeneous catalysis. A heterogeneous catalyst is usually composed of metals, oxides or other materials - acting as the active phase - supported on suitable host structures. The reaction between the reactants, gas or liquid, takes place at the surface of the solid catalyst. As the surface is where the reaction takes place, it is usually organized to be as large as possible per unit of catalyst; finely divided metals, metals embedded in support matrices and metal films are thus commonly used in heterogeneous catalysis.⁵⁻

7

The support, according to the definition of IUPAC,⁸ often plays a non-negligible role as a component in multiphase catalysts and constitutes the catalytic material together with the active phase. It is also called “carrier” and, while usually inert, still contributes to the overall catalytic activity. The relationship between the catalyst and the support should not be deemed as an interdependency but the latter can nevertheless regulate the activity of the former so as to work in a more efficient manner.

Thus, distinct technologies and strategies can enormously influence the catalytic performance of a given active phase; the latter being a balance of seemingly conflicting demands, namely a high activity, a high selectivity, and a long lifetime.⁹⁻¹⁰ Thanks to efficient active phase-support associations, reactions have become more economic, time saving, and sustainable in some cases, so the development of catalytic supports should assist the development of catalysis and the comprehension of catalytic mechanisms.

According to the property of matrices, catalytic supports can be divided into three main groups: inorganic, organic or organic-inorganic hybrid materials (a hybrid material is composed of an intimate mixture of inorganic and organic components which usually interpenetrate on scales of less than 1 μm ¹¹). This introduction will now briefly introduce these materials applied in supported catalysis.

I-1-1) Carbon materials

Carbon materials constitute ideal supporting candidates known for their high surface specific area, chemical and electrochemical inertness, and easy surface modification. These materials are thus widely utilized in supported catalysis for immobilizing active species.¹² Even though they cannot be used under some specific conditions, such as hydrogenation or oxidation at high temperatures (> 700 K for hydrogenation, > 500 K for oxidation), they show numerous superior properties as catalytic supports¹³ including the facts that: (i) they are resistant to acid or basic reaction media and can endure high temperatures during catalysis, (ii) macroscopic shapes and pore sizes can be tuned in order to meet different requirements, (iii) procedures of catalyst recovering and surface modification are facile, (iv) finally it is usually less expensive than other supports. Combining all these advantages, carbon materials are qualified for a large number of industrial reactions.

In 1934, a U.S. patent reported one of the first application utilizing carbon as a support. It was discovered that at 573 K and under 50 to 70 atm of H_2 , sulfur-containing naphthalene could be reduced to tetrahydronaphthalene with a charcoal-supported catalyst containing nickel oxide, molybdenum sulfide, and calcium carbonate.¹⁴ Afterwards, carbon-based catalysts were extensively applied in several representative families of industrial reactions including ammonia synthesis, hydrotreating reactions, and the hydrogenation of carbon oxides.¹² Taking hydrogenation as an example, the

inertness of carbon is of paramount significance when carbon materials are used as supporting matrices. These supporting systems indeed usually comprise two or more metallic phases and, due to carbon inertness, interactions between the metals and/or metal oxides are highly enhanced, thus yielding more active and selective catalysts than those supported on other supports.¹²

More recently, novel crystalline carbon entered our horizon such as graphene¹⁵⁻¹⁷ and carbon nanotubes (CNTs).¹⁸⁻²⁰ These nanocarbon structures generated increasing research interests over the years.²¹⁻²³ Compared with traditional active carbon, which is widely used in industrial processes, nanocarbons have better organized pore structures, more uniform characteristics, reduced number of defects and impurities, etc.²⁴ Regarding their use in industrial catalysis, their high cost, and sometimes the observation of contradictory results remains a challenge in this domain.²⁴

I-1-2) Oxides

Among this category, alumina (Al_2O_3) and silica (SiO_2) are the two most typical oxides that gained great interest in the field of supported catalysis.

Alumina is naturally occurring in its crystalline polymorphic phase, $\alpha\text{-Al}_2\text{O}_3$, as the mineral called corundum, whose varieties form the precious gemstones, ruby and sapphire.²⁵ Another active crystalline phase, $\gamma\text{-Al}_2\text{O}_3$, has become one of the most important catalysts and catalyst supports in the automotive and petroleum industries in early years.²⁶⁻²⁷ Their appropriate surface areas, pore volumes, pore size distributions and acid/base characteristics endowed them outstanding properties in surface chemical composition, local microstructure, and phase composition.²⁸

Even if supported systems based on slightly different precursor–alumina interactions have been reported, electrostatic interactions are predominantly the main driving forces when immobilizing ions on alumina. It is noteworthy however that, in some cases, the immobilization results from the combination of repulsive coulombic force with some specific chemical adsorptions as observed for the adsorptions of cations such as Ni^{2+} , Co^{2+} , and Pb^{2+} onto a positively charged alumina surface.²⁹⁻³⁰

Currently, along with more in-depth research about the catalytic mechanisms at play, some drawbacks concerning alumina supported systems have appeared. For instance, alumina-supported nickel nanoparticles suffered from rapid deactivation in a methane dry reforming process,³¹ or a palladium–alumina system proved to be

sensitive to the presence of water blocking the surface in a methane oxidation process.³² Efforts are thus still required to tune and develop catalytic performances, and although novel alumina-based materials arise, catalytic ranges are yet still too restricted for industrial reactions compared with other oxides like silica, even though alumina is probably still irreplaceable as a well-known support with good alkali-resistance.³³

As mentioned above, the other ubiquitous oxide being intensively studied as support matrix is silica. Besides properties³⁴ and applications³⁵ resembling alumina, silica-based supporting systems with chiral metal catalyst,³⁶ ionic liquid,³⁷ lipase,³⁸ nanoparticles (nickel,³⁹ palladium,⁴⁰ magnetic⁴¹ and organic-inorganic hybrid⁴²) have been reported and used in a wide range of organic transformations. Even though silica, like other supports, may face some leaching problems or impracticalities when it comes to scale-up or industrial scale reactions, synthetic and designing concepts are still supposed to be referential and instructive for other supporting systems.

The source of its high efficiency and versatility in heterogeneous catalysis can be ascribed mainly to two aspects.

Benefiting from mature silanization techniques, the diversified immobilization methods shown in Figure 1 can provide more selectivity when supporting molecular catalysts on silica. For example, when having some troubles obtaining ligand-functionalized organosilanes or facing poor hydrolytic stability of functional organosilanes, modular post-functionalization strategies may be more realistic. Finally, it should be noted that, although these approaches were developed with silica, their principle should be valid for designing other oxide-based catalytic systems.

Another interesting phenomenon verified in numerous works is the enhancement of metal complex catalysis efficiency when immobilized on silica surface.⁴³ Multiple surface effects such as site isolation, concerted catalysis, or confinement effect can enhance catalytic performances, which includes, in addition to enhanced reaction rate, also enhanced regio- and stereoselectivity, as well as enhanced durability.

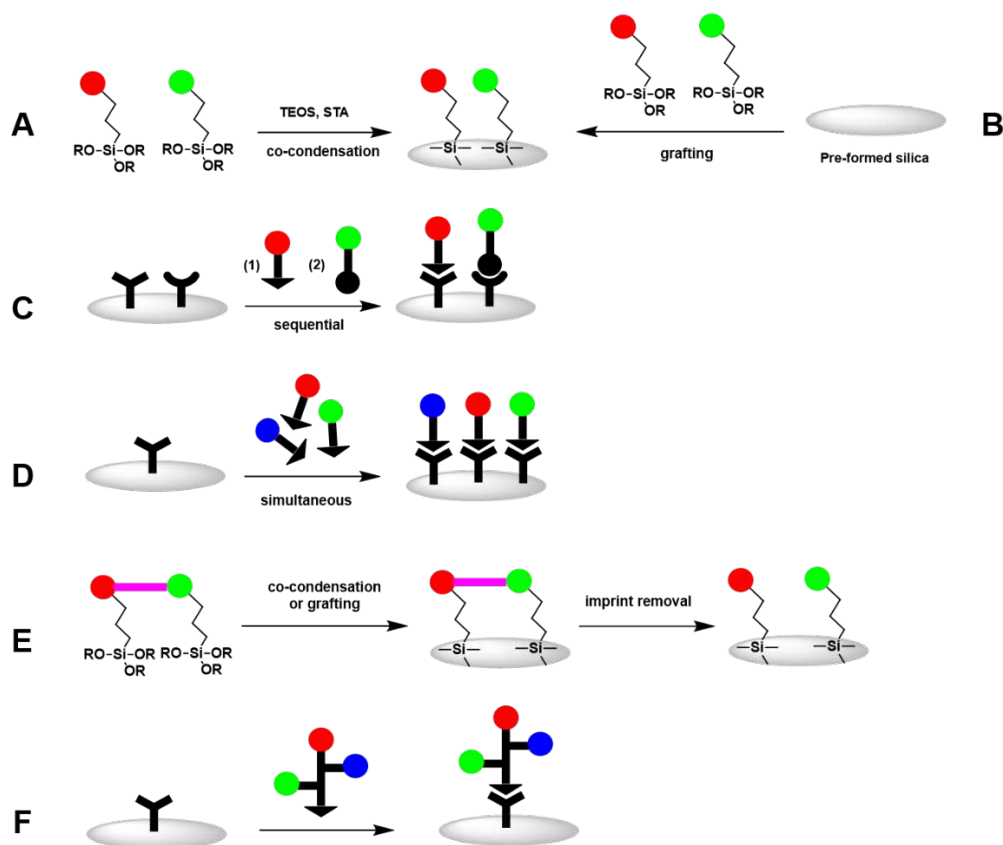


Figure 1. Approaches used for designing multifunctional silica-supported catalysts: (A) co-condensation, (B) grafting, (C) and (D) post-functionalization, (E) molecule imprinting, (F) single molecule (reproduced from ref. ⁴⁴).

Other oxides such as titanium dioxide, are not as representative as alumina and silica in supported catalysis and will therefore not be treated here.

I-1-3) Polymers

Polymers, as a type of organic supporting materials, have retained gigantic attention as well, since the development of their synthesis and characterization methods.⁴⁵⁻⁴⁶ With the involvement of organic synthesis, the operable space for designing supported catalyst systems has become more extensive and flexible than with inorganic materials. Not just compatible with heterogeneous systems, polymer supported catalysis was even utilized under homogeneous conditions,⁴⁷⁻⁴⁸ which demonstrates its uniqueness in this domain.

In contrast to biphasic reactions offered by insoluble inorganic supports, homogenization of supported catalysts may help addressing some deficiencies of heterogeneous systems, including reduced selectivity and reactivity when transferring

the catalysis from *homo-* to *hetero-* environment and some difficulties of characterizations (NMR, MS, TLC, etc.), resulting in the unawareness of catalyst's integrity after recycling experiments.⁴⁹ Furthermore, the easiness for chemical decorations endowed more flexibility when building catalytic systems. For example, PEG as a commercial polymer, possesses either one or two -CH₂OH end groups, which made it easy to prepare a variety of PEG supported ligands and catalysts. The solubility in a wide range of solvents, such as DMF, dichloromethane, toluene, CH₃CN, and water provided a homogeneous environment for the catalysis and a convenience for NMR spectroscopy analyzes, in the meantime, due to the poor solubility in other solvents including hexane, diethyl ether, *tert*-butylmethyl ether (TBME), isopropyl alcohol and cold ethanol, PEG-supported catalysts could be easily recycled through precipitation in these solvents.⁵⁰

It is obvious from this short overview that supports play a predominant role in heterogeneous catalysis. They can bring exclusive supporting catalytic effects such as: (i) dispersing the active phase in order to improve the density of active sites for the envisaged reaction, (ii) improving the stability of the catalysts in the active phase (iii) facilitating the transfer of reagents to the active sites and simplifying the separation procedure at the end of the reaction, (iv) reducing the problem of the formation of local hot spots in the catalyst in some exothermic reactions in order to maintain the selectivity and improve the safety of the operations.⁵¹

I-2) Macroscopically structured catalytic supports

Cellular solids such as cork, wood, sponge, coral, bread, or cake are omnipresent both in nature and human society. Engineered foams made from polymers, metals, ceramic and glasses present unique properties due to their structures comprising stiffness, strength, thermal conductivity and diffusivity, electrical resistivity and so forth, that can be changed by a factor of 1000 or more when compared to natural cellular solids.⁵² Gent and Thomas⁵³ in 1959 gave one of the first sound understanding of the mechanical properties of foamed elastic materials. More recently, a profound comprehension of mechanical, thermal and, in the case of metal foams, electrical properties was built and summarized in the books "Cellular Solids: Structure and Properties"⁵⁴ and "Metal Foams, a Design Guide"⁵⁵.

With the determiner “structured”, catalytic supports enter a more specific topology and morphology with specific benefits. For instance, continuous processes based on Structured Catalytic Supports (SCSs) present several advantages over batch processes due to the efficient mass transfers and low pressure-drop SCSs allow. In addition, SCSs generate an intimate mixing of reactants and allow an easiest separation of the catalyst from the reaction products compared to conventional solid catalysts such as powders or beads.⁵⁶

Solid foams belong to a kind of lattice structured materials that were studied long before attention focused on lattices of other types.⁵² Among the variety of structured catalytic supports, open cell foams are prime candidates. Of ceramic or metallic structure, these host architectures are ideal supports for catalytically active metal (nano)particles.⁵⁷⁻⁵⁹ Thus, efficient solid foam bed reactors have been described, mainly based on silicon carbide or alumina foams coated with a catalytic phase.⁶⁰ These supports have proven to be chemically robust for catalytic reactions under harsh conditions, and generally exhibited good longevity⁶¹ while improving the efficiency⁶² and the selectivity⁶³ of the catalyst compared with conventional supports. However, their expensive price and energy-intensive preparation processes⁶⁴ (**Figure 2**) are main drawbacks, especially given the current considerations of economics and ecology. In addition, these foams are heavy and difficult to handle, contain microcracks and other microstructural defects that considerably reduce their mechanical properties and make them easily breakable. Finally, the presence of closed cells, resulting from their preparation process from polyurethane foams (Fig. 3), renders the reproducibility of reactions uncertain.

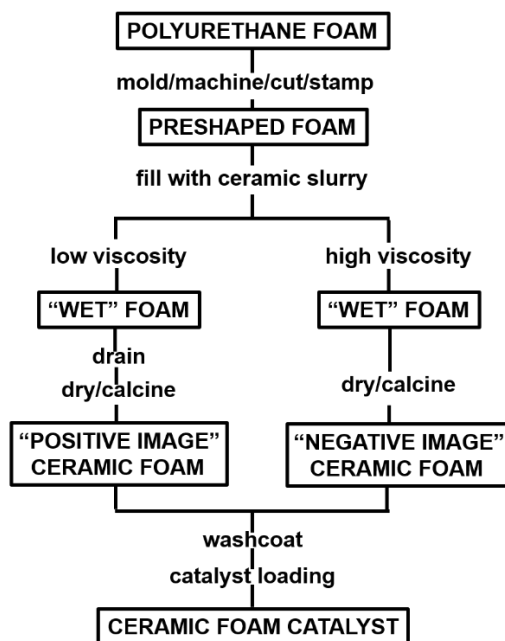


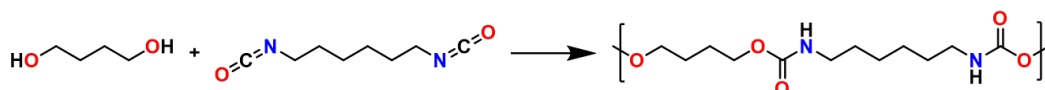
Figure 2. Preparation of ceramic foams (reproduced from ref. 58).

Flexible open cell polymeric foams with their elastomeric properties and readily available sourcing may represent a potential alternative to ceramic or metallic foams.⁶⁵ In particular, open cell polyurethane foams, which are available at low cost due their well-controlled fabrication processes and countless applications,⁶⁶ and which present similar morphological aspects and transport properties (Fig. 3)⁵⁰ seemed attractive. For these reasons, we selected them as a structured catalytic support to conduct our research in this thesis.

I-3) Polyurethane foams

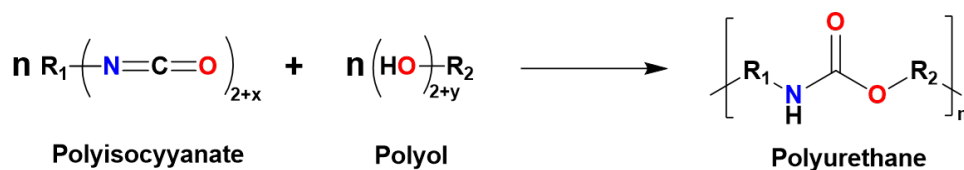
The first polyurethane (PU) was manufactured in **1937** by Otto Bayer at IG Farben in Germany by direct reaction of butanediol with hexamethylene diisocyanate under solvent free conditions (**Scheme 1**).⁶⁷ However, the marketing of PU foams only started in **1952**.⁶⁷ These new materials then rapidly attracted artists and designers who used them to create sculptures, paintings, furniture, textiles and fashion accessories.⁶⁷⁻

68



Scheme 1. Synthesis of first polyurethane by Otto Bayer.

Typically, polyurethanes are synthesized by polymerization reaction between an alcohol and an isocyanate. Alcohols should possess at least two hydroxyl groups per molecule (diols, triols, polyols) for the chain propagation and extension. A similar characteristic is also necessary for the isocyanate. More than one isocyanate group per molecule (diisocyanates, polyisocyanates) is compulsory (**Scheme 2**).



Scheme 2. General synthesis of a polyurethane by reaction of a polyol with a polyisocyanate.

The polyols most often used in the synthesis of polyurethanes are glycols such as polyethylene glycol, polypropylene glycol, and polytetrahydrofuran or polyesters such as poly(ethylene adipate) (**Figure 3A**). The most commonly used polyisocyanates in polyurethane synthesis are aromatic compounds such as 2,4-diisocyanato-1-methylbenzene (TDI), bis(4-isocyanatophenyl)methane (MDI) or aliphatic compounds such as 1,6-diisocyanatohexane (HDI) (**Figure 3B**).⁶⁷

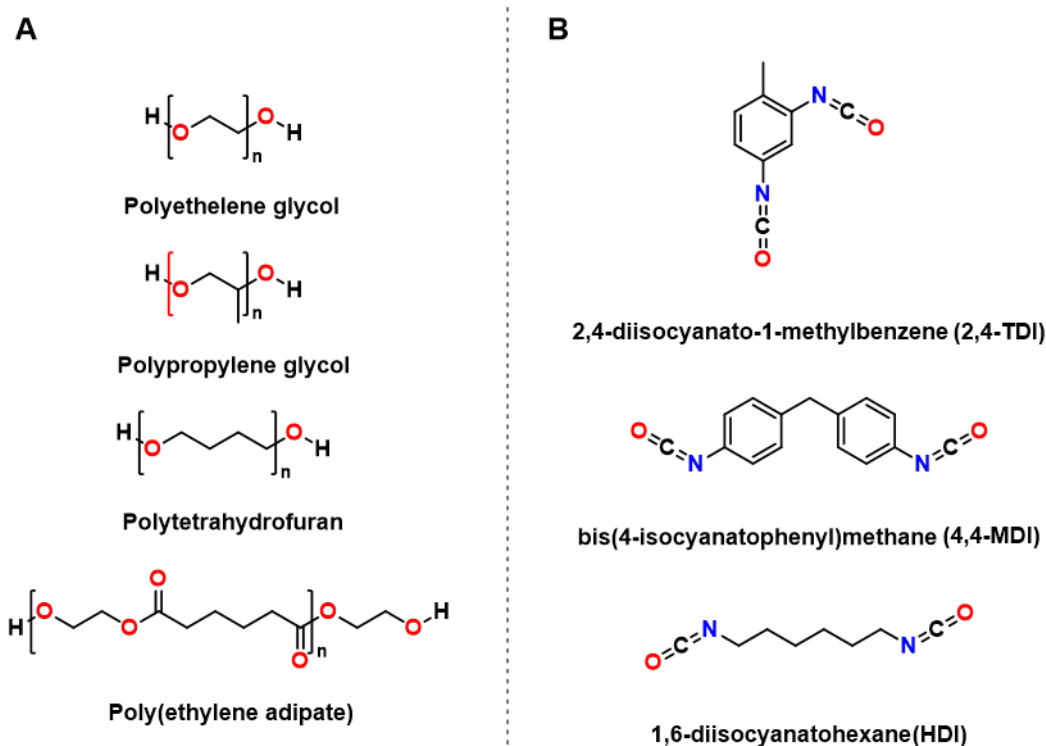


Figure 3. Most used polyols (A) and polyisocyanates (B) in the synthesis of polyurethane

The use of different types of polyol and/or isocyanate will change the properties of the resulting polyurethane. Regarding polyurethane foams, their nature can range from soft and flexible open cell foams to very dense and rigid closed cell foams, depending on the used precursors and on the vulcanization process.⁶⁹ These foams have a wide variety of applications involving their physical and mechanical properties.⁶⁸ When comprised of closed cells, polyurethane foams have excellent mechanical strength and thermal insulation properties, and are typically used for construction, sealing and insulation. In contrast, open cell polyurethane foams are generally used for the manufacture of cushions, mattresses or filters for kitchen hoods, aquariums or hoovers.⁵⁸ In addition, as noted earlier, since these latter foams serve as templates for the manufacture of open cell ceramic and metal foams, they share the same morphological and transport properties.

I-4) Properties of open cell polyurethane foams

Open cell polyurethane foams (PUF) (**Figure 4**) present numerous advantages over traditional catalytic supports. They have a high surface/volume ratio and allow a low pressure drop, even at a high flow rate.^{12,24} They provide effective mass transfers

as well as an intimate mix of the reactants⁷⁰⁻⁷¹ and allow an easy separation of products. In addition, they are commercially available at low cost, non-toxic (polyurethane is used as a biomaterial⁷²), mechanically resistant, elastic and light.^{68, 73} These latter properties make open cell polyurethane foams even advantageous over ceramic and metallic foams, as they can be readily adapted to any types of reactor and used for designing new reactors.



Figure 4. Commercially available open cell polyurethane foams (PUF).

Despite these brilliant properties, the use of PUF as a catalytic support is hampered by its smooth surface. The edges and bridges lack microporosity and thus do not present sufficient adherence to deposit a catalytic phase. Furthermore, traditional coating techniques (washcoat) are incompatible with their limited heat tolerance (max. 80-100 °C). Therefore, finding an efficient, environmentally friendly and industrially applicable method to immobilize catalysts onto the surface of PUF is a true challenge.

In the last five years, several different approaches were reported for the immobilization of a catalytic phase on the surface of polyurethane foams for various applications, including wastewater treatment,⁷⁴ reduction of toxic organic compounds,⁷⁵⁻⁷⁶ aqueous cyanation of aryl halides,⁷⁷ oil/water separation,⁷⁸ and Suzuki coupling reactions.⁷⁹ Although these examples illustrate the versatility of open cell polyurethane foams as SCS, the used immobilization methods were basically all single-purpose-oriented, and a general method is required. Hereafter, we will describe the efforts of the teams of V. Ritleng, D. Edouard, L. Jierry and others towards the

development of a versatile polydopamine coating that proved compatible with several subsequent functionalizations to accomplish a broad spectrum of applications.

I-5) Polydopamine and marine organisms

Marine organisms, in order to attach themselves to submarine surfaces, have developed special mechanisms which purpose is to avert movements by currents and tides so that they can perform normal life functions such as feeding and reproduction. The principles of adhesion for marine worms,⁸⁰ barnacles⁸¹ and mussels⁸²⁻⁸⁵ are all based on glue-like proteins secretion. Numerous studies have shown that mussels can attach to rocks and almost all submarine surfaces.^{80, 85} In particular, a detailed study of the mussel foot protein (mefp-5) revealed the presence of dopamine-like structures (**Figure 5**). It was therefore suggested that polydopamine plays a key role in this adhesion process, which was confirmed experimentally by the work of Messersmith's group.⁸⁶⁻⁸⁷ This seminal work opened a new era for the development of synthetic adhesives and coatings in aqueous media.^{80-85, 87}

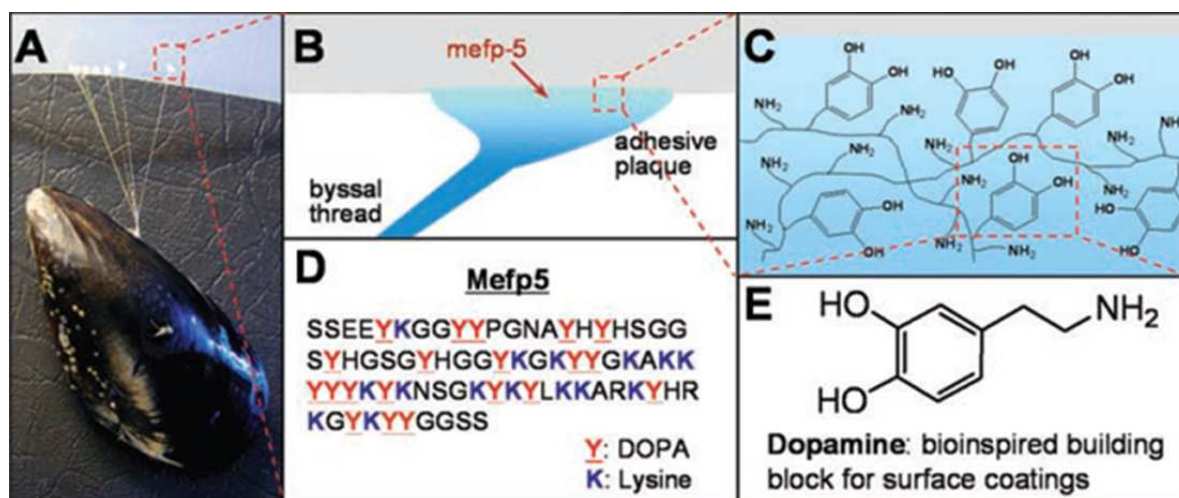


Figure 5. (A) Photograph of a mussel attached to commercial PTFE (B and C) Schematic illustrations of the interfacial location of Mefp-5 and a simplified molecular representation of characteristic amine and catechol groups (D) The amino acid sequence of Mefp-5 (E) Dopamine contains both amine and catechol functional groups found in Mefp-5 and was used as a molecular building block for polymer coatings (reproduced from ref. 86).

I-6) Origin of the adhesive properties of polydopamine and mechanism of formation

The presence of catechol groups in the structure of the mussel foot and other marine animals' adhesive proteins explains in great part their amazing adhesion capability. Catechols are indeed able to interact effectively with nearly all type of surfaces by forming coordination bonds or covalent bonds or weaker interactions such as hydrogen bonds, Van Der Waals interactions and π - π stacking (**Figure 6**).⁸⁸ The combination of all these interactions contribute to the macro adhesive phenomenon observed with mussels and other marine animals.

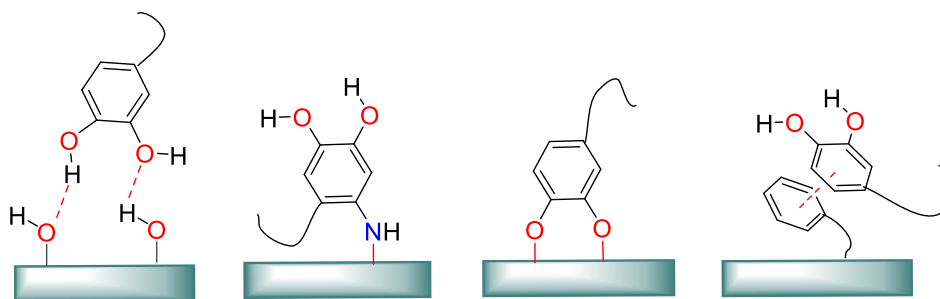


Figure 6. Schematic representation of the four main catechol-surface interactions.

Catechols thus provide a simple and effective mean for functionalizing surfaces, and many natural phenols and polyphenols (**Figure 7**) comprising a high content of dihydroxyphenyl (catechol) and trihydroxyphenyl (gallic acid, GA) moieties are appropriate candidates as coating agents.⁸⁶⁻⁸⁷ Furthermore, these natural compounds have many applications including UV absorption, radical scavenging and metal ion complexation.⁸⁹

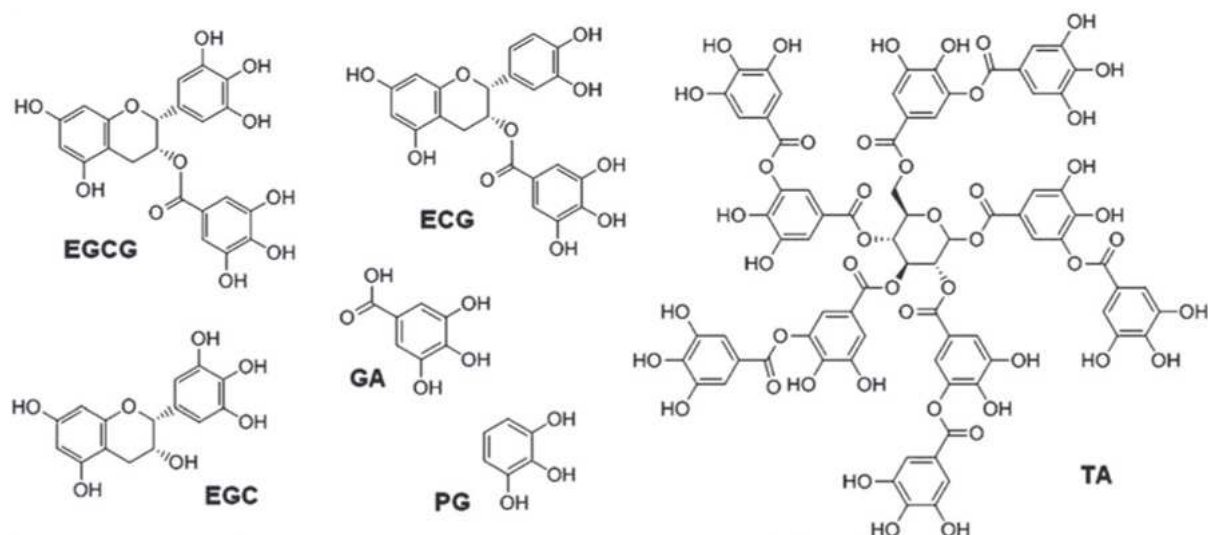


Figure 7. Examples of phenols and polyphenols used as coating agents (reproduced from ref. 89).

However, when comparing the adhesion properties of these polyphenols with those of polydopamine (PDA) generated by self-polymerization of dopamine in the presence of an oxidant under slightly basic conditions ($\text{pH} = 8.5$), PDA as a coating agent still prevails in this field. The amine moieties indeed provide extra binding force that is beneficial for adhesion. Although there is no consensus regarding the precise PDA structure, it is commonly accepted that it is composed of 5,6-dihydroxyindoles and quinhydrones (resulting from the oxidation of the catechol functions) covalently linked together in eumelanin-like oligo-indoles and/or catechol/amine/quinone/indole-type heteropolymers. (**Figure 8**), whose exact composition connectivity and chain lengths depend on the preparation conditions.⁹⁰⁻⁹¹ Furthermore, it is noteworthy that the catechol/*o*-quinone redox couple provides moderately reductive properties to PDA (redox potential +0.53 V vs. NHE at $\text{pH} 7$).⁹⁰⁻⁹²

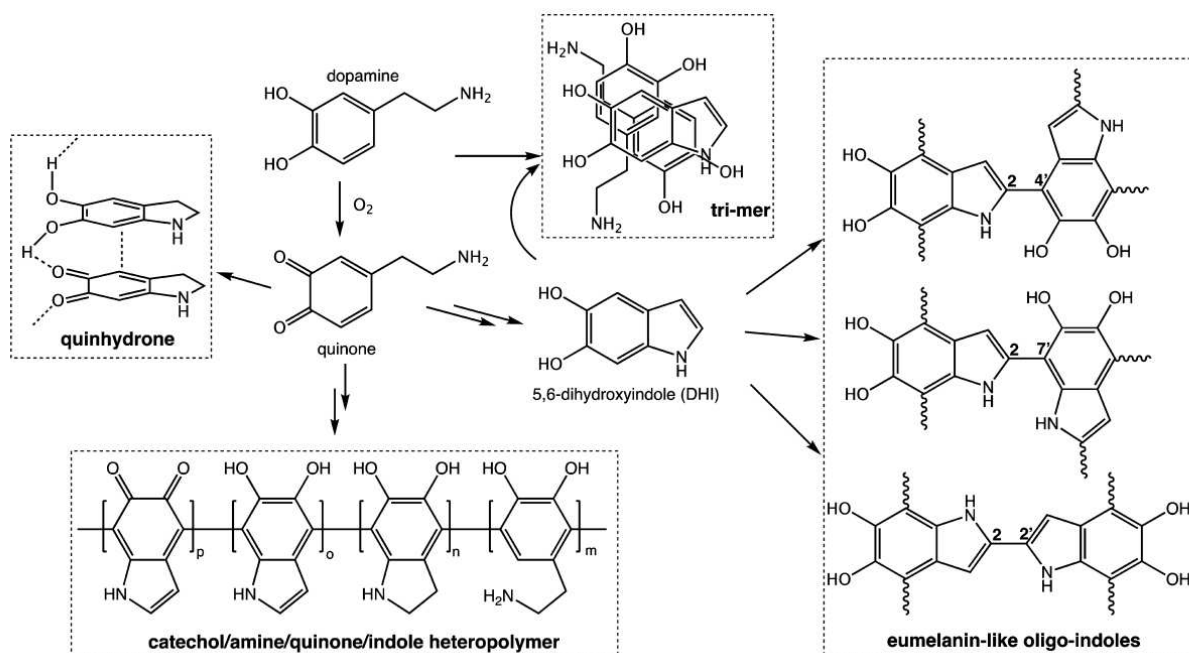


Figure 8. Current theories of polydopamine structure and formation (reproduced from ref. 93).

I-7) PDA as catalyst and catalytic support

As a result of the versatility of its functional groups and of the possibility to undergo hydrogen bonding, imine–enamine or catechol–quinone transformations as well as electron transfer processes, PDA has become a fascinating organocatalyst.⁹⁴⁻⁹⁶ Thus, PDA was used in reactions as varied as aldolizations between benzaldehydes and cyclohexanone,⁸⁸ thiol couplings,⁹⁷ synthesis of nitrogen heterocycles like benzimidazoles,⁹⁸ or electroreduction of CO₂.⁹⁹ Noteworthy, the Liebscher group notably proved that PDA acted as a bi-functional catalyst rather than as an innocent polymer in their reported aldolizations between benzaldehydes and cyclohexanone.⁸⁸

Besides these applications as an organocatalyst, PDA has gained numerous interests as a support matrix in different domains. For instance, PDA can immobilize enzymes and these enzyme-PDA systems can provide better activity and easier recovering and recycling abilities, thus increasing the overall enzyme performance.¹⁰⁰ Noteworthy, despite the strong interaction between the enzymes and the numerous functional groups of PDA, the conformation of enzymes were

not affected. When it comes to environmental pollution, PDA-based materials functionalized with Ag or TiO₂ were utilized for the reduction of toxic substrates such as nitroarenes¹⁰¹⁻¹⁰³ and dyes.¹⁰⁴⁻¹⁰⁷ Interestingly, these PDA-modified TiO₂ or Ag catalysts demonstrated better performances than the pure metal catalysts, highlighting the benefic synergetic effect between the reducing properties of PDA and those of the immobilized metals. Regarding organic synthesis, a wide range of organic reactions including coupling reactions,¹⁰⁸⁻¹¹⁰ oxidation of benzylic carbon,¹¹¹ acetylations,¹¹² cyanation of aryl bromides¹¹³ were reported with Pd-, Au- or organocatalyst-functionalized PDA, and catalytic studies generally demonstrated both excellent stability and recyclability of these PDA-supported systems.

Overall, PDA as an organocatalyst or supporting material has already been proven to be more than promising in the field of catalysis, but its fascinating chemistry for sure will inspire further research and show allow exploring uncharted territories.

I-8) Coating of open cell polyurethane foams (PUF) by PDA

In 2015, Lee *et al.* utilized chromic oxide and sulfuric acid solution to pre-treat a polyurethane (PU) sponge before PDA coating. SEM images of the PU sponge showed the transformation of the smooth and flat surface of the pristine sponge to a rough surface after acid treatment. The acid-etched surface was then coated with a polydopamine layer by treatment with a dopamine solution in the presence of TRIS (pH = 8.5, 10 mM). The resulting foam was washed with deionised water and dried at 60 °C for 6 h (**Figure 9**). Strikingly, the SEM images did not reveal any significant change in surface roughness after coating.¹¹⁴ Therefore, the surface modification of the sponges was confirmed by measuring the contact angle (CA). The excellent water adsorption capacity of thus modified PU sponge was explained by a CA of 0° vs. 110° for the pristine sponge and 65° for the etched sponge.

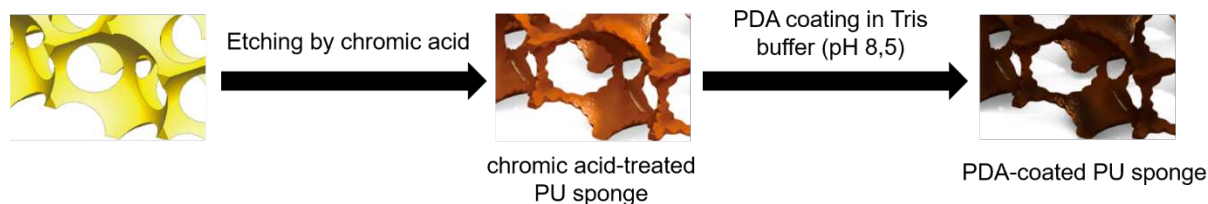


Figure 9. PU Sponge surface modification using chromic acid and PDA (reproduced in part from reference 114).

At the same period, D. Edouard, L. Jierry, V. Rittleng *et al.* reported that PUF foams could be coated by a thin layer of PDA by simple immersion in a solution of dopamine (2 mg/mL) and TRIS (pH = 8.5, 10 mM) at room temperature for 16 h without acid pretreatment.¹¹⁵⁻¹¹⁹ Despite the absence of microporosity at the PUF surface, the successful coating of the entire 3D polymeric material's surface was evidenced by a colour change from light yellow to black (**Figure 10**). The successful coating was further evidenced by low and high magnification SEM images. High magnification images notably revealed the presence of a rough film with randomly dispersed aggregates, as had been previously observed on flat surfaces coated with PDA.

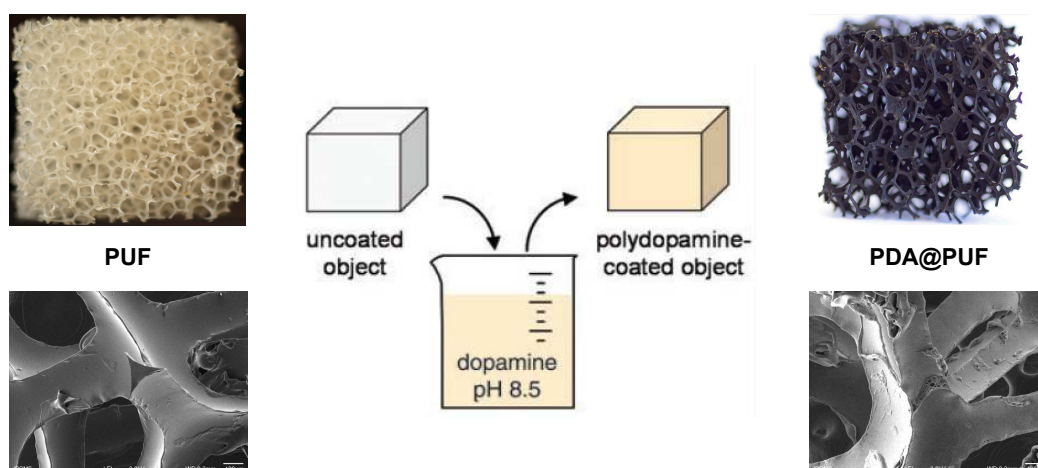


Figure 10. PUF coating of PDA.¹¹⁶

Noteworthy, PUF and PDA@PUF foams were subjected to compression tests to evaluate the influence of the PDA coating on the mechanical properties of pristine PUF. The recorded stress-strain responses (characterized by a typical hysteresis loop⁷³)

showed that the PDA coating does not alter the elastic properties of PUF.¹¹⁶ The thus prepared PDA@PUF catalytic support were then further functionalized with molecular catalysts, metal or metal oxide (nano)particles and metal-organic frameworks by the same authors and others.

I-9) Functionalization of PDA@PUF for catalytic and adsorption applications

I-9-1) Covalent functionalization of PDA@PUF

Messersmith, in its seminal work, and others after, have shown that the catechol and indole moieties present in the PDA structure could react with nucleophiles such as amines or thiols through Michael additions. Catechols can also form Schiff bases by reaction with amines (**Figure 11**).^{86, 90, 120-121}

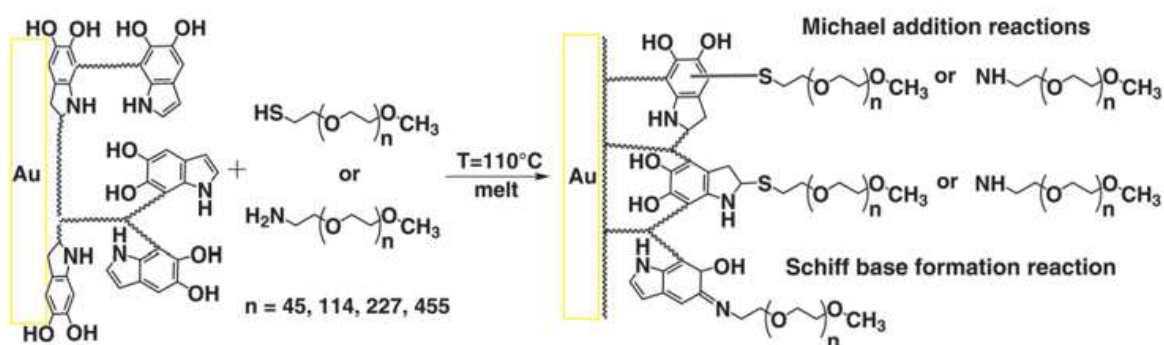


Figure 11. Binding of poly(ethylene oxide) chains to PDA-coated Au substrates by Michael additions and Schiff base formation reactions (reproduced from ref. 90).

To illustrate the possibility of covalently functionalizing a PDA-coated foam with an amine, D. Edouard, L. Jierry, V. Ritleng *et al.* treated a PDA@PUF foam with 5-aminofluorescein (0.5 mg/mL) in an aqueous solution of TRIS (10 mM, pH = 8.5) at 60 °C for 3 h to form Fluo@PDA@PUF (**Figure 12**).¹¹⁵ Successful functionalization all over the surface of the 3D material was demonstrated by confocal fluorescence microscopy.

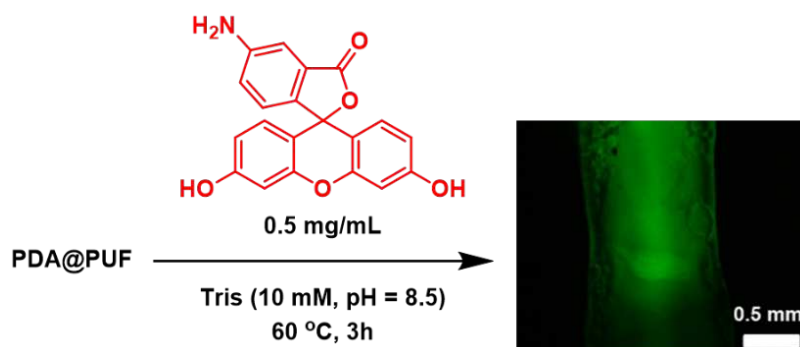


Figure 12. Covalent functionalization of PDA@PUF by Michael addition and/or Schiff base formation reaction with 5-aminofluorescein.¹¹⁵

More recently, the same group covalently anchored both organo- and organometallic catalysts bearing alkoxyethyl arms on the surface of PDA@PUF by an unprecedented silanization process in toluene at 70 °C involving the catechol groups of the mussel-inspired layer (**Figure 13**).¹¹⁸ The thus obtained catalysts, DMAP-TES@PDA@PUF and Ni(NHC)-TES@PDA@PUF, were used as recyclable catalysts for alcohol acylation and aldehyde hydrosilylation, respectively (**Figure 14**). The DMAP-TES@PDA@PUF material in particular could be used for 10 consecutive runs of alcohol acylation without notable activity loss. Remarkably, no leaching was observed nor alteration of the mechanical properties of the flexible support. This approach gives access to highly desirable PDA@PUF-supported single-site heterogeneous catalysts and opens the gate to the use of the large panel of catalysts reported for homogeneous catalysis.

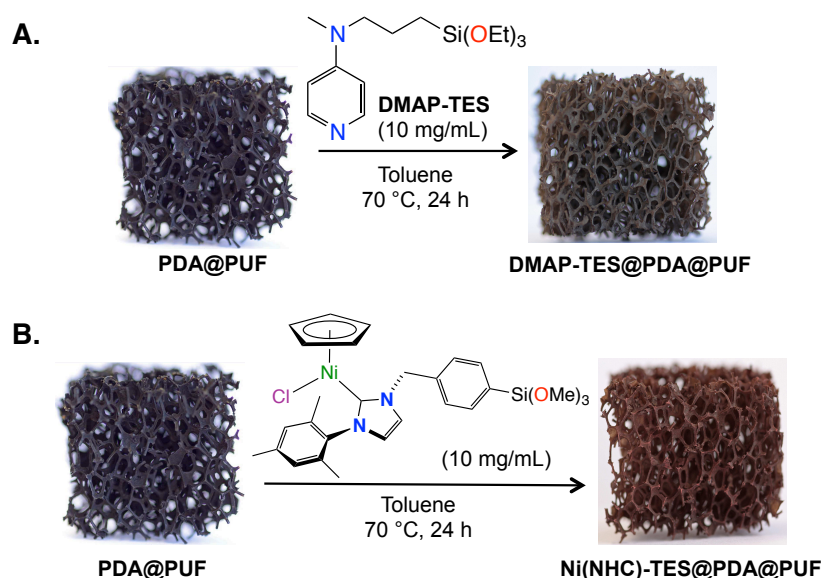


Figure 13. Covalent functionalization of PDA@PUF with DMAP-TES (A) and Ni(NHC)-TES (B) (reproduced from ref. 118)

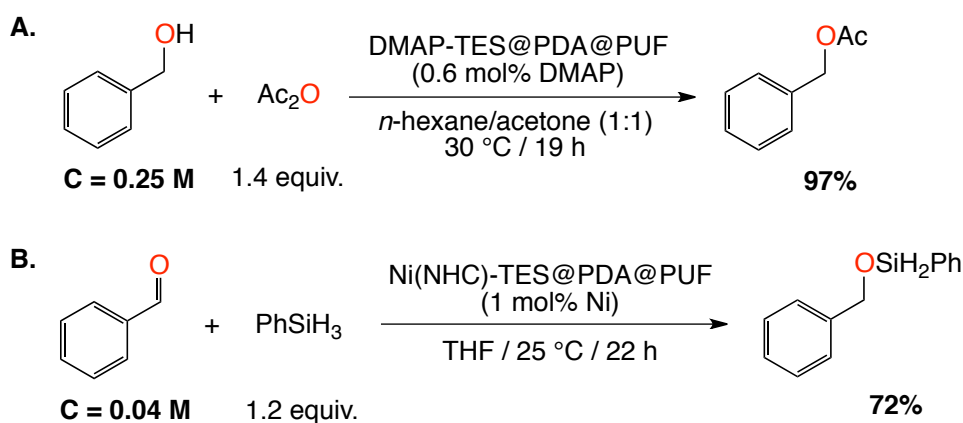


Figure 14. Acylation of benzyl alcohol catalyzed by DMAP-TES@PDA@PUF (A) and hydrosilylation of benzaldehyde catalyzed by Ni(NHC)-TES@PDA@PUF (B).¹¹⁸

I-9-2) Functionalization of PDA@PUF with sodium borohydride

In 2017, PDA@PUF was shown to be an efficient SCS for the removal of methylene blue (MB)¹²² from aqueous solutions in the presence of sodium borohydride. Thus, in the presence of NaBH₄ (0.1 M) at room temperature, complete reduction of MB (0.02 mM in water) to colorless leucomethylene was observed within 25 min after simple immersion of a cubic sample (8 cm³) of PDA@PUF in to the reaction medium (**Figure 15**), and the foam could be used at least 5 times with an almost constant activity.¹¹⁷

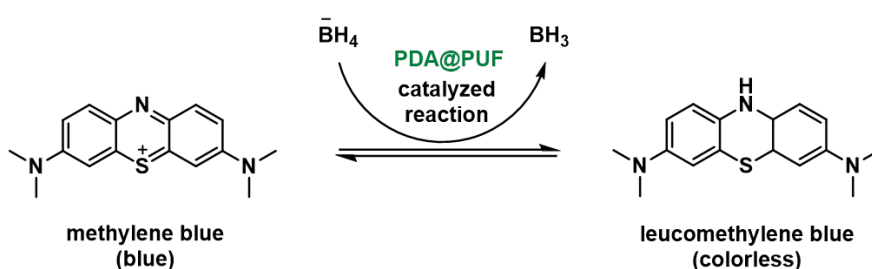


Figure 15. PDA@PUF-catalyzed reduction of MB by NaBH₄.¹¹⁷

Though the role of PDA was supposed to be that of an electron-relay (or redox mediator) between the borohydride and the electron-acceptor dye, the molecular mechanism of this PDA@PUF-catalyzed reduction could not be clearly established.¹¹⁷ Nevertheless, the authors suspected that catechol groups of the PDA layer could

complex the borohydride anions. This assumed behavior was used to prepare $\text{NaBH}_4@\text{PDA}@PUF$ materials by simply immersing $\text{PDA}@PUF$ in an aqueous NaBH_4 solution (0.1 M) for 10 min (**Figure 16**).¹¹⁹

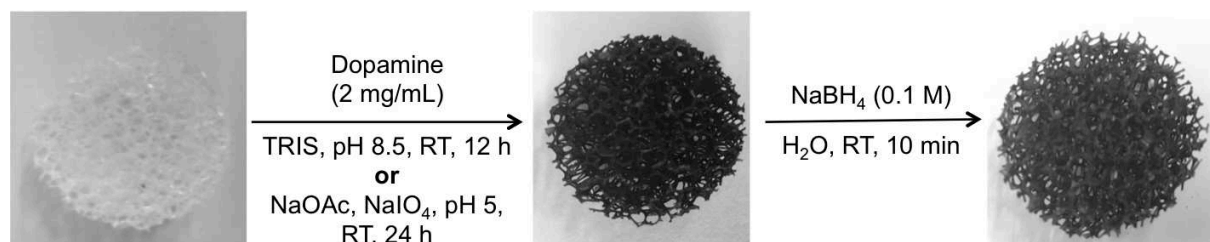


Figure 16. Two-step preparation of $\text{NaBH}_4@\text{PDA}@PUF$ from PUF (reproduced from ref. 119).

Interestingly, cyclic voltammetry measurements tended to confirm the probable complexation of the borohydride ions by the catechol groups of the PDA layer, as a shift of the dopamine oxidation peak by 0.4 V towards the anodic potentials was observed in the presence of NaBH_4 (50 mM in a 10.6 mM aqueous solution of dopamine). Furthermore, the thus obtained $\text{NaBH}_4@\text{PDA}@PUF$ materials proved able to reduce MB (0.02 mM in water) at room temperature in the absence of additional NaBH_4 , and the foam could be used 3 times without noticeable loss of its reducing properties.^{119, 123} In addition, the amount of released boron sub-products is much lower compared to processes using dissolved NaBH_4 , which considerably reduces the environmental impact of this $\text{NaBH}_4@\text{PDA}@PUF$ -based process on the treated wastewater compared to the latter. Finally, $\text{NaBH}_4@\text{PDA}@PUF$ could also reduce benzaldehyde to benzyl alcohol at room temperature (**Figure 17**), which demonstrates the versatility of this material for various reduction reactions.¹¹⁹

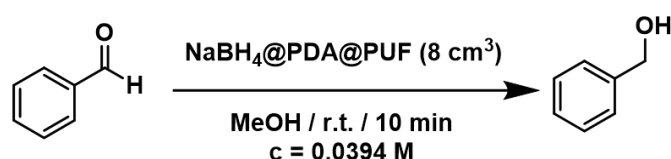


Figure 17. Reduction of benzaldehyde by $\text{NaBH}_4@\text{PDA}@PUF$.

I-9-3) Functionalization of $\text{PUF}@PDA$ with metal (nano)particles

The ability of PDA to reduce metallic cations such as Ag^+ is well documented.¹²⁴ This property has been used to functionalize $\text{PDA}@PUF$ foams with $\text{Ag}(0)$ particles by simply immersing the latter in an aqueous solution of AgNO_3 (50 mM) at room

temperature for 24 h (**Figure 18**).¹¹⁷ The presence of immobilized Ag(0) particles on the surface of the foams was established by scanning electron micrographs combined to energy dispersive X-ray spectroscopy.

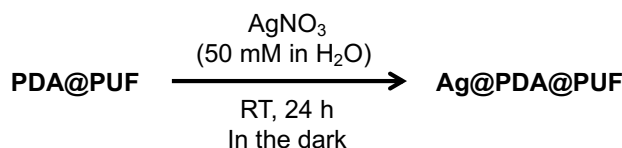


Figure 18. Functionalization of PDA@PUF by *in situ* produced Ag(0) particles.

The catalytic activity of Ag@PDA@PUF was evaluated for the reduction of MB (0.02 mM in water) under conditions similar to those employed with PDA@PUF not pre-functionalised with NaBH₄, *i.e.* in the presence of 0.1 M NaBH₄.¹¹⁷ The Ag particles were found to have a beneficial effect, both on the durability of the SCS, as the foams could be efficiently used for six consecutive runs instead of three without Ag(0) NPs (*vide supra*), and on the reaction kinetics, as the reaction was significantly faster during the first three runs, before showing a comparable activity in the next three runs, which suggested a deactivation of the Ag NPs at this stage.¹¹⁷

PDA@PUF foams were also functionalized with Ru(0) NPs. To achieve that, a PDA@PUF foam was immersed for 24 h at room temperature in a well-stirred suspension of ruthenium NPs in an aqueous medium, previously prepared by reducing RuCl₃·xH₂O with NaBH₄ (**Figure 19**).¹¹⁵

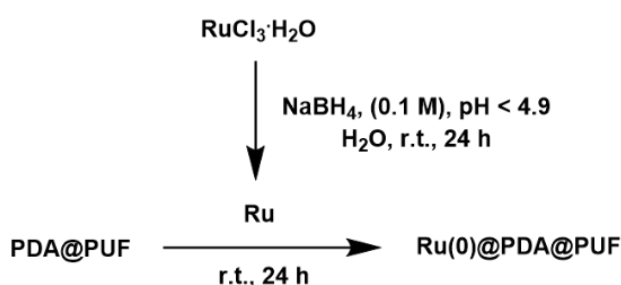


Figure 19. Functionalization of PDA@PUF with Ru(0) NPs.

These Ru(0)@PDA@PUF foams were not characterized, but their catalytic activity was evaluated for the selective hydrogenation of styrene to ethylbenzene under H₂ (60

mL/min) in EtOH at 70 °C: 7% conversion to the desired product was observed after 22 h reaction (**Figure 20**).¹¹⁵

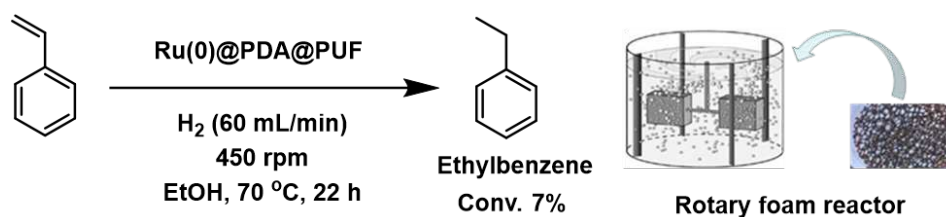


Figure 20. Selective hydrogenation of styrene to ethylbenzene catalyzed by Ru(0)@PDA@PUF.

I-9-4) Functionalization of PDA@PUF with metal oxide nanoparticles

D. Edouard, L. Jierry, V. Ritleng *et al.* also reported the functionalization of PDA@PUF with TiO₂ by simple immersion of a PDA@PUF foam in a well-dispersed suspension of TiO₂ nanoparticles (NPs) in an aqueous medium buffered at a pH of 8.5 for 12 h at 40 °C (**Figure 21**).¹¹⁶ The presence of titanium on the functionalized foam, TiO₂@PDA@PUF, was confirmed by XPS. Elemental mapping by energy dispersive X-ray spectroscopy (EDX) coupled with scanning electron microscopy (SEM) revealed the presence of TiO₂ NPs as micrometric clusters randomly dispersed over the entire surface of the 3D material. An average Ti content of 607 ± 80 mg/kg was determined by ICP-AES. As for the covalently functionalized PDA@PUF catalysts (*vide supra*), compression tests run with PUF, PDA@PUF and TiO₂@PDA@PUF demonstrated that neither the PDA coating nor the functionalization with TiO₂ NPs affected the elastic properties of PUF.

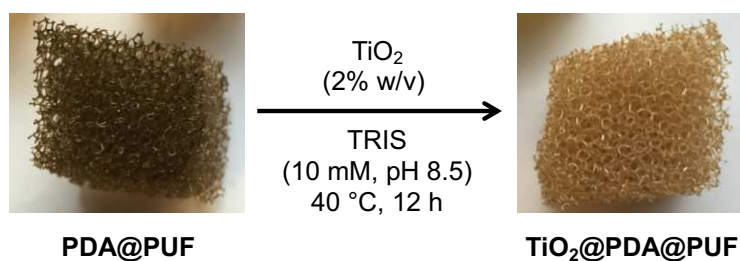


Figure 21. Functionalization of PDA@PUF with TiO₂ nanoparticles.

TiO₂@PDA@PUF was then used for the photodegradation of the harmful dye, acid orange 7 (AO7). For that purpose, the foam was immersed in a 0.028 mM solution of AO7 at room temperature without stirring, and irradiated under UV light (125 W). The photodegradation of AO7 was then monitored by UV-visible spectrometry. Complete degradation of AO7 was observed after 200 min reaction, and the catalyst could be reused at least 5 times without appreciable loss of activity. No titanium leaching was observed by ICP-AES analysis of the solutions (**Figure 22**).¹¹⁶ Noteworthy, an artificially aged TiO₂@PDA@PUF foam - by 5000 compressions to a strain of 25% and 2 compressions to a strain of 75% - showed a remarkably similar activity, and could also be used during 5 catalytic runs with an almost constant activity, thus demonstrating the very high mechanical resistance of these catalytic foams.

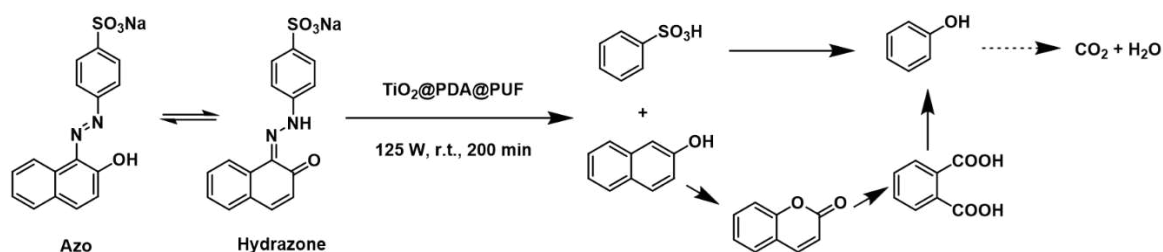


Figure 22. Photocatalysis of AO7 catalyzed by TiO₂@PDA@PUF.

I-9-5) Functionalization of PDA@PUF with carbon materials

PDA@PUF foams were functionalized with activated charcoal (AC) and carbon nanotubes (CNT) in order to combine the advantageous characteristics of PUF foams (high surface-to-volume ratio, low pressure drop and good transport properties) with the high adsorption capacity of these carbon materials,¹²⁵⁻¹²⁸ in order to obtain adsorbents that are more performant and convenient to use than powder-based materials. To obtain the functionalized foams with the highest possible loading of carbon material, PUF foams were immersed twice in aqueous suspensions of the desired carbon materials at room temperature for 24 h: first in an aqueous solution of dopamine (2 mg/mL) buffered at pH 8.5 with 2 g AC or CNT, then in another solution buffered at pH 8.5 with 2 g AC or CNT (**Figure 23**).¹²⁸ Noteworthy, the carbon materials were pretreated with nitric acid (65 %) at 120 °C for 8 h to ensure a better grip on the

PDA's surface. Successful deposition of the carbon materials on the surface of PDA@PUF was demonstrated by TGA measurements and SEM images.



Figure 23. Functionalization of PDA@PUF by AC and CNT.

The activity of the thus obtained adsorbent materials was evaluated for MB adsorption. For this purpose, a cubic sample (8 cm³) of AC@PDA@PUF or CNT@PDA@PUF was simply immersed in a well stirred (700 rpm) solution of MB (50 mL, 0.02 M) at room temperature, and the adsorption of MB was monitored by UV-visible spectrometry. With AC@PDA@PUF, 99% MB was removed after 25 min in the first run. The amount of absorbed MB then gradually decreased from 95% in the second run to 50% in the sixth run. This progressive decrease of the adsorption capacity of AC@PDA@PUF is due to the well-known saturation of the activated charcoal.¹²⁹ In the case of CNT@PDA@PUF, the adsorption performances were much lower than those observed with AC@PDA@PUF. Hence, only 56% MB adsorption was observed after 25 min in the first run, and this decreased much more rapidly to only 8% MB adsorption in sixth run.¹²⁸ The adsorption capacity of AC@PDA@PUF was calculated to be of 245 mg MB / g AC, which is a little lower to what was established for unsupported AC (400 mg/g) but can be easily explained by the fact that the available specific supported area for MB adsorption is lower in the case of the supported AC than in the case of the unsupported AC. Nevertheless, these results established a practical way of exploiting the absorption properties of AC without the usual drawbacks encountered with carbon powders, such as difficult filtration.

I-9-6) Functionalization of PDA@PUF with metal-organic frameworks

In 2018, Yan *et al.*¹³⁰ reported UiO-66-type metal-organic frameworks (MOFs) supported on PDA@PUF membranes: UiO-66-SO₃H-NH₂/PDA@PUF and UiO-66-SO₃H/PDA@PUF. Noteworthy, the acid-base bifunctional UiO-66-type MOFs were prepared directly on PDA@PUF via an *in situ* MHT method (**Figure 24**). The acidity

and basicity of the obtained composites could be easily adjusted by varying the ratio of the organic linkers, monosodium 2-sulfoterephthalate and 2-aminoterephthalic acid. The synthesized materials were thoroughly characterized by SEM, EDS mapping, XRD, BET, FT-IR, XPS and TPD, and their catalytic performances were evaluated in one-pot glucose conversion to 5-hydroxymethylfurfural. High activity under optimized conditions and good stability over 5 runs were observed with UiO-66-SO₃H-NH₂/PDA@PUF having the optimal acid-base site ratio.



Figure 24. Preparation of acid-base bi-functional metal-organic frameworks membranes supported on PDA@PUF and their catalytic application (reproduced from ref. 130).

In 2019, Gong *et al.*¹³¹ introduced a UiO-66-NH₂/graphene oxide (UNG) composite which was loaded on PDA@PUF membranes by simple dip-coating (**Figure 25**). The resulting composite membrane, UNG@PDA@PUF, showed great potential for the practical treatment of differently charged mixed dyes wastewater. Noteworthy, the removal efficiency of MB by UNG@PDA@PUF increased when increasing the pH, whereas the removal efficiency of Congo red (CR) decreased when increasing the pH and that of rhodamine blue (RB) was less affected by the pH of the medium. In filtration experiments with coexisting salt ions, monovalent cations (Na⁺, K⁺) had almost no effect on the removal efficiency of MB, while the divalent cation Ca²⁺ had a slightly negative effect and the divalent anion (SO₄²⁻) promoted the removal efficiency of MB. In the filtration experiments of mixed dyes, UNG@PDA@PUF could simultaneously remove two or three dyes from binary or ternary dyes systems by two-times filtrations.

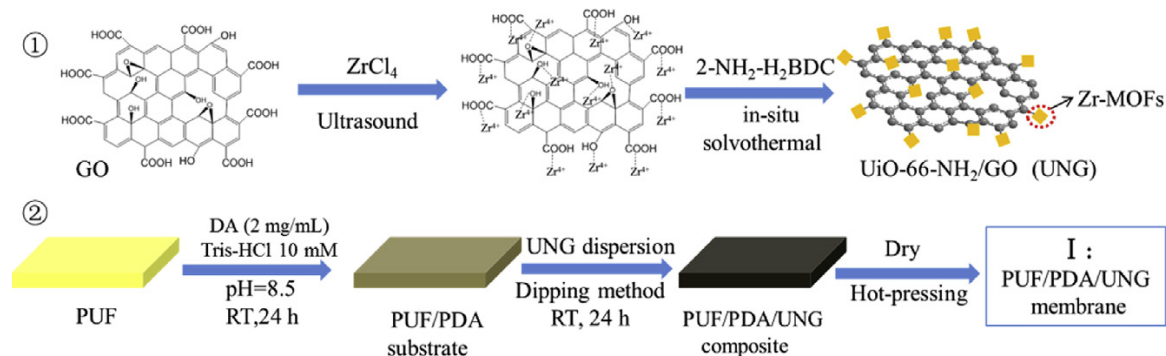


Figure 25. Preparation of the composite membranes (reproduced from ref. 131).

II) Conclusion

The PUF foams were coated with a thin layer of PDA - inspired by the mussel adhesion principle - and were used as a structured support to robustly graft organic or organometallic molecules, an inorganic reductant, metal and metal oxide (nano)particles, carbonaceous materials, and metal organic frameworks for various catalytic and adsorption applications. Based on these seminal works, this thesis aims to covalently anchor organometallic or organic photocatalysts on PDA@PUF to develop easily reusable photocatalysts, as well as to support Pd NPs for various Pd-catalyzed reactions of interest (**Figure 26**).

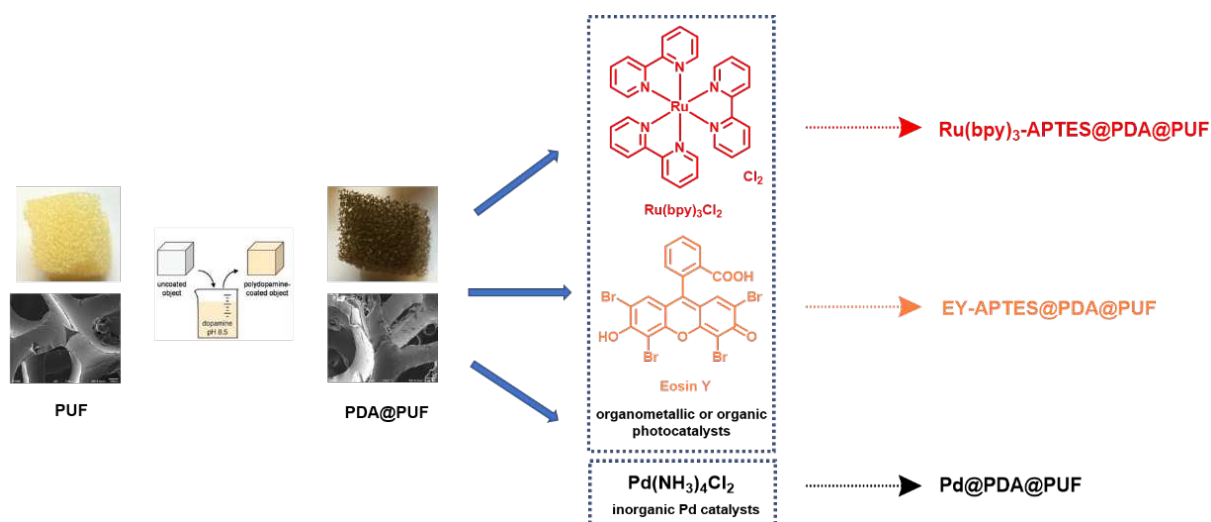


Figure 26. Envisaged PDA@PUF functionalizations.

References

1. Laidler, K. J., A glossary of terms used in chemical kinetics, including reaction dynamics (IUPAC Recommendations 1996). **1996**, 68 (1), 149-192.
2. Bertini, I., *Inorganic and Bio-Inorganic Chemistry - Volume II*. EOLSS Publishers Company Limited: 2009.
3. Kakaei, K.; Esrafil, M. D.; Ehsani, A., Chapter 1 - Introduction to Catalysis. Interface Science and Technology, Kakaei, K.; Esrafil, M. D.; Ehsani, A., Eds. Elsevier: 2019; Vol. 27, pp 1-21.
4. Qing, M.; Su, S.; Wang, L.; Liu, L.; Xu, K.; He, L.; Jun, X.; Hu, S.; Wang, Y.; Xiang, J., Getting insight into the oxidation of SO₂ to SO₃ over V₂O₅-WO₃/TiO₂ catalysts: Reaction mechanism and effects of NO and NH₃. *Chem. Eng. J.* **2019**, 361, 1215-1224.
5. Schlögl, R., Heterogeneous Catalysis. *Angew. Chem. Int. Ed.* **2015**, 54 (11), 3465-3520.
6. Mizuno, N.; Misono, M., Heterogeneous Catalysis. *Chem. Rev.* **1998**, 98 (1), 199-218.
7. Ertl, G.; Knözinger, H.; Weitkamp, J., *Handbook of heterogeneous catalysis*. VCH Weinheim: 1997; Vol. 2.
8. Burwell, R. L., *Pure Appl. Chem.* **1976**, 46 (1), 71-90.
9. Chapter 9. Preparation of catalyst supports, zeolites and mesoporous materials. Studies in Surface Science and Catalysis, van Santen, R. A.; van Leeuwen, P. W. N. M.; Moulijn, J. A.; Averill, B. A., Eds. Elsevier: 1999; Vol. 123, pp 433-457.
10. Chapter 10. Preparation of supported catalysts. Studies in Surface Science and Catalysis, van Santen, R. A.; van Leeuwen, P. W. N. M.; Moulijn, J. A.; Averill, B. A., Eds. Elsevier: 1999; Vol. 123, pp 459-485.
11. Alemán, J. V.; Chadwick, A. V.; He, J.; Hess, M.; Horie, K.; Jones, R. G.; Kratochvíl, P.; Meisel, I.; Mita, I.; Moad, G.; Penczek, S.; Stepto, R. F. T., Definitions of terms relating to the structure and processing of sols, gels, networks, and inorganic-organic hybrid materials (IUPAC Recommendations 2007). **2007**, 79 (10), 1801-1829.
12. Rodríguez-Reinoso, F.; Sepúlveda-Escribano, A., Carbon as Catalyst Support. *Carbon Materials for Catalysis*, 2008; pp 131-155.
13. Patrick, J. W., *Porosity in Carbons: Characterization and Applications*. Wiley: 1995.
14. M. Dunkel, E. D., W. Breuers U.S. patent 1,965,956. 1995.
15. Machado, B. F.; Serp, P., Graphene-based materials for catalysis. *Catal. Sci. Technol.* **2012**, 2 (1), 54-75.
16. Qiu, B.; Xing, M.; Zhang, J., Recent advances in three-dimensional graphene based materials for catalysis applications. *Chem. Soc. Rev.* **2018**, 47 (6), 2165-2216.

17. Navalon, S.; Dhakshinamoorthy, A.; Alvaro, M.; Garcia, H., Carbocatalysis by Graphene-Based Materials. *Chem. Rev.* **2014**, *114* (12), 6179-6212.
18. Serp, P.; Corrias, M.; Kalck, P., Carbon nanotubes and nanofibers in catalysis. *Appl. Catal. A* **2003**, *253* (2), 337-358.
19. Serp, P.; Castillejos, E., Catalysis in Carbon Nanotubes. *ChemCatChem* **2010**, *2* (1), 41-47.
20. Melchionna, M.; Marchesan, S.; Prato, M.; Fornasiero, P., Carbon nanotubes and catalysis: the many facets of a successful marriage. *Catal. Sci. Technol.* **2015**, *5* (8), 3859-3875.
21. Vilatela, J. J.; Eder, D., Nanocarbon Composites and Hybrids in Sustainability: A Review. *ChemSusChem* **2012**, *5* (3), 456-478.
22. Yan, Y.; Shin, W. I.; Chen, H.; Lee, S.-M.; Manickam, S.; Hanson, S.; Zhao, H.; Lester, E.; Wu, T.; Pang, C. H., A recent trend: application of graphene in catalysis. *Carbon Letters* **2021**, *31* (2), 177-199.
23. Yan, Y.; Miao, J.; Yang, Z.; Xiao, F.-X.; Yang, H. B.; Liu, B.; Yang, Y., Carbon nanotube catalysts: recent advances in synthesis, characterization and applications. *Chem. Soc. Rev.* **2015**, *44* (10), 3295-3346.
24. Su, D. S.; Perathoner, S.; Centi, G., Nanocarbons for the Development of Advanced Catalysts. *Chem. Rev.* **2013**, *113* (8), 5782-5816.
25. https://en.wikipedia.org/wiki/Aluminium_oxide#Catalysis.
26. Berty, J. M., CHAPTER 3 - Laboratory Reactors for Catalytic Studies. Applied Industrial Catalysis, Leach, B. E., Ed. Academic Press: 1983; pp 41-67.
27. Hart, L. D.; Lense, E., *Alumina chemicals: science and technology handbook*. John Wiley & Sons: 1990.
28. Trueba, M.; Trasatti, S. P., γ -Alumina as a Support for Catalysts: A Review of Fundamental Aspects. *Eur. J. Inorg. Chem.* **2005**, *2005* (17), 3393-3403.
29. Chu, P.; Petersen, E. E.; Radke, C. J., Modeling wet impregnation of nickel on γ -Alumina. *J. Catal.* **1989**, *117* (1), 52-70.
30. Vordonis, L.; Spanos, N.; Koutsoukos, P. G.; Lycourghiotis, A., Mechanism of adsorption of cobalt(2+) and nickel(2+) ions on the "pure and fluorinated γ -alumina/electrolyte solution" interface. *Langmuir* **1992**, *8* (7), 1736-1743.
31. Margossian, T.; Larmier, K.; Kim, S. M.; Krumeich, F.; Fedorov, A.; Chen, P.; Müller, C. R.; Copéret, C., Molecularly Tailored Nickel Precursor and Support Yield a Stable Methane Dry Reforming Catalyst with Superior Metal Utilization. *J. Am. Chem. Soc.* **2017**, *139* (20), 6919-6927.
32. Velin, P.; Ek, M.; Skoglundh, M.; Schaefer, A.; Raj, A.; Thompsett, D.; Smedler, G.; Carlsson, P.-A., Water Inhibition in Methane Oxidation over Alumina Supported

- Palladium Catalysts. *J. Phys. Chem. C* **2019**, *123* (42), 25724-25737.
33. Sato, T.; Sato, S.; Okuwaki, A.; Tanaka, S.-i., Corrosion Behavior of Alumina Ceramics in Caustic Alkaline Solutions at High Temperatures. *J. Am. Ceram. Soc.* **1991**, *74* (12), 3081-3084.
 34. Chapter 1 Silica: preparation and properties. *Studies in Surface Science and Catalysis*, Vansant, E. F.; Van Der Voort, P.; Vrancken, K. C., Eds. Elsevier: 1995; Vol. 93, pp 3-30.
 35. Chapter 8 Chemical modification of silica: applications and procedures. *Studies in Surface Science and Catalysis*, Vansant, E. F.; Van Der Voort, P.; Vrancken, K. C., Eds. Elsevier: 1995; Vol. 93, pp 149-192.
 36. Shukla, M. S.; Hande, P. E.; Chandra, S., Porous Silica Support for Immobilizing Chiral Metal Catalyst: Unravelling the Activity of Catalyst on Asymmetric Organic Transformations. *ChemistrySelect* **2022**, *7* (23), e202200549.
 37. Wolny, A.; Chrobok, A., Silica-based supported ionic liquid-like phases as heterogeneous catalysts. *Molecules* **2022**, *27* (18), 5900.
 38. Costantini, A.; Califano, V., Lipase immobilization in mesoporous silica nanoparticles for biofuel production. *Catalysts* **2021**, *11* (5), 629.
 39. Abboud, M.; Alnefaie, R.; Alhanash, A., Unsupported and silica-supported nickel nanoparticles: synthesis and application in catalysis. *J. Nanopart. Res.* **2022**, *24* (2), 21.
 40. Díaz-Sánchez, M.; Díaz-García, D.; Prashar, S.; Gómez-Ruiz, S., Palladium nanoparticles supported on silica, alumina or titania: greener alternatives for Suzuki–Miyaura and other C–C coupling reactions. *Environ. Chem. Lett.* **2019**, *17* (4), 1585-1602.
 41. Gawande, M. B.; Monga, Y.; Zboril, R.; Sharma, R. K., Silica-decorated magnetic nanocomposites for catalytic applications. *Coord. Chem. Rev.* **2015**, *288*, 118-143.
 42. Sharma, R. K.; Sharma, S.; Dutta, S.; Zboril, R.; Gawande, M. B., Silica-nanosphere-based organic–inorganic hybrid nanomaterials: synthesis, functionalization and applications in catalysis. *Green Chem.* **2015**, *17* (6), 3207-3230.
 43. Motokura, K.; Ding, S.; Usui, K.; Kong, Y., Enhanced Catalysis Based on the Surface Environment of the Silica-Supported Metal Complex. *ACS Catal.* **2021**, *11* (19), 11985-12018.
 44. Fernandes, A. E.; Jonas, A. M., Design and engineering of multifunctional silica-supported cooperative catalysts. *Catal. Today* **2019**, *334*, 173-186.
 45. Clapham, B.; Reger, T. S.; Janda, K. D., Polymer-supported catalysis in synthetic organic chemistry. *Tetrahedron* **2001**, *57* (22), 4637-4662.
 46. Benaglia, M.; Puglisi, A.; Cozzi, F., Polymer-Supported Organic Catalysts. *Chem. Rev.*

- 2003**, 103 (9), 3401-3430.
47. Dickerson, T. J.; Reed, N. N.; Janda, K. D., Soluble Polymers as Scaffolds for Recoverable Catalysts and Reagents. *Chem. Rev.* **2002**, 102 (10), 3325-3344.
 48. Bergbreiter, D. E.; Tian, J.; Hongfa, C., Using Soluble Polymer Supports To Facilitate Homogeneous Catalysis. *Chem. Rev.* **2009**, 109 (2), 530-582.
 49. Chinnusamy, T.; Hilgers, P.; Reiser, O., Catalysts Bound to Soluble Polymers. Recoverable and Recyclable Catalysts, 2009; pp 77-100.
 50. Lu, J.; Toy, P. H., Organic Polymer Supports for Synthesis and for Reagent and Catalyst Immobilization. *Chem. Rev.* **2009**, 109 (2), 815-838.
 51. Edouard, D.; Lacroix, M.; Huu, C. P.; Luck, F., Pressure drop modeling on SOLID foam: State-of-the art correlation. *Chem. Eng. J.* **2008**, 144 (2), 299-311.
 52. Ashby, M. F., The properties of foams and lattices. *Philos. Trans. Royal Soc. A: Math, Phys. Eng. Sci.* **2006**, 364 (1838), 15-30.
 53. Gent, A. N.; Thomas, A. G., The deformation of foamed elastic materials. *J. Appl. Polym. Sci.* **1959**, 1 (1), 107-113.
 54. Ashby, M. F.; Gibson, L. J., Cellular solids: structure and properties. *Press Syndicate of the University of Cambridge, Cambridge, UK* **1997**, 175-231.
 55. Ashby, M. F.; Evans, T.; Fleck, N. A.; Hutchinson, J.; Wadley, H.; Gibson, L., *Metal foams: a design guide*. Elsevier: 2000.
 56. Bakker, J. J. W.; Groendijk, W. J.; de Lathouder, K. M.; Kapteijn, F.; Moulijn, J. A.; Kreutzer, M. T.; Wallin, S. A., Enhancement of Catalyst Performance Using Pressure Pulses on Macroporous Structured Catalysts. *Ind. Eng. Chem. Res.* **2007**, 46 (25), 8574-8583.
 57. Giani, L.; Groppi, G.; Tronconi, E., Mass-Transfer Characterization of Metallic Foams as Supports for Structured Catalysts. *Ind. Eng. Chem. Res.* **2005**, 44 (14), 4993-5002.
 58. Richardson, J. T.; Peng, Y.; Remue, D., Properties of ceramic foam catalyst supports: pressure drop. *Appl. Catal. A* **2000**, 204 (1), 19-32.
 59. Lacroix, M.; Nguyen, P.; Schweich, D.; Pham Huu, C.; Savin-Poncet, S.; Edouard, D., Pressure drop measurements and modeling on SiC foams. *Chem. Eng. Sci.* **2007**, 62 (12), 3259-3267.
 60. Duong-Viet, C.; Ba, H.; El-Berrichi, Z.; Nhut, J.-M.; Ledoux, M. J.; Liu, Y.; Pham-Huu, C., Silicon carbide foam as a porous support platform for catalytic applications. *New J. Chem.* **2016**, 40 (5), 4285-4299.
 61. Ou, X.; Piliitsis, F.; Jiao, Y.; Zhang, Y.; Xu, S.; Jennings, M.; Yang, Y.; Taylor, S. F. R.; Garforth, A.; Zhang, H.; Hardacre, C.; Yan, Y.; Fan, X., Hierarchical Fe-ZSM-5/SiC foam catalyst as the foam bed catalytic reactor (FBCR) for catalytic wet peroxide oxidation (CWPO). *Chem. Eng. J.* **2019**, 362, 53-62.

62. Feng, L.; Liu, Y.; Jiang, Q.; Liu, W.; Wu, K.-H.; Ba, H.; Pham-Huu, C.; Yang, W.; Su, D. S., Nanodiamonds @ N, P co-modified mesoporous carbon supported on macroscopic SiC foam for oxidative dehydrogenation of ethylbenzene. *Catal. Today* **2020**, *357*, 231-239.
63. Jiao, Y.; Ou, X.; Zhang, J.; Fan, X., Structured ZSM-5 coated SiC foam catalysts for process intensification in catalytic cracking of n-hexane. *Reaction Chem. Eng.* **2019**, *4* (2), 427-435.
64. Chen, B.; Dingerdissen, U.; Krauter, J. G. E.; Lansink Rotgerink, H. G. J.; Möbus, K.; Ostgard, D. J.; Panster, P.; Riermeier, T. H.; Seebald, S.; Tacke, T.; Trauthwein, H., New developments in hydrogenation catalysis particularly in synthesis of fine and intermediate chemicals. *Appl. Catal. A* **2005**, *280* (1), 17-46.
65. Gama, N. V.; Ferreira, A.; Barros-Timmons, A., Polyurethane foams: Past, present, and future. *Materials* **2018**, *11* (10), 1841.
66. Szycher PhD, M. E., *Szycher's Handbook of Polyurethanes (2nd ed.)*. CRC Press. 2012.
67. Dutta, A. S., 2 - Polyurethane Foam Chemistry. Recycling of Polyurethane Foams, Thomas, S.; Rane, A. V.; Kanny, K.; V.K, A.; Thomas, M. G., Eds. William Andrew Publishing: 2018; pp 17-27.
68. Engels, H.-W.; Pirkl, H.-G.; Albers, R.; Albach, R. W.; Krause, J.; Hoffmann, A.; Casselmann, H.; Dormish, J., Polyurethanes: Versatile Materials and Sustainable Problem Solvers for Today's Challenges. *Angew. Chem. Int. Ed.* **2013**, *52* (36), 9422-9441.
69. Foam-Tech What is the difference between open-cell and closed-cell polyurethane foams? [http://www.foam-tech.com/products/urethane foam/open closed cell.htm](http://www.foam-tech.com/products/urethane%20foam/open_closed_cell.htm) (accessed January 23).
70. Giani, L.; Groppi, G.; Tronconi, E., Heat Transfer Characterization of Metallic Foams. *Ind. Eng. Chem. Res.* **2005**, *44* (24), 9078-9085.
71. Richardson, J. T.; Remue, D.; Hung, J. K., Properties of ceramic foam catalyst supports: mass and heat transfer. *Appl. Catal. A* **2003**, *250* (2), 319-329.
72. Rahimi, A.; Mashak, A., Review on rubbers in medicine: natural, silicone and polyurethane rubbers. *Plast. Rubber Compos.* **2013**, *42* (6), 223-230.
73. Gong, L.; Kyriakides, S.; Jang, W. Y., Compressive response of open-cell foams. Part I: Morphology and elastic properties. *Int. J. Solids Struct.* **2005**, *42* (5), 1355-1379.
74. Pattanayak, D. S.; Mishra, J.; Nanda, J.; Sahoo, P. K.; Kumar, R.; Sahoo, N. K., Photocatalytic degradation of cyanide using polyurethane foam immobilized Fe-TCP-SS-TiO₂-rGO nano-composite. *J. Environ. Manag.* **2021**, *297*, 113312.
75. Khan, M. S. J.; Khan, S. B.; Kamal, T.; Asiri, A. M., Agarose biopolymer coating on

- polyurethane sponge as host for catalytic silver metal nanoparticles. *Polymer Testing* **2019**, *78*, 105983.
76. Jin, Q.; Ma, L.; Zhou, W.; Chintalapalle, R.; Shen, Y.; Li, X., Strong interaction between Au nanoparticles and porous polyurethane sponge enables efficient environmental catalysis with high reusability. *Catal. Today* **2020**, *358*, 246-253.
 77. Khajeh Dangolani, S.; Sharifat, S.; Panahi, F.; Khalafi-Nezhad, A., Immobilized palladium nanoparticles on a cyclodextrin-polyurethane nanosponge (Pd-CD-PU-NS): An efficient catalyst for cyanation reaction in aqueous media. *Inorg. Chim. Acta* **2019**, *494*, 256-265.
 78. Satria, M.; Saleh, T. A., Facile approach of eco-friendly superhydrophilic/underwater superoleophobic zinc-functionalized polyurethane foams for continuous oil-water separation. *J. Mol. Liquids* **2022**, *367*, 120341.
 79. Sahoo, L.; Mondal, S.; Beena, N. C.; Gloskovskii, A.; Manju, U.; Topwal, D.; Gautam, U. K., 3D Porous Polymeric-Foam-Supported Pd Nanocrystal as a Highly Efficient and Recyclable Catalyst for Organic Transformations. *ACS Appl. Mater. Interfaces* **2021**, *13* (8), 10120-10130.
 80. Sun, C. J.; Srivastava, A.; Reifert, J. R.; Waite, J. H., Halogenated DOPA in a Marine Adhesive Protein. *The Journal of Adhesion* **2009**, *85* (2-3), 126-138.
 81. Kamino, K., Novel barnacle underwater adhesive protein is a charged amino acid-rich protein constituted by a Cys-rich repetitive sequence. *Biochem. J.* **2001**, *356* (2), 503-507.
 82. Lin, Q.; Gourdon, D.; Sun, C.; Holten-Andersen, N.; Anderson, T. H.; Waite, J. H.; Israelachvili, J. N., Adhesion mechanisms of the mussel foot proteins mfp-1 and mfp-3. *Proc. Natl. Acad. Sci. U.S.A.* **2007**, *104* (10), 3782-3786.
 83. Petrone, L.; Kumar, A.; Sutanto, C. N.; Patil, N. J.; Kannan, S.; Palaniappan, A.; Amini, S.; Zappone, B.; Verma, C.; Miserez, A., Mussel adhesion is dictated by time-regulated secretion and molecular conformation of mussel adhesive proteins. *Nature Commun.* **2015**, *6* (1), 8737.
 84. Farsad, N.; Sone, E. D., Zebra mussel adhesion: Structure of the byssal adhesive apparatus in the freshwater mussel, *Dreissena polymorpha*. *J. Structur. Bio.* **2012**, *177* (3), 613-620.
 85. Lee, B. P.; Messersmith, P. B.; Israelachvili, J. N.; Waite, J. H., Mussel-Inspired Adhesives and Coatings. *Annual Rev. Mater. Res.* **2011**, *41*, 99-132.
 86. Lee, H.; Dellatore, S. M.; Miller, W. M.; Messersmith, P. B., Mussel-Inspired Surface Chemistry for Multifunctional Coatings. *Science* **2007**, *318* (5849), 426-430.
 87. Lee, H.; Scherer, N. F.; Messersmith, P. B., Single-molecule mechanics of mussel adhesion. *Proc. Natl. Acad. Sci. U.S.A.* **2006**, *103* (35), 12999-13003.

88. Saiz-Poseu, J.; Mancebo-Aracil, J.; Nador, F.; Busqué, F.; Ruiz-Molina, D., The Chemistry behind Catechol-Based Adhesion. *Angew. Chem. Int. Ed.* **2019**, *58* (3), 696-714.
89. Sileika, T. S.; Barrett, D. G.; Zhang, R.; Lau, K. H. A.; Messersmith, P. B., Colorless Multifunctional Coatings Inspired by Polyphenols Found in Tea, Chocolate, and Wine. *Angew. Chem. Int. Ed.* **2013**, *52* (41), 10766-10770.
90. Pop-Georgievski, O.; Verreault, D.; Diesner, M.-O.; Proks, V.; Heissler, S.; Rypáček, F.; Koelsch, P., Nonfouling Poly(ethylene oxide) Layers End-Tethered to Polydopamine. *Langmuir* **2012**, *28* (40), 14273-14283.
91. Ponzio, F.; Barthès, J.; Bour, J.; Michel, M.; Bertani, P.; Hemmerlé, J.; d'Ischia, M.; Ball, V., Oxidant Control of Polydopamine Surface Chemistry in Acids: A Mechanism-Based Entry to Superhydrophilic-Superoleophobic Coatings. *Chem. Mater.* **2016**, *28* (13), 4697-4705.
92. Steenken, S.; Neta, P., One-electron redox potentials of phenols. Hydroxy- and aminophenols and related compounds of biological interest. *J. Phys. Chem.* **1982**, *86* (18), 3661-3667.
93. Ryu, J. H.; Messersmith, P. B.; Lee, H., Polydopamine Surface Chemistry: A Decade of Discovery. *ACS Appl. Mater. Interfaces* **2018**, *10* (9), 7523-7540.
94. Molnár, Á., Polydopamine – its Prolific Use as Catalyst and Support Material. *ChemCatChem* **2020**, *12* (10), 2649-2689.
95. Wang, Z.; Zou, Y.; Li, Y.; Cheng, Y., Metal-Containing Polydopamine Nanomaterials: Catalysis, Energy, and Theranostics. *Small* **2020**, *16* (18), 1907042.
96. Liebscher, J., Chemistry of Polydopamine – Scope, Variation, and Limitation. *Eur. J. Org. Chem.* **2019**, *2019* (31-32), 4976-4994.
97. Du, Y.; Yang, H.-C.; Xu, X.-L.; Wu, J.; Xu, Z.-K., Polydopamine as a Catalyst for Thiol Coupling. *ChemCatChem* **2015**, *7* (23), 3822-3825.
98. Pawar, S. A.; Chand, A. N.; Kumar, A. V., Polydopamine: An Amine Oxidase Mimicking Sustainable Catalyst for the Synthesis of Nitrogen Heterocycles under Aqueous Conditions. *ACS Sustainable Chem. Eng.* **2019**, *7* (9), 8274-8286.
99. Coskun, H.; Aljabour, A.; De Luna, P.; Farka, D.; Greunz, T.; Stifter, D.; Kus, M.; Zheng, X.; Liu, M.; Hassel, A. W., Biofunctionalized conductive polymers enable efficient CO₂ electroreduction. *Science Adv.* **2017**, *3* (8), e1700686.
100. Ansari, S. A.; Husain, Q., Potential applications of enzymes immobilized on/in nano materials: A review. *Biotechnol. Adv.* **2012**, *30* (3), 512-523.
101. Zeng, T.; Zhang, X.-l.; Niu, H.-y.; Ma, Y.-r.; Li, W.-h.; Cai, Y.-q., In situ growth of gold nanoparticles onto polydopamine-encapsulated magnetic microspheres for catalytic reduction of nitrobenzene. *Appl. Catal. B* **2013**, *134-135*, 26-33.

102. Li, Y.; Zhu, L.; Wang, B.; Mao, Z.; Xu, H.; Zhong, Y.; Zhang, L.; Sui, X., Fabrication of Thermoresponsive Polymer-Functionalized Cellulose Sponges: Flexible Porous Materials for Stimuli-Responsive Catalytic Systems. *ACS Appl. Mater. Interfaces* **2018**, *10* (33), 27831-27839.
103. Liu, Y.; Li, G.; Qin, R.; Chen, D., Surface-Engineered Polydopamine Particles as an Efficient Support for Catalytic Applications. *Langmuir* **2016**, *32* (51), 13675-13686.
104. Mao, Y.; Jiang, W.; Xuan, S.; Fang, Q.; Leung, K. C.-F.; Ong, B. S.; Wang, S.; Gong, X., Rod-like β -FeOOH@poly(dopamine)-Au-poly(dopamine) nanocatalysts with improved recyclable activities. *Dalton Trans.* **2015**, *44* (20), 9538-9544.
105. Syres, K.; Thomas, A.; Bondino, F.; Malvestuto, M.; Grätzel, M., Dopamine Adsorption on Anatase TiO₂(101): A Photoemission and NEXAFS Spectroscopy Study. *Langmuir* **2010**, *26* (18), 14548-14555.
106. Hou, X.; Cai, Y.; Song, X.; Wu, Y.; Zhang, J.; Wei, Q., Electrospun TiO₂ nanofibers coated with polydopamine for enhanced sunlight-driven photocatalytic degradation of cationic dyes. *Surf. Interface Anal.* **2019**, *51* (2), 169-176.
107. Li, W.; Ma, Z.; Bai, G.; Hu, J.; Guo, X.; Dai, B.; Jia, X., Dopamine-assisted one-step fabrication of Ag@AgCl nanophotocatalyst with tunable morphology, composition and improved photocatalytic performance. *Appl. Catal. B* **2015**, *174-175*, 43-48.
108. Dubey, A. V.; Kumar, A. V., A biomimetic magnetically recoverable palladium nanocatalyst for the Suzuki cross-coupling reaction. *RSC Adv.* **2016**, *6* (52), 46864-46870.
109. Xie, A.; Zhang, K.; Wu, F.; Wang, N.; Wang, Y.; Wang, M., Polydopamine nanofilms as visible light-harvesting interfaces for palladium nanocrystal catalyzed coupling reactions. *Catal. Sci. Technol.* **2016**, *6* (6), 1764-1771.
110. Kunfi, A.; Szabó, V.; Mastalir, Á.; Bucsi, I.; Mohai, M.; Németh, P.; Bertóti, I.; London, G., Palladium on Polydopamine: Its True Potential in Catalytic Transfer Hydrogenations and Heck Coupling Reactions. *ChemCatChem* **2017**, *9* (16), 3236-3244.
111. Majumdar, B.; Bhattacharya, T.; Sarma, T. K., Gold Nanoparticle-Polydopamine-Reduced Graphene Oxide Ternary Nanocomposite as an Efficient Catalyst for Selective Oxidation of Benzylic C(sp³)-H Bonds Under Mild Conditions. *ChemCatChem* **2016**, *8* (10), 1825-1835.
112. Veisi, H.; Taheri, S.; Hemmati, S., Preparation of polydopamine sulfamic acid-functionalized magnetic Fe₃O₄ nanoparticles with a core/shell nanostructure as heterogeneous and recyclable nanocatalysts for the acetylation of alcohols, phenols, amines and thiols under solvent-free conditions. *Green Chem.* **2016**, *18* (23), 6337-6348.
113. Gazdag, T.; Kunfi, A.; London, G., Cyanation of aryl bromides with K₄[Fe(CN)₆] using

- polydopamine supported Pd nanoparticle catalysis: formation of magnetite during the reaction. *React. Kinet. Mech. Catal.* **2018**, *125* (2), 567-581.
114. Seok, S.; Shin, S.; Lee, T. J.; Jeong, J.-M.; Yang, M.; Kim, D. H.; Park, J. Y.; Lee, S. J.; Choi, B. G.; Lee, K. G., Multifunctional Polyurethane Sponge for Polymerase Chain Reaction Enhancement. *ACS Appl. Mater. Interfaces* **2015**, *7* (8), 4699-4705.
115. Edouard, D.; Ritleng, V.; Jierry, L.; Chau Dalencon, N. T. T., Process of modification of the surface properties of cellular elastomeric foams. WO2016012689A2, 2016.
116. Pardieu, E.; Chau, N. T. T.; Dintzer, T.; Romero, T.; Favier, D.; Roland, T.; Edouard, D.; Jierry, L.; Ritleng, V., Polydopamine-coated open cell polyurethane foams as an inexpensive, flexible yet robust catalyst support: a proof of concept. *Chem. Commun.* **2016**, *52* (25), 4691-4693.
117. Lefebvre, L.; Kelber, J.; Jierry, L.; Ritleng, V.; Edouard, D., Polydopamine-coated open cell polyurethane foam as an efficient and easy-to-regenerate soft structured catalytic support (S2CS) for the reduction of dye. *J. Environ. Chem. Eng.* **2017**, *5* (1), 79-85.
118. Ait Khouya, A.; Mendez Martinez, M. L.; Bertani, P.; Romero, T.; Favier, D.; Roland, T.; Guidal, V.; Bellière-Baca, V.; Edouard, D.; Jierry, L.; Ritleng, V., Coating of polydopamine on polyurethane open cell foams to design soft structured supports for molecular catalysts. *Chem. Commun.* **2019**, *55* (79), 11960-11963.
119. Lefebvre, L.; Kelber, J.; Mao, X.; Ponzio, F.; Agusti, G.; Vigier-Carrière, C.; Ball, V.; Jierry, L.; Ritleng, V.; Edouard, D., Borohydride-functionalized polydopamine-coated open cell polyurethane foam as a reusable soft structured material for reduction reactions: Application to the removal of a dye. *Environ. Prog. Sustain. Energy* **2019**, *38* (2), 329-335.
120. Yang, J.; Cohen Stuart, M. A.; Kamperman, M., Jack of all trades: versatile catechol crosslinking mechanisms. *Chem. Soc. Rev.* **2014**, *43* (24), 8271-8298.
121. Wu, J.; Zhang, L.; Wang, Y.; Long, Y.; Gao, H.; Zhang, X.; Zhao, N.; Cai, Y.; Xu, J., Mussel-Inspired Chemistry for Robust and Surface-Modifiable Multilayer Films. *Langmuir* **2011**, *27* (22), 13684-13691.
122. Rafatullah, M.; Sulaiman, O.; Hashim, R.; Ahmad, A., Adsorption of methylene blue on low-cost adsorbents: A review. *J. Hazard. Mater.* **2010**, *177* (1), 70-80.
123. Edouard, D.; Lefebvre, L.; Jierry, L.; Ritleng, V.; Kelber, J. Reduction kit, reducing composition and use of said kit and composition, WO2018020146A1, 2018.
124. Liu, Y.; Ai, K.; Lu, L., Polydopamine and Its Derivative Materials: Synthesis and Promising Applications in Energy, Environmental, and Biomedical Fields. *Chem. Rev.* **2014**, *114* (9), 5057-5115.
125. Gómez, V.; Larrechi, M. S.; Callao, M. P., Kinetic and adsorption study of acid dye

- removal using activated carbon. *Chemosphere* **2007**, 69 (7), 1151-1158.
126. Zohre, S.; Ataallah, S. G.; Mehdi, A., Experimental study of methylene blue adsorption from aqueous solutions onto carbon nano tubes. *Int. J. Water Res. Environ. Eng.* **2010**, 2147483647 (2), 016-028.
127. Kennedy, L. J.; Vijaya, J. J.; Sekaran, G.; Kayalvizhi, K., Equilibrium, kinetic and thermodynamic studies on the adsorption of m-cresol onto micro- and mesoporous carbon. *J. Hazard. Mater.* **2007**, 149 (1), 134-143.
128. Lefebvre, L.; Agusti, G.; Bouzeggane, A.; Edouard, D., Adsorption of dye with carbon media supported on polyurethane open cell foam. *Catal. Today* **2018**, 301, 98-103.
129. Chandra, T. C.; Mirna, M. M.; Sudaryanto, Y.; Ismadji, S., Adsorption of basic dye onto activated carbon prepared from durian shell: Studies of adsorption equilibrium and kinetics. *Chem. Eng. J.* **2007**, 127 (1), 121-129.
130. Zhang, Y.; Zhao, J.; Wang, K.; Gao, L.; Meng, M.; Yan, Y., Green Synthesis of Acid-Base Bi-functional UiO-66-Type Metal-Organic Frameworks Membranes Supported on Polyurethane Foam for Glucose Conversion. *ChemistrySelect* **2018**, 3 (32), 9378-9387.
131. Li, J.; Gong, J.-L.; Zeng, G.-M.; Zhang, P.; Song, B.; Cao, W.-C.; Fang, S.-Y.; Huan, S.-Y.; Ye, J., The performance of UiO-66-NH₂/graphene oxide (GO) composite membrane for removal of differently charged mixed dyes. *Chemosphere* **2019**, 237, 124517.

Chapter I

[Ru(bpy)₃]²⁺-functionalized polydopamine-coated polyurethane foam as an easily reusable macroscopic heterogeneous catalyst for visible-light photocatalysis

Chapter I

[Ru(bpy)₃]²⁺-functionalized polydopamine-coated polyurethane foam as an easily reusable macroscopic heterogeneous catalyst for visible-light photocatalysis

Table of contents

I) Introduction.....	67
II) Results and discussion	69
II-1) Preparation and characterization of Ru(bpy) ₃ -APTES@PDA@PUF.....	69
II-2) Photocatalytic activity of Ru(bpy) ₃ -APTES@PDA@PUF	75
II-3) Catalyst recycling and leaching tests	79
III) Conclusion and perspectives	85
IV) Experimental section.....	85
IV-1) Materials and methods	85
IV-2) Experimental procedures.....	87
IV-2-1) Open cell polyurethane foam (PUF) coating with polydopamine (PDA)	87
IV-2-2) Functionalization of PDA@PUF with APTES	87
IV-2-3) Synthesis of 2,2'-bipyridine-4-carboxylic acid.....	88
IV-2-4) Coupling of 2,2'-bipyridine-4-carboxylic acid with APTES@PDA@PUF	89
IV-2-5) Synthesis of <i>cis</i> -[Ru(bpy) ₂ Cl ₂].2H ₂ O	89
IV-2-6) Coordination of <i>cis</i> -[Ru(bpy) ₂ Cl ₂].2H ₂ O on BPY-APTES@PDA@PUF.....	90
IV-2-7) Synthesis of <i>N</i> -phenyl-tetrahydroisoquinoline	90
IV-2-8) General procedure for the oxidative homocoupling of benzylic amines photocatalyzed by Ru(bpy) ₃ -APTES@PDA@PUF.....	90
IV-2-9) General procedure for the cross-dehydrogenative couplings photocatalyzed by Ru(bpy) ₃ -APTES@PDA@PUF	91
IV-2-10) Ru(bpy) ₃ -APTES@PDA@PUF recovery and reuse in successive photocatalytic experiments	91

IV-2-11) Ru leaching influence on the course of a photocatalytic process	91
V) References	92

Abstract

This chapter introduces an easy-to-handle, highly reusable and efficient macroscopic $[\text{Ru}(\text{bpy})_3]^{2+}$ -based catalyst for applications in visible-light-induced photocatalysis. The structured heterogeneous photocatalyst was obtained by post-functionalization of a redox-non innocent polydopamine-coated open cell polyurethane foam (PDA@PUF) via a silanization process of the mussel-inspired adhesive layer with 3-(triethoxysilyl)propan-1-amine (APTES), followed by an EDC-mediated coupling with [2,2'-bipyridine]-4-carboxylic acid and further complexation of $[\text{Ru}(\text{bpy})_2\text{Cl}_2]$ (bpy = 2,2'-bipyridine). The successful covalent grafting of APTES on the PDA layer of PUF and further functionalization all over the foam' surface with $[\text{Ru}(\text{bpy})_3]^{2+}$ was suggested by ^{29}Si CP-MAS NMR and XPS spectroscopies, ICP-AES analyses and SEM-EDX elemental mapping. As a proof of concept, the performance of the as-prepared $\text{Ru}(\text{bpy})_3\text{-APTES@PDA@PUF}$ catalyst was investigated in model benzylic amine homocouplings and cross dehydrogenative couplings under visible-light irradiation and molecular oxygen as a green oxygen source. The macroscopic catalyst proved catalytically effective in both reactions, showing very good functional group tolerance and excellent reusability in an easy-to-carry "dip-and-play" mode for at least 6 runs. Impressively, an improvement of the catalytic performances was even observed in both reactions, which most likely results from a modification of the uppermost layer of polydopamine that renders the visible-light photocatalyst more accessible, as suggested by the progressive color lightening of the catalytic foams, the smoothing of their surface and XPS analyses.

1) Introduction

Visible-light photoredox catalysis, as a powerful and effective tool in organic synthesis, has become a prominent topic through single-electron or energy transfer processes under mild reaction conditions.¹⁻² In particular, $[\text{Ru}(\text{bpy})_3]^{2+}$ has shown its applicability in a myriad of visible-light-induced reactions under fluorescent light bulb, LED or sunlight irradiation, including, among others, asymmetric Csp³-H alkylations,³⁻⁴ reductive dehalogenations,⁵⁻⁶ oxidative hydroxylations,⁷ cycloadditions,⁸⁻¹² coupling reactions¹³⁻¹⁵ and free radical polymerizations.¹⁶⁻¹⁷ Despite this impressive versatility, important limitations arise from (i) the high cost and toxicity of ruthenium, (ii) the high molar extinction coefficient of $[\text{Ru}(\text{bpy})_3]^{2+}$ that hampers light penetration into the solution and causes dramatically reduced reaction rates when scaling-up reactions in traditional batch reactors due to the low surface area to volume ratio of the latter.¹⁸ Possible answers to these limitations go through the immobilisation of the photocatalyst (PC) on a solid support, incorporation in supramolecular systems, or transformation into amphiphilic or other specific derivatives compatible with liquid-liquid phase-separation conditions to develop easily recoverable and reusable heterogeneous

visible-light PCs,¹⁹ and/or the use of continuous flow reactors.²⁰

Immobilized catalytic systems may additionally allow (i) a better control of the reaction efficiency and selectivity through the tuning of the environment in the vicinity of the photocatalytic centers, (ii) an improvement of their photostability and a decrease of the self-quenching process through functionalization of the photosensitizer and spatial separation of the catalytic centers, and (iii) the use in solvents where the complexes are insoluble or inactive. In terms of hosting matrix, a vast array of strategies were studied up to now to immobilize visible-light active transition metal complexes, including straightforwardly supported or sophisticated systems based on carbon nitrides,²¹ graphene,²² MOFs,²³ or supramolecular assembly.²⁴ Even though all these reusable solid- or liquid-phase heterogeneous PCs were prepared and effectively applied in various types of light-induced transformations, the whole catalytic processes seemed somewhat short of some dexterities and proceeding conveniences for scale up procedures, as they lacked some practicability or compatibility of supporting materials. The expectation for more applicable heterogeneous PCs is that the building blocks should be easily obtainable at low environmental and economic cost, the preparation of the supported PC simple, and the application more diversified.

On the other hand, polydopamine (PDA) has been demonstrated to act as an efficient visible-light-harvesting material²⁵⁻²⁶ and redox mediator²⁷ able to accelerate the rate of photoinduced electron transfer via a two-electron and two-proton redox-coupling mechanism;²⁸ two properties that can clearly be beneficial in heterogeneously photocatalyzed processes.²⁹⁻
33

In this context, we report here our studies toward the immobilization of $[\text{Ru}(\text{bpy})_3]^{2+}$ on redox non-innocent, easy-to-prepare and easy-to-handle PDA-coated open cell polyurethane foams (PUF),^{27, 34-39} which possess sufficiently large pores to allow efficient light penetration inside the whole three-dimensional structure as well as efficient transport properties under flow conditions, and which - due to their lightweight and flexibility - can be easily engineered and adapted to any kind of (photo)reactor.³⁹

Thanks to the presence of catechol moieties on the surface of the PDA adhesive layer, (3-aminopropyl)triethoxysilane (APTES) was readily anchored on PDA@PUF, accomplishing an interfacial amination so as to support the PC via subsequent EDC-mediated coupling with [2,2'-bipyridine]-4-carboxylic acid and further complexation with $[\text{Ru}(\text{bpy})_2\text{Cl}_2]$. The resulting $\text{Ru}(\text{bpy})_3\text{-APTES@PDA@PUF}$ material was then characterized by a combination of ²⁹Si CP-MAS NMR and XPS spectroscopies, ICP-AES analyses, SEM microscopy and SEM-EDX elemental mapping, and its catalytic activity studied in model oxidative benzylic amine homocouplings and C-H bond functionalizations of *N*-phenyl-tetrahydroisoquinoline under visible-light irradiation and O₂ as a green oxygen source.⁴⁰⁻⁴⁵ The macroscopic catalyst proved catalytically effective in both reactions with a very good functional group tolerance and showed

excellent reusability for at least 6 runs in an easy-to-carry “dip-and-play” mode. Impressively, although some Ru leaching was measured, an improvement of the catalytic performances was even observed in both reactions, which most likely results from a modification of the uppermost layer of polydopamine that renders the $[\text{Ru}(\text{bpy})_3]^{2+}$ photocatalyst more accessible, as revealed by the progressive color change of the catalytic foams from dark brown to dark red or orange, the smoothing of their surface, and XPS analyses.

II) Results and discussion

II-1) Preparation and characterization of $\text{Ru}(\text{bpy})_3\text{-APTES@PDA@PUF}$

The chosen strategy for the immobilization of $[\text{Ru}(\text{bpy})_3]\text{Cl}_2$ at the surface of polydopamine-coated open cell polyurethane foams (PDA@PUF) relies on the previously-established proof of concept regarding the feasibility to covalently graft a molecular catalyst bearing an alkoxysilyl arm by condensation of the latter with the catechol groups of the mussel-inspired layer.³⁶ Thus, after coating a cubic sample of PUF of ca. 1.5 cm × 1.5 cm × 3 cm with a thin layer of PDA by simple immersion in an aqueous solution of dopamine at room temperature buffered at a pH of 8.5, close to that of a marine environment, and several washings with water,³⁵⁻³⁶ the resulting PDA@PUF material was functionalized with $[\text{Ru}(\text{bpy})_3]\text{Cl}_2$ in three steps via (i) a silanization process with 3-(triethoxysilyl)propan-1-amine (APTES), (ii) the EDC-mediated coupling of [2,2'-bipyridine]-4-carboxylic acid with the resulting amino-functionalized foam, and (iii) the complexation of ruthenium to the anchored bipyridine units by reaction with *cis*- $[\text{Ru}(\text{bpy})_2]\text{Cl}_2$ (**Figure 1**). This progressive functionalization of PDA@PUF was preferred to that implying the prior synthesis of the triethoxysilyl-functionalized $[\text{Ru}(\text{bpy})_3]\text{Cl}_2$ derivative, followed by the silanization process, due to the impossibility to maintain the integrity of the triethoxysilyl groups in the envisaged reaction conditions, although such a strategy, if possible, may have led to a higher ruthenium loading.

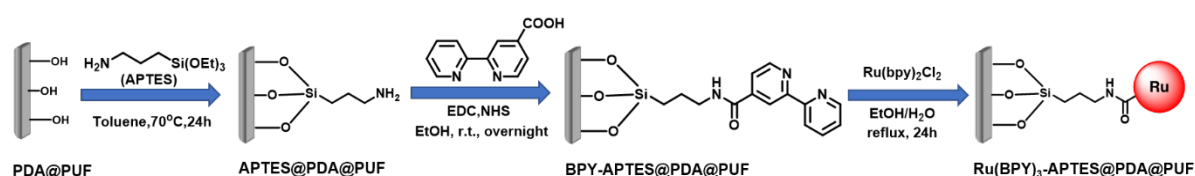


Figure 1. Functionalization strategy of PDA@PUF for the immobilization of $\text{Ru}(\text{bpy})_3^{2+}$

Specifically, the silanization of PDA@PUF was conducted with APTES in toluene at 70 °C for 24 h (**Figure 1**). The successful covalent anchoring of APTES on the foam surface was established by ²⁹Si CP-MAS NMR spectroscopy. The NMR spectrum indeed revealed signals at -64.3 ppm, -56.4 ppm, -53.4 ppm and -42.0 ppm (**Figure 2**), demonstrating the presence of

T_1 , T_2 as well as cross-linked T_3+T_3' and T_4+T_4' substructures⁴⁶ similarly to what can be observed with covalently anchored APTES on a silica matrix.⁴⁷ In addition, ICP-AES measurements on several samples of APTES@PDA@PUF revealed a mean Si content of 3.763 ± 0.041 g/kg, and high magnification SEM images showed a rough surface characteristic of the PDA coating on PUF (**Figure 3**).³⁵⁻³⁶ Finally, SEM-EDX spectroscopy suggested a relatively homogeneous distribution of Si on the surface of APTES@PDA@PUF as expected (**Figure 4**).

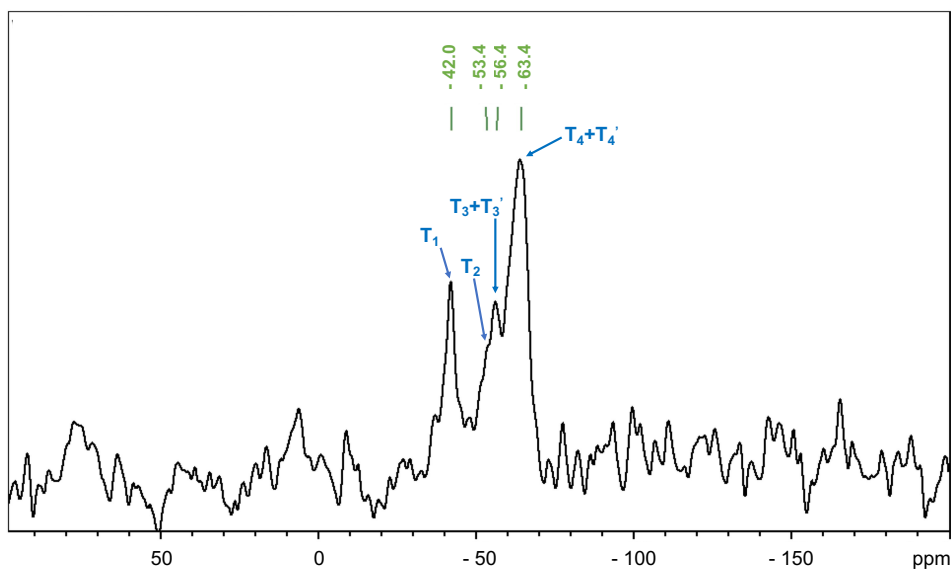


Figure 2. ^{29}Si CP-MAS NMR spectrum of APTES@PDA@PUF

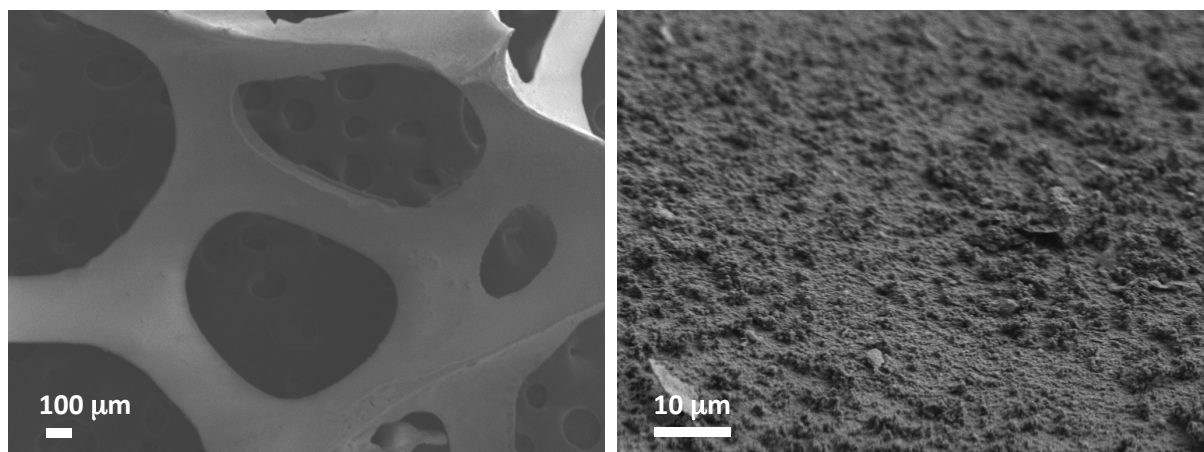
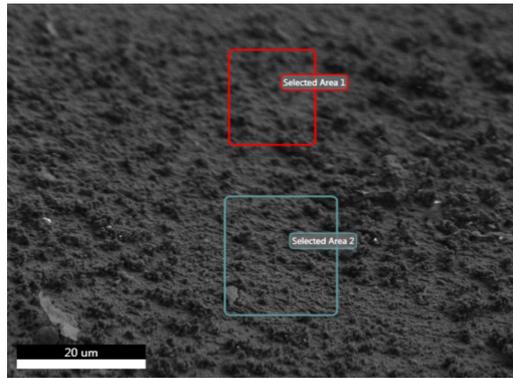
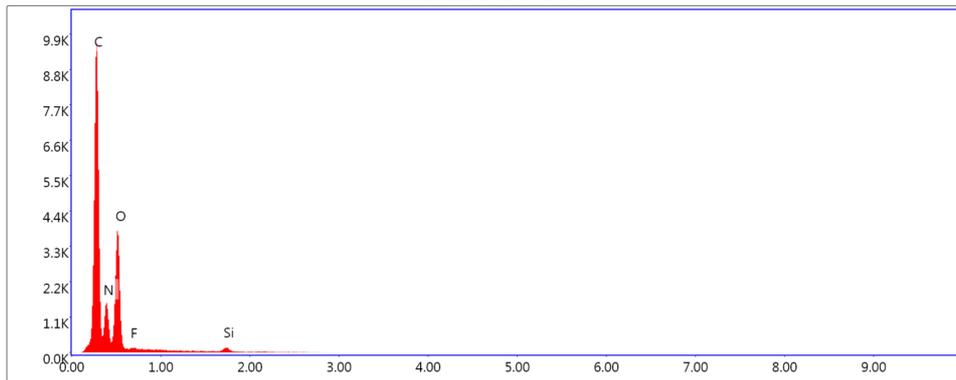


Figure 3. SEM images at different magnification of APTES@PDA@PUF



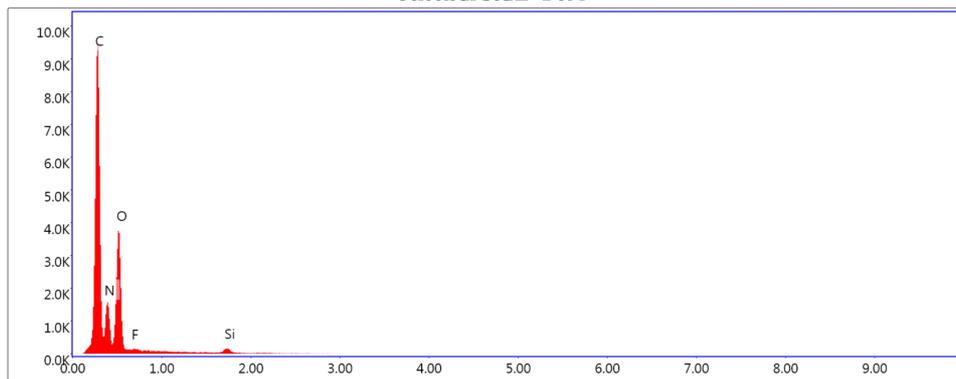
Selected Area 1 - Det 1



Lsec: 48.4 0 Cnts 5.740 keV Det: Octane Elite 25

Element	Weight %	Atomic %	Net Int.	Error %
C K	72.2	78.4	1322.5	8.2
N K	9.0	8.4	151.4	28.3
O K	12.7	10.4	423.5	27.2
F K	0.1	0.0	5.9	31.2
Si K	6.0	2.8	25.2	19.0

Selected Area 2 - Det 1



Lsec: 48.4 0 Cnts 5.740 keV Det: Octane Elite 25

Element	Weight %	Atomic %	Net Int.	Error %
C K	71.9	78.0	1300.6	8.3
N K	9.6	8.9	158.3	28.1
O K	12.9	10.5	422.7	27.0
F K	0.0	0.0	2.3	31.1
Si K	5.7	2.6	27.0	18.7

Figure 4. SEM image of APTES@PDA@PUF with selected areas for EDX spectroscopy (top), corresponding EDX spectra and quantitative results (middle and bottom)

After this silanization step, the primary amine groups of APTES present on the foam surface were reacted with 2,2'-bipyridine-4-carboxylic acid under EDC activating conditions in ethanol at room temperature to furnish the bpy-functionalized foam, BPY-APTES@PDA@PUF (**Figure 1**). SEM images confirmed the integrity of the foam with the absence of apparent modification of the surface (**Figure 5**) and ICP-AES the preservation of the silicon anchor, though the mean Si content diminished to 2.462 ± 0.025 g/kg, most likely in reason some cross-linked silicon crust losses.

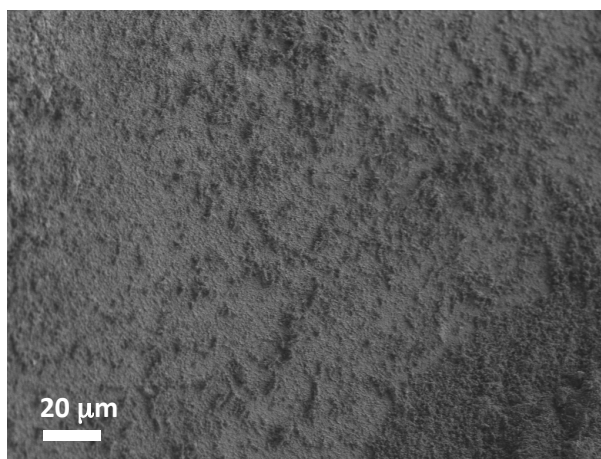


Figure 5. High magnification SEM image of BPY-APTES@PDA@PUF

The subsequent coordination of $[\text{Ru}(\text{bpy})_2\text{Cl}_2]$ on BPY-APTES@PDA@PUF was conducted in a hydro-alcoholic solution at $95\text{ }^\circ\text{C}$ for 24 h. The black colour of BPY-APTES@PDA@PUF turned dark brown, indicating a modification of the foam coating and the probable successful coordination of the $[\text{Ru}(\text{bpy})_2]^{2+}$ moiety to the anchored 2,2'-bipyridine. Accordingly, ICP-AES measurements on several samples of $\text{Ru}(\text{bpy})_3$ -APTES@PDA@PUF revealed a mean Ru content of 2.024 ± 0.027 g/kg as well as a Si content of 1.564 ± 0.020 g/kg. Low magnification SEM images revealed a slight corrugation of the struts edges, as was observed previously for other PDA@PUF foams functionalized by a molecular catalyst via a similar silanization process.³⁶ Higher magnification images showed a rough film structure with numerous scattered PDA aggregates, typical of PDA coating on a PUF,³⁵⁻³⁶ similarly to what was observed on APTES@PDA@PUF and BPY-APTES@PDA@PUF foams (**Figure 6**). SEM micrographs combined to EDX spectroscopy revealed a relatively homogeneous distribution of C, N, O, Si and Ru over the foam surface, without apparent aggregates or segregations area, ensuring a good structural homogeneity of the material as well as a homogeneous distribution of the photocatalyst (**Figures 7 and 8**).

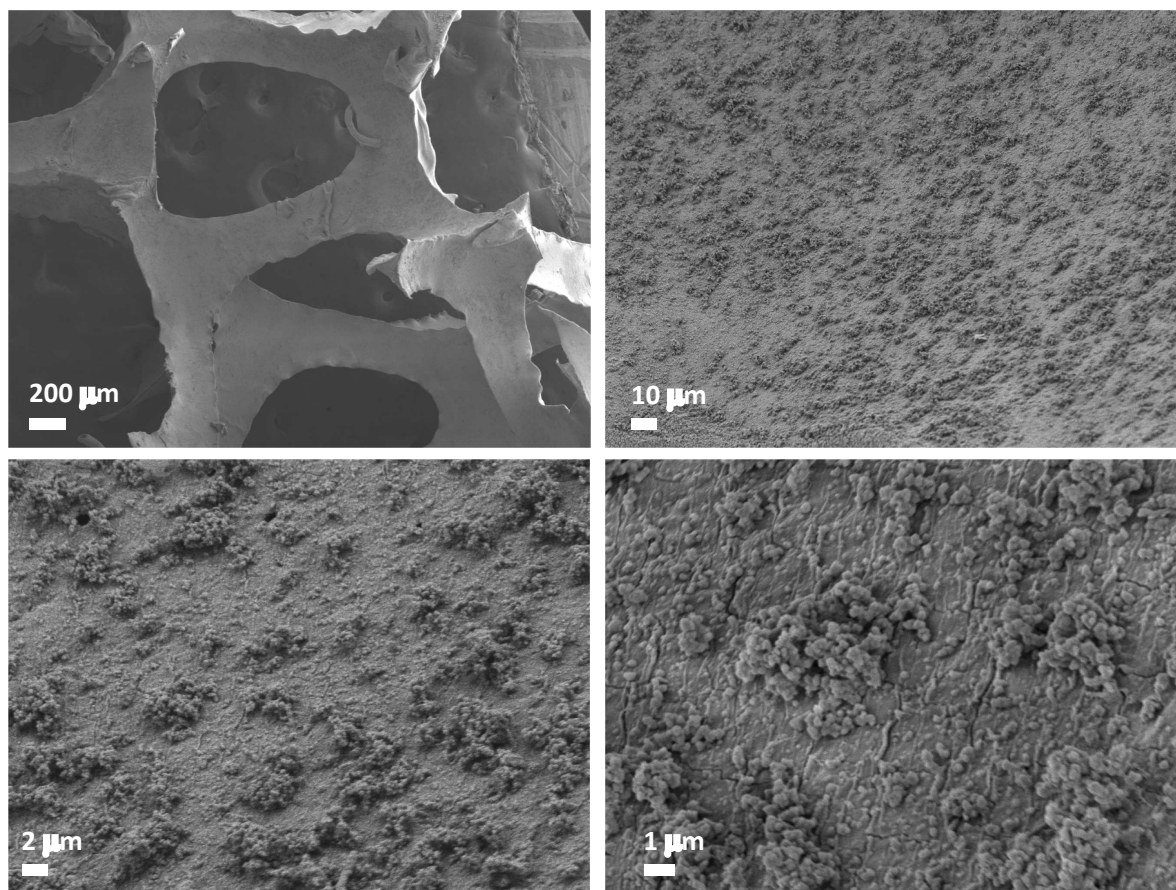


Figure 6. SEM images of as-synthesized Ru(bpy)₃-APTES@PDA@PUF with different magnifications.

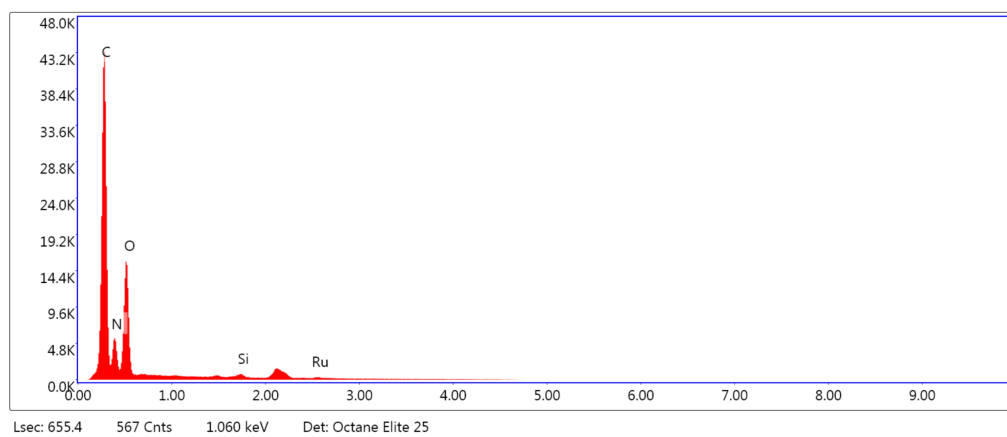


Figure 7. EDX spectrum of as-synthesized Ru(bpy)₃-APTES@PDA@PUF (corresponding to the field of view shown in **Figure 8**).

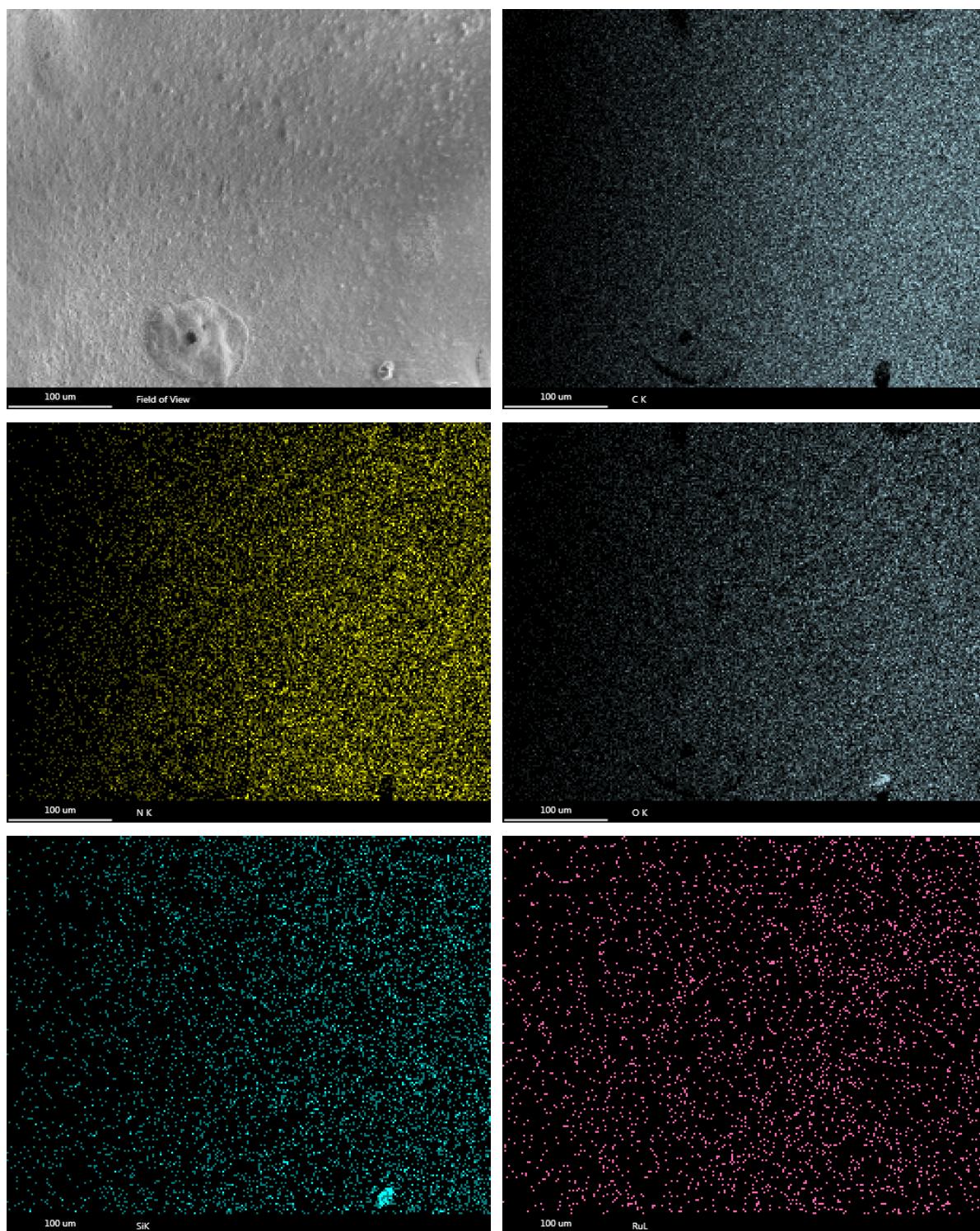


Figure 8. SEM-EDX mapping of C, N, O, Si and Ru elements on as-synthesized Ru(bpy)₃-APTES@PDA@PUF.

X-ray photoelectron spectroscopy (XPS) was performed to gain further information about the chemical composition at the topmost surface (i.e.: 9 ± 2 nm) of Ru(bpy)₃-APTES@PDA@PUF. In agreement with the result of the EDX spectroscopy, the XPS survey scan and high-resolution spectra revealed the core level of O1s, N1s, C1s, Si2p and Ru3d elements (**Figures 9** and **10**). Unfortunately, the peak value for Ru3d_{5/2} could not be

determined with precision due to the weak signal-to-noise ratio and that due to Ru3d_{3/2} could not be observed as it overlapped with the C1s peak (**Figure 10**), therefore rendering assignment to a specific ruthenium species and/or oxidation state difficult.⁴⁸

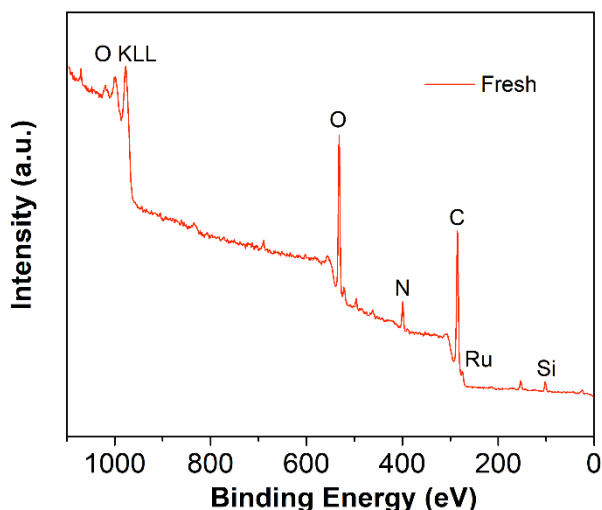


Figure 9. XPS survey spectrum of as-synthesized Ru(bpy)₃-APTES@PDA@PUF.

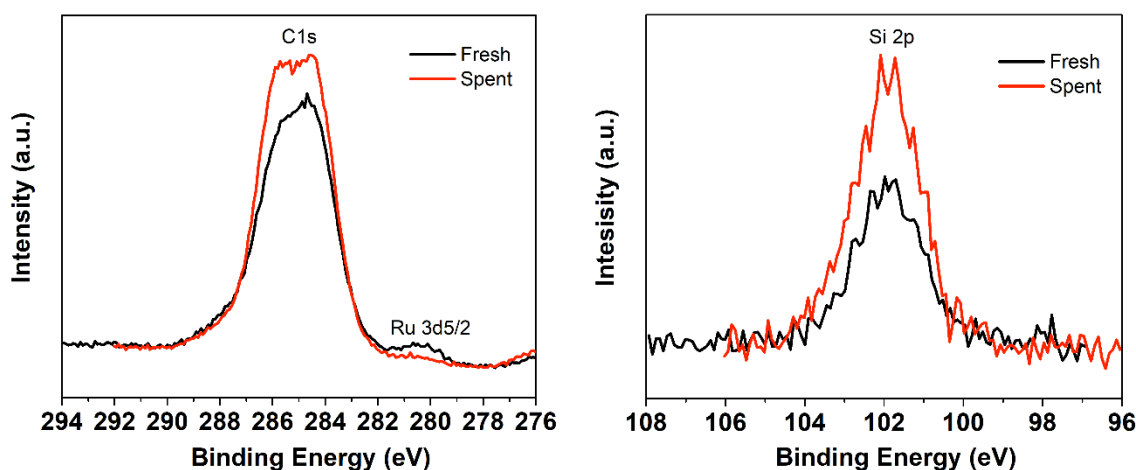


Figure 10. High resolution XPS spectra of C1s, Ru3d_{5/2} (left) and Si2p (right) core level regions of Ru(bpy)₃-APTES@PDA@PUF: as-synthesized (black), spent after six cycles of oxidative homocoupling of benzylamine (red).

II-2) Photocatalytic activity of Ru(bpy)₃-APTES@PDA@PUF

As electrophilic intermediates, imines play a crucial role in the preparation of pharmaceuticals, pesticides and fine chemicals.⁴⁹⁻⁵⁰ A strong stoichiometric oxidant such as 2-iodoxybenzoic acid or N-tert-butylbenzene-sulfinimidoyl chloride is usually required for their preparation from amines. Recently, however, efforts have been devoted to the development of heterogeneous visible-light photocatalysts for these transformations.⁴⁸ In particular,

immobilized transition metal complexes have been studied to develop functional group-tolerant photocatalytic processes, using O₂ as the oxidant.¹⁹ Herein, Ru(bpy)₃-APTES@PDA@PUF catalyst was thoroughly investigated in visible-light-induced oxidative couplings of benzylic amines under mild conditions.

Initial studies focussed on the oxidative homocoupling of benzylamine under O₂ at 30-35°C (due to LED light heating) using a cubic sample of Ru(bpy)₃-APTES@PDA@PUF of ca. 1.5 cm × 1.5 cm × 3 cm, whose mass was adjusted to have a Ru loading of 0.9 mol% as a catalyst. Solvents and lights were found to have a prominent influence on the conversion. In acetonitrile under blue light (LED, 18W), the reaction conversion reached 59 % after 24 h (Table 1, entry 1) and 90% after 48 h (entry 6). Solvents such as MeOH, toluene and CH₃CN/H₂O all proved less suitable for the reaction under similar conditions, giving much lower conversions after 24 h (entries 2-4). The use of white light (LED, 24 W) also resulted in lower conversion after 24 h (entry 5). Not surprisingly,⁵¹ the reactive rate of the supported catalyst was much slower than that of its homogeneous counterpart, [Ru(bpy)₃Cl₂],6H₂O, which achieved 84% conversion in 1 h under similar conditions (entry 7). Nevertheless, the benefit in using the foam lies in that the foam could be reused multiple times, tolerating repeated solvents rinsing and immersions without apparent deactivation, as a single sample of Ru(bpy)₃-APTES@PDA@PUF was used for these optimization studies. Furthermore, as expected, the absence of catalyst or light led to the absence of reactions conversions (entries 8 and 9), thus demonstrating that Ru-supported catalysis was at the origin of a typical photocatalytic mechanism. Finally, the use of a cubic sample of PDA@PUF (entry 10) resulted in the absence of reaction, showing that the support by itself does not affect the catalytic process.

With these optimized conditions in hands (CH₃CN, 18W blue LED light, 48 h), the scope of the homocouplings was then briefly evaluated with a single sample of Ru(bpy)₃-APTES@PDA@PUF (1.5 cm × 1.5 cm × 3 cm, 0.9 mol% Ru) (**Figure 11**). *para*-Substituted benzylamines bearing electron-donating methoxy or *t*-butyl substituents were converted in high yields (95% and 89%) within 48 h reaction time, similarly to benzylamine. In contrast, when benzylamine was *para*-substituted with electron-withdrawing substituents such as trifluoromethyl and chloride, slightly lower conversions of 77% and 82% conversion were observed after 48 h reaction, in agreement with the literature, as electron-poor benzylamines typically give lower yields in this type of oxidative couplings^{40, 43-44, 40-45}. Additionally, the photocatalytic activity of Ru(bpy)₃-APTES@PDA@PUF was explored for the oxidative homocoupling of the heterocyclic amine, 2-pyridinemethanamine, resulting in 77% conversion after 48 h. Noteworthy, the catalytic foam seemed stable and robust all along the scope study, as suggested by these results.

Table 1. Optimization of the reaction conditions for the oxidative coupling of benzylamine under visible light and O₂ using Ru(bpy)₃-APTES@PDA@PUF as photocatalyst.^a

Entry	Catalyst	Solvent	Time (h)	GC conv. (%)
1 ^b	Ru(bpy) ₃ -APTES@PDA@PUF	CH ₃ CN	24	59
2 ^b	Ru(bpy) ₃ -APTES@PDA@PUF	toluene	24	29
3 ^b	Ru(bpy) ₃ -APTES@PDA@PUF	MeOH	25	11
4 ^b	Ru(bpy) ₃ -APTES@PDA@PUF	CH ₃ CN/H ₂ O (4/1)	24	48
5 ^c	Ru(bpy) ₃ -APTES@PDA@PUF	CH ₃ CN	24	47
6 ^b	Ru(bpy) ₃ -APTES@PDA@PUF	CH ₃ CN	48	90
7 ^b	[Ru(bpy) ₃ Cl ₂], 6 H ₂ O	CH ₃ CN	1	84
8 ^d	Ru(bpy) ₃ -APTES@PDA@PUF	CH ₃ CN	24	0
9 ^b	no catalyst	CH ₃ CN	24	0
10 ^b	PDA@PUF	CH ₃ CN	24	0

^a benzylamine (0.5 mmol), Ru(bpy)₃-APTES@PDA@PUF (1.5 cm × 1.5 cm × 3 cm, 0.9 mol% Ru) or [Ru(bpy)₃Cl₂].6H₂O (8 mol%) or PDA@PUF (1.5 cm × 1.5 cm × 3 cm) or no catalyst, solvent (10 mL), O₂ balloon, visible light, 30~40 °C due to LED light heat, 1000 rpm. ^b 18 W blue LED light ^c 24 W white LED light ^d Reaction run in the dark.

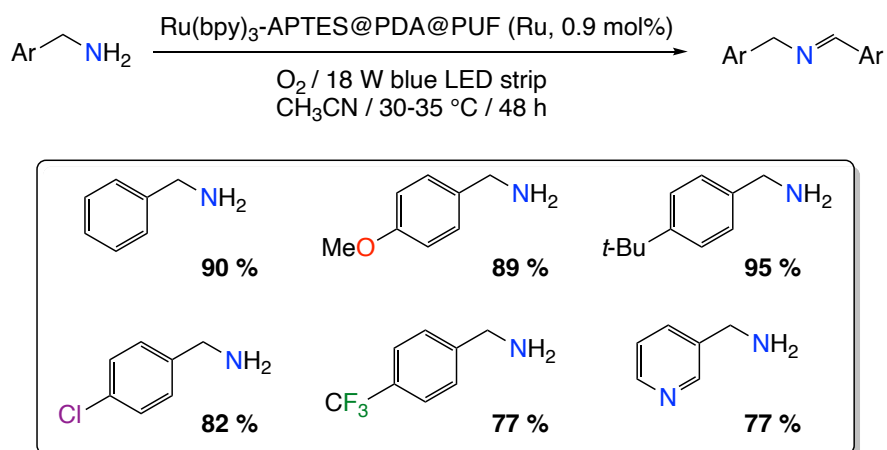


Figure 11. Oxidative homocoupling of benzylic amines using Ru(bpy)₃-APTES@PDA@PUF as photocatalyst.

In order to further probe and evaluate the photocatalytic performances of Ru(bpy)₃-APTES@PDA@PUF, oxidative C–H bond functionalizations of *N*-phenyl-tetrahydroisoquinoline were selected as a second type of model reactions given the universality

of this elegant reaction for [Ru(bpy)₃Cl₂]-mediated photocatalysis.^{19,40-42, 45} Using a cubic sample of Ru(bpy)₃-APTES@PDA@PUF of ca. 1.5 cm × 1.5 cm × 3 cm, whose mass was adjusted to have a Ru loading of 4.5 mol% as photocatalyst, O₂ as oxidant, under an 18W blue LED light, we first focused on the reaction between *N*-phenyl-tetrahydroisoquinoline and nitromethane in order to optimize the reactions conditions (**Table 1**). As observed for the oxidative homocoupling of benzylic amines, solvents were found to have a significant influence on the progress of the reaction, and, in agreement with the literature,^{19,41} methanol was found to be the one giving the best results. Thus, in methanol at ca. 35 °C, the reaction yield could reach up to 83 % after 24 h reaction when a large excess of nitromethane (20 equiv.) was used (**Table 2**).

Table 2. Optimization of the reaction conditions for the nitromethanation of *N*-phenyl-tetrahydroisoquinoline under visible light and O₂ using Ru(bpy)₃-APTES@PDA@PUF as photocatalyst.^a

Entry	Solvent	Isolated yield (%)
1	MeOH	48
2	EtOH	37
3	<i>i</i> -PrOH	33
4	MeOH/H ₂ O (1/1)	trace
5	MeOH/H ₂ O (9/1)	41
6	1,4-dioxane	-
7	CH ₃ CN	19
8	THF	-
9 ^b	MeOH	83

^a Reaction conditions: 2-phenyl-1,2,3,4-tetrahydroisoquinoline (0.1 mmol), nitromethane (1 mmol), Ru(bpy)₃-APTES@PDA@PUF (1.5 cm × 1.5 cm × 3 cm, 4.5 mol% Ru), solvent (10 mL), O₂ balloon, 18 W blue LED light, 30-35 °C due to LED light heat, 24 h, 1000 rpm. ^b Nitromethane (2 mmol).

With these conditions in hands (NuH (20 equiv.), MeOH, 18W blue LED light, 24 h), the scope of this cross dehydrogenative coupling was then evaluated with a short series of nucleophiles, using a single sample of Ru(bpy)₃-APTES@PDA@PUF (1.5 cm × 1.5 cm × 3 cm, 4.5 mol% Ru). All investigated nucleophiles, including secondary phosphine oxides, gave the desired reaction compounds in yields varying from 23 to 62% (**Figure 12**). Satisfyingly again, the heterogeneous photocatalyst proved stable throughout the reaction scope

investigation, as it could be used for one substrate after another without any apparent deactivation or inhibition.

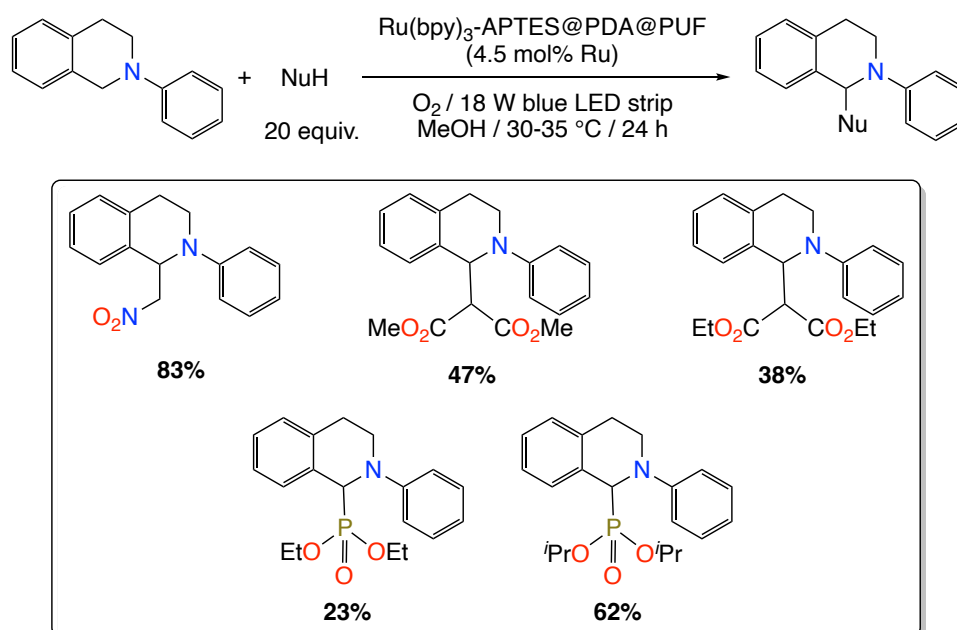


Figure 12. Photocatalytic C–C/C–P couplings of *N*-phenyl-tetrahydroisoquinoline with various nucleophiles using Ru(bpy)₃-APTES@PDA@PUF as photocatalyst.

II-3) Catalyst recycling and leaching tests

For heterogeneous catalytic systems, the recovery from liquid media and reuse of the catalyst are of great significance. With powdered catalysts, tedious and time-consuming work-up procedures, as well as problems of catalyst loss are usually inevitable. The macroscopically structured catalyst used in the present work allows one to operate the product/catalyst separation in a much easier way as the catalyst can be just taken out from the reaction medium followed by a short washing step to remove the adsorbed liquid on its surface before reuse.

To shed more light on the recycling properties of Ru(bpy)₃-APTES@PDA@PUF that could be foreseen from the optimization and scope studies (*vide supra*), six consecutive runs of benzylamine oxidative homocoupling and of *N*-phenyl-tetrahydroisoquinoline nitromethanation were conducted; each with a single sample of freshly prepared Ru(bpy)₃-APTES@PDA@PUF (1.5 cm × 1.5 cm × 3 cm, 4.5 μmol Ru) that was simply removed from the reaction medium and washed in various solvents under sonication after each run, before being reused. Strikingly, the photocatalytic activity stayed at an excellent level for the 6 runs in both reactions, with a notable improvement of the observed GC conversions or NMR yields from run 1 to 3 in the oxidative benzylamine coupling (**Figure 13A**) and from run 1 to 6 in the nitromethanation of *N*-phenyl-tetrahydroisoquinoline (**Figure 13B**). The reason for this gradual improvement of

the photocatalytic activity of Ru(bpy)₃-APTES@PDA@PUF is not clear but we suspect it could be related to a degradation of the uppermost layer of the PDA coating as suggested by the colour lightening of the foam from dark brown to brown-red or even orange depending on the considered reaction (**Figure 14**).

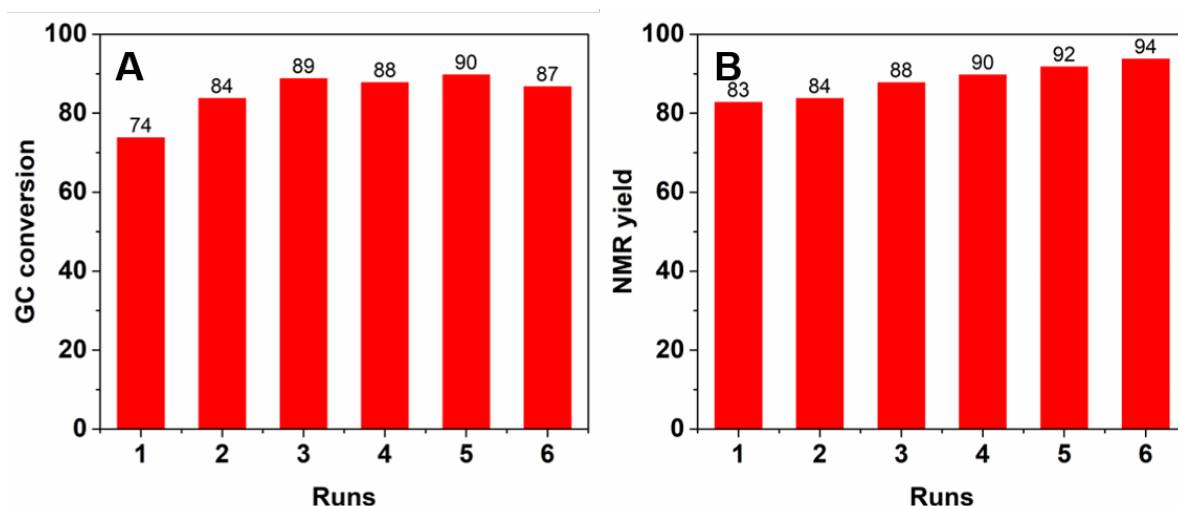


Figure 13. GC conversion and NMR yield measured over the 6 successive runs of oxidative homocoupling of benzylamine (A) and of nitromethanation of *N*-phenyl-tetrahydroisoquinoline (B) catalysed by a single sample of Ru(bpy)₃-APTES@PDA@PUF in each case. Benzylamine homocoupling conditions: benzylamine (0.5 mmol), Ru(bpy)₃-APTES@PDA@PUF (1.5 cm × 1.5 cm × 3 cm, 0.9 mol% Ru), CH₃CN (10 mL), O₂ balloon, 18 W blue LED light, ca. 35 °C, 48 h, 1000 rpm. Aza-Henry conditions: 2-phenyl-1,2,3,4-tetrahydroisoquinoline (0.1 mmol), nitromethane (2 mmol), Ru(bpy)₃-APTES@PDA@PUF (1.5 cm × 1.5 cm × 3 cm, 4.5 mol% Ru), MeOH (10 mL), O₂ balloon, 18 W blue LED light, ca. 35 °C, 24 h, 1000 rpm.

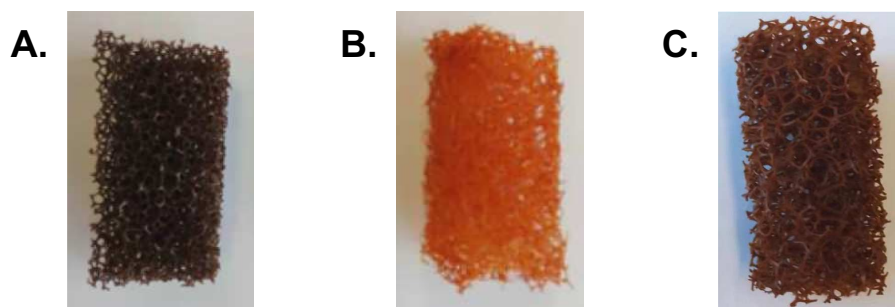


Figure 14. Photographs of Ru(bpy)₃-APTES@PDA@PUF: as-synthesized (A), spent after six cycles of oxidative homocoupling of benzylamine (B), spent after six cycles of nitromethanation of *N*-phenyl-tetrahydroisoquinoline (C).

To try to gain some insight about this apparent modification of the foam surface, the spent foam after 6 cycles of oxidative benzylamine coupling was submitted to SEM and SEM-EDX analyses. Low magnification SEM images showed a higher degree of corrugation of the struts edges (**Figure 15**), due most probably to repeated solvent swelling in the polymeric foam.³⁶ In contrast, higher magnification images revealed a smoother surface with less numerous scattered PDA aggregates (**Figure 15**), which may be at the origin of the observed colour

lightening as well as of a better access of the substrates to the immobilised Ru catalyst which, in return, could explain the progressive increase of activity observed over the cycling tests.

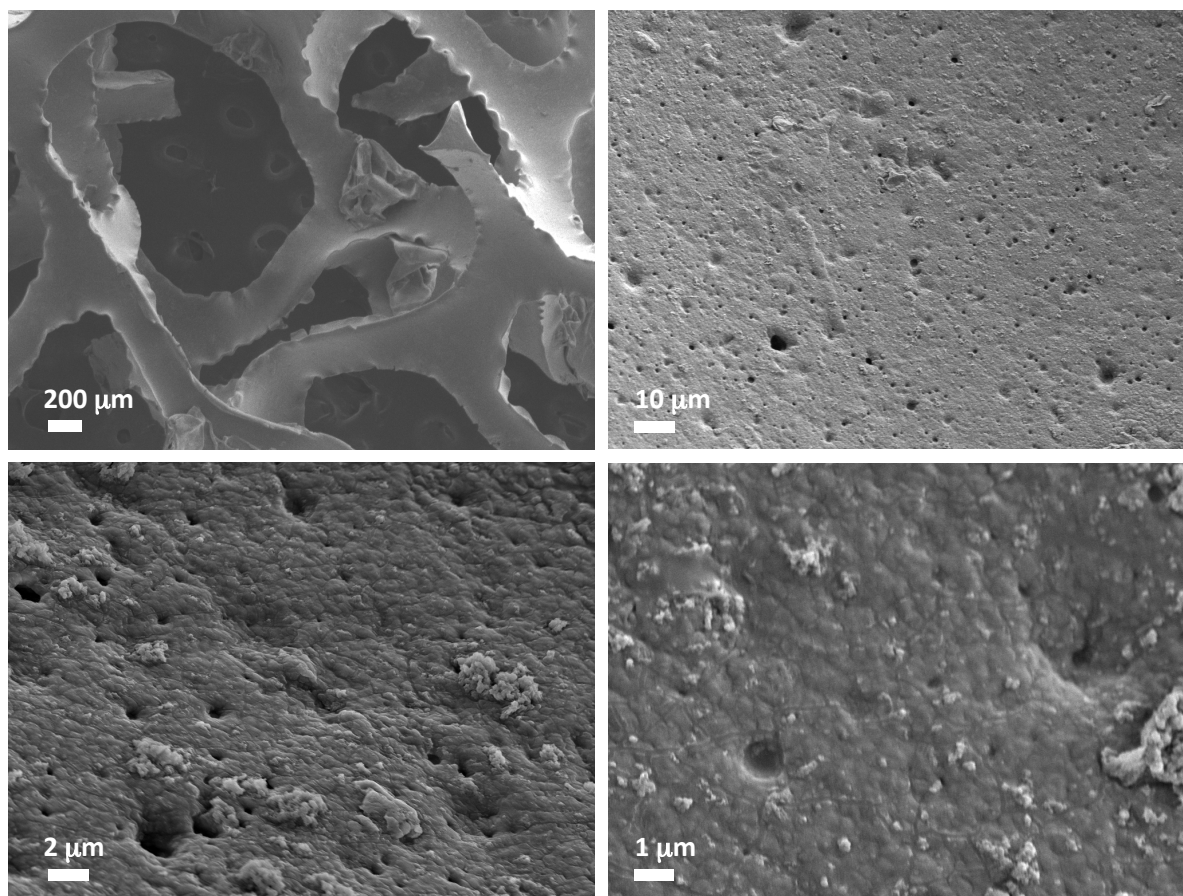


Figure 15. SEM images with different magnifications of spent Ru(bpy)₃-APTES@PDA@PUF after six cycles of oxidative homocoupling of benzylamine.

Noteworthy, the elemental distribution over the foam surface did not seem to be significantly affected by this surface smoothing as SEM-EDX elemental mapping still showed a relatively homogeneous distribution of C, N, O, Si and Ru elements over the foam surface without apparent aggregates or segregations area (**Figures 16 and 17**).

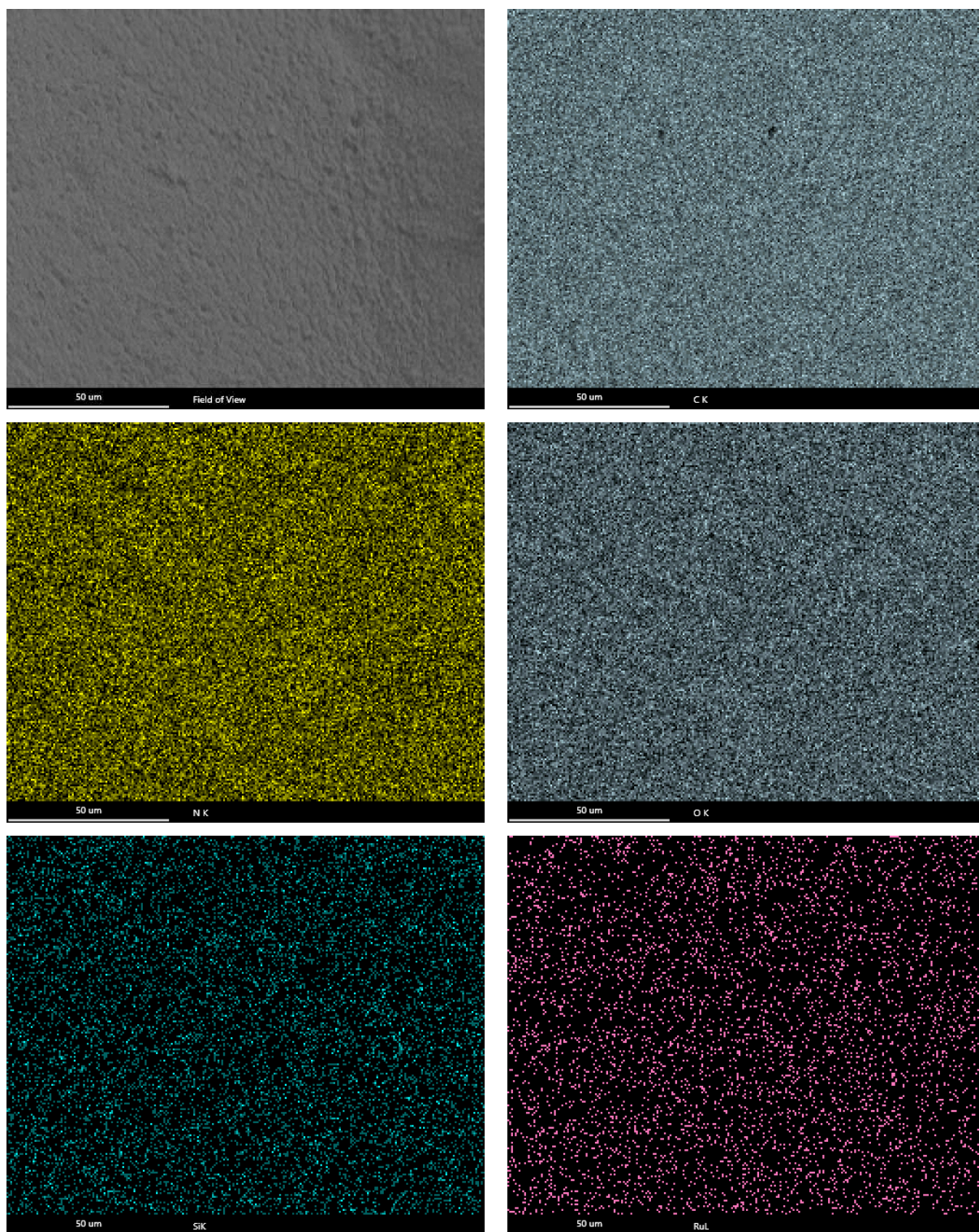


Figure 16. SEM-EDX mapping of C, N, O, Si and Ru elements on spent $\text{Ru}(\text{bpy})_3\text{-APTES@PDA@PUF}$ after six cycle of oxidative benzylamine homocoupling.

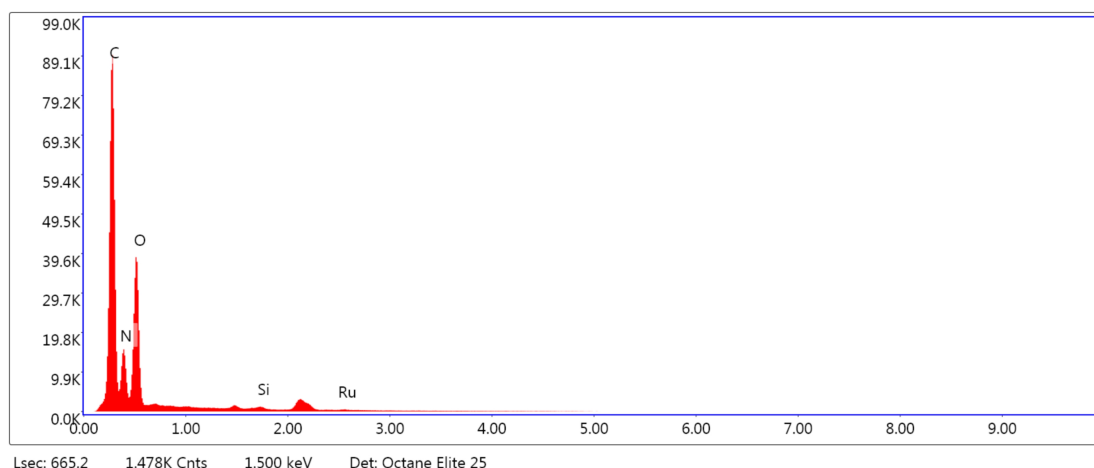


Figure 17. EDX spectrum of spent Ru(bpy)₃-APTES@PDA@PUF after six cycles of oxidative benzylamine homocoupling (corresponding to the field of view shown in **Figure 16**).

In agreement with these results, the XPS survey scan spectrum still showed the core level of O1s, N1s, C1s, Si2p and Ru3d elements (**Figure 18**). When compared to that of the as-synthesized foam, the high-resolution spectra of the C1s, Ru3d_{5/2} and Si2p core level regions however revealed that some C had been oxidized, which correlates well with the reaction conditions of the cycling tests, and that the relative level of Ru3d_{5/2} had decreased, while that of Si2p had increased, at least on the topmost surface which may explain the better accessibility of the Ru photocatalyst (**Figure 10**). This was confirmed by ICP-AES analyses of the spent Ru(bpy)₃-APTES@PDA@PUF catalytic material, which indicated a loss of Ru of about 30% (1.404 ± 0.016 g/kg vs. 2.024 ± 0.027 g/kg for the as synthesized foam) while the amount of Si level did not vary significantly (1.564 ± 0.020 to 1.633 ± 0.018 g/kg). Noteworthy this Ru loss was also confirmed by ICP-AES analyses of the reaction solutions, which indicated a similar loss of about 30% over the 6 cycles, but with decreasing amounts at each run, *i.e.*: from 3.77 ± 0.02 mg/kg in the first run to 1.56 mg/kg ± 0.01 in the last one. All this suggests that the catechol-silicon linkage, whether linear or cross-linked, was stable enough to sustain the reaction conditions along the six cycling runs, in agreement with our previous results on supported molecular catalysts bearing an alkoxysilyl anchoring arm on PDA@PUF foams. Furthermore, the fact that, despite this stability of the catechol-silicon linkage, some Ru leaching was observed, suggest however that either some Ru(bpy)₂Cl₂ was simply adsorbed on the PDA layer or more likely that the amide linkage between the siloxytriethylamino anchor and the bipyridine was not stable under the reaction conditions.

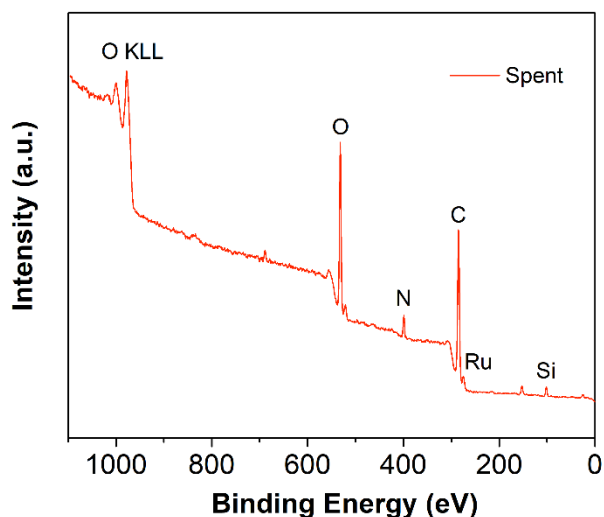


Figure 18. XPS survey spectra of spent Ru(bpy)₃-APTES@PDA@PUF after six cycles of oxidative homocoupling of benzylamine.

Finally, to evaluate the influence of the Ru leaching in the liquid reaction medium on the progress of a photocatalytic process with an as-synthesized sample of Ru(bpy)₃-APTES@PDA@PUF, a control experiment was carried out where, after 8 h reaction, the reaction solution of a *N*-phenyl-tetrahydroisoquinoline nitromethanation was split into two equal portions; one of which was allowed to continue the reaction in the presence of the catalytic foam while the other was maintained under similar conditions but without the catalytic foam. While the NMR yield was of 7% after the first 8 h reaction, it reached 60 % after 24 h in the case of the foam-catalysed reaction and only 21% in the case of the blank reaction (**Figure 19**). This shows that, at least for the first run with an as-synthesized foam, the leached Ru has a non-negligible influence on the reaction course but that most of the activity is nevertheless due to the heterogeneous catalyst.

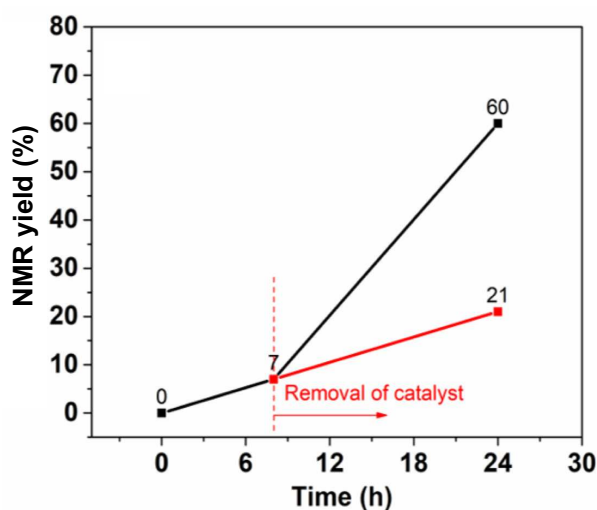


Figure 19. Leaching test with a sample of as-synthesized Ru(bpy)₃-APTES@PDA@PUF for the nitromethanation of *N*-phenyl-tetrahydroisoquinoline.

III) Conclusion and perspectives

In summary, we have prepared macroscopic Ru(bpy)₃-functionalized open cell polymeric foams that functioned as a versatile heterogeneous photocatalyst. Following a simple dip-coating protocol of an open cell polyurethane foam in an aqueous solution of dopamine, the resulting polydopamine-coated foam, PDA@PUF, was functionalized with Ru(bpy)₃²⁺ via a three-step route involving a silanization process of the mussel-inspired adhesive layer with APTES, the subsequent EDC-mediated coupling with [2,2'-bipyridine]-4-carboxylic acid and the complexation of the anchored bipyridine with [Ru(bpy)₂Cl₂].

The resulting Ru(bpy)₃-APTES@PDA@PUF material acted as an efficient heterogeneous photocatalyst for both oxidative benzylic amine homocouplings and cross dehydrogenative couplings under visible-light irradiation and molecular oxygen as a green oxygen source, and showed excellent reusability for at least 6 runs in an easy-to-carry “dip-and-play” mode allowed by its macroscopic structure. Despite the fact that about 30% ruthenium leaching was observed over the 6 cycling tests – which most probably results from the sensitivity of the amide linkage but not from that of the alkoxy-silyl anchor, as demonstrated by ICP-AES analyses – an improvement of the catalytic performances was observed over the successive cycling tests in both reactions. As suggested by a combination of photographs, SEM and XPS analyses, this unexpected improvement most likely results from a modification of the uppermost layer of polydopamine that renders the [Ru(bpy)₃]²⁺ photocatalyst more accessible.

Provided that more solid chemical links than the amide linkage will be used in the future, these results pave the way for the design of easy-to-handle long-lived heterogeneous photocatalysts whose easy-to-engineer flexible macroscopic structure with large pores allowing efficient mass transfers, low pressure drop, and easy light penetration should permit their use under flow conditions in industrial photoreactors.

IV) Experimental section

IV-1) Materials and methods

Unless otherwise stated, all reagents and solvents were used as provided by commercial suppliers without any further purification/treatment. Polyurethane open cell foams (20 PPI, TCL 40100 soft white reticulated) were given by FoamPartner. Dopamine hydrochloride (008896), EDC hydrochloride (024810), *N*-hydroxysuccinimide (005022) and 3-aminopropyltriethoxysilane (ISI0010-98) were purchased from Fluorochem. Tris base (99.9+% - T1503), ammonium acetate (≥98% - A7330), 2-acetylpyridine (≥99% - W325104) and crotonaldehyde (≥99% - 262668) were purchased from Sigma-Aldrich. 4-Chlorobenzylamine

(97+% - A13984), 4-*tert*-butylbenzylamine (98% - L20394), 3-(aminomethyl) pyridine (98+% - B23634) were provided by Alfa Aesar. 4-(Trifluoromethyl) benzylamine (97% - 375830010) was purchased from Acros Organics. 4-Methoxybenzylamine (>97.0% - M0870), 2,2'-bipyridyl (>99.0% - B0468) were provided by TCI. RuCl₃·xH₂O (40-43% Ru, 99.9% Ru - 44-5880) was purchased from Strem Chemicals. Ru(bpy)₂Cl₂·2H₂O,⁵² 2,2'-bipyridine-4-carboxylic acid⁵³⁻⁵⁴ and *N*-phenyl-tetrahydroisoquinoline⁵⁵⁻⁵⁶ were prepared according to published procedures. 18.2 MΩ deionized water (TOC < 1 ppb), supplied by a Q20 Millipore system, was used for the preparation of aqueous solutions and washing procedures with water. Purifications by column chromatography were carried out with Macherey-Nagel silica gel 60 (0.04-0.63 mm). RGB LED strip light (Govee, H6190) was manufactured by Shenzhen Intellirocks Tech Co. Ltd.

Scanning electron microscopy (SEM) measurements were recorded with a Hitachi SU8010 FE-SEM microscope at 3 kV at room temperature. No metallization of the samples was done, but their borders were covered with a metallic tape to evacuate the excess of charge.

Elemental mapping by scanning electron microscopy-energy dispersive X-ray spectroscopy (SEM-EDX) was investigated with a Zeiss Gemini SEM 500 FEG EDAX Octane Elite EDX detector. The X-rays emitted upon electron irradiation were acquired in the range 0–20 keV. Quantification was done using the standard-less ZAF correction method in the Team EDS software from EDAX.

X-ray Photoelectron Spectroscopy (XPS) was carried out in an ultrahigh vacuum (UHV) spectrometer equipped with a VSW Class WA hemispherical electron analyzer and a monochromatic Al K α X-ray source (1486.6 eV). Survey and high-resolution spectra were recorded in constant pass energy mode (90 and 22 eV, respectively). Binding energies were calibrated by referring to the C 1s peak at 284.4 eV. Shirley-type background subtraction and fitting of the spectra were done with the software package Casa XPS vs. 2.3. High resolution XPS peaks deconvolution has been accomplished with mixed Guassian-Lorentian curves using XPS Peak 4.1 software minimizing the mean squared error. The Ru 3d peak was fitted using one single Ru^{II} representing metallic and oxidized Ru species. For the fitting of C 1s five components were used corresponding to the various chemical states of the carbon support.

Inductively coupled plasma-atomic emission spectrometry (ICP-AES). For Ru loading determination, Ru(bpy)₃-APTES@PDA@PUF samples were mineralized with aqua regia (2 mL HCl, 1 mL HNO₃) at 185 °C for 50 min under pressure (Multiwave ECO, Anton Paar). A blank test was carried out in parallel under the same conditions. Ru quantification in the clear obtained solutions was realized by ICP-AES (Varian 720ES) at two wavelengths: Ru 245.657 nm and Ru 267.876 nm. Measurements were performed by the Plateforme Analytique des Inorganiques of the Institut Pluridisciplinaire Hubert Curien (UMR CNRS 7178), Strasbourg, France.

Gas chromatographic (GC) analyses were carried out on an Agilent 7820A instrument equipped with a HP-1 column (30 m, 0.35 mm, 0.25 μm), with hydrogen as gas carrier and tetradecane as the internal standard. The retention times and GC responses in terms of area versus concentration of the reagents and products were calibrated by using pure components diluted in an acetone solution at various concentrations. The conversion and product distribution were calculated from the GC results.

Solution NMR spectra were recorded at 298 K on a Bruker Avance III HD 400 MHz spectrometer operating at 400.13 MHz for ^1H and at 100.61 MHz for ^{13}C . The chemical shifts are referenced to the residual deuterated or ^{13}C solvent peaks. Chemical shifts (δ) and coupling constants (J) are expressed in ppm and Hz respectively (see the Supporting Information).

For solid-state NMR spectra, the foam samples were frozen into $\text{N}_2(l)$ and grinded. The grinded foams were then packed in 4 mm ZrO_2 rotors under air. The ^{29}Si CP-MAS experiments spectra were recorded at 298 K on a Bruker Solid State DSX 300 MHz NMR spectrometer operating at 69.66 MHz, and equipped with a Bruker 4 mm $^1\text{H}/\text{X}$ CP-MAS probe. A shaped Cross-Polarization pulse sequence with tangential modulation on both channels was used with the following parameters: the spinning speed was set to 10 kHz, the spectral width to 30 kHz, the contact time was in the range of 1 ms, the proton RF field was around 55 kHz for decoupling (using SPINAL 64 sequence) and 40 kHz for contact, with a recycle delay of 5s. The spectra were calibrated with respect an external PDMS sample (-35.1 ppm).

IV-2) Experimental procedures

IV-2-1) Open cell polyurethane foam (PUF) coating with polydopamine (PDA)

The procedure was adapted from our published procedure.³⁴⁻³⁵ Dopamine hydrochloride (2 mg/mL) was dissolved in an aqueous solution (500 mL) of Tris base (10 mM) buffered to pH 8.5 with aqueous HCl (1 M). Four cubic samples of PUF (*ca.* 1.5 cm \times 1.5 cm \times 3 cm) were immersed in the stirred solution for 17 h at RT. The solution turned quickly orange, then slowly black. The resulting PDA-coated foams (PDA@PUF) were then taken out of the solution, dried in an oven at 80 $^\circ\text{C}$ for 1.5 h, washed in vigorously stirred water (3 \times 10 min in 500 mL,) and dried again in an oven at 80 $^\circ\text{C}$.

IV-2-2) Functionalization of PDA@PUF with APTES

A cubic sample of PDA@PUF (*ca.* 1.5 cm \times 1.5 cm \times 3 cm) was washed in vigorously stirred toluene (3 \times 25 mL) at room temperature for a few minutes, and dried under vacuum prior to the functionalization.

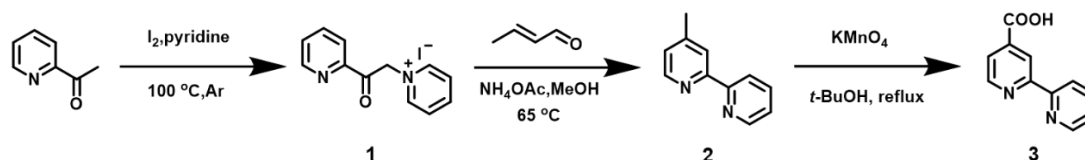
A stirring bar and the cubic sample of PDA@PUF were introduced in a Schlenk tube, that was then put under argon. This was followed by the additions of anhydrous toluene (25 mL) and APTES (0.23 mL, 1 mmol). After 24 h of stirring at 70 $^\circ\text{C}$, the resulting APTES-

functionalized foam, APTES@PDA@PUF, was removed from the reaction medium, washed for a few minutes in vigorously stirred toluene (3 × 25 mL), and then dried under vacuum.

APTES@PDA@PUF was characterized by ²⁹Si CP-MAS NMR, SEM, SEM-EDX, and ICP-AES revealing a mean Si content of 3.763 ± 0.041 g/kg.

IV-2-3) Synthesis of 2,2'-bipyridine-4-carboxylic acid

The synthesis of the 2,2'-bipyridine-4-carboxylic acid was adapted from published procedures⁵³⁻⁵⁴ through a three-step process without rigorous purification midway (**Scheme 1**).



Scheme 1. Synthetic path for the preparation of 2,2'-bipyridine-4-carboxylic acid

To iodine (20.6 g, 81.2 mmol) under argon were added pyridine (60 mL) and 2-acetylpyridine (8.3 mL, 74 mmol). The mixture was then stirred at 100 °C overnight. After the mixture was cooled to room temperature, the product was filtered and recrystallized in ethanol to afford **1** as a black solid (12.5 g, 52% yield). The collected ¹H and ¹³C{¹H} NMR data were in agreements with the literature. ¹H NMR (DMSO-*d*₆, 400.13 MHz): δ 9.07–9.01 (m, 2H, CHN), 8.88 (dt, ³J = 4.7, ⁴J = 1.3 Hz, 1H, CHN), 8.79–8.71 (m, 1H), 8.33–8.26 (m, 2H), 8.15 (td, ³J = 7.7, ⁴J = 1.7, 1H), 8.07 (dt, ³J = 7.9, ⁴J = 1.2, 1H), 7.84 (ddd, ³J = 7.6, ³J = 4.7, ⁴J = 1.4, 1H), 6.54 (s, 2H, CH₂). ¹³C{¹H} NMR (DMSO-*d*₆, 100.61 MHz): δ 191.4 (CO), 150.4 (CCO), 149.5, 146.3, 146.3, 138.1, 129.1, 127.7, 122.0, 66.6 (CH₂).

A solution of **1** (9.66 g, 30 mmol), ammonium acetate (11.4 g, 15 mmol) and crotonaldehyde (5.8 ml, 70 mmol) in MeOH (100 mL) was heated under stirring to 65 °C overnight. The solvent was then evaporated in a rotary evaporator until a little methanol remained and the resulting black oil extracted with hexane (5 × 50 mL). The combined organic extracts were washed with saturated brine and dried over MgSO₄. After removal of the solvent, crude **2** (2.2 g, 88% yield) was obtained as a dark yellow liquid without further purification. The collected ¹H NMR data were in agreements with the literature. ¹H NMR (CDCl₃, 400.13 MHz): δ 8.68 (ddd, ³J = 4.8, ⁴J = 1.8, J = 0.9, 1H), 8.54 (dd, ³J = 4.9, ⁴J = 0.8, 1H), 8.39 (dt, ³J = 8.0, ⁴J = 1.1, 1H), 8.23 (dt, ³J = 1.7, ⁴J = 0.8, 1H), 7.81 (td, ³J = 7.8, ⁴J = 1.8, 1H), 7.30 (ddd, ³J = 7.5, ³J = 4.8, ⁴J = 1.2, 1H), 7.13 (ddd, ³J = 4.9, ⁴J = 1.7, ⁴J = 0.8, 1H), 2.44 (s, 3H, CH₃).

Dispersion of **2** (1.8 g, 10.6 mmol) in *t*-BuOH/H₂O (1:1, 180 mL) was followed by the addition of KMnO₄ (3.5 g, 22.2 mmol). The reaction mixture was then refluxed for 1 h. After cooling the medium to room temperature, another portion of KMnO₄ (3.5 g, 22.2 mmol) was added, and the reaction mixture refluxed for another 18 h. The medium was then cooled to

room temperature, and filtrated through a Celite pad that was washed with ethanol (ca. 50 mL). Subsequently, most of the ethanol was removed under vacuum, and the pH of the remaining aqueous solution adjusted to 4 with concentrated aqueous HCl. The resulting white precipitate was filtrated, washed with a little amount of cold water, and dried under vacuum. The collected ^1H and $^{13}\text{C}\{^1\text{H}\}$ NMR data were in agreement with the literature and confirmed the obtention of **3** (1.2 g, 57% yield). ^1H NMR (DMSO- d_6 , 400 MHz): δ 8.88–8.85 (m, 1H), 8.82 (s, 1H), 8.72 (d, $^3J = 4.7$, 1H), 8.41 (d, $^3J = 7.9$, 1H), 7.97 (tt, $^3J = 8.0$, $^4J = 2.2$, 1H), 7.86 (dd, $^3J = 5.0$, $^4J = 1.6$, 1H), 7.49 (dd, $^3J = 7.7$, $^4J = 4.9$, 1H). $^{13}\text{C}\{^1\text{H}\}$ NMR (DMSO- d_6 , 100.61 MHz): δ 166.2 (CO), 156.4 (CCO), 154.4, 150.5, 149.6, 139.5, 137.6, 124.7, 123.1, 120.7, 119.5.

IV-2-4) Coupling of 2,2'-bipyridine-4-carboxylic acid with APTES@PDA@PUF

A cubic sample of APTES@PDA@PUF (ca. 1.5 cm \times 1.5 cm \times 3 cm) was washed for a few minutes in vigorously stirred ethanol (25 mL) at room temperature before use.

A stirring bar was introduced in a Schlenk tube. This was followed by the additions of ethanol (25 mL), 2,2'-bipyridine-4-carboxylic acid (40 mg, 0.2 mmol), *N*-hydroxysuccinimide (34 mg, 0.3 mmol) and EDC hydrochloride (0.4 mmol, 76 mg), in this order. After 0.5 h, the cubic sample of APTES@PDA@PUF was then immersed into the stirred solution for 20 h at room temperature. The resulting bipyridine-coupled foam, BPY-APTES@PDA@PUF, was then washed in acetone (3 \times 30 mL), water (2 \times 30 mL) and ethanol (2 \times 30 mL), and dried under vacuum.

BPY-APTES@PDA@PUF was characterized by SEM and ICP-AES revealing a mean Si content of 2.462 ± 0.025 g/kg.

IV-2-5) Synthesis of *cis*-[Ru(bpy) $_2$ Cl $_2$] \cdot 2H $_2$ O

The synthesis was adapted from a published procedure.⁵² Ruthenium(III) chloride trihydrate (2 g, 8.2 mmol), 2,2'-bipyridine (2.59 g, 16.6 mmol), and LiCl (2.33 g, 55.0 mmol) were dissolved in reagent grade *N,N*-dimethylformamide (67 mL) in a 100 mL round-bottomed flask equipped with a reflux condenser. The mixture was stirred and refluxed overnight by heating in an oil bath. After it was cooled to room temperature, the reaction medium was poured into acetone (340 mL) and then placed in freezer at -28 °C to allow crystallization. The resulting dark violet solid (1.04 g, 24.3% yield) was collected by filtration, washed with acetone, water and diethyl ether, and then dried under vacuum. The collected ^1H and $^{13}\text{C}\{^1\text{H}\}$ NMR data are in agreement with the literature. ^1H NMR (DMSO- d_6 , 400.13 MHz): δ 9.97 (ddd, $^3J = 5.6$, $^4J = 1.6$, $^4J = 0.7$ Hz, 1H), 8.64 (dt, $^3J = 8.2$, $^4J = 1.2$, 1H), 8.51–8.45 (m, 1H), 8.09–8.03 (m, 1H), 7.77 (ddd, $^3J = 7.3$, $^3J = 5.6$, $^4J = 1.3$, 1H), 7.68 (ddd, $^3J = 8.1$, $^3J = 7.4$, $^4J = 1.5$, 1H), 7.51 (ddd, $^3J = 5.7$, $^4J = 1.5$, $^4J = 0.7$, 1H), 7.10 (ddd, $J = 7.3$, 5.8, 1.4 Hz, 1H). $^{13}\text{C}\{^1\text{H}\}$ NMR (DMSO- d_6 , 100.61 MHz): δ 160.2, 158.2, 153.2, 152.0, 134.6, 133.3, 125.3, 125.3, 122.8,

122.5.

IV-2-6) Coordination of *cis*-[Ru(bpy)₂Cl₂]-2H₂O on BPY-APTES@PDA@PUF

A stirring bar and the cubic sample of BPY-APTES@PDA@PUF (ca. 1.5 cm × 1.5 cm × 3 cm) were introduced in a Schlenk tube. This was followed by the addition of 25 mL of H₂O/EtOH (1:1) and of Ru(bpy)₂Cl₂·2H₂O (52 mg, 0.1 mmol). The reaction medium was then heated under stirring by putting the tube in an oil bath at 95 °C. After 24 h reaction, the resulting Ru-coordinated foam, Ru(bpy)₃-APTES@PDA@PUF, was removed from the solution and then rinsed with ethanol (3 × 30 mL), H₂O (2 × 30 mL), and acetonitrile (2 × 30 mL).

Ru(bpy)₃-APTES@PDA@PUF was characterized by SEM-EDX, XPS, and ICP-AES revealing a mean Si content of 1.564 ± 0.020 g/kg and Ru content of 2.024 ± 0.027 g/kg).

IV-2-7) Synthesis of *N*-phenyl-tetrahydroisoquinoline

The synthesis was adapted from published procedures.⁵⁵⁻⁵⁶ In a 50 mL Schlenk tube were placed copper(I) iodide (190 mg, 1 mmol) and potassium phosphate (4.25 g, 20.0 mmol). The tube was evacuated under vacuum and backfilled with argon several times. 2-Propanol (10.0 mL), ethylene glycol (1.1 mL, 20.0 mmol), 1,2,3,4-tetrahydroisoquinoline (1.90 mL, 15.0 mmol) and iodobenzene (1.1 mL, 10.0 mmol) were added successively via syringes at room temperature. The reaction mixture was heated at 90 °C for 24 h and then allowed to cool to room temperature. Diethyl ether (50 mL) and water (70 mL) were then added. The aqueous layer was separated and extracted with diethyl ether (2 × 50 mL). The combined organic extracts were washed with brine and dried over magnesium sulfate. After solvent removal under vacuum, the remaining residue was purified via flash column chromatography on silica (petroleum ether/ethyl acetate, 40:1) to give the desired product as a dark yellow oil (541 mg, 26% yield). The collected ¹H and ¹³C{¹H} NMR data were in agreements with the literature. ¹H NMR (CDCl₃, 400.13 MHz): δ 7.33–7.27 (m, 2H, H_{Ar}), 7.21–7.13 (m, 4H, H_{Ar} and *m*-H_{Ph}), 6.99 (dt, ³J = 7.8, ⁴J = 1.1, 2H, *o*-H_{Ph}), 6.83 (tt, ³J = 7.3, ⁴J = 1.1 Hz, 1H, *p*-H_{Ph}), 4.42 (s, 2H, CH₂N), 3.57 (t, ³J = 5.9 Hz, 2H, CH₂CH₂N), 3.00 (t, *J* = 5.8 Hz, 2H, CH₂CH₂N). ¹³C{¹H} NMR (CDCl₃, 100.61 MHz): δ 150.7 (*ipso*-H_{Ph}), 135.0 (H_{Ar}), 134.6 (H_{Ar}), 129.4 (*m*-H_{Ph}), 128.7 (H_{Ar}), 126.7 (H_{Ar}), 126.5 (H_{Ar}), 126.2 (H_{Ar}), 118.8 (*p*-H_{Ph}), 115.3 (*o*-H_{Ph}), 50.9 (CH₂N), 46.7 (CH₂N), 29.3 (CH₂CH₂N).

IV-2-8) General procedure for the oxidative homocoupling of benzylic amines photocatalyzed by Ru(bpy)₃-APTES@PDA@PUF

A stirring bar and the cubic sample of Ru(bpy)₃-APTES@PDA@PUF of ca. 1.5 cm × 1.5 cm × 3 cm, whose mass (225 mg) was adjusted in function of its Ru content established by ICP-AES (0.202 wt%) to have a Ru loading of 4.5 μmol, were introduced in a Schlenk tube.

Acetonitrile (10 mL) was then added to immerse totally the foam. This was followed by the addition of the benzylamine (0.5 mmol). The tube was then closed with a rubber septum, its atmosphere quickly evacuated under vacuum and backfilled with O₂ several times. Under O₂, supplied by a balloon, the tube was placed under the irradiation of an 18 W LED blue light and the mixture was stirred (1000 rpm) at room temperature for 48 h. It is noteworthy that light irradiation induced some heat aggregation around the Schlenk tube but the temperature did never exceed 35 °C. The conversion of the amines to the imines was determined by GC and/or by ¹H NMR spectroscopy after solvent removal.

IV-2-9) General procedure for the cross-dehydrogenative couplings photocatalyzed by Ru(bpy)₃-APTES@PDA@PUF

A stirring bar and the cubic sample of Ru(bpy)₃-APTES@PDA@PUF of ca. 1.5 cm × 1.5 cm × 3 cm, whose mass (225 mg) was adjusted in function of its Ru content established by ICP-AES (0.202 wt%) to have a Ru loading of 4.5 μmol, were introduced in a Schlenk tube. Methanol (10 mL) was then added to immerse totally the foam. This was followed by the addition of N-phenyl-tetrahydroisoquinoline (21 mg, 0.1 mmol) and of the nucleophile (2 mmol). The tube was then closed with a rubber septum, its atmosphere quickly evacuated under vacuum and backfilled with O₂ several times. Under O₂, supplied by a balloon, the tube was placed under the irradiation of an 18 W LED blue light and the mixture was stirred (1000 rpm) at room temperature for 24 h. It is noteworthy that light irradiation induced some heat aggregation around the Schlenk tube but the temperature did never exceed 35 °C. The conversion was determined by ¹H NMR spectroscopy after solvent removal.

IV-2-10) Ru(bpy)₃-APTES@PDA@PUF recovery and reuse in successive photocatalytic experiments

The above-described general procedures for the photocatalytic benzylamine oxidative couplings and N-phenyl-tetrahydroisoquinoline alkylations were followed using benzylamine (55 μL, 0.5 mmol) for the oxidative homocouplings, N-phenyl-tetrahydroisoquinoline (21 mg, 0.1 mmol) and nitromethane (107 μL, 2 mmol) for the aza-Henry alkylations, and a cubic sample of Ru(bpy)₃-APTES@PDA@PUF of ca. 1.5 cm × 1.5 cm × 3 cm (225 mg, 0.202 wt% Ru, *i.e.*: 4.5·10⁻³ mmol) as catalyst for each reaction type. After each photocatalytic run, the Ru(bpy)₃-APTES@PDA@PUF foam was removed from the reaction medium, washed by immersing it successively in acetone (3 × 15 mL) and H₂O (3 × 15 mL) for 30 min under sonication each time, and then dried under vacuum.

IV-2-11) Ru leaching influence on the course of a photocatalytic process

In this control experiment aiming at evaluating the importance of ruthenium leaching on

the reaction progress of a cross dehydrogenative coupling, the above-described general procedure was followed using N-phenyl-tetrahydroisoquinoline (21 mg, 0.1 mmol), nitromethane (107 μ L, 2 mmol), and a cubic sample of as-synthesized Ru(bpy)₃-APTES@PDA@PUF of ca. 1.5 cm \times 1.5 cm \times 3 cm (225 mg, 0.202 wt% Ru, i.e.: 4.5 \cdot 10⁻³ mmol) as catalyst, excepted that, after 8 h reaction, an aliquot (50 μ L) of the medium was removed to monitor the progress of the reaction by ¹H NMR and 10 mL of methanol was added to the medium. The reaction medium was then immediately split into two equal portions of 10 mL - one with the photocatalytic foam and the other without the foam - that were each allowed to continue to react under similar conditions (ca. 30-35 °C, O₂, 18W LED blue light). After 16 h more, the courses of both the blank and foam-catalyzed reactions were monitored by removing aliquots (50 μ L) and analysing them by ¹H NMR.

V) References

1. Arias-Rotondo, D. M.; McCusker, J. K., The photophysics of photoredox catalysis: a roadmap for catalyst design. *Chem. Soc. Rev.* **2016**, *45* (21), 5803-5820.
2. Prier, C. K.; Rankic, D. A.; MacMillan, D. W., Visible light photoredox catalysis with transition metal complexes: applications in organic synthesis. *Chem. Rev.* **2013**, *113* (7), 5322-5363.
3. Nicewicz, D. A.; MacMillan, D. W., Merging photoredox catalysis with organocatalysis: the direct asymmetric alkylation of aldehydes. *Science* **2008**, *322* (5898), 77-80.
4. Li, M.; Sang, Y.; Xue, X.-S.; Cheng, J.-P., Origin of Stereocontrol in Photoredox Organocatalysis of Asymmetric α -Functionalizations of Aldehydes. *J. Org. Chem.* **2018**, *83* (6), 3333-3338.
5. Narayanam, J. M.; Tucker, J. W.; Stephenson, C. R., Electron-transfer photoredox catalysis: development of a tin-free reductive dehalogenation reaction. *J. Am. Chem. Soc.* **2009**, *131* (25), 8756-8757.
6. Beatty, J. W.; Stephenson, C. R., Amine functionalization via oxidative photoredox catalysis: methodology development and complex molecule synthesis. *Acc. Chem. Res.* **2015**, *48* (5), 1474-1484.
7. Zou, Y. Q.; Chen, J. R.; Liu, X. P.; Lu, L. Q.; Davis, R. L.; Jørgensen, K. A.; Xiao, W. J., Highly efficient aerobic oxidative hydroxylation of arylboronic acids: photoredox catalysis using visible light. *Angew. Chem. Int. Ed.* **2012**, *51* (3), 784-788.
8. Ischay, M. A.; Anzovino, M. E.; Du, J.; Yoon, T. P., Efficient visible light photocatalysis of [2+2] enone cycloadditions. *J. Am. Chem. Soc.* **2008**, *130* (39), 12886-12887.
9. Yoon, T. P.; Ischay, M. A.; Du, J., Visible light photocatalysis as a greener approach to photochemical synthesis. *Nat. Chem.* **2010**, *2* (7), 527-532.
10. Yoon, T. P., Visible light photocatalysis: The development of photocatalytic radical ion

- cycloadditions. *ACS Catal.* **2013**, 3 (5), 895-902.
11. Pali, P.; Shukla, G.; Saha, P.; Singh, M. S., Photo-oxidative Ruthenium(II)-Catalyzed Formal [3 + 2] Heterocyclization of Thioamides to Thiadiazoles. *Org. Lett.* **2021**, 23 (10), 3809-3813.
 12. Zhao, L.-M.; Lei, T.; Liao, R.-Z.; Xiao, H.; Chen, B.; Ramamurthy, V.; Tung, C.-H.; Wu, L.-Z., Visible-Light-Triggered Selective Intermolecular [2+2] Cycloaddition of Extended Enones: 2-Oxo-3-enoates and 2,4-Dien-1-ones with Olefins. *J. Org. Chem.* **2019**, 84 (14), 9257-9269.
 13. Zhang, K.; Qiao, L.; Xie, J.; Lin, Z.; Li, H.; Lu, P.; Wang, Y., Visible-Light-Induced C(sp²)-C(sp³) Coupling Reaction for the Regioselective Synthesis of 3-Functionalized Coumarins. *J. Org. Chem.* **2021**, 86 (14), 9552-9562.
 14. Zhang, H.-Y.; Chen, J.; Lu, C.-C.; Han, Y.-P.; Zhang, Y.; Zhao, J., Visible-Light-Induced C(sp²)-C(sp³) Cross-Dehydrogenative-Coupling Reaction of N-Heterocycles with N-Alkyl-N-methylanilines under Mild Conditions. *J. Org. Chem.* **2021**, 86 (17), 11723-11735.
 15. Jouffroy, M.; Primer, D. N.; Molander, G. A., Base-Free Photoredox/Nickel Dual-Catalytic Cross-Coupling of Ammonium Alkylsilicates. *J. Am. Chem. Soc.* **2016**, 138 (2), 475-478.
 16. Xu, J.; Jung, K.; Boyer, C., Oxygen tolerance study of photoinduced electron transfer-reversible addition-fragmentation chain transfer (PET-RAFT) polymerization mediated by Ru(bpy)₃Cl₂. *Macromolecules* **2014**, 47 (13), 4217-4229.
 17. Yeow, J.; Xu, J.; Boyer, C., Polymerization-Induced Self-Assembly Using Visible Light Mediated Photoinduced Electron Transfer-Reversible Addition-Fragmentation Chain Transfer Polymerization. *ACS Macro Letters* **2015**, 4 (9), 984-990.
 18. Douglas, J. J.; Sevrin, M. J.; Stephenson, C. R. J., Visible Light Photocatalysis: Applications and New Disconnections in the Synthesis of Pharmaceutical Agents. *Org. Proc. Res. Dev.* **2016**, 20 (7), 1134-1147.
 19. Yakushev, A. A.; Abel, A. S.; Averin, A. D.; Beletskaya, I. P.; Cheprakov, A. V.; Ziankou, I. S.; Bonneviot, L.; Bessmertnykh-Lemeune, A., Visible-light photocatalysis promoted by solid- and liquid-phase immobilized transition metal complexes in organic synthesis. *Coord. Chem. Rev.* **2022**, 458, 214331.
 20. Hsieh, H.-W.; Coley, C. W.; Baumgartner, L. M.; Jensen, K. F.; Robinson, R. I., Photoredox Iridium-Nickel Dual-Catalyzed Decarboxylative Arylation Cross-Coupling: From Batch to Continuous Flow via Self-Optimizing Segmented Flow Reactor. *Org. Proc. Res. Dev.* **2018**, 22 (4), 542-550.
 21. Mori, K.; Tatsumi, D.; Iwamoto, T.; Masui, Y.; Onaka, M.; Yamashita, H., Ruthenium(II)-Bipyridine/NanoC₃N₄ Hybrids: Tunable Photochemical Properties by

- Using Exchangeable Alkali Metal Cations. *Chem. Asian J.* **2018**, *13* (10), 1348-1356.
22. Li, X.; Hao, Z.; Zhang, F.; Li, H., Reduced graphene oxide-immobilized tris(bipyridine)ruthenium(II) complex for efficient visible-light-driven reductive dehalogenation reaction. *ACS Appl. Mater. Interfaces* **2016**, *8* (19), 12141-12148.
23. Pang, J.; Yuan, S.; Qin, J.-S.; Lollar, C. T.; Huang, N.; Li, J.; Wang, Q.; Wu, M.; Yuan, D.; Hong, M.; Zhou, H.-C., Tuning the ionicity of stable metal-organic frameworks through ionic linker installation. *J. Am. Chem. Soc.* **2019**, *141* (7), 3129-3136.
24. Wu, Y.-P.; Yang, B.; Tian, J.; Yu, S.-B.; Wang, H.; Zhang, D.-W.; Liu, Y.; Li, Z.-T., Postmodification of a supramolecular organic framework: visible-light-induced recyclable heterogeneous photocatalysis for the reduction of azides to amines. *Chem. Commun.* **2017**, *53* (100), 13367-13370.
25. Xie, A.; Zhang, K.; Wu, F.; Wang, N.; Wang, Y.; Wang, M., Polydopamine nanofilms as visible light-harvesting interfaces for palladium nanocrystal catalyzed coupling reactions. *Catal. Sci. Technol.* **2016**, *6* (6), 1764-1771.
26. Lee, M.; Kim, J. U.; Lee, J. S.; Lee, B. I.; Shin, J.; Park, C. B., Mussel-Inspired Plasmonic Nanohybrids for Light Harvesting. *Adv. Mater.* **2014**, *26* (26), 4463-4468.
27. Lefebvre, L.; Kelber, J.; Jierry, L.; Ritleng, V.; Edouard, D., Polydopamine-coated open cell polyurethane foam as an efficient and easy-to-regenerate soft structured catalytic support (S2CS) for the reduction of dye. *J. Environ. Chem. Eng.* **2017**, *5* (1), 79 - 85.
28. Kim, J. H.; Lee, M.; Park, C. B., Polydopamine as a Biomimetic Electron Gate for Artificial Photosynthesis. *Angew. Chem. Int. Ed.* **2014**, *53* (25), 6364-6368.
29. Xia, P.; Liu, M.; Cheng, B.; Yu, J.; Zhang, L., Dopamine Modified g-C₃N₄ and Its Enhanced Visible-Light Photocatalytic H₂-Production Activity. *ACS Sustainable Chem. Eng.* **2018**, *6* (7), 8945-8953.
30. Yu, Z.; Li, F.; Yang, Q.; Shi, H.; Chen, Q.; Xu, M., Nature-Mimic Method To Fabricate Polydopamine/Graphitic Carbon Nitride for Enhancing Photocatalytic Degradation Performance. *ACS Sustainable Chem. Eng.* **2017**, *5* (9), 7840-7850.
31. Wang, H.; Lin, Q.; Yin, L.; Yang, Y.; Qiu, Y.; Lu, C.; Yang, H., Biomimetic Design of Hollow Flower-Like g-C₃N₄@PDA Organic Framework Nanospheres for Realizing an Efficient Photoreactivity. *Small* **2019**, *15* (16), 1900011.
32. Zhang, C.; Yang, H.-C.; Wan, L.-S.; Liang, H.-Q.; Li, H.; Xu, Z.-K., Polydopamine-Coated Porous Substrates as a Platform for Mineralized β -FeOOH Nanorods with Photocatalysis under Sunlight. *ACS Appl. Mater. Interfaces* **2015**, *7* (21), 11567-11574.
33. Mao, W.-X.; Lin, X.-J.; Zhang, W.; Chi, Z.-X.; Lyu, R.-W.; Cao, A.-M.; Wan, L.-J., Core-shell structured TiO₂@polydopamine for highly active visible-light photocatalysis. *Chem. Commun.* **2016**, *52* (44), 7122-7125.
34. Edouard, D.; Ritleng, V.; Jierry, L.; Chau, N. T. T., Method for modifying the surface

- properties of elastomer cellular foams. WO 2016012689A2. 2016.
35. Pardieu, E.; Chau, N. T. T.; Dintzer, T.; Romero, T.; Favier, D.; Roland, T.; Edouard, D.; Jierry, L.; Ritleng, V., Polydopamine-coated open cell polyurethane foams as an inexpensive, flexible yet robust catalyst support: a proof of concept. *Chem. Commun.* **2016**, 52 (25), 4691-4693.
 36. Ait Khouya, A.; Martinez, M. L. M.; Bertani, P.; Romero, T.; Favier, D.; Roland, T.; Guidal, V.; Bellière-Baca, V.; Edouard, D.; Jierry, L.; Ritleng, V., Coating of polydopamine on polyurethane open cell foams to design soft structured supports for molecular catalysts. *Chem. Commun.* **2019**, 55 (79), 11960-11963.
 37. Lefebvre, L.; Kelber, J.; Mao, X.; Ponzio, F.; Agusti, G.; Vigier-Carrière, C.; Ball, V.; Jierry, L.; Ritleng, V.; Edouard, D., Borohydride-functionalized polydopamine-coated open cell polyurethane foam as a reusable soft structured material for reduction reactions: Application to the removal of a dye. *Environ. Prog. Sustain. Energy* **2019**, 38 (2), 329-335.
 38. Birba, L.; Ritleng, V.; Jierry, L.; Agusti, G.; Fongarland, P.; Edouard, D., An efficient bio-inspired catalytic tool for hydrogen release at room temperature from a stable borohydride solution. *Int. J. Energy Res.* **2020**, 44 (13), 10612-10627.
 39. Ponzio, F.; Kelber, J.; Birba, L.; Rekab, K.; Ritleng, V.; Jierry, L.; Edouard, D., Polydopamine film coating on polyurethane foams as efficient "sunscreen". Application to photocatalysis under UV irradiation. *Environ. Technol. Innov.* **2021**, 23, 101618.
 40. Chen, J.; Cen, J.; Xu, X.; Li, X., The application of heterogeneous visible light photocatalysts in organic synthesis. *Catal. Sci. Technol.* **2016**, 6 (2), 349-362.
 41. Condie, A. G.; González-Gómez, J. C.; Stephenson, C. R. J., Visible-Light Photoredox Catalysis: Aza-Henry Reactions via C-H Functionalization. *J. Am. Chem. Soc.* **2010**, 132 (5), 1464-1465.
 42. Zhi, Y.; Ma, S.; Xia, H.; Zhang, Y.; Shi, Z.; Mu, Y.; Liu, X., Construction of donor-acceptor type conjugated microporous polymers: A fascinating strategy for the development of efficient heterogeneous photocatalysts in organic synthesis. *Appl. Catal. B* **2019**, 244, 36-44.
 43. Lan, X.; Liu, X.; Zhang, Y.; Li, Q.; Wang, J.; Zhang, Q.; Bai, G., Unveiling Charge Dynamics in Acetylene-Bridged Donor- π -Acceptor Covalent Triazine Framework for Enhanced Photoredox Catalysis. *ACS Catal.* **2021**, 11 (12), 7429-7441.
 44. Li, S.; Li, L.; Li, Y.; Dai, L.; Liu, C.; Liu, Y.; Li, J.; Lv, J.; Li, P.; Wang, B., Fully Conjugated Donor-Acceptor Covalent Organic Frameworks for Photocatalytic Oxidative Amine Coupling and Thioamide Cyclization. *ACS Catal.* **2020**, 10 (15), 8717-8726.
 45. Wang, C.; Xie, Z.; deKrafft, K. E.; Lin, W., Light-Harvesting Cross-Linked Polymers for Efficient Heterogeneous Photocatalysis. *ACS Appl. Mater. Interfaces* **2012**, 4 (4), 2288-

2294.

46. Albert, K.; Pfeleiderer, B.; Bayer, E.; Schnabel, R., Characterization of chemically modified glass surfaces by ^{13}C and ^{29}Si CP/MAS NMR spectroscopy. *J. Colloid Interf. Sci.* **1991**, *142* (1), 35-40.
47. Vejayakumaran, P.; Rahman, I. A.; Sipaut, C. S.; Ismail, J.; Chee, C. K., Structural and thermal characterizations of silica nanoparticles grafted with pendant maleimide and epoxide groups. *J. Colloid Interf. Sci.* **2008**, *328* (1), 81-91.
48. Balcerzak, J.; Redzynia, W.; Tyczkowski, J., In-situ XPS analysis of oxidized and reduced plasma deposited ruthenium-based thin catalytic films. *Appl. Surf. Sci.* **2017**, *426*, 852-855.
49. Martin, S. F., Recent applications of imines as key intermediates in the synthesis of alkaloids and novel nitrogen heterocycles. *Pure Appl. Chem.* **2009**, *81* (2), 195-204.
50. Iwanejko, J.; Wojaczyńska, E., Cyclic imines—preparation and application in synthesis. *Org. Biomol. Chem.* **2018**, *16* (40), 7296-7314.
51. Hübner, S.; de Vries, J. G.; Farina, V., Why Does Industry Not Use Immobilized Transition Metal Complexes as Catalysts? *Adv. Synth. Catal.* **2016**, *358* (1), 3-25.
52. Lay, P. A.; Sargeson, A. M.; Taube, H.; Chou, M. H.; Creutz, C., Cis-Bis(2,2-Bipyridine-N,N') Complexes of Ruthenium (III)/(II) and Osmium (III)/(II). *Inorg. Synth.* **1986**, 291-299.
53. Huang, Y.; Lin, Q.; Wu, J.; Fu, N., Design and synthesis of a squaraine based near-infrared fluorescent probe for the ratiometric detection of Zn^{2+} ions. *Dyes Pigm.* **2013**, *99* (3), 699-704.
54. Constable, E. C.; Figgemeier, E.; Housecroft, C. E.; Olsson, J.; Zimmermann, Y. C., Electrochemical probing of ground state electronic interactions in polynuclear complexes of a new heteroditopic ligand. *Dalton Trans.* **2004**, (13), 1918-1927.
55. Kwong, F. Y.; Klapars, A.; Buchwald, S. L., Copper-catalyzed coupling of alkylamines and aryl iodides: An efficient system even in an air atmosphere. *Org. Lett.* **2002**, *4* (4), 581-584.
56. Ma, P.; Liu, Y.; Chen, L.; Zhao, X.; Yang, B.; Zhang, J., Photocatalyst-and additive-free decarboxylative alkylation of N-aryl tetrahydroisoquinolines induced by visible light. *Org. Chem. Front.* **2021**, *8* (11), 2473-2479.

Chapter II

Polydopamine-coated polyurethane foams as a structured support for the development of an easily reusable heterogeneous photocatalyst based on Eosin Y

Chapter II

Polydopamine-coated polyurethane foams as a structured support for the development of an easily reusable heterogeneous photocatalyst based on Eosin Y

Table of contents

I) Introduction.....	99
II) Results and discussion	108
II-1) Preparation and characterization of EY-APTES@PDA@PUF based on post-functionalization of PDA@PUF.....	108
II-2) Photocatalytic studies	111
III) Conclusion and perspectives	120
IV) Experimental part.....	121
IV-1) Materials and methods	121
IV-2) Experimental procedures.....	122
IV-2-1) Open cell polyurethane foam (PUF) coating with polydopamine (PDA)	122
IV-2-2) Functionalization of PDA@PUF with APTES.....	122
IV-2-3) Coupling of neutral eosin Y with APTES@PDA@PUF	122
IV-2-4) Preparation of EY-APTES@PDA@PUF in a one-pot procedure from PDA@PUF	123
IV-2-5) Preparation of EY-PDA@PUF	123
IV-2-6) General procedure for the oxidation of 2-methyl-5-nitro-isoquinolin-2-ium iodide photocatalyzed by EY-APTES@PDA@PUF	123
IV-2-7) General procedures for the oxidation of sulfides to sulfoxides photocatalyzed by EY-APTES@PDA@PUF or EY-PDA@PUF	124
IV-2-8) Reusability procedure.....	124
IV-2-9) <i>Stop-and-go</i> experiment for the oxidation of <i>p</i> -tolyl methyl sulfide	124
V) References	125

Abstract

In this chapter we try to introduce a more sustainable alternative to the heterogeneous macroscopic Ru(bpy)₃-APTES@PDA@PUF photocatalyst developed in the first chapter by immobilizing the organic dye, eosin Y, on PDA@PUF. The structured heterogeneous photocatalyst was obtained by post-functionalization of PDA@PUF via the same silanization process of the mussel-inspired adhesive layer with 3-(triethoxysilyl)propan-1-amine (APTES) and a similar EDC-mediated coupling of the resulting amino-functionalized foam, but with eosin Y instead of [2,2'-bipyridine]-4-carboxylic acid. After characterization of the resulting EY-APTES@PDA@PUF foam by ²⁹Si CP-MAS NMR, ICP-AES, SEM and SEM-EDX, it was first tested as heterogeneous photocatalyst for the oxidation of 2-methyl-5-nitroisoquinolin-2-ium iodide to the corresponding isoquinolone. Despite a good efficiency under white light (24W LED) irradiation and excellent reusability in an easy-to-carry “dip-and-play” mode for at least 6 runs, the yellow color of the reaction solution combined to a change of aspect of the catalytic foam from red to brownish suggested some eosin Y leaching. To better apprehend the influence of EY leaching on photocatalytic efficiency of EY-APTES@PDA@PUF, its catalytic activity was next investigated for the oxidation of sulfides to sulfoxides, a reaction that is completely silent in the absence of a photocatalyst. A high efficiency under white light irradiation (24W) was observed for its first use. However, recycling tests highlighted a fast deactivation in this case, and a stop-and-go experiment clearly evidenced the occurrence of eosin leaching. As a non-negligible simple adsorption of eosin Y on the PDA layer coupled to a low efficiency of the EDC-mediated coupling reaction with the grafted amine groups were suspected to be the origin of this phenomenon, an EY-APTES1@PDA@PUF foam was then prepared via a one-pot protocol implying the coupling of eosin Y with APTES in the presence of COMU instead of EDC prior to the covalent anchoring procedure by condensation of the alkoxy silane groups of APTES with the catechols of PDA. Alternatively, a one-step coating-and-functionalization strategy implying an *in situ* coupling of dopamine with eosin Y was adopted to generate an EY-PDA@PUF foam without APTES. Both macroscopic photocatalysts similarly showed high efficiency for their first use in a model oxidation of sulfide to sulfoxides reaction. However, recycling tests again highlighted fast deactivation due to important eosin Y leaching. The combination of PDA and eosin Y may thus not be appropriate to anchor robustly eosin Y on PUF.

1) Introduction

Organic photoredox catalysts represent attractive alternatives in visible-light photocatalysis to expensive and potentially toxic noble metal-based photocatalysts such as [Ru(bpy)₃]Cl₂ or [Ir(dF(CF₃)ppy)₂(bpy)](PF₆). Organic dyes are indeed typically less toxic,

easier to handle, and available at lower cost as they can be readily synthesized from natural feedstock.¹ In addition, due to the fact they avoid metal coordination, they often exhibit superior solubility in organic solvents.¹⁻² The growing interest in their development is also driven by the fact that they often compare to or even outperform transition metal-based photocatalysts.³⁻⁴ Furthermore, due to their inherent potent reactivity, they are much more than simple alternatives to transition metal-based photocatalysts and can allow access to unique reactivities.⁵

Among the variety of existing organic photoredox catalysts (**Figure 1**),⁵ eosin Y (EY) is by far one of the most studied organic dye for its photocatalytic properties in organic synthesis.^{1-2,6} In particular, EY has demonstrated high catalytic efficiency in various organic synthetic transformations, including reduction,⁷⁻⁸ oxidation,⁹⁻¹⁰ arylation¹¹ and trifluoromethylation reactions,¹²⁻¹³ radical polymerizations,¹⁴⁻¹⁸ as well as cooperative catalysis.¹⁹⁻²¹ In this work aiming at providing an even more sustainable alternative to Ru(bpy)₃-APTES@PDA@PUF, we thus naturally selected this dye as a model to investigate the possibility of developing an easily reusable heterogeneous macroscopic photocatalyst based on an organic photoredox catalyst.

The photocatalytic properties of eosin Y rely on its redox potential: the oxidation potential range is between -1.06 V and 1.10 V, whereas reduction potential range stands between +0.78 V and +0.83 V (**Figure 2A**). The maximum of absorption wave is located around 539 nm, with a molar extinction coefficient $\epsilon = 60\,803\text{ M}^{-1}\text{ cm}^{-1}$ (Fig. 2B).²²⁻²⁴ Green LEDs that have their maximum emission around 530 nm are thus usually employed as light sources for the activation of eosin Y. Upon excitation by such light, eosin Y undergoes a rapid inter-system crossing from the ground state **EY** to the lowest energy triplet state ^{triplet}**EY***. It must be noted here however that a direct singlet-triplet transition being forbidden, the light actually excites the electrons of EY to a higher excited singlet state ^{singlet}**EY*** from where they rapidly relax to the lowest excited singlet state, and that it is only then that the excited electrons undergo an intersystem crossing to the active triplet state ^{triplet}**EY*** (**Figure 2A**).²³⁻²⁴ The latter then follows a reductive or oxidative quenching cycle depending on whether it receives a single electron from an electron donor reactant **RQ** or loses a single electron by reaction with an electron acceptor reactant **OQ** (**Figure 3**). The resulting radical anion or cation then reacts with another electron acceptor **A** or electron donor **D** to regenerate the **PC** (*i.e.*: **EY**) while the radical cation and anion of the reactants recombine to form the desired product. In addition to this classical photoredox catalytic cycle, the photoexcited state of eosin Y may also induce energy transfer process.²⁵

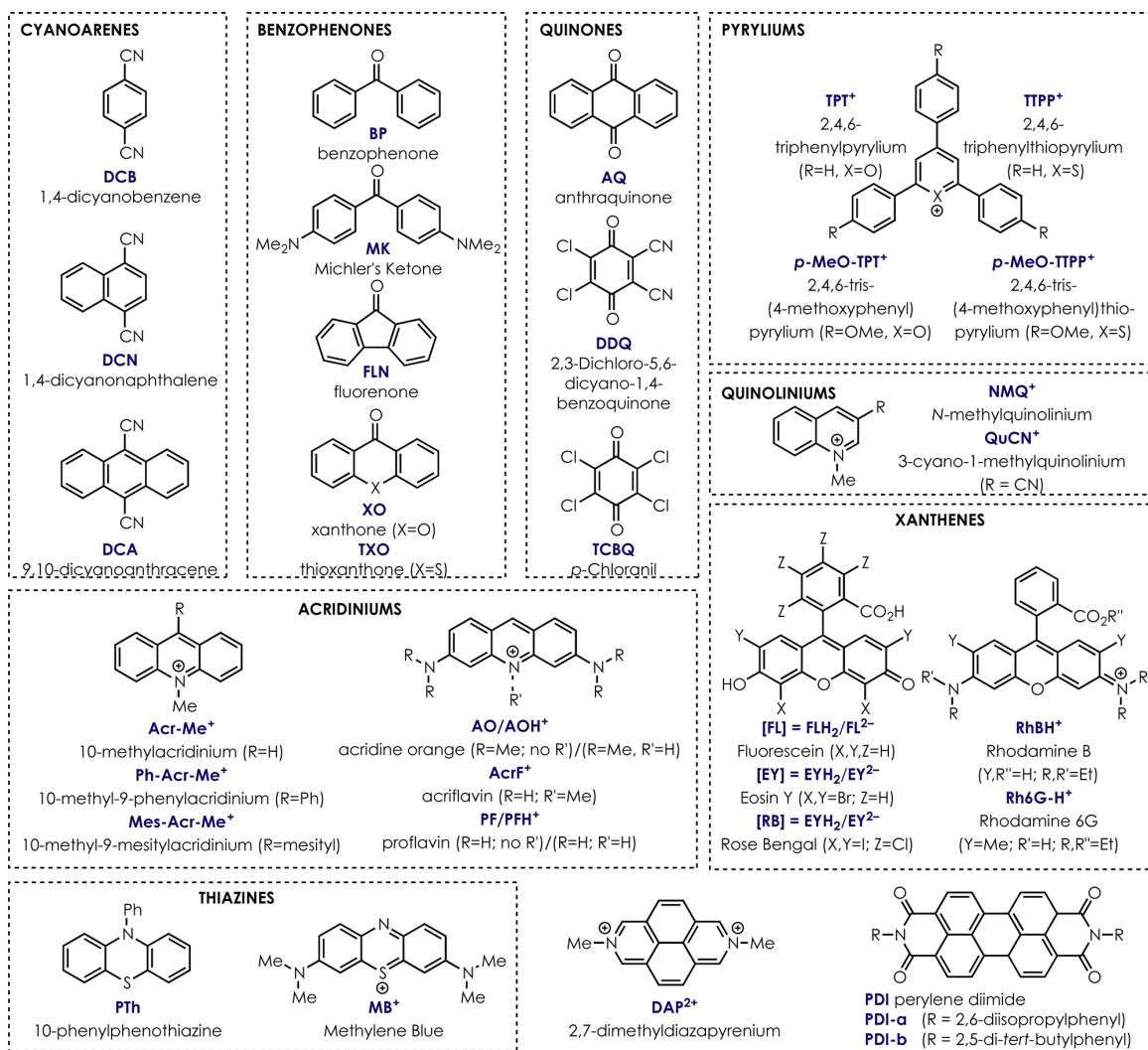


Figure 1. Common organic photoredox catalysts (reproduced from ref. 5).

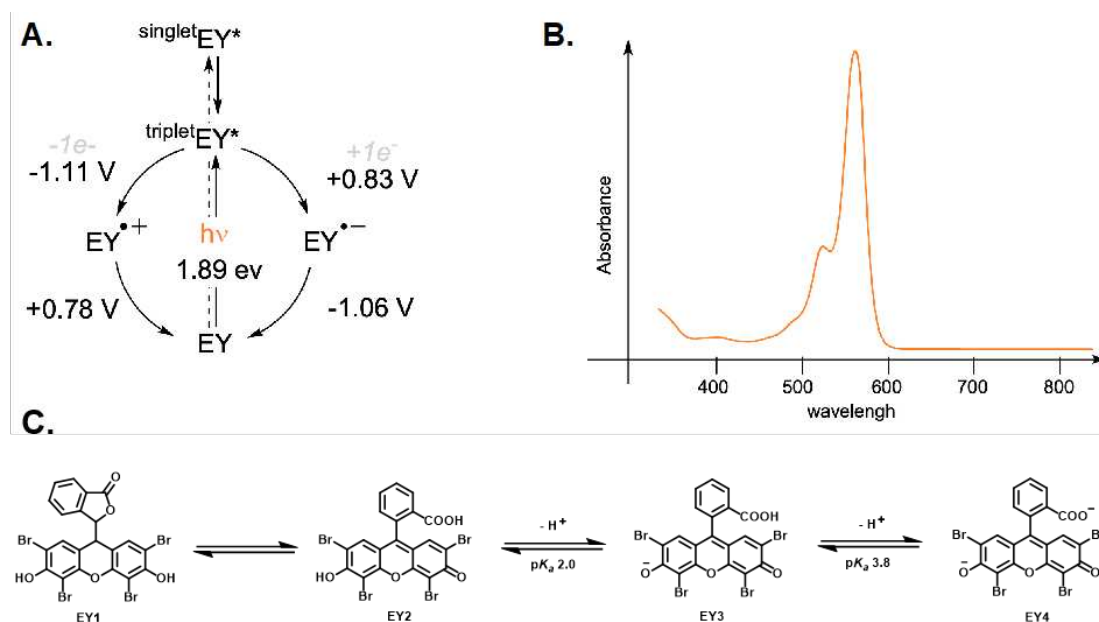


Figure 2. (A) Oxidative and reductive quenching cycles of eosin Y with their respective potentials. (B) Eosin Y absorption spectrum in ethanol. (C) Eosin Y equilibrates in solution (reproduced from ref. 6).

It is noteworthy that although there are four different forms of Eosin Y in equilibrium in solution: spirocyclic (EY1), neutral (EY2), monoanionic (EY3) and dianionic (EY4) (**Figure 2C**),²⁶ only EY3 and EY4 are catalytically active and the presence of minor amounts of impurities in the solvents or reactants is sufficient to shift the acid–base equilibria in either direction. Nevertheless, their respective contents are rarely studied and established, and it is commonly accepted to use either EY2 or EY4 to designate eosin Y without further precision on the real composition in the reactive medium.

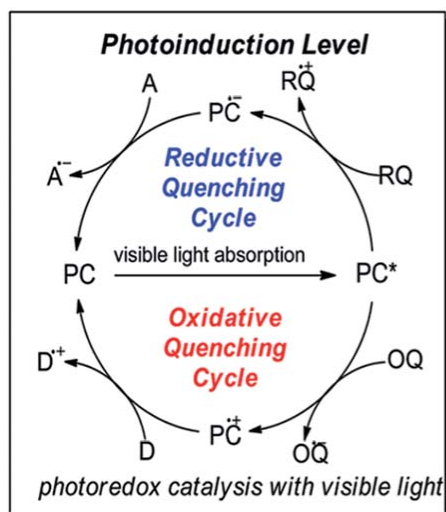


Figure 3. Generic illustration of a molecular photoredox cycle (reproduced from ref. 1).

According to the Beer-Lambert-Bouguer law,²⁷ photochemical reactions carried out in conventional batch reactors will be exposed to a non-uniform distribution of radiations due to the photon transport attenuation effect. Consequently, the reaction medium near the middle or the wall of the reactor will be exposed to different intensities of irradiation, thus causing different reaction rates. While this phenomenon can be easily overcome in small reaction flasks by a strong stirring, when it comes to large photochemical reactors, this non-uniform situation may give rise to the over-irradiation of external zones generating the formation of undesired byproducts.¹ One possible solution to solve this issue consists in conducting the catalysis under heterogeneous conditions with the PC anchored to a solid support as light irradiation into the solution will then not be hampered by the molar extinction coefficient of the dissolved PC. Additionally, with this method, the workup isolation and purification procedures will be simplified, and the catalyst can potentially be easily reused several times. This strategy has already been largely applied to EY with solid supports as varied as silica particles,^{18, 28} graphene oxide,²⁹ metal-organic frameworks,³⁰⁻³¹ polymeric supports,^{10, 32-35} glass wool,³⁶ and magnetic nanoparticles³⁷ have been utilized for EY immobilization. To the best of our knowledge, EY has however never been supported on a macroscopic three-dimensionally structured support such as open cell foams. Selected examples with various immobilization

approaches going from non-covalent bonding to covalent bonding are discussed below.

In 2019, M. Selvaraj, *et. al.* reported the immobilization of eosin Y on the commercially available Amberlite IRA 900 chloride resin through a simple anion exchange reaction (**Figure 4**).¹⁰ The maximum loading of eosin Y reached 1.39 mmol per gram of resin. The efficiency of the polymer-supported photocatalyst was evaluated for the oxidation of thioethers to sulfoxides as well as for the oxidative hydroxylation of phenylboronic acids to phenols. The former reaction was preferentially conducted in acetonitrile:water (8:2) under a 3 W green LED irradiation and air as oxidant in the presence of 3 mol% eosin Y. Yields varying between 63 and 91% were observed with various aryl alkyl sulfides after 6 h reaction at room temperature (RT) (**Scheme 1**). Moderate to good yields were also observed for the hydroxylation of phenylboronic acids to phenols under slightly different conditions: 5 mol% eosin Y, 14W compact fluorescent lamp, air, 36 h, RT. Leaching of the dye was observed when using the most eosin Y-loaded resin. The leaching was almost completely suppressed when using a polymer resin with a lesser amount of dye (0.46 mmol/g). Noteworthy, despite the observed eosin Y leaching, the heterogeneous catalyst could be used six times without important loss of its catalytic efficiency.

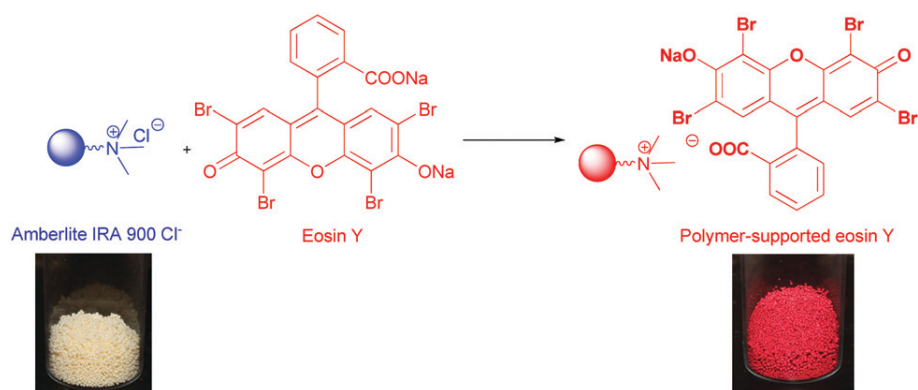
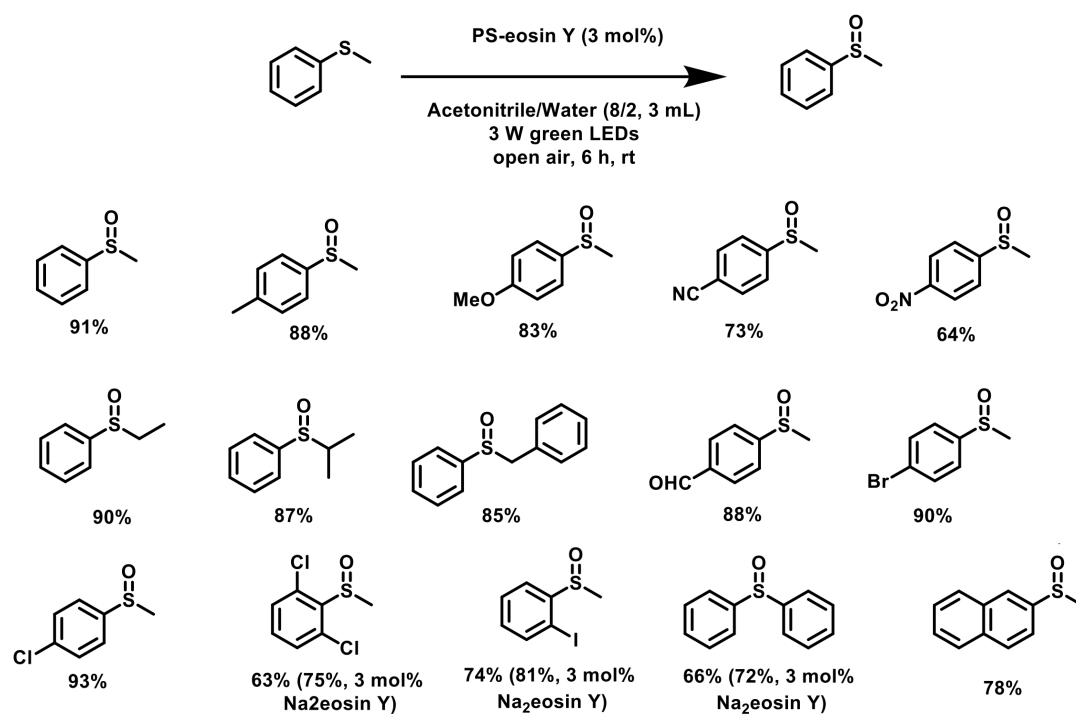


Figure 4. Immobilization of eosin Y on Amberlite IRA 900 chloride resin via an anion exchange reaction (reproduced from ref. 10)



Scheme 1. Oxidation of sulfides to sulfoxides catalyzed by the Amberlite-supported eosin Y.

The same year, P. Li, G.-W. Wang, *et. al.* reported a magnetic nanoparticle-supported eosin Y bis-benzyltriethylammonium salt (MNPs-Eosin Y) that proved efficient in C-C and C-P coupling reactions of sp^3 C-H bonds adjacent to the nitrogen atom of tetrahydroisoquinoline derivatives with pronucleophiles such as nitroalkanes, malononitrile, dimethyl malonate and H-phosphonate diesters under 3W green LED irradiation and air as oxidant at RT (**Figure 5**).³⁷ The supported catalyst was prepared through a lengthy four-step procedure involving (i) silica-coating of magnetic Fe_3O_4 nanoparticles (MNPs), (ii) benzyl chloride anchoring through condensation of a trimethoxysilyl side-arm with the surface silanols of the $SiO_2@Fe_3O_4$ MNPs, (iii) reaction of the benzyl chloride-functionalized MNPs with triethylamine (iv) treatment of the resulting ammonium salt-functionalized MNPs with eosin Y in a 3:1 mixture of acetone/water (**Figure 6**). A loading of 0.1 mmol of eosin Y per gram was determined via spectrophotometric method. Good to excellent yields were obtained in all studied cross-dehydrogenative couplings (Figure 5). Noticeably, the catalyst could be easily separated from the reaction medium by using an external permanent magnet and could be reused at least eight times with no evident loss of activity and minimal levels of eosin leaching, as indicated by the absence of detection in the crude reactions' mixtures of the characteristic absorption of eosin Y by spectrometric measurements.

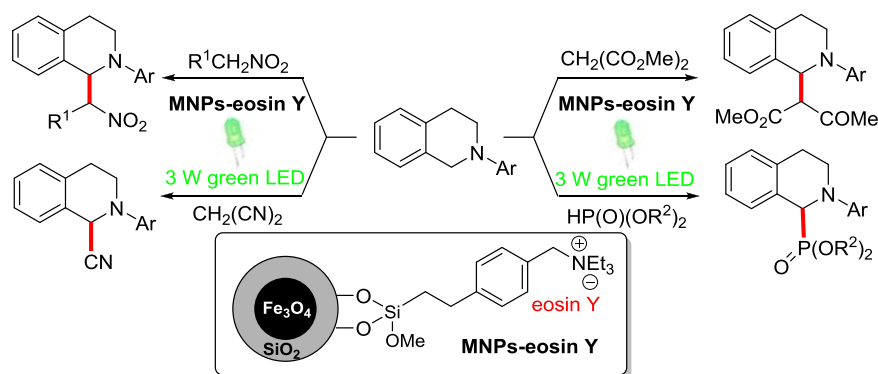


Figure 5. Magnetic nanoparticles supported eosin Y for visible light oxidative C-C and C-P bond formation (reproduced from ref. 37).

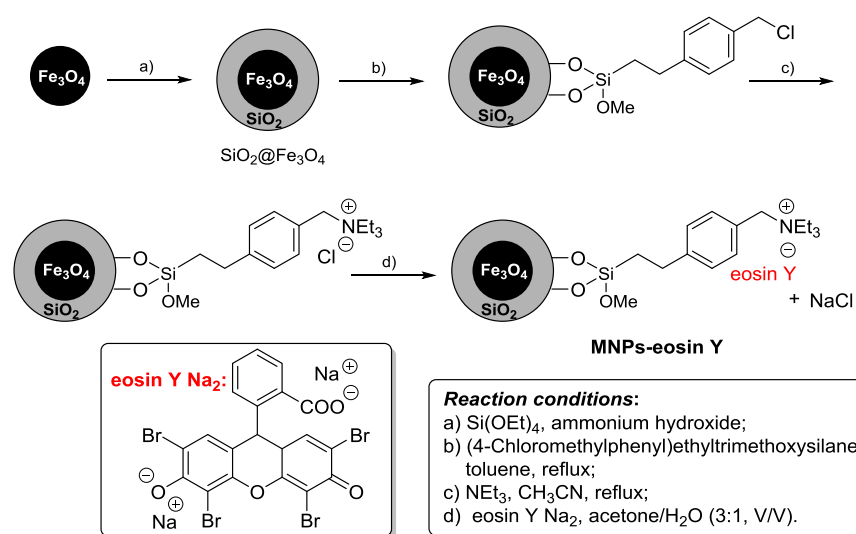
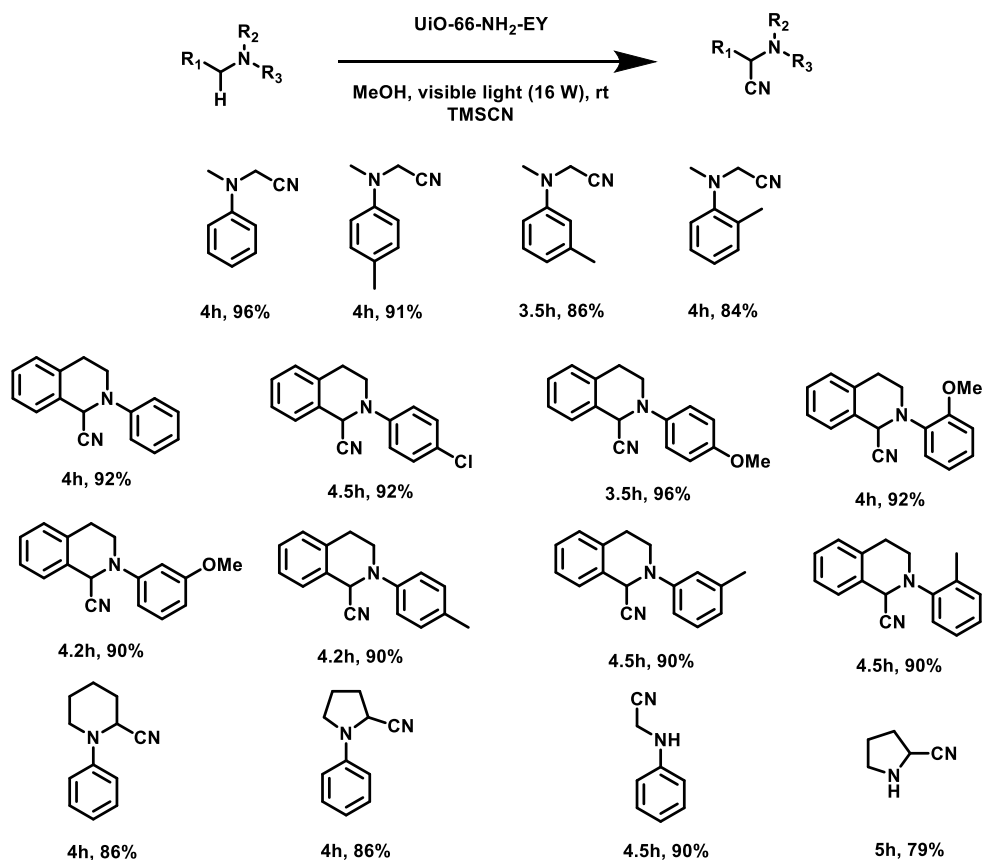


Figure 6. Four-step preparation of the magnetic nanoparticle-supported eosin Y bis-benzyltriethylammonium salt (reproduced from ref. 37).

The covalent anchoring of eosin Y in an amine-functionalized Zr(IV) metal-organic framework (UiO-66-NH₂) was reported by Kahn *et al.* in 2019. Specifically, eosin Y was introduced in the framework via a single-step dehydrating coupling of the carboxyl group of dianionic eosin Y with the primary amine groups of UiO-66-NH₂ by using *N,N*-dicyclohexylcarbodiimide (DCC) as the dehydrating reagent in DMF. The thus obtained heterogeneous photocatalyst was used for the α -cyanation of secondary and tertiary amines via C–H bond functionalization with TMSCN as the cyanide source in methanol at room temperature under irradiation with a 16 W visible-light source. *N,N*-dimethylanilines and cyclic amines, such as piperidine, pyrrolidine and tetrahydroisoquinoline furnished the α -aminonitrile products with good to excellent yield (79-96%) (**Scheme 2**). Impressively, EY@UiO-66-NH₂ catalyst could be used for up to 10 runs without any significant loss in activity. Furthermore, in addition to the traditional advantages provided by heterogeneous catalysis, the UiO-66-NH₂ metal-organic framework played a significant role in the development of catalytic activity of the

heterogeneous photocatalyst whose performance was found to be superior to that of homogeneous eosin Y.



Scheme 2. Substrate scope for the α -cyanation of amines photocatalyzed by the UiO-66-NH₂-supported eosin Y.

In 2020, C. Boyer, J. Xu *et al.* described the immobilization of eosin Y onto commercially available cotton threads (i.e.: cellulose type material with surface hydroxyl groups) via a similar single-step DCC coupling method in the presence of 4-(dimethylamino)pyridine (DMAP) in CH₂Cl₂ at RT (Fig. 7A).³⁸ Quantification of immobilized eosin Y on the cotton thread was done by UV-vis analysis of the reaction and rinsing solutions; one meter of EY@cotton thread was found to contain around 2.8 mg catalyst. Negligible leaching (0.003 wt.%) was observed after 2 days of soaking in DMSO, CH₂Cl₂, DMF, MeOH, THF, H₂O and CH₃CN, and scanning electron microscopy (SEM) images revealed no difference in the fibrous microstructure before and after immobilization suggesting that the DCC coupling does not alter the cotton thread. The resulting EY@cotton PC was then utilized for the oxidation of thioanisole to methylsulfinylbenzene as well as for photoinduced electron/energy transfer – reversible addition-fragmentation chain transfer (PET-RAFT) polymerizations (Fig. 7B and 7C). The sulfide oxidation reaction was preferentially conducted in a 5:2 CH₃CN/H₂O mixture under

green light irradiation (0.45 mW/cm^2) and air as oxidant in the presence of 16.8 mg of eosin Y for 1 mmol of thioanisole at room temperature. Under these conditions, around 45% yield was observed after 28 h reaction for 6 successive runs, indicating no significant loss in catalytic efficiency over time. Thus, less than 0.011 wt% leaching was measured. In the PET-RAFT polymerization reactions, well-defined polymers were synthesized by the polymerization of various monomers in different solvents using RAFT agent such as 2-cyano-2-propyl dodecyl trithiocarbonate (CPDTC) and triethylamine as a co-catalyst under green light (0.45 mW/cm^2) (Fig. 7C). Remarkably, recyclability of EY@cotton was also possible for this polymerization reaction, although in this case, a slight drop in catalytic performance ($< 5\%$) was observed after 5 cycles, as well as minor EY leaching and a slight discoloration of the EY@cotton material, which was attributed to the presence of reducing agents in the medium.

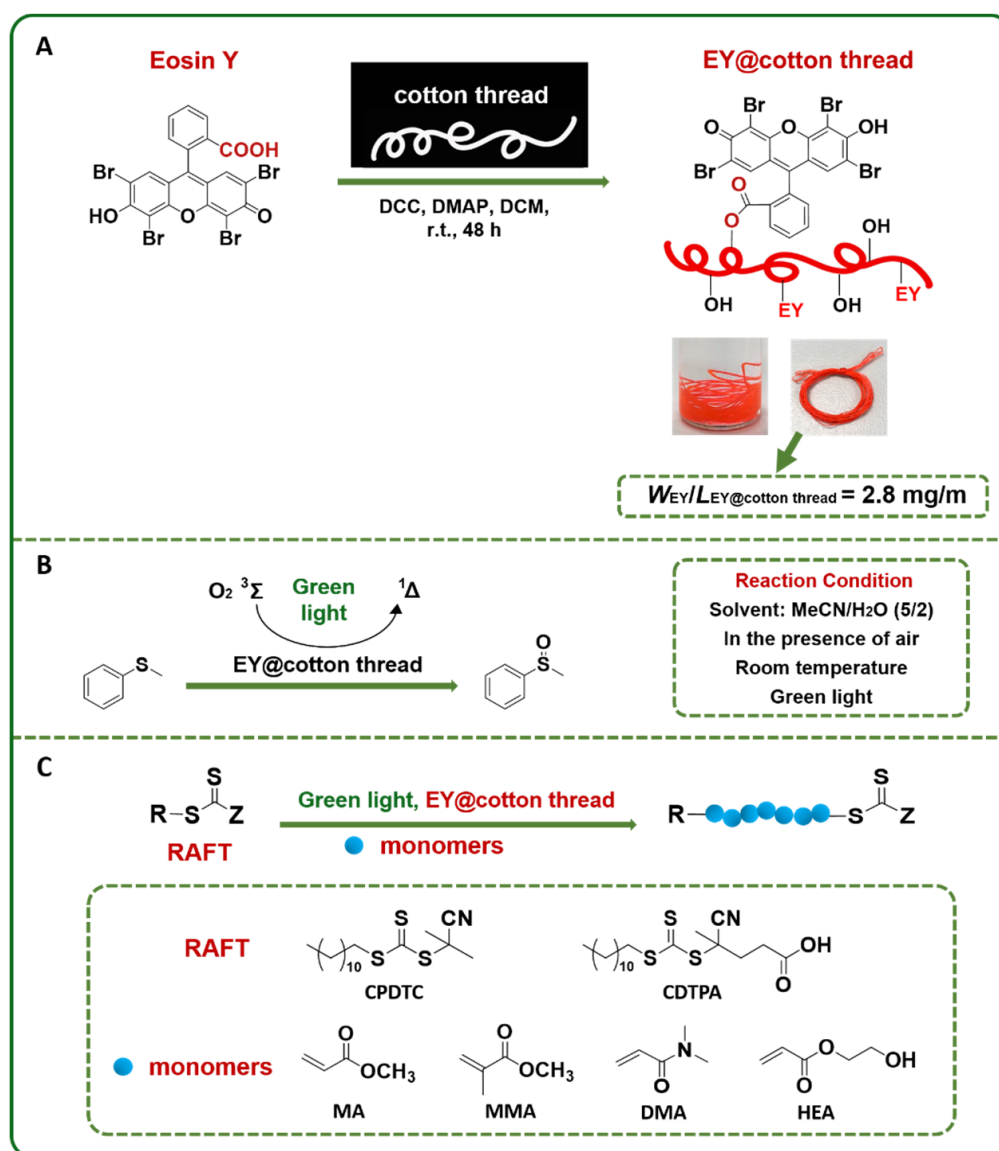


Figure 7. (A) Single-step immobilization process of EY onto cotton threads. (B) Oxidation of thioanisole catalyzed by EY@cotton thread in the air. (C) Polymer synthesis by PET-RAFT polymerization catalyzed by EY@cotton thread. (reproduced from ref. 38).

In 2020, C. Scaiano, *et. al.* introduced novel heterogeneous photocatalysts based on glass wool.³⁶ To facilitate the attachment of the photocatalysts to the surface, the authors modified the glass wool surface by the introduction of amino groups via a silanization reaction with (3-aminopropyl)triethoxysilane (APTES). Thereafter, the photocatalysts were anchored onto the glass surface by using DCC for amide formation as in the previous examples (**Figure 8**). After full characterization, the catalytic activity of the thus heterogenized photocatalysts were then evaluated for the aerobic oxidative hydroxylation of phenylboronic acid and the singlet oxygen mediated photooxidation of 9,10-dimethylantracene (DMA) to the corresponding 9,10-endoperoxide (DMA-O₂). While EY@GW, proved poorly reactive for the hydroxylation of phenylboronic, it proved efficient for the photooxidation of DMA in acetonitrile at room temperature under green LED (520 nm), and could be used for five runs with only little apparent activity decrease and no apparent EY leaching.

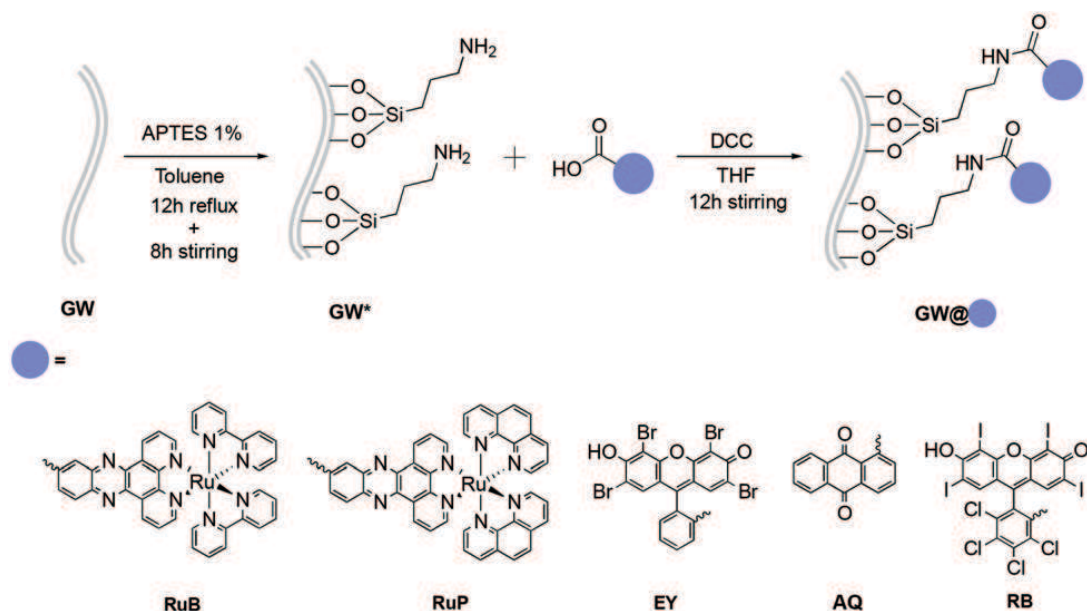


Figure 8. Glass wool functionalization with various photocatalysts including eosin Y via a silanization process with APTES and a DCC-mediated coupling (reproduced from ref. ³⁶).

In this chapter, we present our results toward the immobilization of eosin Y onto the tree-dimensional macroscopic support PDA@PUF.

II) Results and discussion

II-1) Preparation and characterization of EY-APTES@PDA@PUF based on post-functionalization of PDA@PUF

The first strategy for the immobilization of EY at the surface of polydopamine-coated open cell polyurethane foams (PDA@PUF) mimics the one followed for the immobilization of

$[\text{Ru}(\text{bpy})_3]^{2+}$ except that no metal complexation step was necessary (see Chapter I). Thus, after coating a cubic sample of PUF of ca. 2 cm × 2 cm × 2 cm with a thin layer of PDA by simple immersion in an aqueous solution of dopamine at room temperature buffered at a pH of 8.5, and several washings with water,³⁹ the resulting PDA@PUF material was functionalized with eosin Y in two steps via (i) the same silanization process with 3-(triethoxysilyl)propan-1-amine (APTES) in toluene at 70 °C for 24 h, (ii) a similar EDC-mediated coupling of the resulting amino-functionalized foam, but with eosin Y instead of [2,2'-bipyridine]-4-carboxylic acid (**Figure 9**). Specifically, APTES@PDA@PUF was treated with neutral eosin Y in the presence of 1.5 equiv. of *N*-hydroxysuccinimide (NHS), and 2 equiv. of EDC hydrochloride in ethanol at room temperature. The successful grafting of eosin Y was visible to the naked eye by a striking colour change from black in APTES@PDA@PUF to red in EY-APTES@PDA@PUF.

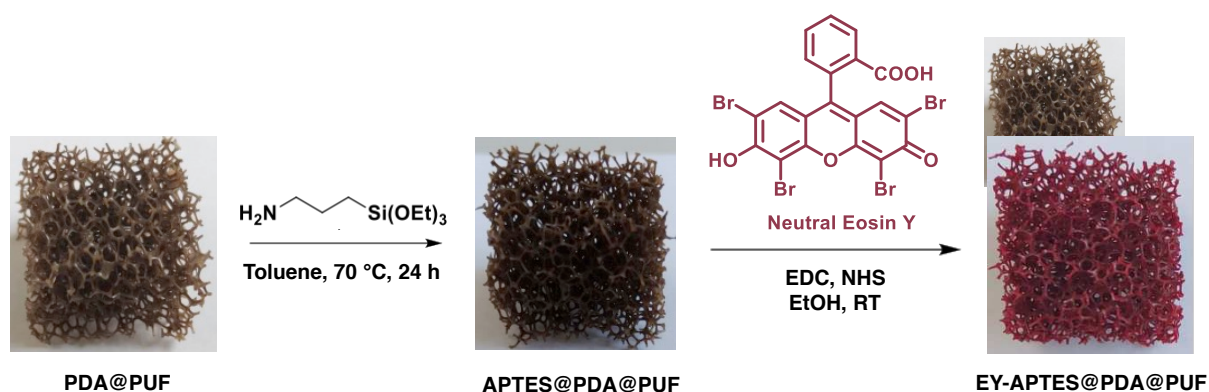


Figure 9. Post-functionalization strategy of PDA@PUF for eosin Y immobilization.

After thorough washing procedures of EY-APTES@PDA@PUF in acetone and $\text{CH}_3\text{CN}/\text{H}_2\text{O}$ (1:1), mean Si and Br contents of 2.544 ± 0.077 g/kg and 1.051 ± 0.029 g/kg were measured by ICP-AES, respectively. The ^{29}Si CP-MAS NMR spectrum revealed signals between -65.1 ppm and -42.5 ppm (**Figure 10**), similarly to what was observed with APTES@PDA@PUF (see Chapter I), which suggests the preservation of the T_1 , T_2 as well as cross-linked $T_3+T'_3$ and $T_4+T'_4$ substructures⁴⁰ after the EDC-mediated coupling, and highlights the robustness of the silicon–catechol bonding formed in the first step of the post-functionalization strategy.

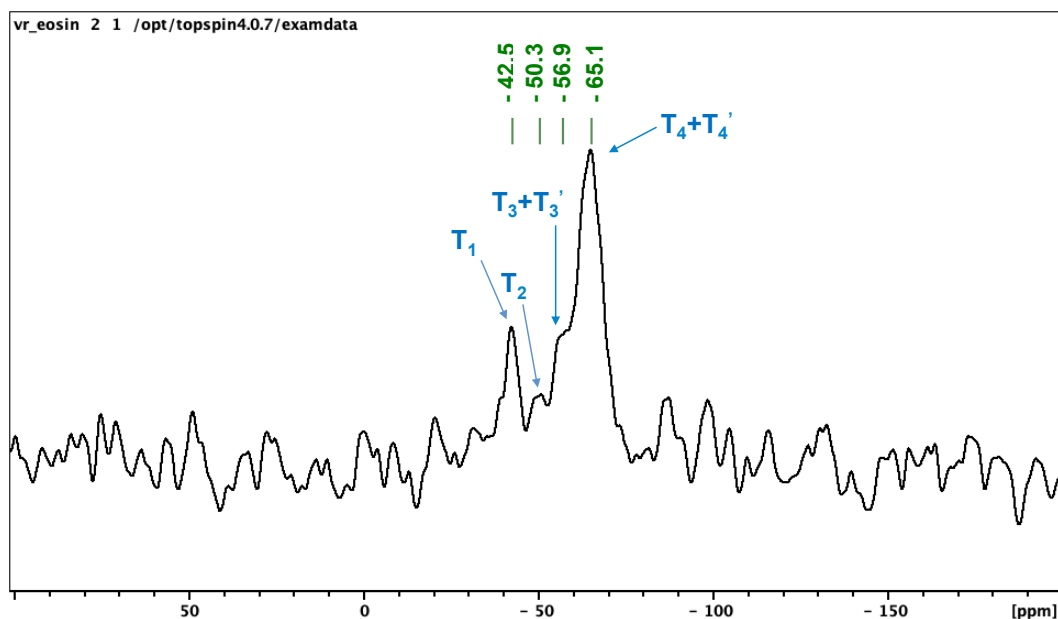


Figure 10. ^{29}Si CP-MAS NMR spectrum of EY-APTES@PDA@PUF.

Low magnification SEM images of EY-APTES@PDA@PUF did not reveal obvious corrugation of the struts edges (**Figure 11**), as was observed previously for $\text{Ru}(\text{bpy})_3\text{-APTES@PDA@PUF}$ (see Chapter I) or other PDA@PUF foams functionalized by a molecular catalyst via a similar silanization process.⁴¹ Higher magnification images showed a rough film structure with scattered PDA aggregates, typical of PDA coating on a PUF,³⁹ similarly to what was observed on $\text{Ru}(\text{bpy})_3\text{-APTES@PDA@PUF}$ (**Figure 11**). EDX spectroscopy confirmed the presence of C, N, O, Si and Br elements on the foam surface (**Figure 12**), though the latter was not detected on all selected areas, most probably in reason of its relatively low loading.

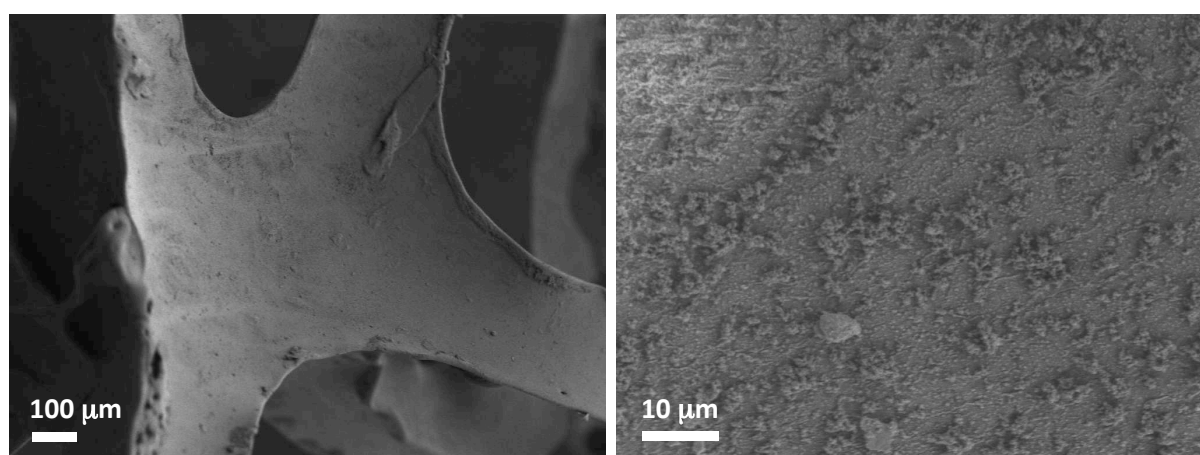


Figure 11. SEM images of as-synthesized EY-APTES@PDA@PUF with different magnifications.

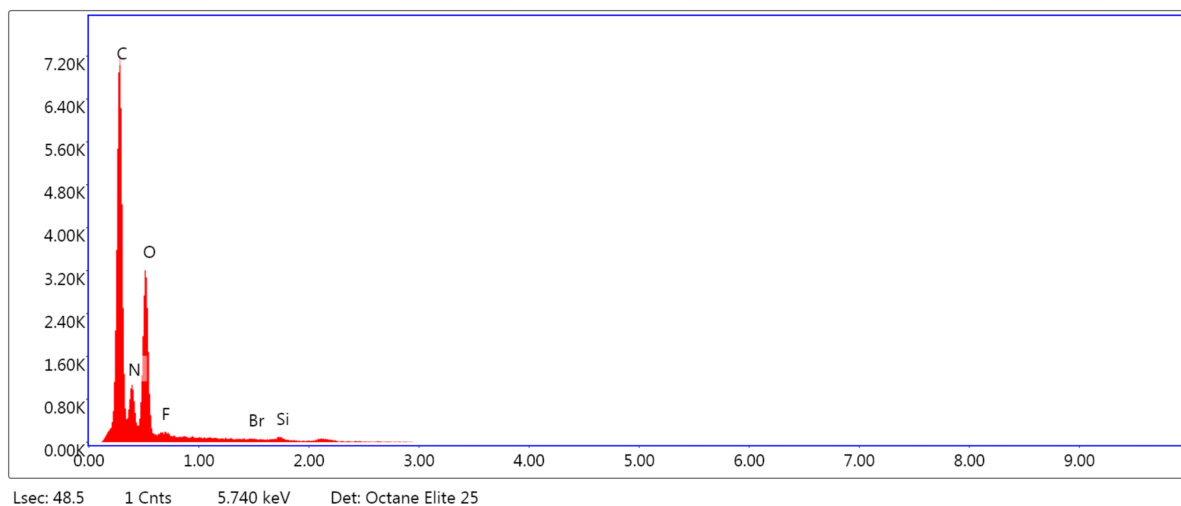


Figure 12. EDX spectrum of as-synthesized EY-APTES@PDA@PUF

II-2) Photocatalytic studies

It has been widely reported that under visible-light irradiation, EY is capable of converting molecular oxygen to singlet oxygen.^{36,42-43} Singlet oxygen is a highly reactive species for a large number of organic reactions,⁴⁴⁻⁴⁵ including the oxidation of *N*-alkylpyridinium salts to quinolones and isoquinolones⁴⁶ and of sulfides to sulfoxides^{10,38,47} that were chosen as model reactions for the study of the photocatalytic properties of EY-APTES@PDA@PUF.

N-Heterocycles containing a pyridine moiety such as quinolines and isoquinolines are privileged scaffolds that occupy key roles in many medically related molecules.⁴⁸ Similarly, quinolones and isoquinolones exhibit diverse biological and pharmaceutical activities, including anticancer,⁴⁹ antibiotic,⁵⁰ antiviral, and antihypertensive activities.⁵¹ It is therefore highly desirable to develop convenient, efficient and practical transformations from readily available quinolines and isoquinolines to quinolones and isoquinolones, and eosin Y has recently been reported to act as a highly efficient and environmentally friendly homogeneous photocatalyst for the visible light-mediated aerobic oxidation of *N*-alkylpyridinium salts at room temperature with air as a “green” oxidant.⁴⁶ This reaction thus seemed to be a perfect case study to evaluate the photocatalytic properties of our EY-functionalized foams.

Initial studies focused on the oxidation of 2-methyl-5-nitroisoquinolin-2-ium iodide in the presence of Cs₂CO₃ as base under air at 30-35 °C (due to LED light heating) using eosin Y (2 mol%) or a cubic sample of EY-APTES@PDA@PUF of ca. 2 cm × 2 cm × 2 cm whose mass was adjusted to have an eosin Y loading of 0.46 mol%, as catalysts (Table 1). Solvents and lights were found to have a prominent influence on the reaction yield. In THF under 24 W white LED light irradiation, the reaction yield reached 71% after 18 h reaction with eosin Y as catalyst, which was significantly lower from what was reported by H. Fu *et al.*⁴⁶ under 40 W compact

fluorescent light (CFL) irradiation at room temperature (entry 1 vs. entry 2). Running the reaction in ethanol under otherwise similar conditions resulted in a similar yield (entry 3), but running it in CH₃CN resulted in a significant improvement as the expected oxidation product could be isolated in 96% yield after 18 h reaction (entry 4). The latter conditions were therefore chosen for evaluating the photocatalytic properties of our macroscopic heterogeneous catalyst, at the exception that the solvent volume had to be increased from 2 to 8 mL in order to allow the complete immersion of the 2 cm × 2 cm × 2 cm foam. Satisfyingly, despite the four-fold decrease of the reactants' concentrations and a little more than a 4-fold decrease of the catalyst loading (0.46 mol% vs. 2 mol%), a 70% isolated yield was obtained after the same reaction time with EY-APTES@PDA@PUF (entry 5). Noteworthy however, 44% yield was obtained in the absence of a photocatalyst under otherwise similar reaction conditions (entry 6), which may explain the previous result, at least in part, and shows that the reaction occurs in the absence of a catalyst under these conditions. Still, it is 1.6 times faster in the presence of our macroscopic photocatalyst.

Table 1. Optimization of the reaction conditions for the oxidation of 2-methyl-5-nitro-isoquinolin-2-ium iodide under visible light and air using eosin Y or EY-APTES@PDA@PUF as photocatalyst.

Entry	Catalyst	Solvent	Light	Time (h)	Isolated yield (%)
1 ^a	Eosin Y	THF	40W CFL	6	94
2 ^b	Eosin Y	THF	24W white LED	18	71
3 ^b	Eosin Y	EtOH	24W white LED	18	76
4 ^b	Eosin Y	CH ₃ CN	24W white LED	18	96
5 ^c	EY-APTES@PDA@PUF	CH ₃ CN	24W white LED	18	70
6 ^d	-	CH ₃ CN	24W white LED	18	44

^a Result from reference 46: 2-methyl-5-nitro-isoquinolin-2-ium iodide (0.2 mmol), Cs₂CO₃ (0.3 mmol), eosin Y (2 mol%), THF (2 mL), ambient air, 40W CFL, room temperature. ^b 2-methyl-5-nitro-isoquinolin-2-ium iodide (0.2 mmol), Cs₂CO₃ (0.3 mmol), eosin Y (2 mol%), solvent (2 mL), air balloon, 24W white LED, ca. 35 °C due to LED light heat. ^c 2-methyl-5-nitro-isoquinolin-2-ium iodide (0.2 mmol), Cs₂CO₃ (0.3 mmol), EY-APTES@PDA@PUF (2 cm × 2 cm × 2 cm, 0.46 mol% EY), CH₃CN (8 mL), air balloon, 24W white LED, ca. 35 °C due to LED light heat, 650 rpm. ^d 2-methyl-5-nitro-isoquinolin-2-ium iodide (0.5 mmol), Cs₂CO₃ (0.75 mmol), no catalyst, CH₃CN (20 mL), air balloon, 24W white LED, ca. 35 °C due to LED light heat.

Encouraged by these results, we next decided to evaluate the reusability of EY-APTES@PDA@PUF. For that purpose, six consecutive runs of 2-methyl-5-nitro-isoquinolin-

2-ium iodide aerobic oxidation under visible light irradiation were conducted with a single sample of freshly prepared EY-APTES@PDA@PUF (2 cm × 2 cm × 2 cm, 0.46 mol% EY), that was simply removed from the reaction medium and washed successively with acetone, water and acetonitrile after each run, before being reused. Satisfyingly, the activity maintained at the same level for the six runs (**Figure 13**). It is noteworthy however that the reaction media after each run were slightly coloured in orange, suggesting some eosin Y leaching. Accordingly, the foam became more brownish (**Figure 14**) and ICP-AES analysis of the used foam after these 6 catalytic runs indicated a Si loss of about 22%.

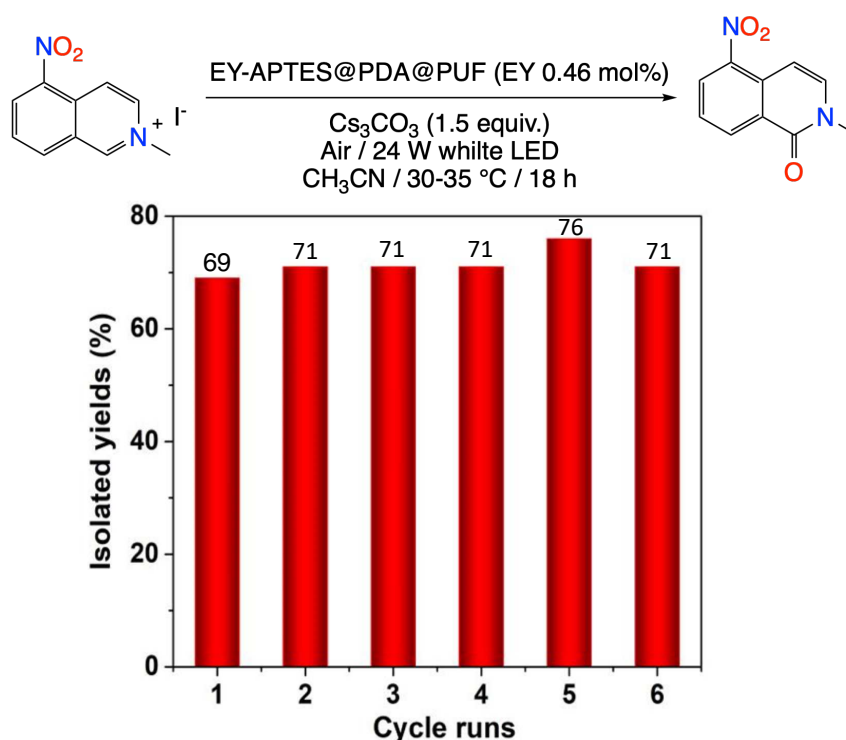


Figure 13. Isolated yields measured over the six successive runs of 2-methyl-5-nitro-isoquinolin-2-ium iodide oxidation photocatalyzed by a single sample of EY-APTES@PDA@PUF. Reaction conditions: 2-methyl-5-nitro-isoquinolin-2-ium iodide (0.2 mmol), Cs₂CO₃ (0.3 mmol), EY-APTES@PDA@PUF (2 cm × 2 cm × 2 cm, 0.46 mol% EY), CH₃CN (8 mL), air balloon, 24W white LED, ca. 35 °C due to LED light heat, 650 rpm.



Figure 14. Photograph of the spent EY-APTES@PDA@PUF foam after six cycles of 2-methyl-5-nitro-isoquinolin-2-ium iodide oxidation.

To try to gain some insight about this apparent modification of the foam surface, the spent foam after 6 cycles of methyl pyridinium salt oxidation was submitted to SEM and SEM-EDX analyses. As for Ru(bpy)₃-APTE@PDA@PUF (Chapter I), low magnification SEM images showed a higher degree of corrugation of the struts edges, due most probably to repeated solvent swelling in the polymeric foam,⁴¹ while, higher magnification images revealed a smoother surface with less numerous scattered PDA aggregates (**Figure 15**). EDX spectroscopy confirmed the presence of C, N, O, and Si elements on the foam surface but did not show any Br anymore (**Figure 16**). Adsorbed Cs coming from the used base was detected instead.

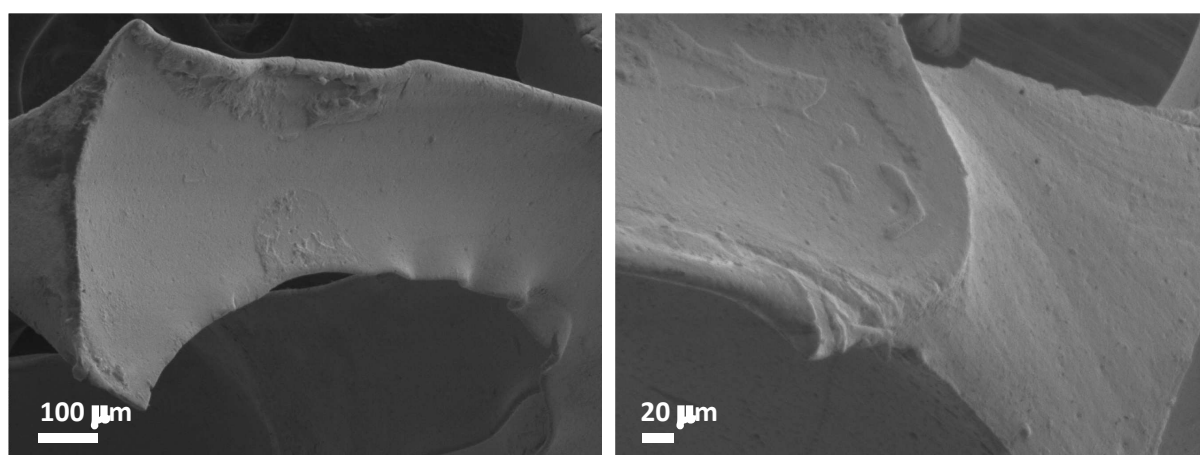


Figure 15. SEM images with different magnifications of spent EY-APTES@PDA@PUF after six cycles of 2-methyl-5-nitro-isoquinolin-2-ium iodide oxidation.

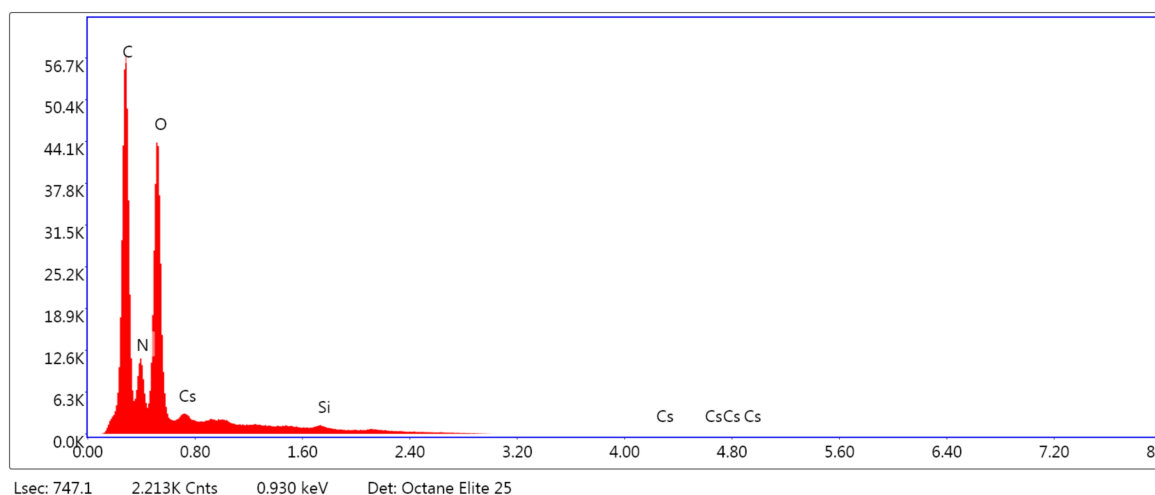


Figure 16. EDX spectrum of spent EY-APTES@PDA@PUF after six cycles of 2-methyl-5-nitro-isoquinolin-2-ium iodide oxidation.

To get more insight to the photocatalytic properties of EY-APTES@PDA@PUF and better apprehend the influence of EY leaching on these, we next investigated a reaction of interest where the presence of PC is absolutely essential for its progress:^{10, 38} the oxidation of sulfides

to sulfoxides. Sulfoxides are among the most prevalent and important functional groups found in diverse natural products and pharmaceutical molecules.⁵² In addition, sulfoxides are synthetic intermediates for the construction of various organic compounds.⁵³⁻⁵⁴

Initial studies focused on the oxidation of methyl *p*-tolyl sulfide to its corresponding sulfoxide under 24 W white LED irradiation at 30-35 °C (due to LED light heating) using eosin Y (0.5 mol%) or a cubic sample of EY-APTES@PDA@PUF of ca. 2 cm × 2 cm × 2 cm, whose mass was adjusted to have an eosin Y loading of 0.18 mol%, as catalysts (Table 2). Solvents and air or O₂ atmosphere were found to have a prominent influence on the reaction yield. In CH₃CN/H₂O (3:1) under air, the reaction yield reached 84% after 6 h reaction with eosin Y as catalyst, giving a turnover number (TON) of 168 and a turnover frequency (TOF) of 28 h⁻¹ (entry 1). Running the reaction with EY-APTES@PDA@PUF (0.18 mol% EY) in the same solvent mixture but with 5-fold lower concentration (to allow the complete immersion of the macroscopic catalyst) resulted in only 36% yield after 18 h reaction, thus in a slightly higher TON (200 vs. 168) but a 2.5 slower TOF (entry 2), while running it in pure CH₃CN or CH₃CN/H₂O (1:1) resulted in very low yields, TON and TOF (entries 3 and 4). Satisfyingly however, switching to an O₂ atmosphere and to 4:1 mixture of CH₃CN/H₂O allowed to observe almost full conversion after 48 h reaction, reaching a TON of 544 and TOF of 11.3 h⁻¹.

Table 2. Optimization of the reaction conditions for the oxidation of methyl *p*-tolyl sulfide under visible light using eosin Y or EY-APTES@PDA@PUF as photocatalyst.^a

Entry	Catalyst	Solvent	Time (h)	NMR yield (%)	TON ^d	TOF (h ⁻¹) ^e
1 ^a	Eosin Y	CH ₃ CN/H ₂ O (3:1)	6	84	168	28
2 ^b	EY-APTES@PDA@PUF	CH ₃ CN/H ₂ O (3:1)	18	36	200	11.1
3 ^b	EY-APTES@PDA@PUF	CH ₃ CN	18	0	0	0
4 ^b	EY-APTES@PDA@PUF	CH ₃ CN/H ₂ O (1:1)	18	9	50	2.8
5 ^c	EY-APTES@PDA@PUF	CH ₃ CN/H ₂ O (4:1)	48	98	544	11.3

^a Conditions: methyl *p*-tolyl sulfide (1 mmol), eosin Y (0.5 mol% EY), CH₃CN/H₂O (3:1) (8 mL), 24 W white LED, air balloon, 30-35 °C due to LED light heat. ^b methyl *p*-tolyl sulfide (0.5 mmol), EY-APTES@PDA@PUF (2 cm x 2 cm x 2 cm, 0.18 mol% EY), solvent (20 mL), 24W white LED, air balloon, 30-35 °C due to LED light heat, 1000 rpm. ^c methyl *p*-tolyl sulfide (0.5 mmol), EY-APTES@PDA@PUF (2 cm x 2 cm x 2 cm, 0.18 mol% EY), CH₃CN/H₂O (4:1) (20 mL), 24W white LED, O₂ balloon, 30-35 °C due to LED light heat, 1000 rpm. ^d TON expressed as the yield / catalyst loading. ^e TOF (h⁻¹) expressed as the TON / reaction time (h).

With these optimized reaction conditions in hands: EY-APTES@PDA@PUF (2 cm x 2 cm x 2 cm, 0.18 mol% EY), CH₃CN/H₂O (4:1) (20 mL), 24W white LED, O₂ balloon, 30-35 °C, 48 h, recycling tests were then performed with a single sample of freshly prepared EY-APTES@PDA@PUF. In contrast to what was observed for the oxidation of 2-methyl-5-nitroisoquinolin-2-ium iodide (**Figure 13**), a gradual decrease of the NMR yield was observed, from 98% in the 1st run to 59% in the 5th run (**Figure 17**), which tended to confirm that there might exist some catalysts leaching or deactivation. Accordingly, ICP-AES analyses of the used foam after these 5 catalytic runs indicated an eosin Y loss of 34% with a Br content of 0.691 ± 0.019 g/kg vs. 1.051 ± 0.029 g/kg in the as-synthesized foam.

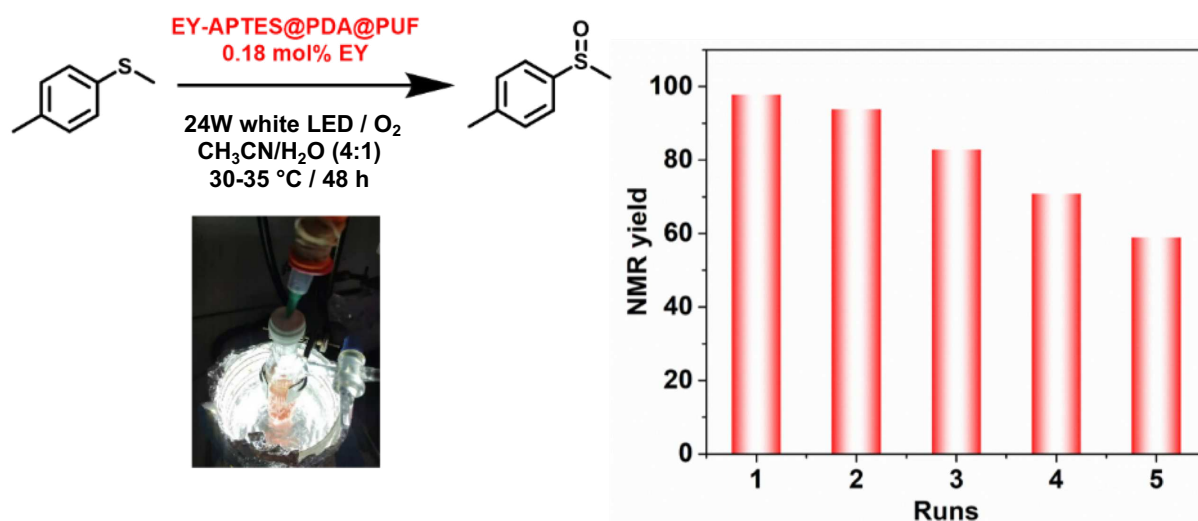


Figure 17. Isolated yields measured over five successive runs of *p*-tolyl methyl sulfide oxidation photocatalyzed by a single sample of EY-APTES@PDA@PUF. Reaction conditions: methyl *p*-tolyl sulfide (0.5 mmol), EY-APTES@PDA@PUF (2 cm x 2 cm x 2 cm, 0.18 mol% EY), CH₃CN/H₂O (4:1) (20 mL), 24W white LED, O₂ balloon, 30-35 °C due to LED light heat, 1000 rpm.

A stop-and-go experiment run with an as-synthesized EY-APTES@PDA@PUF foam under similar reaction conditions showed that the *p*-tolyl methyl sulfide oxidation does not stop when the foam is removed from the liquid medium, which unambiguously confirmed that eosin Y was leaching (**Figure 18**). The reaction rate during the 10 h reaction run without the macroscopic photocatalyst even slightly increased compared with the first 20 h reaction in the presence of the foam-based catalyst.

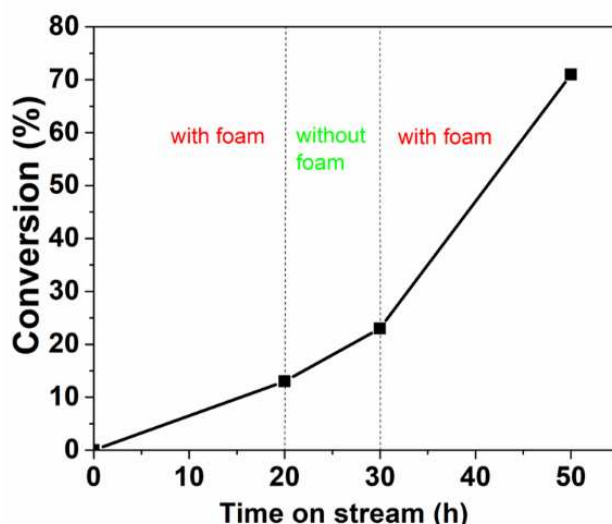
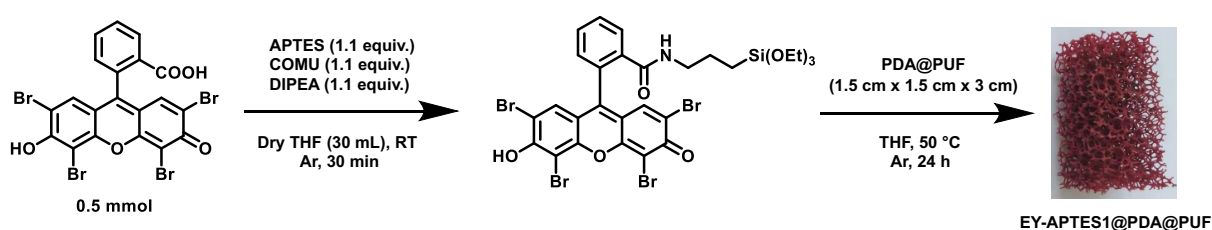


Figure 18. Stop-and-go experiment on *p*-tolyl methyl sulfide oxidation with EY-APTES@PDA@PUF. Reaction conditions: methyl *p*-tolyl sulfide (0.5 mmol), EY-APTES@PDA@PUF (2 cm x 2 cm x 2 cm, 0.18 mol% EY), CH₃CN/H₂O (4:1) (20 mL), 24W white LED, O₂ balloon, 30-35 °C due to LED light heat, 1000 rpm.

A non-negligible adsorption of eosin Y on the PDA layer coupled to a low efficiency of the EDC-mediated coupling reaction with the grafted amine groups were suspected to be the origin of this phenomenon. Other strategies for preparing the supported photocatalyst were therefore considered. In a first attempt, in order to minimize the simple adsorption of eosin Y onto PDA and to have a more efficient eosin-APTES coupling, eosin Y was coupled to APTES prior to the covalent anchoring procedure to PDA@PUF, and this in the presence of COMU instead of EDC (**Scheme 3**). For that purpose, neutral eosin Y was reacted with 1.1 equiv. of APTES in the presence of 1.1 equiv. of COMU and 1.1 equiv. of diisopropylethylamine (DIPEA) in THF for 30 min at RT, before introducing a PDA-coated PUF into the medium and increasing the reaction temperature to 50 °C for 24 h. The thus obtained red EY-APTES1@PDA@PUF foam was then washed successively with acetone, water and acetonitrile under 24W white LED irradiation, before vacuum drying.



Scheme 3. One-pot COMU-mediated eosin-Y-APTES coupling and APTES-PDA condensation for anchoring EY-APTES on PDA@PUF

Next EY-APTES1@PDA@PUF was tested for the oxidation of *p*-tolyl methyl sulfide in three successive runs under the exact same conditions that were used for EY-APTES@PDA@PUF. Significant leaching was again observed (**Figure 19**). While only 24 h

reaction was sufficient to reach 97% conversion in the first run, which suggested a higher initial eosin Y loading than with the sequential grafting process, the conversion dropped to 64% after 24 h reaction in the second run and to 49% in the third run. Owing to this severe deactivation, further characterization was not carried out.

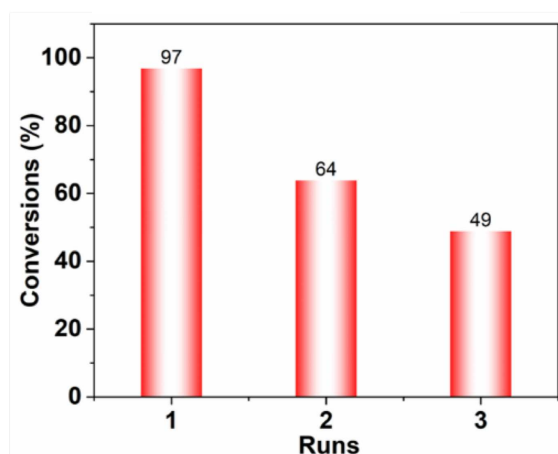
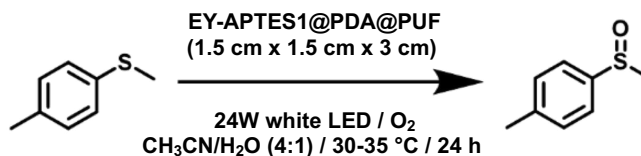
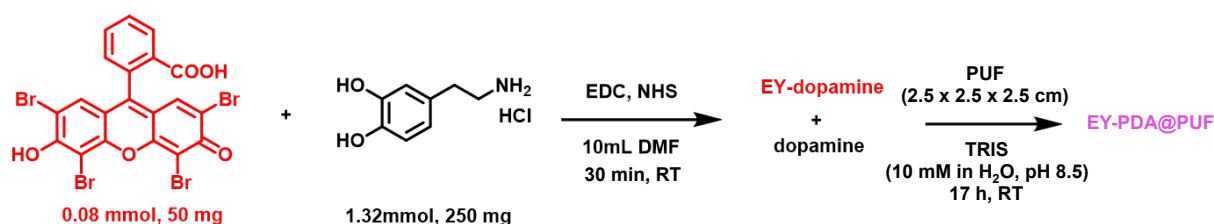


Figure 19. Isolated yields measured over three successive runs of *p*-tolyl methyl sulfide oxidation photocatalyzed by a single sample of EY-APTES1@PDA@PUF. Reaction conditions: methyl *p*-tolyl sulfide (0.5 mmol), EY-APTES1@PDA@PUF (1.5 cm x 1.5 cm x 3 cm), CH₃CN/H₂O (4:1) (20 mL), 24W white LED, O₂ balloon, 30-35 °C due to LED light heat, 1000 rpm

A completely different strategy was then considered. After an EDC-mediated coupling of eosin Y with dopamine in the presence of a large excess of the latter, the resulting mixture was placed under dopamine self-polymerization conditions to generate an EY-PDA hybrid coating in the presence of a cubic sample of PUF (2.5 cm x 2.5 cm x 2.5 cm) and provide a EY-PDA@PUF material without APTES (**Scheme 4**). Following this procedure, the resulting very dark red foam was dried in an oven at 80 °C for 1 h, and then washed with acetone and acetonitrile until the washings were colorless.



Scheme 4. Hybrid EY-PDA coating of PUF.

The catalyst efficiency and reusability of EY-PDA@PUF was then evaluated for the

oxidation of thioanisole. Satisfyingly, the conversion of thioanisole to the corresponding sulfoxide reached 99% in only 14 h for the 1st run. However, the conversion decreased to 75% in the 3rd run and this tendency continued until the 5th run with only 20% conversion (**Figure 20**), suggesting considerable eosin Y leaching in this case as well. Furthermore, when EY-PDA@PUF was rinsed under supersonic bath conditions right after the synthesis, the conversion of thioanisole dropped directly to 31%, strongly suggesting that a large amount of adsorbed EY instead of grafted EY existed in this case as well.

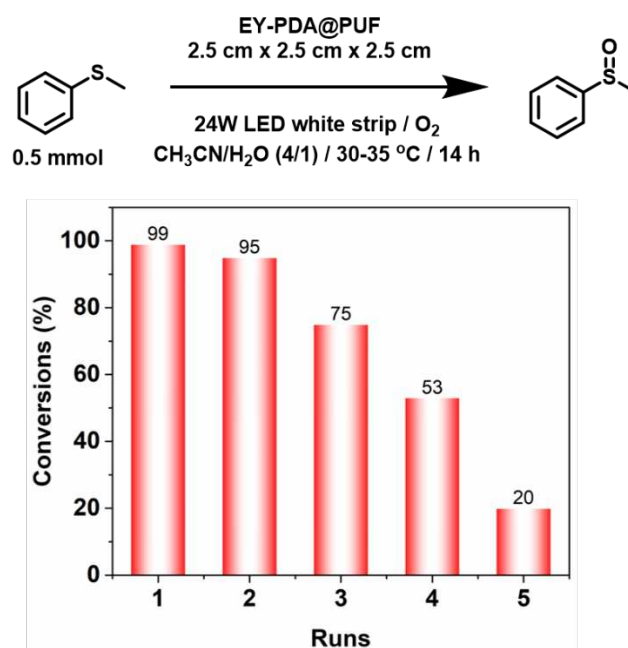


Figure 20. Isolated yields measured over five successive runs of thioanisole oxidation photocatalyzed by a single sample of EY-PDA@PUF. Reaction conditions: thioanisole (0.5 mmol), EY-PDA@PUF (2.5 cm x 2.5 cm x 2.5 cm), CH₃CN/H₂O (4:1) (20 mL), 24W white LED, O₂ balloon, 30-35 °C due to LED light heat, 1000 rpm

To exclude any potential effect from this specific reaction type, we then studied the nitromethanation of *N*-phenyl-tetrahydroisoquinoline, which was successfully catalyzed by Ru(bpy)₃-APTES@PDA@PUF (see Chapter I). Unfortunately, a similar catalyst deactivation phenomenon was observed.

Compared with supported the EY catalysts described in the introduction, the stability of our PDA@PUF supported catalysts is disappointing, suggesting that PDA may not be an ideal support matrix for eosin Y or other similar dyes.

III) Conclusion and perspectives

In summary, we have prepared EY-APTES@PDA@PUF, EY-APTES1@PDA@PUF and PDA-EY@PUF foams that functioned as photocatalysts for the oxidation of *N*-alkylpyridinium salts to quinolones and isoquinolones and of sulfides to sulfoxides under visible-light

irradiation. Following a simple dip-coating protocol of PUF into an aqueous solution of dopamine buffered to a pH of 8.5, PDA@PUF was functionalized with eosin Y, either via a two-step process involving silanization with APTES and EDC-mediated coupling with eosin Y, or via a one-pot protocol implying the coupling of eosin Y with APTES prior to the covalent anchoring procedure by condensation of the alkoxysilane groups with the catechols of PDA. Alternatively, a one-step coating-and-functionalization strategy implying the *in situ* coupling of dopamine with eosin Y was adopted to generate EY-PDA@PUF. All three macroscopic photocatalyst showed high efficiency for their first use in a model oxidation of sulfide to sulfoxides reaction. However, recycling tests highlighted fast deactivation due to important eosin Y leaching. This was clearly demonstrated in the case of EY-APTES@PDA@PUF by a stop-and-go experiment and ICP-AES measurements that showed a 34% eosin Y loss after five runs. The combination of PDA and eosin Y may thus not be appropriate to anchor robustly eosin Y on PUF.

IV) Experimental section

IV-1) Materials and methods

All reagents and solvents were used as provided by commercial suppliers without any further purification/treatment. Polyurethane open cells foams (20 PPI, TCL 40100 soft white reticulated) were given by FoamPartner. Eosin Y (T0035) and 4-(methylthio)toluene (M0949) were purchased from TCI. Dopamine hydrochloride (008896), EDC hydrochloride (024810), N-hydroxysuccinimide (005022), 3-aminopropyltriethoxysilane (ISI0010-98) and thioanisole (002945) were purchased from Fluorochem. Tris base (99.9+% - T1503) was purchased from Sigma-Aldrich. COMU (344284) was provided by Acros Organics. 2-Methyl-5-nitroisoquinolin-2-ium iodide was prepared according to a published procedure.⁵⁵ 18.2 MΩ deionized water (TOC < 1 ppb), supplied by a Q20 Millipore system, was used for the preparation of aqueous solutions and washing procedures with water. RGB LED strip light (Govee, H6190) was manufactured by Shenzhen Intellirocks Tech Co. Ltd. Purifications by column chromatography were carried out with Macherey silica gel (Kielselgel 60). TraceMetal grade HCl 37 % (Fisher Chemical) and Rotipuran Supra HNO₃ 69 % (Roth) were used for ICP-AES analyses. Element standards were purchased from CPI international.

Scanning electron microscopy (SEM) measurements were recorded with a Hitachi SU8010 FE-SEM microscope at 3 kV at room temperature. No metallization of the samples was done, but their borders were covered with a metallic tape to evacuate the excess of charge.

Elemental mapping by scanning electron microscopy-energy dispersive X-ray spectroscopy (SEM-EDX) was investigated with a Zeiss Gemini SEM 500 FEG EDAX Octane

Elite EDX detector. The X-rays emitted upon electron irradiation were acquired in the range 0–20 keV. Quantification was done using the standard-less ZAF correction method in the Team EDS software from EDAX.

Inductively coupled plasma-atomic emission spectrometry (ICP-AES) measurements were performed by the Plateforme Analytique of the Institut Pluridisciplinaire Hubert Curien (UMR CNRS 7178), Strasbourg, France.

Gas chromatographic (GC) analyses were done on a GC Agilent with FID detectors using Agilent HP1 column (30 m, 0.35 mm, 0.25 μ m), with hydrogen as gas carrier and with tetradecane as the internal standard. The retention times and GC responses in terms of area versus concentration of the reagents and products were calibrated by using pure components directly transferred from reactive solutions. The conversion and product distribution were calculated from the GC results.

Solution NMR spectra were recorded at 298 K on a Bruker Avance III HD 400 MHz spectrometer operating at 400.13 MHz for ^1H . The chemical shifts are referenced to the residual deuterated. Chemical shifts (δ) and coupling constants (J) are expressed in ppm and Hz respectively.

For solid-state NMR spectra, the foam samples were frozen into $\text{N}_2(l)$ and grinded. The grinded foams were then packed in 4 mm ZrO_2 rotors under air. The ^{29}Si CP-MAS experiments spectra were recorded at 298 K on a Bruker Solid State DSX 300 MHz NMR spectrometer operating at 69.66 MHz, and equipped with a Bruker 4 mm $^1\text{H}/\text{X}$ CP-MAS probe. A shaped Cross-Polarization pulse sequence with tangential modulation on both channels was used with the following parameters: the spinning speed was set to 10 kHz, the spectral width to 30 kHz, the contact time was in the range of 1 ms, the proton RF field was around 55 kHz for decoupling (using SPINAL 64 sequence) and 40 kHz for contact, with a recycle delay of 5s. The spectra were calibrated with respect an external PDMS sample (-35.1 ppm).

IV-2) Experimental procedures

IV-2-1) Open cell polyurethane foam (PUF) coating with polydopamine (PDA)

A cubic sample of PDA@PUF of ca. 2 cm \times 2 cm \times 2 cm was coated with PDA as described in Chapter I.

IV-2-2) Functionalization of PDA@PUF with APTES

A cubic sample of PDA@PUF of ca. 2 cm \times 2 cm \times 2 cm was functionalized with APTES as described in Chapter I. A similar mean Si content of 3.763 ± 0.041 g/kg was established by ICP-AES.

IV-2-3) Coupling of neutral eosin Y with APTES@PDA@PUF

A cubic sample of APTES@PDA@PUF (ca. 2 cm × 2 cm × 2 cm) was washed for a few minutes in vigorously stirred toluene (3 × 25 mL) before use.

A stirring bar was introduced in a Schlenk tube. This was followed by the additions of ethanol (20 mL), eosin Y (65 mg, 0.1 mmol), *N*-hydroxysuccinimide (17 mg, 0.15 mmol) and EDC hydrochloride (38 mg, 0.2 mmol) in this order. After 0.5 h of stirring, the cubic sample of APTES@PDA@PUF) was then immersed into the solution for overnight stirring at room temperature. The resulting eosin Y-coupled foam, EY-APTES@PDA@PUF, was then washed in acetone (10 × 60 mL) and CH₃CN/H₂O (4:1) (2 × 60 mL), and dried under vacuum.

EY-APTES@PDA@PUF was characterized by SEM, EDX, ²⁹Si CP-MAS NMR and ICP-AES revealing mean Si and Br contents of 2.544 ± 0.077 g/kg and 1.051 ± 0.029 g/kg, respectively.

IV-2-4) Preparation of EY-APTES@PDA@PUF in a one-pot procedure from PDA@PUF

A stirring bar, neutral eosin Y (324 mg, 0.50 mmol) and COMU (235 mg, 0.55 mmol) were introduced in a Schlenk tube. The atmosphere was then evacuated under vacuum and back-filled with argon, three times. Freshly distilled THF (25 mL), *N,N*-diisopropylethylamine (0.12 mL, 0.75 mmol) and APTES (0.26 mL, 0.55 mmol) were subsequently added, and the mixture stirred for 30 min under argon at room temperature. A sample of PDA@PUF (ca. 1.5 cm × 1.5 cm × 3 cm) was then immersed into the solution and the mixture was stirred for 24 h under argon at 50 °C. The resulting EY-APTES@PDA@PUF foam was washed under vigorous stirring overnight (each time) in acetone (60 mL), H₂O (60 mL) and CH₃CN (60 mL) under 24W white LED irradiation, and then dried under vacuum.

IV-2-5) Preparation of EY-PDA@PUF

A 25 mL round-bottomed flask was charged with neutral eosin Y (50 mg, 0.08 mmol), *N*-hydroxysuccinimide (10 mg, 0.08 mmol), EDC hydrochloride (16 mg, 0.08 mmol) and DMF (5 mL). After 10 min of stirring at room temperature, dopamine hydrochloride (250 mg, 1.32 mmol) was added and the mixture was reacted for 30 min at the same temperature. The reaction mixture was then poured into a beaker containing an aqueous solution (125 mL) of Tris base (10 mM) buffered to pH 8.5 with aqueous HCl (1 M). A cubic sample of pristine PUF (ca. 2.5 cm × 2.5 cm × 2.5 cm) was immersed in the beaker and the reaction mixture stirred for 17 h at room temperature. The resulting very dark red EY-PDA@PUF foam was then taken out from the beaker and dried in an oven at 80 °C for 1 h. This was followed by thorough washings under vigorous stirring in acetone (60 mL) and CH₃CN (60 mL), and drying under vacuum.

IV-2-6) General procedure for the oxidation of 2-methyl-5-nitro-isoquinolin-2-ium iodide

photocatalyzed by EY-APTES@PDA@PUF

A stirring bar and a cubic sample of EY-APTES@PDA@PUF of ca. 2 cm × 2 cm × 2 cm, whose mass (280 mg) was adjusted in function of its Br content established by ICP-AES (0.105 wt%) to have an EY loading of 0.925 μmol, were introduced in a 10 mL Schlenk tube.^a

2-Methyl-5-nitroisoquinolin-2-ium iodide (0.2 mmol), Cs₂CO₃ (0.3 mmol) and acetonitrile (8 mL) were then added so that the foam was totally immersed.^a The tube was sealed with a rubber septum equipped with an air balloon and the reaction mixture stirred at room temperature (650 rpm) under irradiation with a 24 W white LED strip for 24 h. Water (8 mL) was then added and the product was extracted with ethyl acetate (8 mL × 2). After purification by chromatography on silica (petroleum ether/ethyl acetate, V/V = 1/1) and solvent removal, the oxidation product was obtained as a yellow solid and its identity confirmed by ¹H NMR in CDCl₃.

^a: the foam was compressed in these conditions.

IV-2-7) General procedures for the oxidation of sulfides to sulfoxides photocatalyzed by EY-APTES@PDA@PUF or EY-PDA@PUF

A stirring bar and the cubic sample of EY-APTES@PDA@PUF of ca. 2 cm × 2 cm × 2 cm, whose mass (280 mg) was adjusted in function of its Br content established by ICP-AES (0.105 wt%) to have a EY loading of 0.925 μmol, were introduced in a 50 mL Schlenk tube.^a

Acetonitrile/water (4:1) (20 mL) was then added to immerse the foam. This was followed by the addition of *p*-tolyl methyl sulfide (for EY-APTES@PDA@PUF and EY-APTES1@PDA@PUF) or thioanisole (for EY-PDA@PUF) (0.5 mmol). The tube was then sealed with a rubber septum, degassed, and refilled with O₂ several times, and finally equipped with an O₂ balloon. The reaction mixture was vigorously stirred (1000 rpm) at room temperature and aliquots of the reaction medium were periodically removed by syringe to determine the conversion of sulfides by GC analysis or, after removal of solvents under reduced pressure, by ¹H NMR in CDCl₃.

^a: the foam was not compressed in these conditions.

IV-2-8) Reusability procedure

After each run, the foam was separated from the liquid then washed with acetone (3 × 30 mL), H₂O (3 × 30 mL) and acetonitrile (3 × 30 mL), dried under vacuum and re-used as described above.

IV-2-9) Stop-and-go experiment for the oxidation of *p*-tolyl methyl sulfide

In this control experiment conducted for checking the occurrence of eosin Y leaching into

the liquid medium, the above-described general procedure for the oxidation of sulfides to sulfoxides was followed using *p*-tolyl methyl sulfide (0.5 mmol) in CH₃CN/H₂O (4:1) (20 mL), an O₂ balloon, a 24W white LED strip, and a cubic sample of EY-APTES@PDA@PUF of ca. 2 cm × 2 cm × 2 cm, whose mass (280 mg) was adjusted in function of its Br content established by ICP-AES (0.105 wt%) to have a EY loading of 0.925 μmol, as catalyst, except that, after 20 h reaction, the EY-APTES@PDA@PUF foam was removed from the reaction medium for 10 h. Then, EY-APTES@PDA@PUF was reintroduced in the reacting vessel for 20 h. During the whole process, the O₂ atmosphere was maintained. The course of the reaction was monitored by sampling the reaction medium at T = 20, 30, and 50 h, and analyzing the removed aliquots (50 μL) by GC.

V) References

1. Srivastava, V.; Singh, P. P., Eosin Y catalysed photoredox synthesis: a review. *RSC Adv.* **2017**, 7 (50), 31377-31392.
2. Hari, D. P.; König, B., Synthetic applications of eosin Y in photoredox catalysis. *Chem. Commun.* **2014**, 50 (51), 6688-6699.
3. Pitre, S. P.; McTiernan, C. D.; Ismaili, H.; Scaiano, J. C., Mechanistic Insights and Kinetic Analysis for the Oxidative Hydroxylation of Arylboronic Acids by Visible Light Photoredox Catalysis: A Metal-Free Alternative. *J. Am. Chem. Soc.* **2013**, 135 (36), 13286-13289.
4. Huang, L.; Zhao, J.; Guo, S.; Zhang, C.; Ma, J., Bodipy Derivatives as Organic Triplet Photosensitizers for Aerobic Photoorganocatalytic Oxidative Coupling of Amines and Photooxidation of Dihydroxynaphthalenes. *J. Org. Chem.* **2013**, 78 (11), 5627-5637.
5. Romero, N. A.; Nicewicz, D. A., Organic Photoredox Catalysis. *Chem. Rev.* **2016**, 116 (17), 10075-10166.
6. Herbrink, F.; Camarero González, P.; Krstic, M.; Puglisi, A.; Benaglia, M.; Sanz, M. A.; Rossi, S., Eosin Y: Homogeneous Photocatalytic In-Flow Reactions and Solid-Supported Catalysts for In-Batch Synthetic Transformations. *Appl. Sci.* **2020**, 10 (16), 5596.
7. Zhang, L.; Zhou, Q.; Kang, S. Z.; Li, X. Q.; Mu, J. Visible Light Photocatalytic Hydrogen Evolution from Water Reduction Using Eosin y Containing Trace Vitamin B12 as a Light Harvesting Unit, *Adv. Mater. Res.* **2013**, 724-725, 753-756.
8. Yang, X.-J.; Chen, B.; Zheng, L.-Q.; Wu, L.-Z.; Tung, C.-H., Highly efficient and selective photocatalytic hydrogenation of functionalized nitrobenzenes. *Green Chem.* **2014**, 16 (3), 1082-1086.
9. Rueping, M.; Zhu, S.; Koenigs, R. M., Photoredox catalyzed C–P bond forming

- reactions — visible light mediated oxidative phosphorylations of amines. *Chem. Commun.* **2011**, 47 (30), 8679-8681.
10. Sridhar, A.; Rangasamy, R.; Selvaraj, M., Polymer-supported eosin Y as a reusable photocatalyst for visible light mediated organic transformations. *New Journal of Chemistry* **2019**, 43 (46), 17974-17979.
 11. Hari, D. P.; Schroll, P.; König, B., Metal-Free, Visible-Light-Mediated Direct C–H Arylation of Heteroarenes with Aryl Diazonium Salts. *J. Am. Chem. Soc.* **2012**, 134 (6), 2958-2961.
 12. Cantillo, D.; de Frutos, O.; Rincón, J. A.; Mateos, C.; Kappe, C. O., Continuous Flow α -Trifluoromethylation of Ketones by Metal-Free Visible Light Photoredox Catalysis. *Org. Lett.* **2014**, 16 (3), 896-899.
 13. Pham, P. V.; Nagib, D. A.; MacMillan, D. W. C., Photoredox Catalysis: A Mild, Operationally Simple Approach to the Synthesis of α -Trifluoromethyl Carbonyl Compounds. *Angew. Chem. Int. Ed.* **2011**, 50 (27), 6119-6122.
 14. Kitano, H.; Ramachandran, K.; Scranton, A. B., Free Radical Shadow Cure Initiated Using Two-Component and Three-Component Initiator Systems. *Int. J. Photoenergy* **2012**, 2012, 213846.
 15. Avens, H. J.; Bowman, C. N., Mechanism of cyclic dye regeneration during eosin-sensitized photoinitiation in the presence of polymerization inhibitors. *J. Polym. Sci. A Polym. Chem.* **2009**, 47 (22), 6083-6094.
 16. Xu, J.; Shanmugam, S.; Duong, H. T.; Boyer, C., Organo-photocatalysts for photoinduced electron transfer-reversible addition–fragmentation chain transfer (PET-RAFT) polymerization. *Polym. Chem.* **2015**, 6 (31), 5615-5624.
 17. Yeow, J.; Chapman, R.; Xu, J.; Boyer, C., Oxygen tolerant photopolymerization for ultralow volumes. *Polym. Chem.* **2017**, 8 (34), 5012-5022.
 18. Shanmugam, S.; Xu, S.; Adnan, N. N. M.; Boyer, C., Heterogeneous Photocatalysis as a Means for Improving Recyclability of Organocatalyst in “Living” Radical Polymerization. *Macromolecules* **2018**, 51 (3), 779-790.
 19. Neumann, M.; Földner, S.; König, B.; Zeitler, K., Metal-Free, Cooperative Asymmetric Organophotoredox Catalysis with Visible Light. *Angew. Chem. Int. Ed.* **2011**, 50 (4), 951-954.
 20. Neumann, M.; Zeitler, K., A Cooperative Hydrogen-Bond-Promoted Organophotoredox Catalysis Strategy for Highly Diastereoselective, Reductive Enone Cyclization. *Chem. Eur. J.* **2013**, 19 (22), 6950-6955.
 21. Nicewicz, D. A.; MacMillan, D. W. C., Merging Photoredox Catalysis with Organocatalysis: The Direct Asymmetric Alkylation of Aldehydes. *Science* **2008**, 322 (5898), 77-80.

22. Penzkofer, A.; Beidoun, A.; Daiber, M., Intersystem-crossing and excited-state absorption in eosin Y solutions determined by picosecond double pulse transient absorption measurements. *J. Lumin.* **1992**, *51* (6), 297-314.
23. Penzkofer, A.; Beidoun, A., Triplet-triplet absorption of eosin Y in methanol determined by nanosecond excimer laser excitation and picosecond light continuum probing. *Chem. Phys.* **1993**, *177* (1), 203-216.
24. Penzkofer, A.; Beidoun, A.; Speiser, S., Singlet excited-state absorption of eosin Y. *Chem. Phys.* **1993**, *170* (1), 139-148.
25. Zhang, J.; Wang, L.; Liu, Q.; Yang, Z.; Huang, Y., Synthesis of α,β -unsaturated carbonyl compounds via a visible-light-promoted organocatalytic aerobic oxidation. *Chem. Commun.* **2013**, *49* (99), 11662-11664.
26. Majek, M.; Filace, F.; von Wangelin, A. J., On the mechanism of photocatalytic reactions with eosin Y. *Beilstein journal of organic chemistry* **2014**, *10* (1), 981-989.
27. Lambert, J. H., *J. H. Lambert, ... Photometria, sive de Mensura et gradibus luminis, colorum et umbrae.* sumptibus viduae E. Klett: 1760.
28. Satoh, M.; Shirai, K.; Saitoh, H.; Yamauchi, T.; Tsubokawa, N., Photografting of polymers onto nanosized silica surface initiated by eosin moieties immobilized onto the surface. *J. Polym. Sci. A Polym. Chem.* **2005**, *43* (3), 600-606.
29. Mou, Z.; Dong, Y.; Li, S.; Du, Y.; Wang, X.; Yang, P.; Wang, S., Eosin Y functionalized graphene for photocatalytic hydrogen production from water. *Int. J. Hydrog. Energy* **2011**, *36* (15), 8885-8893.
30. Wang, J.; Liu, Y.; Li, Y.; Xia, L.; Jiang, M.; Wu, P., Highly Efficient Visible-Light-Driven H₂ Production via an Eosin Y-Based Metal–Organic Framework. *Inorg. Chem.* **2018**, *57* (13), 7495-7498.
31. Kumar, G.; Solanki, P.; Nazish, M.; Neogi, S.; Kureshy, R. I.; Khan, N.-u. H., Covalently hooked EOSIN-Y in a Zr(IV) framework as visible-light mediated, heterogeneous photocatalyst for efficient CH functionalization of tertiary amines. *J. Catal.* **2019**, *371*, 298-304.
32. Yu, X.; Yang, Z.; Qiu, B.; Guo, S.; Yang, P.; Yu, B.; Zhang, H.; Zhao, Y.; Yang, X.; Han, B.; Liu, Z., Eosin Y-Functionalized Conjugated Organic Polymers for Visible-Light-Driven CO₂ Reduction with H₂O to CO with High Efficiency. *Angew. Chem. Int. Ed.* **2019**, *58* (2), 632-636.
33. Tang, L.; Li, T.; Zhuang, S.; Lu, Q.; Li, P.; Huang, B., Synthesis of pH-Sensitive Fluorescein Grafted Cellulose Nanocrystals with an Amino Acid Spacer. *ACS Sustainable Chem. Eng.* **2016**, *4* (9), 4842-4849.
34. Li, X.; Zhang, Y. C.; Zhao, Y.; Zhao, H. P.; Zhang, B.; Cai, T., Xanthene Dye-Functionalized Conjugated Porous Polymers as Robust and Reusable Photocatalysts

- for Controlled Radical Polymerization. *Macromolecules* **2020**, *53* (5), 1550-1556.
35. Zhao, Y.; Shao, S.; Xia, J.; Huang, Y.; Zhang, Y. C.; Li, X.; Cai, T., Hydrophilic ultrafiltration membranes with surface-bound eosin Y for an integrated synthesis-separation system of aqueous RAFT photopolymerization. *J. Mater. Chem. A* **2020**, *8* (19), 9825-9831.
 36. Teixeira, R. I.; de Lucas, N. C.; Garden, S. J.; Lanterna, A. E.; Scaiano, J. C., Glass wool supported ruthenium complexes: versatile, recyclable heterogeneous photoredox catalysts. *Catal. Sci. Technol.* **2020**, *10* (5), 1273-1280.
 37. Li, P.; Wang, G.-W.; Zhu, X.; Wang, L., Magnetic nanoparticle-supported eosin Y ammonium salt: An efficient heterogeneous catalyst for visible light oxidative C–C and C–P bond formation. *Tetrahedron* **2019**, *75* (25), 3448-3455.
 38. Chu, Y.; Huang, Z.; Liu, R.; Boyer, C.; Xu, J., Scalable and Recyclable Heterogeneous Organo-photocatalysts on Cotton Threads for Organic and Polymer Synthesis. *ChemPhotoChem* **2020**, *4* (10), 5201-5208.
 39. Pardieu, E.; Chau, N. T. T.; Dintzer, T.; Romero, T.; Favier, D.; Roland, T.; Edouard, D.; Jierry, L.; Ritleng, V., Polydopamine-coated open cell polyurethane foams as an inexpensive, flexible yet robust catalyst support: a proof of concept. *Chem. Commun.* **2016**, *52* (25), 4691-4693.
 40. Albert, K.; Pfeleiderer, B.; Bayer, E.; Schnabel, R., Characterization of chemically modified glass surfaces by ¹³C and ²⁹Si CP/MAS NMR spectroscopy. *J. Colloid Interf. Sci.* **1991**, *142* (1), 35-40.
 41. Ait Khouya, A.; Mendez Martinez, M. L.; Bertani, P.; Romero, T.; Favier, D.; Roland, T.; Guidal, V.; Bellière-Baca, V.; Edouard, D.; Jierry, L.; Ritleng, V., Coating of polydopamine on polyurethane open cell foams to design soft structured supports for molecular catalysts. *Chem. Commun.* **2019**, *55* (79), 11960-11963.
 42. Scholz, M.; Dëdic, R.; Breitenbach, T.; Hála, J., Singlet oxygen-sensitized delayed fluorescence of common water-soluble photosensitizers. *Photochem. Photobiol. Sci.* **2013**, *12* (10), 1873-1884.
 43. Lutkus, L. V.; Rickenbach, S. S.; McCormick, T. M., Singlet oxygen quantum yields determined by oxygen consumption. *J. Photochem. Photobiol. A: Chem.* **2019**, *378*, 131-135.
 44. Ghogare, A. A.; Greer, A., Using Singlet Oxygen to Synthesize Natural Products and Drugs. *Chem. Rev.* **2016**, *116* (17), 9994-10034.
 45. Zamadar, M.; Greer, A., Singlet Oxygen as a Reagent in Organic Synthesis. *Handbook of Synthetic Photochemistry*, 2009; pp 353-386.
 46. Jin, Y.; Ou, L.; Yang, H.; Fu, H., Visible-Light-Mediated Aerobic Oxidation of N-Alkylpyridinium Salts under Organic Photocatalysis. *J. Am. Chem. Soc.* **2017**, *139* (40),

14237-14243.

47. Bonesi, S. M.; Fagnoni, M.; Albini, A., Photosensitized Electron Transfer Oxidation of Sulfides: A Steady-State Study. *Eur. J. Org. Chem.* **2008**, 2008 (15), 2612-2620.
48. Carey, J. S.; Laffan, D.; Thomson, C.; Williams, M. T., Analysis of the reactions used for the preparation of drug candidate molecules. *Org. Biomol. Chem.* **2006**, 4 (12), 2337-2347.
49. Claassen, G.; Brin, E.; Crogan-Grundy, C.; Vaillancourt, M. T.; Zhang, H. Z.; Cai, S. X.; Drewe, J.; Tseng, B.; Kasibhatla, S., Selective activation of apoptosis by a novel set of 4-aryl-3-(3-aryl-1-oxo-2-propenyl)-2(1H)-quinolinones through a Myc-dependent pathway. *Cancer Lett.* **2009**, 274 (2), 243-249.
50. Forbis, R. M.; Rinehart, K. L. Jr., Nybomycin. VII. Preparative routes to nybomycin and deoxynybomycin. *J. Am. Chem. Soc.* **1973**, 95 (15), 5003-5013.
51. Afonso, A.; Weinstein, J.; Gentles, M. J., Antiviral compounds and antihypertensive compounds. WO9203327, 1992.
52. Goncharov, N.; Orekhov, A. N.; Voitenko, N.; Ukolov, A.; Jenkins, R.; Avdonin, P., Chapter 41 - Organosulfur Compounds as Nutraceuticals. Nutraceuticals, Gupta, R. C., Ed. Academic Press: Boston, 2016; pp 555-568.
53. Huang, X.; Maulide, N., Sulfoxide-Mediated α -Arylation of Carbonyl Compounds. *J. Am. Chem. Soc.* **2011**, 133 (22), 8510-8513.
54. Carreno, M. C., Applications of Sulfoxides to Asymmetric Synthesis of Biologically Active Compounds. *Chem. Rev.* **1995**, 95 (6), 1717-1760.
55. Wang, G.; Hu, W.; Hu, Z.; Zhang, Y.; Yao, W.; Li, L.; Fu, Z.; Huang, W., Carbene-catalyzed aerobic oxidation of isoquinolinium salts: efficient synthesis of isoquinolinones. *Green Chem.* **2018**, 20 (14), 3302-3307.

Chapter III

Pd-functionalized polydopamine-coated polyurethane foam as a highly reusable structured catalyst for selective alkyne semi-hydrogenation and Suzuki coupling under air

Chapter III

Pd-functionalized polydopamine-coated polyurethane foam as a highly reusable structured catalyst for selective alkyne semi-hydrogenation and Suzuki coupling under air

Table of contents

I) Introduction.....	133
II) Results and discussion	135
II-1) Preparation and characterization of Pd@PDA@PUF.....	135
II-2) Semi-hydrogenation of alkynes	139
II-2-1) Semi-hydrogenation of phenylacetylene	140
II-2-2) Semi-hydrogenation of other alkynes.....	142
II-3) Suzuki coupling of aryl bromides and phenylboronic acid under mild aerobic conditions	146
II-4) Catalyst recycling, leaching test and evidence of progressive Pd(II) reduction.....	148
III) Conclusion and perspectives	154
IV) Experimental section.....	155
IV-1) Materials and methods	155
IV-2) Experimental procedures.....	157
IV-2-1) Open cell polyurethane foam (PUF) coating with polydopamine (PDA)	157
IV-2-2) Functionalization of PDA@PUF with [PdCl ₂ (NH ₃) ₄] · H ₂ O.....	157
IV-2-3) General procedure for the catalytic alkyne-to-alkene hydrogenations with Pd@PDA@PUF.....	157
IV-2-4) General procedure for the Suzuki cross-couplings of arylboronic acid and aryl bromides with Pd@PDA@PUF under aerobic conditions	158
IV-2-5) Pd@PDA@PUF recovery and reuse in successive semi-hydrogenation and Suzuki reactions	158
IV-2-6) <i>Stop-and-go</i> experiment for the semi-hydrogenation of 4-octyne with Pd@PDA@PUF.....	159
IV-2-7) Alkyne vs. alkene competing hydrogenation with Pd@PDA@PUF	159

IV-2-8) Phenylacetylene-to-styrene hydrogenation with $[\text{Pd}(\text{NH}_3)_4\text{Cl}_2] \cdot \text{H}_2\text{O}$	159
V) References	160

Abstract

Polyurethane foams (PUF) were coated with a thin layer of polydopamine (PDA), and Pd strongly anchored onto PDA via simple immersion of PDA@PUF in a hydro-alcoholic solution of Pd(NH₃)₄Cl₂·H₂O at room temperature under air to afford Pd@PDA@PUF foams. XPS showed the absence of initial reduction of palladium despite the redox properties of PDA, and HR-SEM and SEM-EDX suggested a coordination of evenly dispersed Pd(II) ions by the catechol moieties of the PDA layer, thus resulting in a single atom-type dispersion of the active phase. The “dip-and-play” catalytic pattern of Pd@PDA@PUF and high dispersion of Pd on the surface guaranteed high activity, selectivity and reusability in alkyne semi-hydrogenations and in Suzuki couplings under air without prior reduction procedures. Self-enhancing properties, observed in recycling and control experiments, were explained by XPS as the chelated Pd(II) ions were gradually reduced to isolated (coordinated) Pd(0) atoms under hydrogenation or Suzuki coupling reaction conditions.

1) Introduction

The semi-hydrogenation of alkynes to alkenes is of paramount importance either in industrial or in organic synthetic domain¹⁻², but the selective production of olefins from alkynes requires catalysts able to both hydrogenate the triple bond and hamper over-hydrogenation toward alkanes. In addition, these catalysts should limit the undesired double bond isomerization³. In this respect, supported Pd nanoparticle-based catalysts⁴⁻⁸ are among the best candidates in terms of activity, but they often suffer from moderate selectivity⁹. Typical approaches to improve it¹⁰ rely on the modification of the Pd nanoparticles (NPs) by the addition of N-, P-, or S-containing ligands¹¹⁻¹³ or on the ‘doping’ with a less active metal.¹⁴⁻¹⁵ A typical example in this domain is the famous Lindlar catalyst, where Pd/CaCO₃ is partially poisoned by the addition of Pb and quinoline. However, the use of Pb requires a precise control of its location with respect to the Pd active phase and represents a serious limit for the eco-sustainable use of the Lindlar catalyst. A more recent approach relies on the strategy of active site isolation, that includes the development of single atom-based catalysts^{10, 16}. These attractive strategies with, in some cases, selectivity up to 99% and reuse up to 10 times, may however be not so valuable if one cannot carry on the scale-up process for industrial implementation in a practical and highly operable manner with cost competitiveness and in an eco-friendly mode. For instance, Lu *et al.*¹⁷ reported an unsupported nanoporous palladium (PdNPore), whilst Kuwahara *et al.*¹⁸ introduced a yolk-shell nanostructured composite composed of Pd nanoparticles (NPs), aminopolymers, and poly(ethylenimine) (PEI) confined in hollow silica spheres, and Shen *et al.*¹⁹ recently described a two-dimensionality (2D) enhanced interface-confined effect that led to the strong interaction between lead (Pb) species

and the ultrathin 2D palladium nanosheets (Pd NSs). These various catalysts exhibited high conversion and chemoselectivity in semi-hydrogenation of phenylacetylene and other alkynes, as well as superior recyclability ensuring the catalyst reuse for several times. However, the adopted catalyst designs are tedious, time-consuming and energy-intensive. A simpler and easier to scale-up catalyst production strategy is thus still desirable, but remains challenging.

This challenge prompted us to consider palladium-driven heterogeneous catalysis with PDA-coated open cell polyurethane foams (PDA@PUF) as a non-innocent support for the semi-hydrogenation of alkynes and possibly other organic transformations. Indeed, polydopamine is known to act as an efficient chelating agent towards a variety of metals, such as Ag^+ , Au^+ , Pd^{2+} , Pt^{2+} salts etc.²⁰⁻²¹, forming stable complexes, and moreover to be able to reduce these metal ions thanks to the reductive properties of the catechol moieties. Accordingly, the generation of such PDA-supported palladium complexes can be regarded as an “open gate” for the convenient and rapid preparation of heterogeneous Pd(0) catalysts. Inspired by this concept, catalytic composites based on polydopamine-supported palladium have been successfully prepared and applied in ammonia borane hydrolysis, various cross-couplings and nitroarene transfer hydrogenation²²⁻²⁴, endowing this topic a brilliant future.

In this chapter, we put forward an effective and straightforward approach for the preparation of Pd-functionalized polydopamine-coated polyurethane foams starting from a commercial PUF, dopamine, and $[\text{Pd}(\text{NH}_3)_4]\text{Cl}_2 \cdot \text{H}_2\text{O}$. The whole process leaves no doubt that the preparation of the macroscopic catalytic object is unprecedentedly facile and highly efficient with merely two successive operations of dipping, stirring and rinsing at room temperature. This simple route lowers the threshold for catalyst preparation by several order of magnitude compared to current site isolation strategies. Furthermore, the catalytic performance of the resulting Pd@PDA@PUF catalytic material in a pattern of “dip-and-play” mode reaches high standard in efficiency, versatility and stability. Thus, the as-prepared catalyst displays high catalytic performance in the selective semi-hydrogenation of various alkynes, as well as in Suzuki coupling reactions, and moreover shows remarkable stability for 15 cycling tests. Noteworthy, XPS, HR-SEM and SEM-EDX data suggest an initial chelation of the Pd(II) salt by the catechol/*o*-quinone moieties of the PDA layer, which would result in a “single atom” nature of the active phase that would be at the origin of Pd@PDA@PUF’s high alkene selectivity in alkyne hydrogenation catalysis. Furthermore, in the absence of necessity of a prior reduction procedure to generate an active phase, self-enhancing catalytic properties have been observed along the recycling experiments, both in the semi-hydrogenation reactions and in the Suzuki couplings under air. These were explained by XPS that showed a progressive reduction of the immobilized Pd(II) salt to an active Pd(0) phase along the catalytic tests.

ICP-AES measurements on several samples of Pd@PDA@PUF revealed a mean Pd loading of 2.437 ± 0.323 g/kg (0.244 ± 0.032 wt%). High-resolution scanning electron microscopy (HR-SEM) images of as-synthesized Pd@PDA@PUF are displayed in **Figure 3**. Low magnification images (top) show that the PDA was coated on the whole surface of PUF as a rough film at the macroscopic level, while higher magnification images (bottom) reveal that the rough film structure is constituted of numerous scattered polymers aggregates typical of PDA coating on a PUF.²⁵⁻²⁶ No Pd particles could be identified, suggesting a relatively small size for the latter or, more likely, a molecular nature of the immobilized palladium species as the catechol moieties of the PDA layer may simply act as a chelating ligand substituting two chloride or NH₃ ligands of [Pd(NH₃)₄Cl₂] \cdot H₂O²⁷⁻²⁸, which could result in a single atom-type distribution of Pd over the surface. No TEM characterization could however be carried out on to confirm or infirm this assumption. The elastic character of the PUF host substrate indeed prevented it to be cut into thin slices for the observation, even after a freezing step in liquid N₂ had been attempted to enhance its rigidity.

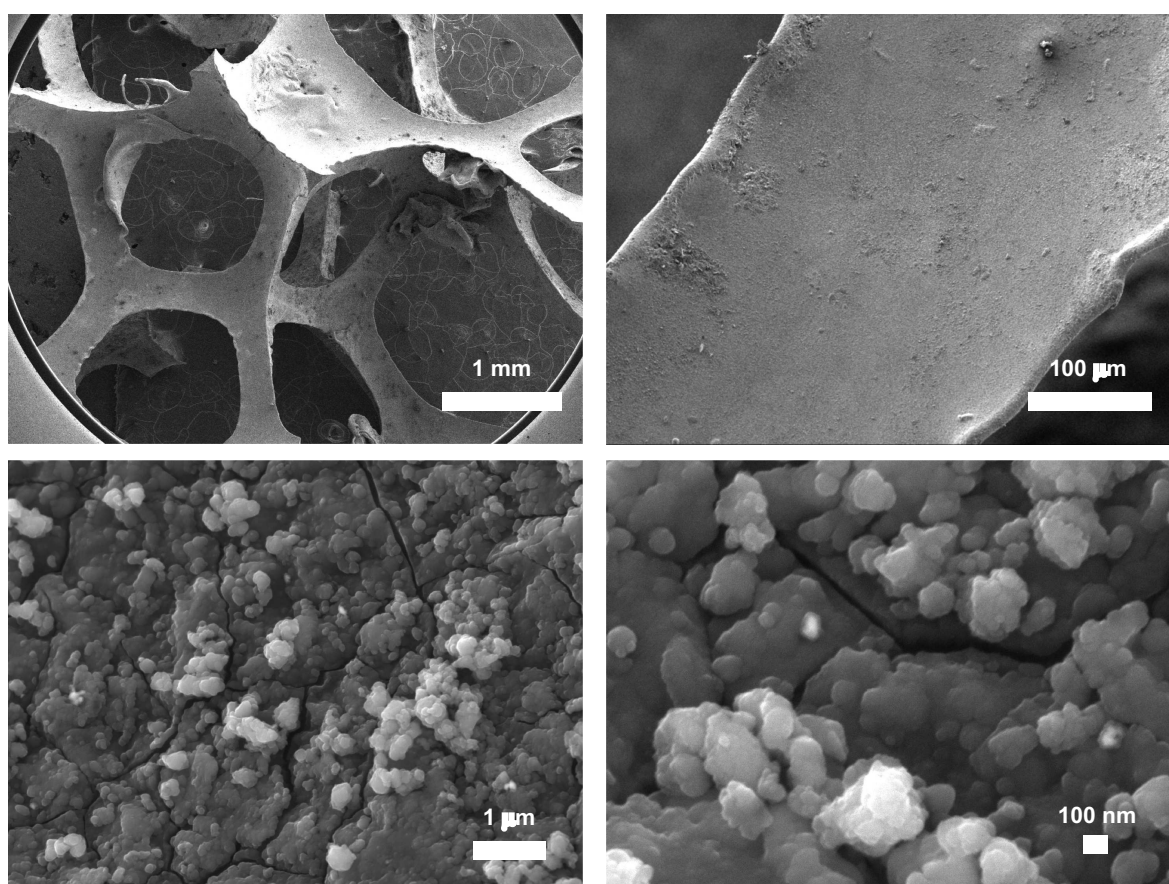


Figure 3. HR-SEM images with different magnifications of as-synthesized Pd@PDA@PUF.

SEM micrographs combined to energy dispersive X-ray spectroscopy (EDX) revealed a quasi-uniform distribution of Pd over the foam surface (**Figure 4**), without apparent aggregates or segregation areas, ensuring a relatively good structural homogeneity of the material.

Besides, a similarly homogeneous distribution of C, O and N was also observed, highlighting the homogeneous PDA coating on PUF. Noteworthy, no Cl was detected, and the mapping of the O atoms coincides almost perfectly with that of the Pd, further highlighting a possible simple coordination of the Pd complex by the catechol moieties.

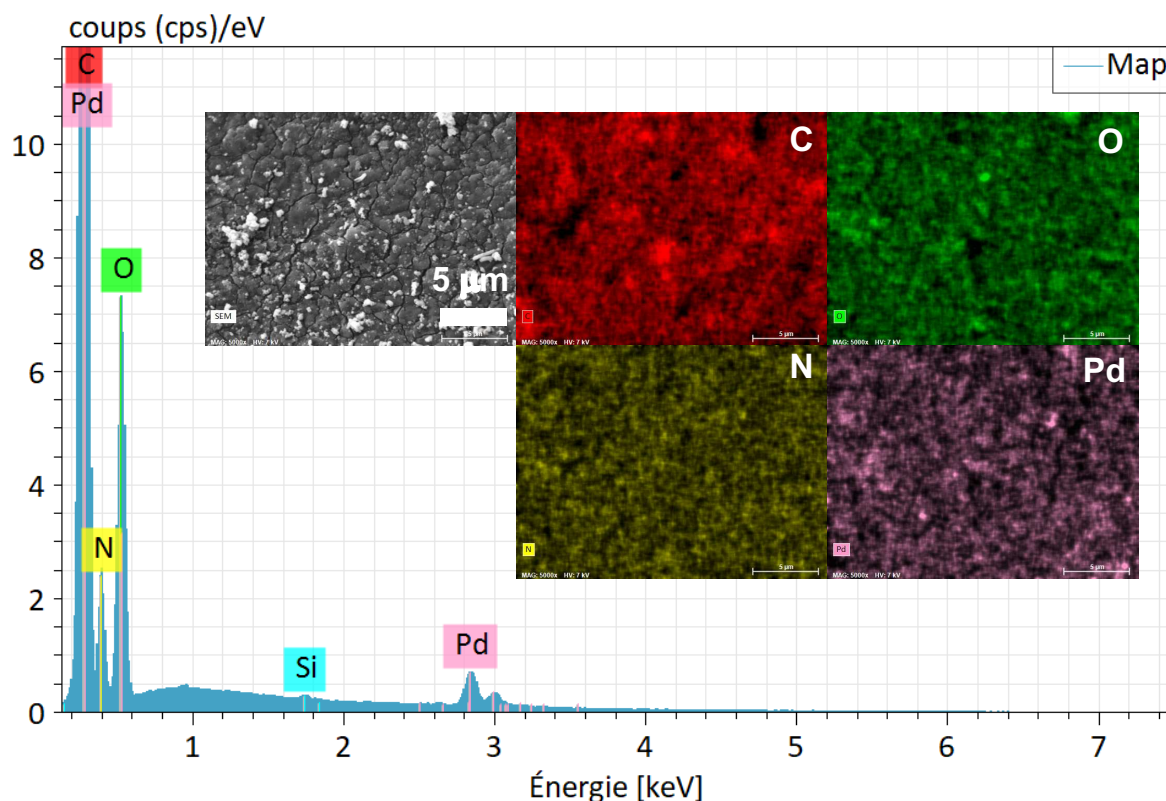


Figure 4. SEM-EDX spectrum and elemental mapping of as-synthesized Pd@PDA@PUF.

X-ray photoelectron spectroscopy (XPS) was performed to gain information on the oxidation state of Pd, as well as on the nature of its interaction with the PDA layer. In agreement with the result of the EDX spectroscopy, the XPS survey scan spectrum of as-synthesized Pd@PDA@PUF indicated the presence of O, N, Pd and C elements (**Figure 5**). The high-resolution Pd 3d XPS core level region clearly accounted for Pd(II) species with binding energy of the 3d_{5/2} peak at 337.2 eV (**Figure 6A**). At odds with the standard redox potential of PDA that lies at about +0.3 V/NHE while that of the Pd²⁺/Pd⁰ redox couple lies at +0.99 V/NHE²⁹ and with some literature precedents, such as the immobilization of K₂PdCl₄ on PDA-coated cotton microfiber which resulted in the partial reduction of Pd(II) salt to Pd(0) NPs,³⁰ but in agreement with other reports where no reduction of Pd(II) to Pd(0) upon immobilization of a Pd salt on PDA was observed,³¹ the PDA layer coated on PUF seems here to initially serve as a pure adhesive layer without reduction of the Pd(II) precursor. Again, this highlights a possible simple coordination of the Pd(II) species by the catechol moieties of the PDA layer.

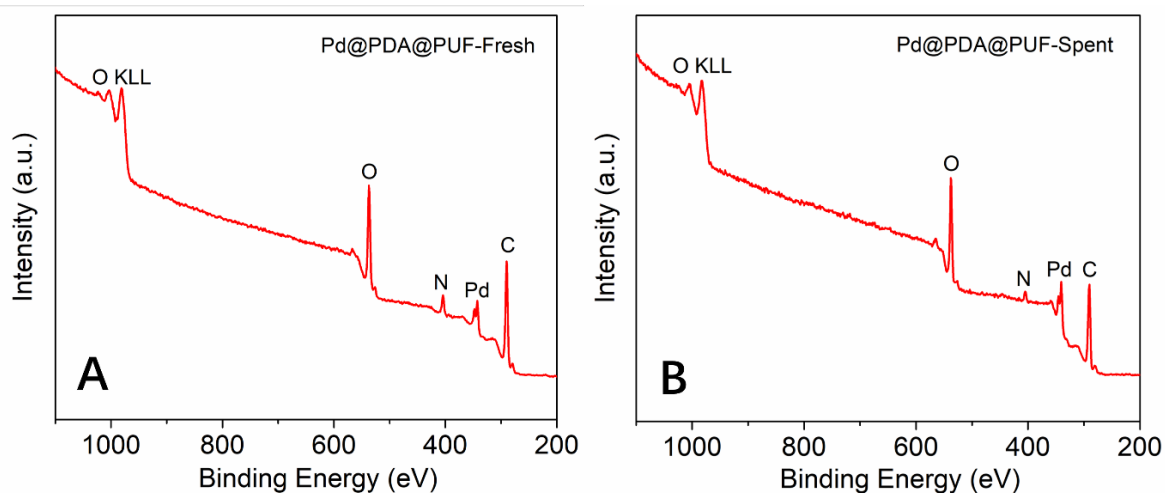


Figure 5. XPS survey spectra of Pd@PDA@PUF: (A) as-synthesized, (B) spent (after 15 cycling tests).

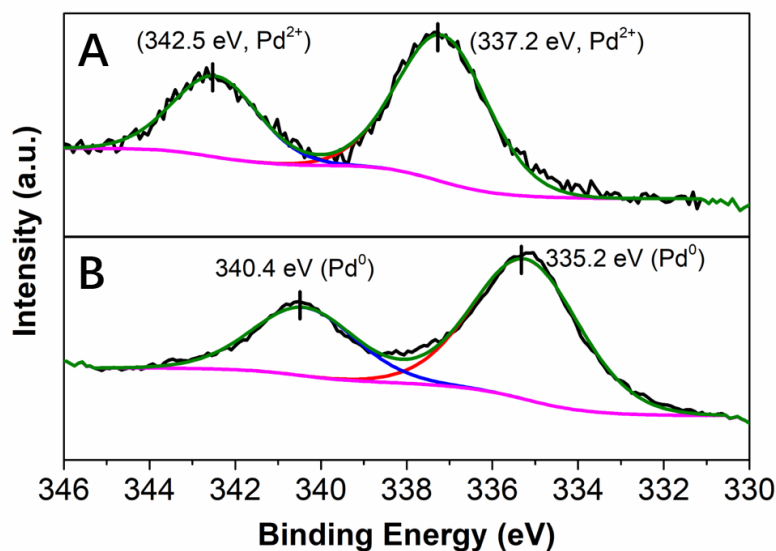


Figure 6. High resolution XPS spectra of the Pd 3d core level region of Pd@PDA@PUF: (A) as-synthesized, (B) spent (after 15 cycling tests).

XRD failed to evidence diffraction peaks corresponding to palladium phases for as-synthesized Pd@PDA@PUF (**Figure 7**), most likely because of the low palladium loading on the support (0.244 ± 0.032 wt%), but probably also because of the small size of the palladium particles or molecular species. For the sake of completeness, thermogravimetric analysis (TGA) of PUF, PDA@PUF and as-synthesized Pd@PDA@PUF materials were also recorded. The polymeric materials all presented similar results (**Figure 8**), thereof showing the absence of obvious variations of the materials composition in agreement with the low loadings of PDA and Pd onto the pristine PUF.

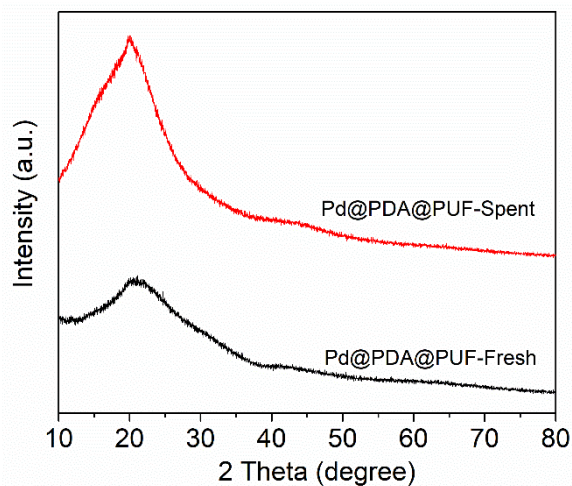


Figure 7. XRD profiles of Pd@PDA@PUF: black curve, as-synthesized; red curve, spent (after 15 cycling tests).

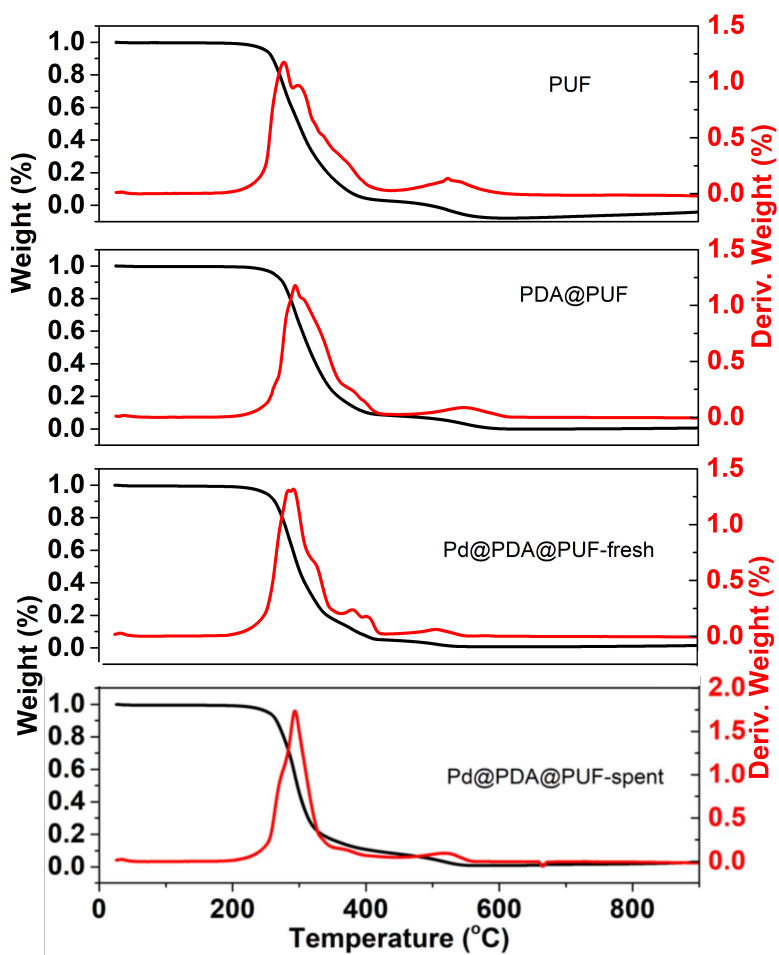


Figure 8. TGA curves of PUF, PDA@PUF, as-synthesized Pd@PDA@PUF and spent Pd@PDA@PUF (after 15 cycling tests).

II-2) Semi-hydrogenation of alkynes

Pd@PDA@PUF (0.244 ± 0.032 wt%), in the form of cubic samples of ca. 8 cm^3 whose masses were adjusted in function of their Pd content to have a Pd loading of $7 \mu\text{mol}$, was investigated as catalyst for the selective semi-hydrogenation of aliphatic, aromatic, terminal and internal alkynes (0.076 to 0.3 M, giving Pd loadings of 0.46 to 0.12 mol%) in ethanol at room temperature under a constant flow rate of H_2 (2 to 13 mL/min) into the solution to maintain its concentration constant during the whole duration of the catalytic processes.

II-2-1) Semi-hydrogenation of phenylacetylene

The semi-hydrogenation of phenylacetylene (PA) to styrene (ST) is of great significance as this aromatic alkyne is an unwanted component of the gaseous reagent steams used in polystyrene production plants, which removal is compulsory to avoid the deactivation and poisoning of the polymerization catalysts.⁵ PA was thus selected as a model substrate for our initial studies.

Optimization studies (see the Supporting Information) conducted with this substrate at various concentrations (0.076 to 0.3 M) and under various H_2 flow rates (2 to 13 mL/min) allowed to establish an optimal H_2 flow rate of 13 mL/min and alkyne concentration of 0.3 M (Pd loading of 0.12 mol%). Under these optimized conditions, a selectivity to ST as high as 95% at 98% conversion could be observed after 4.25 h of reaction, giving a TON of 776 (expressed as the number of (mol of PA converted to ST)/(mol_{Pd})) and a TOF of 183 h^{-1} (**Figure 9**). Using an initial PA concentration of 0.15 M (Pd loading of 0.23 mol%) under otherwise similar conditions, led to comparable TOF (188 h^{-1}) and ST selectivity (95% at 91% conversion), but of course to a lower TON (376) (**Table S1** and **Figure S1**). Satisfyingly, in both cases, ethylbenzene (EB) started to be produced appreciably only after full conversion of PA into ST. Such results may be explained by the fact that PA displays high adsorption properties on Pd@PDA@PUF, which could prevent ST to be adsorbed before all PA is consumed. The formation rate of EB is indeed almost similar to that of ST, which tends to show that the two successive hydrogenation reactions are initiated on similar active sites.

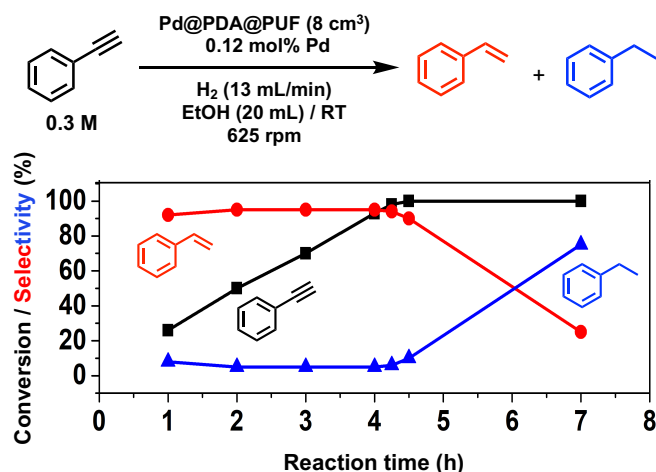


Figure 9. Hydrogenation of phenylacetylene with Pd@PDA@PUF (8 cm³); black squares: PA conversion; red circles, ST selectivity; blue triangles: EB selectivity. Reaction conditions: PA (6 mmol), Pd (7.10⁻³ mmol, 0.12 mol%), EtOH (20 mL), H₂ flow rate (13 mL/min), room temperature, 625 rpm.

For comparison, the catalysis based on the unsupported precursor, [Pd(NH₃)₄Cl₂].H₂O (0.23 mol% Pd), was investigated under similar conditions: PA (3 mmol), EtOH (20 mL), RT, H₂ (13 mL/min). 91% PA conversion with 95% ST selectivity was observed after 1 h reaction (TON = 376, TOF = 376 h⁻¹), which is just twice as fast as what was observed with Pd@PDA@PUF under the same conditions (*vide supra* and **Table S1**). This shows that PDA@PUF, as a support, retained the selectivity of the homogeneous Pd catalyst, which is very rare,³² while rendering it easily recyclable (*vide infra*) in contrast to the latter, which yielded a suspension of a black solid at the end of the hydrogenation reaction (**Figure 10**), most likely Pd(0) particles.

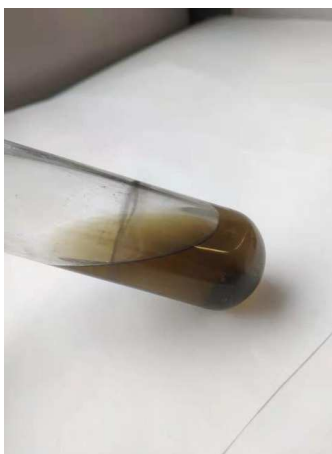


Figure 10. Photo of the reaction medium after the hydrogenation of phenylacetylene with [Pd(NH₃)₄Cl₂].H₂O (0.23 mol%).

These interesting results prompted us to compare the catalytic performance of our easily prepared Pd@PDA@PUF catalyst with state-of-the-art Pd-systems. As can be seen in **Table 1**, Pd@PDA@PUF compares well with or even outperforms, in terms of reaction conditions,

selectivity and/or TON, many catalytic systems, which preparation typically implies much more complex synthetic paths aimed at the fine tailoring of the active phases (entries 2-10) or at the production of highly dispersed, size- and shape-controlled nanocomposites (entries 9-12) up to single atom catalysts (entries 13-15). The only notable exception is the graphdiyne-supported Pd single-atom catalyst Pd^S-GDY, which can achieve TON as high as 12586 with an exceptional selectivity of 99.3 (entry 14). However, this latter necessitates a tedious synthetic process compared to our Pd@PDA@PUF material, which precludes its use on an industrial scale.

Table 1. Liquid-Phase Hydrogenation Catalysts for the Selective PA-to-ST Reduction

Entry	Catalyst	Solvent	T (K)	P (bar)	t (min)	Conv. (%) ^a	Select. (%) ^a	TON ^b
1	Pd@PDA@PUF ^c	EtOH	298	1	255	98	95	776
2 ³³	^{0.9} Pd/C ^d	EtOH	298	1	55	98	96	165
3 ³⁴	SiO ₂ @CuFe ₂ O ₄ -Pd ^e	<i>n</i> -hexane	-	1	150	98	98	224
4 ¹⁹	Pd-Pb NSS ^f	EtOH	313	4	30	100	95.8	549
5 ³⁵	Pd/Ag@CeO ₂ -1.5 ^g	EtOH	313	15	720	97	99	9.6
6 ³⁴	Lindlar cat. (Aldrich) ^h	<i>n</i> -hexane	-	1	150	82	92	176
7 ³⁶	Lindlar cat. (NHU Co.) ^j	EtOH	303	1	270	5	>99	309
8 ³⁷	Lindlar cat. (TCI) ^j	CH ₃ CN	303	1	60	86	99	327
9 ³⁶	Pd/mpg-C ₃ N ₄ ^k	EtOH	303	1	85	100	94	1037
10 ³⁷	MWCNTs-Fe ₃ O ₄ -Cu ₂ O-Pd ^l	CH ₃ CN	303	1	90	100	98	377
11 ³⁸	PyC ₁₂ S-Pd/VC ^m	CH ₂ Cl ₂	303	1	300	98	94	980
12 ¹⁸	Pd+PEI(L)@HSS ⁿ	MeOH/1,4 -dioxane	303	1	240	97	87	169
13 ³⁹	Pd ^S -GDY ^o	EtOH	298	2	120	100	99.3	12586
14 ⁴⁰	Pd _{0.18} Cu ₁₅ /Al ₂ O ₃ ^p	<i>n</i> -hexane	298	6.9	480	90	94	-
15 ⁴¹	Pd ₁ /SBA-15@N-C ^q	EtOH	323	1	10	96	93	893

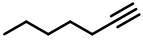
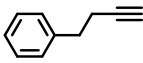
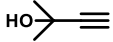
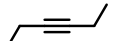
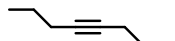
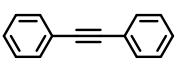
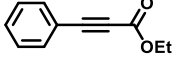
^a PA conversion and ST selectivity determined by GC analysis. ^bTurnover number expressed as (mol of PA converted to ST)/(mol_{Pd}). Pd loading in the catalytic material (and in the reaction medium): ^c0.244 wt% (0.12 mol%), ^d0.924 wt% (0.57 mol%), ^e4.15wt% (0.43 mol%), ^f2.6 wt% (0.175 mol%), ^g8 wt% (10 mol%), ^h5wt% (0.43 mol%), ⁱ1 wt% (0.016 mol%), ^j5wt% (0.26 mol%), ^k5.64 wt% (0.091 mol%), ^l1.67 wt% (0.26 mol%), ^m1 wt% (0.094 mol%), ⁿ(0.5 mol%), ^o0.42 wt% (0.0079 mol%), ^p0.18 at%, ^q0.12 wt% (0.1 mol%).

II-2-2) Semi-hydrogenation of other alkynes

Next, the catalytic activity of Pd@PDA@PUF was evaluated in other alkyne semi-hydrogenation reactions, including those of terminal and internal aliphatic alkynes, as well as aromatic and functionalized alkynes. Satisfyingly, under similar conditions than those used for PA's hydrogenation, they all provided excellent conversions with good to excellent alkene selectivity, showing Pd@PDA@PUF's versatility in the wide field of heterogeneous semi-

hydrogenation processes (**Table 2**).

Table 2. Semi-hydrogenation of various alkynes catalyzed by Pd@PDA@PUF^a

Entry	Substrate	Time (h)	Conv. (%) ^b	Alkene sel. (%) ^b	Z/E ratio ^b
1		1.8	97	98	-
2 ^c		3.3	> 99	99	-
3		1.8	97	96	-
4		1.3	99	94	-
5		1.5	> 99	99	1/0 ^d
6		1.5	> 99	99	37/1
7		3	98	85	16/1
8		4	99	88	7/1

^a Reaction conditions: alkyne (3 mmol), Pd@PUF@PDA (8 cm³, Pd: 0.23 mol%), EtOH (20 mL), room temperature, H₂ flow (13 mL/min), 625 rpm. ^bDetermined by GC or ¹H NMR ^cReaction conducted at 10 °C. ^dNo (*E*)-3-hexene detected by GC.

More specifically, excellent results were obtained for all investigated terminal alkynes (1-heptyne, 4-phenyl-1-butyne, 2-methylbut-3-yn-2-ol) with alkene selectivity ranging from 94 to 98% at conversions of 97 to 99% (**Table 3**, entries 1,3 and 4), and over-hydrogenation to the corresponding alkane or double-bond isomerization being only appreciable after the full alkyne consumption (**Figures 11A-D**). In the case of 1-heptyne, the alkene selectivity could even be increased to 99% at full alkene conversion by lowering the reaction temperature to 10 °C (**Table 2**, entry 2 and **Figure 11B**).

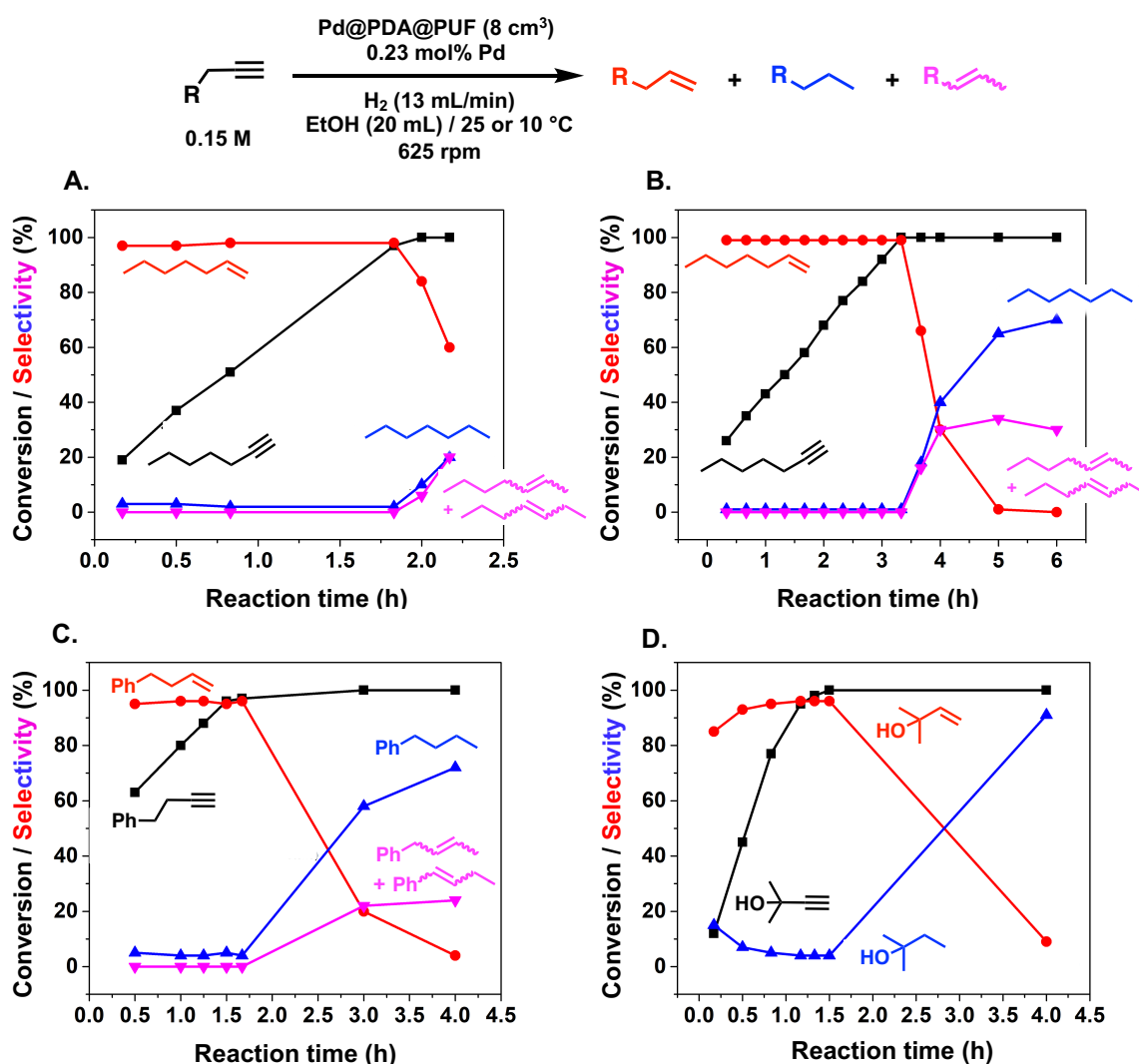


Figure 11. Hydrogenation with Pd@PDA@PUF of 1-heptyne at 25 °C (A), 1-heptyne at 10 °C (B), 4-phenyl-1-butyne at 25 °C (C), 2-methylbut-3-yn-2-ol at 25 °C (D); black squares: alkyne conversion; red circles, 1-alkene selectivity; blue triangles: alkane selectivity.; pink triangle: 1-alkene isomerization products. Reaction conditions: alkyne (3 mmol), Pd ($7 \cdot 10^{-3}$ mmol, 0.23 mol%), EtOH (20 mL), H₂ flow rate (13 mL/min), 25 or 10 °C, 625 rpm.

The semi-hydrogenation of aliphatic internal alkynes such as 3-hexyne and 4-octyne proved even more selective with selectivity as high as 99% to the (*Z*)-alkene at full alkyne conversion (**Table 2**, entries 5 and 6). Most impressively, this selectivity was maintained to very high levels even several hours after all the alkyne had been consumed as isomerization to the (*E*)-alkene or over-hydrogenation to the fully saturated hydrocarbon proved to be very slow (**Figure 12A and B**). To further highlight the aptitude of Pd@PDA@PUF to selectively hydrogenate 3-hexyne to (*Z*)-3-hexene, we performed a competitive experiment starting from a mixture of 60% 3-hexyne and 40% (*Z*)-3-hexene. During the first 50 min of the catalytic test, we observed a totally selective conversion of the alkyne to (*Z*)-3-hexene without any appreciable competition of the hydrogenation of the latter to hexane. Remarkably, Pd@PDA@PUF maintained a complete chemoselectivity even after complete consumption of

3-hexyne (after ca. 50 min) (**Figure 12C**). Such gain of selectivity compared to the semi-hydrogenation of terminal alkynes (*vide supra*) might be attributed, on one side, to the less favourable double-bond isomerization of the resulting alkene, and on the other side, to the increased steric hindrance around the double bond, which makes harder its further hydrogenation to the alkane.

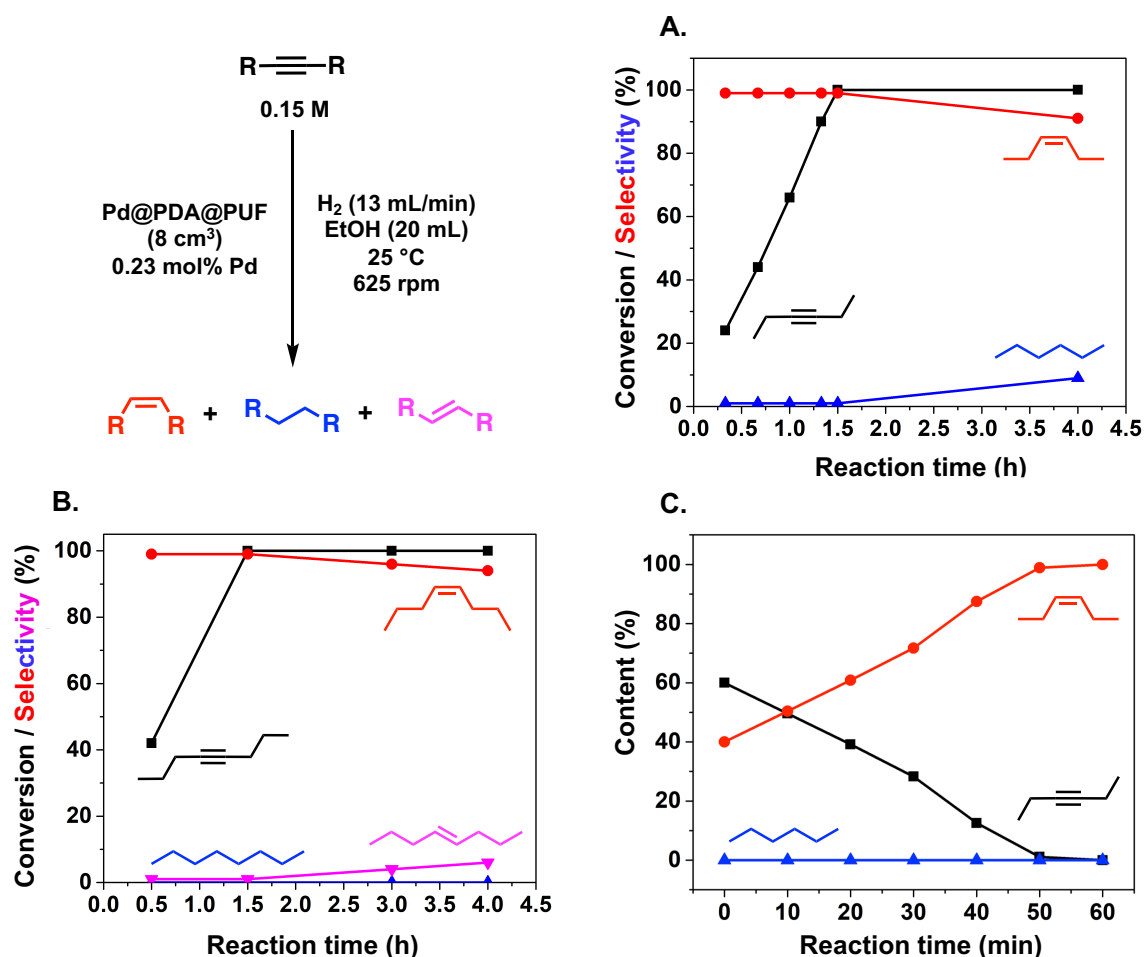


Figure 12. Hydrogenation with Pd@PDA@PUF (8 cm³) of 3-hexyne (A), 4-octyne (B), a 60:40 mixture of 3-hexyne and (Z)-3-hexene (C); black squares: alkyne conversion (A and B) or content (C); red circles, (Z)-alkene selectivity (A and B) or content (C); blue triangles: alkane selectivity.; pink triangle: (E)-alkene selectivity. Reaction conditions: alkyne (3 mmol) (A and B) or alkyne (1.8 mmol) and alkene (1.2 mmol) (C), Pd (7·10⁻³ mmol, 0.23 mol%), EtOH (20 mL), H₂ flow rate (13 mL/min), 25 °C, 625 rpm.

In the case of the bulky aromatic alkyne, 1,2-diphenylacetylene, the alkene selectivity (Z/E ratio of 16:1) was only of 85% at full alkyne conversion (**Table 2**, entry 7), as 1,2-diphenylethane started to form from the beginning of the reaction. Furthermore, (E)-1,2-diphenylethylene was detected in amounts varying between 10 and 5% throughout the whole process, while the amount of (Z)-1,2-diphenylethylene varied between 85 and 80% during the first 3 h before diminishing gradually when all the starting alkyne had been consumed, *i.e.*: after 3 h reaction (**Figure 13**). Such result might be attributed to the aromatic rings, which could provide easier access to the double-bond after the initial alkyne-to-alkene hydrogenation

through π - π -interaction with the PDA layer²⁸, compared to saturated alkenes, which readily decoordinate after the initial alkyne-to-alkene hydrogenation.

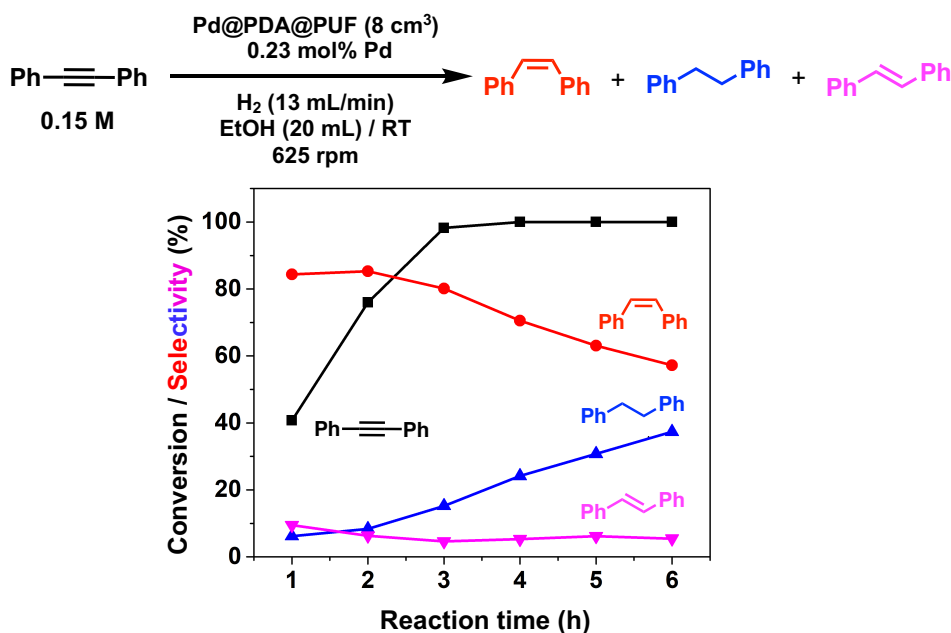


Figure 13. Hydrogenation with Pd@PDA@PUF (8 cm³) of 1,2-diphenylacetylene; black squares: alkyne conversion; red circles, (Z)-alkene selectivity; blue triangles: alkane selectivity; pink triangle: (E)-alkene selectivity. Reaction conditions: 1,2-diphenylethylene (3 mmol), Pd (7.10⁻³ mmol, 0.23 mol%), EtOH (20 mL), H₂ flow rate (13 mL/min), 25 °C, 625 rpm.

Finally, in the case of ethyl-3-phenylpropynoate (**Table 2**, entry 8), it is worth noting that the ester functionality was not affected by the hydrogenation, but similarly to what was observed with 1,2-diphenylacetylene, full consumption of the alkyne took a longer time (4 h) than with aliphatic alkynes or PA, and non-negligible amounts of the alkane (12%) and (E)-alkene (in a 1:7 ratio with the Z-isomer) were observed at this point.⁴²

Among all studied substrates, aliphatic alkynes clearly give higher alkene selectivity than aromatic alkynes, particularly in the case of symmetric internal alkynes with which overhydrogenation to alkanes is hardly observed, even after prolonged reaction times. In agreement with the HR-SEM and SEM-EDX data, which suggest a very small size of the immobilized Pd species, a possible explanation of Pd@PDA@PUF high alkene selectivity may be related to the possible chelation of Pd(II) ions by the catechol moieties of the PDA layer, which would result in a “single atom”-type dispersion of the active phase.

II-3) Suzuki coupling of aryl bromides and phenylboronic acid under mild aerobic conditions

The Pd-catalyzed Suzuki cross-coupling, as one of the most powerful methods for the

construction of biaryl compounds, is extensively utilized in the synthesis of natural products or pharmaceuticals, as well as in the preparation of organic electronics⁴³⁻⁴⁵. It thus aroused our curiosity to check whether our catalyst system was efficient in catalyzing this type of reactions.

Initial studies focused on the coupling under air of phenylboronic acid with chloro- or bromobenzene in EtOH/H₂O (1:1) (8 mL) at 65 °C in the presence of K₂CO₃ as base and of cubic samples of Pd@PDA@PUF (0.244 ± 0.032 wt%) of ca. 8 cm³ as catalytic material, whose masses were adjusted to have a Pd loading of 7 μmol, *i.e.*: of 1.4 or 0.23 mol% depending on the amount of aryl bromide (0.5 or 3.0 mmol).

With a catalytic loading of 1.4 mol% Pd, only 20% conversion of chlorobenzene to biphenyl was observed after 23 h reaction (**Table 3**, entry 1). However, when bromobenzene was used instead of chlorobenzene, 88% conversion to biphenyl was observed after 3 h and 96% after 4 h (entries 2 and 3). Satisfyingly, a similar conversion was observed after the same reaction time when increasing the amount of bromobenzene 6-fold (conversely diminishing the Pd loading to 0.23 mol%), thus allowing to reach a TON of 426 and a TOF of 107 h⁻¹ (entry 4). In this case also, Pd@PDA@PUF displayed a high catalytic efficiency without any pre-activation procedures, and this moreover, under aerobic conditions in aqueous medium in the absence of a phosphine ligand.⁴⁶⁻⁴⁹

Table 3. Optimization of the Suzuki coupling with Pd@PDA@PUF^a

Entry	X	Pd loading (mol%)	Time (h)	Conv. (%) ^b	TOF (h ⁻¹)
1	Cl	1.4	23	20	0.62
2	Br	1.4	3	88	21
3	Br	1.4	4	96	17
4	Br	0.23	4	98	107

^a Reaction conditions: halobenzene (0.5-3 mmol), phenylboronic acid (0.6-3.6 mmol), K₂CO₃ (0.75-4.5 mmol), Pd@PUF@PDA (8 cm³, Pd: 1.4-0.23 mol%), EtOH/H₂O (1:1) (8 mL), 65 °C, 625 rpm.

^b Determined by GC or NMR.

With these optimized conditions in hand, we then briefly examined the scope of the coupling reaction by varying the nature of the aryl bromide (**Figure 14**). The reaction proceeded with high efficiency for all five *para*-substituted bromobenzene substrates

examined, whether they bear electron-donating or electron-withdrawing groups, and isolated yields ranging from 90 to 97% were obtained after 4 h reaction. The reaction of 2-bromonaphthalene, in contrast, originated in a slightly reduced activity with only 83% isolated yield after 4 h reaction. The sterically crowded 2-bromobiphenyl and 3-bromo-4-methoxytoluene were coupled efficiently, giving isolated yields of 86 and 94%, respectively. Finally, the *ortho*-ester-substituted aryl bromide, methyl 2-bromobenzoate, gave the expected biaryl compound in 64% isolated yield after 4 h reaction. These results show that both sensitive functionalities and sterically crowded substrates are well tolerated by Pd@PDA@PUF.

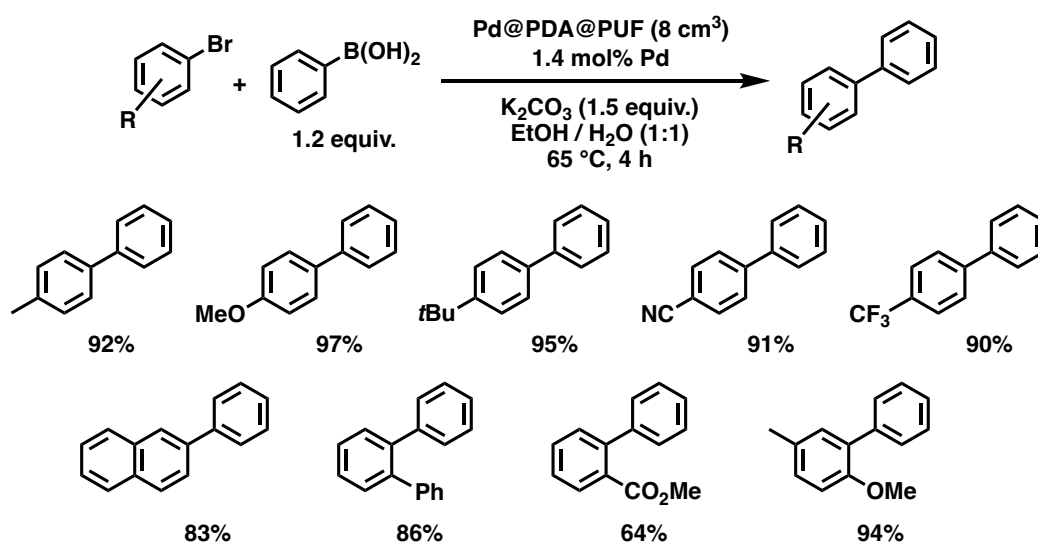


Figure 14. Scope of the Pd@PDA@PUF-catalyzed Suzuki cross-coupling.

II-4) Catalyst recycling, leaching test and evidence of progressive Pd(II) reduction

Reusability, a criterion of great significance in evaluating heterogeneous catalytic systems operated in liquid-phase medium, is normally measured as the relative activity of the catalyst maintained in successive runs of a given catalytic reaction. In the case of powdered catalyst, the product-catalyst separation is generally carried out via physical methods, such as filtration or centrifugation. Such methods are tedious on practical use and time-consuming, along with problems linked to catalyst loss. The macroscopic catalyst used in the present work allows one to operate the product-catalyst separation in a much easier way as the catalyst can be just taken out from the reaction medium followed by a short washing step to remove the adsorbed liquid on its surface before reuse.

To shed more light on the recycling properties of Pd@PDA@PUF, 15 consecutive catalytic runs were conducted with a single cubic sample of Pd@PDA@PUF (8 cm³, Pd: 7 μmol, *i.e.*: 0.23 mol% for all reactions as 3 mmol of substrate were used in each case), consisting in 5 runs of semi-hydrogenation of PA, followed by 5 runs of Suzuki coupling of bromobenzene

with phenylboronic acid, and then again 5 runs of PA semi-hydrogenation (**Figure 15**).

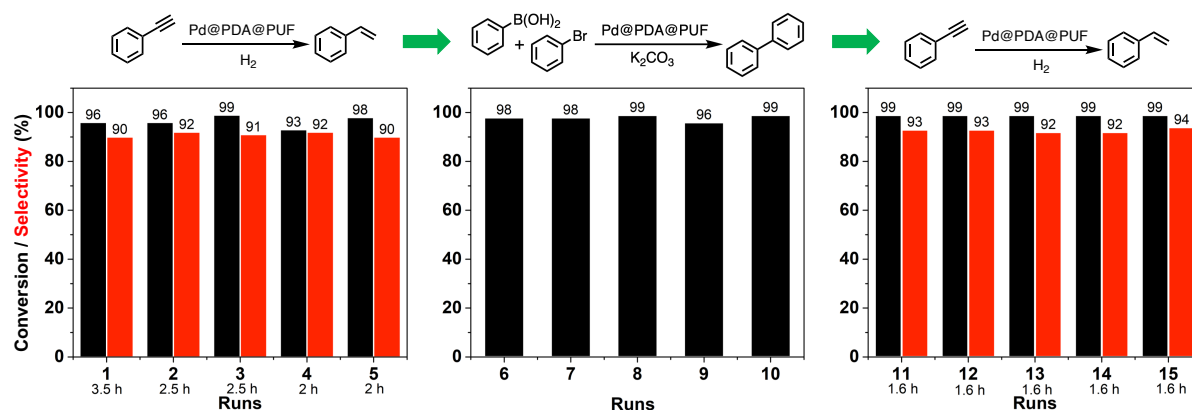


Figure 15. Conversion and selectivity measured over the 15 successive runs of semi-hydrogenation of phenylacetylene (runs 1 to 5 and 11 to 15) and Suzuki coupling of bromobenzene with phenylboronic acid (runs 6 to 10) catalysed by a single cubic sample of Pd@PDA@PUF (8 cm³, Pd: 0.23 mol%). Hydrogenation's conditions: phenylacetylene (3 mmol), EtOH (20 mL), H₂ flow rate (13 mL/min), 25 °C, 625 rpm. Suzuki coupling's conditions: bromobenzene (3 mmol), phenylboronic acid (3.6 mmol), K₂CO₃ (4.5 mmol), EtOH/H₂O (1:1) (8 mL), 65 °C.

During the first 5 runs of semi-hydrogenation, the time necessary to consume nearly all PA decreased from 3.5 h in run 1 to 2 h in run 5, while the ST selectivity maintained at 91 ± 1 %, thereof suggesting a gradual improvement of the catalytic activity of Pd@PDA@PUF over these first 5 runs. The next 5 runs of Suzuki coupling each resulted in 97.5 ± 1.5 % conversion in 4 h reaction, showing no apparent variation of catalytic activity. Finally, the 5 last runs of semi-hydrogenation demonstrated the extremely high stability of the foam-based catalyst, as both the reaction rate and the selectivity remained unchanged for the whole set of tests with 99% conversion and 93% ± 1 % of ST selectivity after 1.6 h reaction for run 11 to 15. Noteworthy, 45 mmol of substrates (PA and bromobenzene) were efficiently converted over these 15 runs with just 7 μmol of Pd, which corresponds to Pd loading 0.0156 mol% if one takes into consideration the total amount of converted substrates.

It must be highlighted here that despite the fact that Pd@PDA@PUF experienced 65 °C for 4 h in a basic environment during the coupling reactions and that it was washed with water and organic solvents (ethanol and ethyl acetate) in an ultrasonic bath after each coupling reaction, the activity in the subsequent semi-hydrogenation tests (*i.e.*: runs 11 to 15) did not drop down, but even slightly increased. A determining requirement to establish whether Pd@PDA@PUF was competent in accomplishing such recycling experiment was that the catalyst could endure prolonged rinsing steps like ultrasonic bath washings. To our delight, Pd@PDA@PUF achieved this goal, maintaining both high conversion and selectivity from the beginning to the end. PUF (structured catalytic support), PDA (adhesive layer), and Pd precursor (active species), after a facile combination, thus constitute a very stable heterogeneous structured catalyst for both semi-hydrogenation and Suzuki coupling reactions.

Even more satisfyingly, the performance of semi-hydrogenation catalysis showed an interesting development during the first runs of catalysis due, most probably, to the progressive reduction of the immobilized Pd, as shown by XPS analyses (*vide infra*).

ICP-AES analyses of the Pd content of both the foam after these 15 cycling tests and the reaction medium confirmed the robust anchoring of Pd. No Pd was indeed detected in the reaction solution after the first run of semi-hydrogenation reaction, although the most important catalyst leaching is typically expected during the first run. Moreover, the Pd content of the Pd@PDA@PUF foam after the cycling tests showed only negligible deviation (2.205 mg/g) compared to the value measured for the as-synthesized foam (2.758 mg/g). This absence or quasi-absence of leaching was further demonstrated by a stop-and-go experiment that was carried out for the hydrogenation of 4-octyne with a fresh Pd@PDA@PUF foam. The latter indeed evidenced the quenching of the reaction as soon as Pd@PDA@PUF was removed from the reaction medium, and the restart of the reaction when the foam was re-immersed (**Figure 16**).

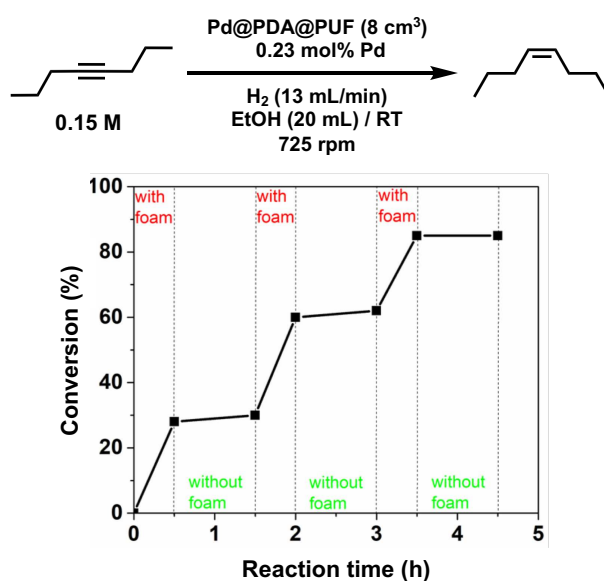


Figure 16. Stop-and-go experiment on 4-octyne' semi-hydrogenation with Pd@PDA@PUF. Reaction conditions: 4-octyne (3 mmol), Pd@PUF@PDA (8 cm³, Pd: 0.23 mol%), EtOH (20 mL), H₂ flow rate (13 mL/min), room temperature, 625 rpm

Furthermore, the surface of the spent catalyst after these 15 cycling tests remained remarkably similar compared to that of the as-synthesized Pd@PDA@PUF foam, as revealed by HR-SEM (**Figure 17**). In particular, high magnification images still show numerous scattered polymers aggregates typical of PDA coating, and again, no Pd particles could be identified. This further suggests an initial simple coordination of the Pd(II) ions, and moreover shows the absence of mobility of the active phase even after reduction to Pd(0). Accordingly, SEM micrographs combined to EDX spectroscopy again showed a quasi-uniform distribution of C, O, N and Pd without notable aggregates or segregations area (**Figure 18**).

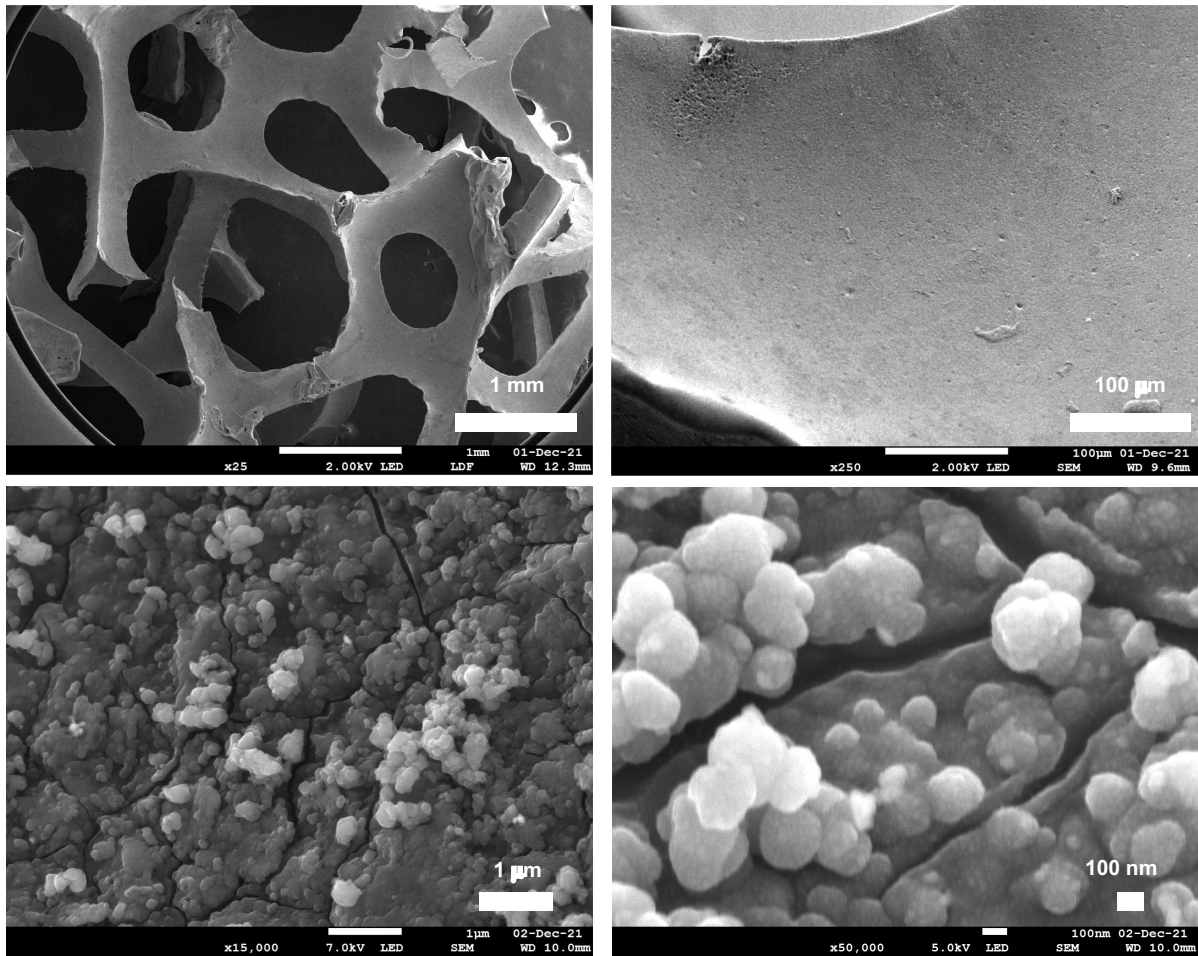


Figure 17. HR-SEM images with different magnifications of spent Pd@PDA@PUF (after 15 cycling tests).

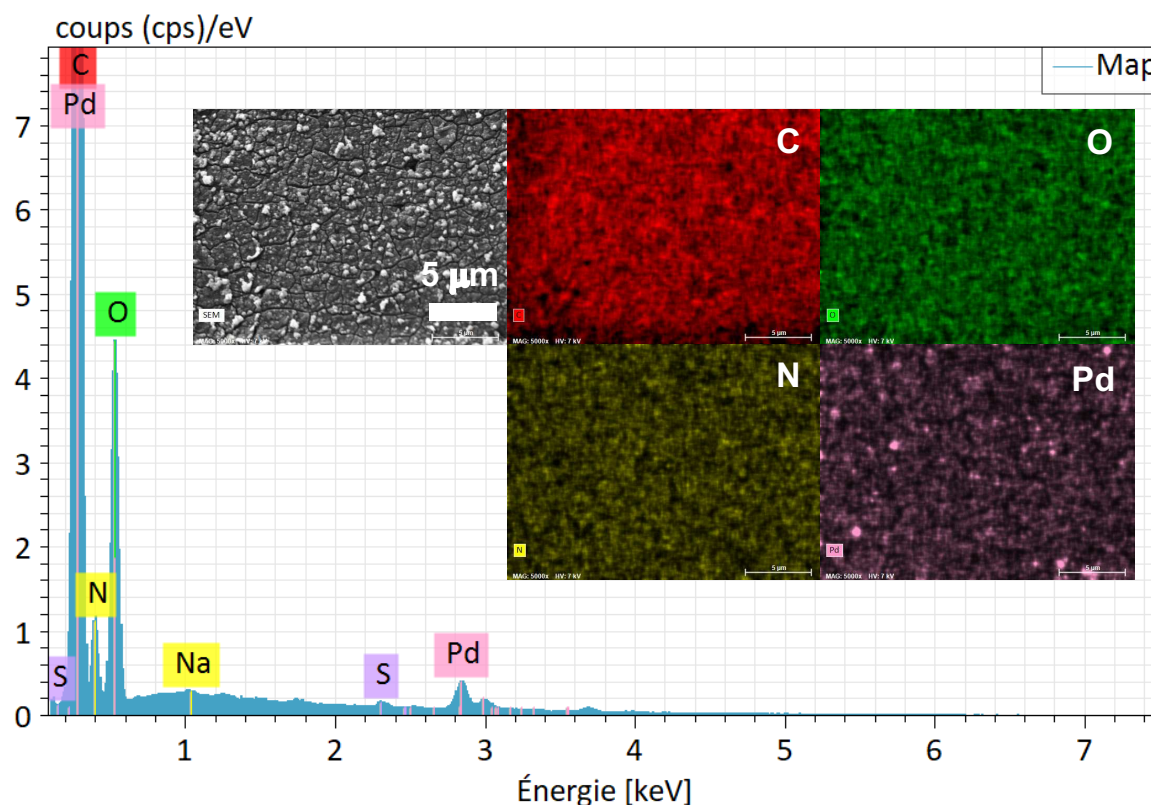


Figure 18. SEM-EDX spectrum and elemental maps of spent Pd@PDA@PUF (after 15 cycling tests).

To gain more information about the absence of necessity of prior-catalysis time-and-energy consuming reduction procedures and the possible reduction of the immobilized Pd(II) species under the catalytic conditions, XPS measurements were performed (i) on the Pd@PDA@PUF foam that has been used for the cycling tests (**Figure 6B**), and (ii) on foams that have been used for a single run of semi-hydrogenation of PA or of Suzuki coupling of bromobenzene and phenylboronic acid (**Figure 19**). In contrast to what was observed for the as-synthesized foam (**Figure 6A**), only Pd(0) was observed on the spent Pd@PDA@PUF foam after 15 catalytic runs of alkyne hydrogenation and Suzuki coupling (**Figure 6B**). Remarkably, this zero-oxidation state could be observed even after letting the foam standing in air for weeks, revealing a stabilizing effect of the PDA layer through surface interaction with the anchored metal (*vide infra*). Noteworthy however, this full reduction of the immobilized Pd(II) species to Pd(0) is not the result of a 'one-shot-process'. Thus, as can be seen in **Figure 19**, Pd(II) was only partially reduced to Pd(0) after a single catalytic run, either in semi-hydrogenation or Suzuki coupling. This result explains the observed activity of as-synthesized Pd@PDA@PUF without prior reduction, the reaction mixtures being sufficiently reductive to activate the switch-on transformation of the Pd@PDA@PUF catalytic material, as well as the gradual improvement of the catalytic activity of Pd@PDA@PUF observed over the first 5 runs of the cycling tests and in the optimization study (**Figure S1**). Furthermore, it is worth mentioning that the Pd(II) immobilized species was reduced at varying degrees depending on

the nature of the reaction. Thus, approximately 25% Pd(II) was reduced to Pd(0) after one run of semi-hydrogenation reaction⁵⁰ while ca. 57% Pd(0) was formed after one Suzuki coupling, suggesting (i) that the Suzuki coupling reaction medium is more reductive than the alkyne hydrogenation one, (ii) that a classical Pd(0)/Pd(II) mechanism⁵¹ is occurring, even though the cross-coupling was carried out in open vessel under air. Furthermore, the easy reduction of Pd(II) to Pd(0) observed in our experiments may be attributed, at least in part, to the small dimension, or even coordinated ions state, of the active phase. Indeed, for larger Pd nanoparticles, the reduction could be more tedious at low temperature due to the slow diffusion of oxygen out and of dihydrogen in, throughout the oxide particle.

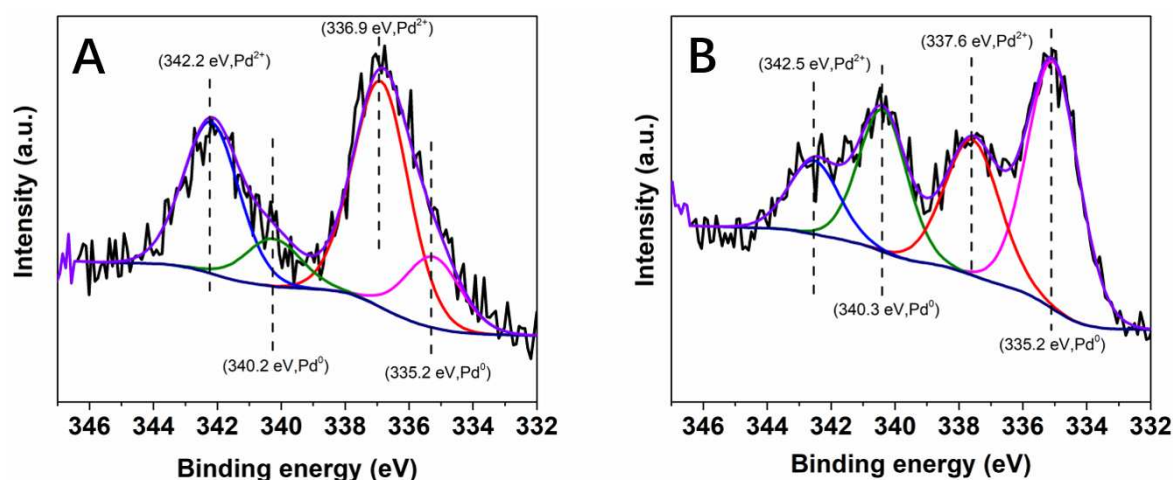


Figure 19. High-resolution XPS spectra of the Pd 3d core level region of Pd@PDA@PUF: (A) after one run of semi-hydrogenation of phenylacetylene, (B) after one run of Suzuki coupling of bromobenzene and phenylboronic acid.

The high-resolution XPS spectra of the C 1s core level region (**Figure 20**) of as-synthesized and spent Pd@PDA@PUF catalyst after 15 cycling tests suggest a non-innocent behaviour of the PDA layer. In the C 1s spectrum of the pristine Pd@PUF@PDA foam, four peaks at 284.4, 285.8 eV, 287.2 eV and 289.2 eV can be assigned to the C=C, C-C/C-N/C-O, C=O, and O-C=O groups of polydopamine, respectively (**Figure 20A**)⁵⁰. The C1s spectrum of the spent foam shows the same four peaks, but their intensity varied significantly compared to the as-synthesized catalyst, owing to a probable reductive alteration of the catechol/*o*-quinone ratio of the PDA layer. Specifically, the area of the C=C peak increased by 15% while that of the C=O peak decreased by 8%, which suggests that a non-negligible proportion of *o*-quinone-like groups has been reduced to catechols after the 15 cycling tests. We suspect that this partial reduction of the PDA layer helps preventing the re-oxidation of Pd(0) to Pd(II) when the foam is exposed to air (*vide supra*), and explain the formidable stability of the Pd@PDA@PUF catalyst overtime.

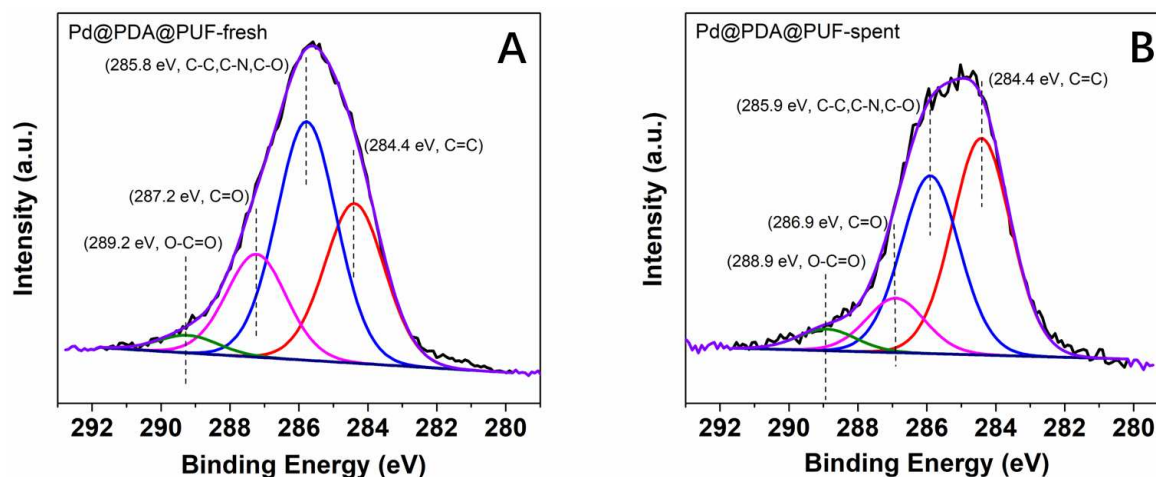


Figure 20. High-resolution XPS spectra of the C 1s core level region of Pd@PDA@PUF: (A) as-synthesized, (B) spent (after 15 cycling tests).

III) Conclusion and perspectives

In summary, we have developed an effective and general strategy to readily prepare Pd@PDA@PUF foams that can operate as a versatile and highly reliable heterogeneous catalyst without a prior-reduction procedure. Pd@PDA@PUF foams are prepared by a simple dip-coating protocol of PDA-coated PUF in a hydro-alcoholic solution of Pd(NH₃)₄Cl₂·H₂O at room temperature, and such an easy-to-make composite acts as an efficient and reusable heterogeneous catalyst for the semi-hydrogenation of alkynes under 1 atm H₂ at ambient temperature, giving remarkably high alkene selectivity (up to 99%) at full alkyne conversion, as well as for the Suzuki coupling of aryl bromides under aerobic conditions.

Moreover, the Pd@PDA@PUF catalyst is extremely stable and showed decay neither in activity nor in selectivity when running the hydrogenation and coupling reactions for 15 cycles altogether with thorough washing procedures in an ultrasonic bath between each catalytic run. The as-recovered catalyst even displayed improved catalytic performance due to both the progressive *in situ* reduction of the Pd(II) immobilized species into Pd(0), as demonstrated by XPS studies, and to the presence of strong interaction between Pd and the non-innocent adhesive PDA layer, which prevents re-oxidation of the Pd active phase during the air exposure between two cycling tests, as well as Pd leaching into the medium.

Furthermore, the very small size of the Pd species, as shown by HR-SEM and SEM-EDX studies, suggest an initial simple coordination of the Pd(II) ions by the catechol moieties of the PDA layer. The resulting “single atom”-type dispersion of the active phase and the absence of aggregation of the reduced Pd overtime may be at the origin of the very high selectivity observed in alkyne semi-hydrogenations.

The easy-to-engineer character of the size and shape of the Pd@PDA@PUF catalyst, as

well as its efficient mass transfer and transport properties, allow foreseeing relatively easy scale-up procedures and adaptation to continuous flow processes, and studies in this direction are currently under way in our laboratories.

All in all, we believe this “dip-and-play” catalytic mode and easy adaptation to any kind of reactor will stimulate the design of new generations of heterogeneous catalysts and opens the gate for a wider range of applications by virtue of its unprecedentedly facile preparation and excellent catalytic and reusable performance.

IV) Experimental section

IV-1) Materials and methods

Unless otherwise stated, all reagents and solvents were used as provided by commercial suppliers without any further purification or treatment. Polyurethane open cells foams (20 pores per inch, TCL 40100 soft white reticulated) were given by FoamPartner. Dopamine hydrochloride (008896) and 1,2-diphenylethyne (95% - 464554) were purchased from Fluorochem. Tris base (99.9+% - T1503), styrene (99% - 24,086-9) 4-bromotoluene (98% - B82200), *trans*-stilbene (96% - 13,993-9), heptane (99% - 650536) and [PdCl₂(NH₃)₄].H₂O (≥99.9% - 323438) were purchased from Sigma-Aldrich. 1-Heptyne (99% - A11130), ethyl phenylpropiolate (98% - L00603), 2-methyl-3-butyn-2-ol (98% - L07593), phenylacetylene (98% - A12139), benzenboronic acid (98% - A14257), 4-bromobenzonitrile (98% - A10914), 1-bromo-4-tert-butylbenzene (97% - A15924), 4-bromobenzotrifluoride (99% - A15942), 2-methoxybenzenboronic acid (97% - B21071), 2-bromotoluene (99% - A12315), methyl 2-bromobenzoate were (99% - A12435) and 2-bromobiphenyl (98% - B21840) were purchased from Alfa Aesar. Bromobenzene (99% - 106682500), 4-bromoanisole (98% - 106630050) and 2-bromonaphthalene (99% - 179710250) were purchased from Acros Organics. Chlorobenzene (>98% - C1948). 4-phenyl-1-butene (>98% - P0161), 4-phenyl-1-butyne (P0358), 4-octyne (>99% - O0127), *cis*-4-octene (>95% - O0135), 3-hexyne (>97% - H0430), 4-octane (>97% - O0022), 2-methyl-3-buten-2-ol (>97% - M0178), *trans*-3-hexene (>99% - H0399), *trans*-4-octene (>99% - O0136), *cis*-3-hexene (>97% - H0398), ethyl (*E*)-cinnamate (>99% - C0359) and 3-bromo-4-methoxytoluene (>97% - B3032) were provided by TCI. Ethyl 3-phenylpropanoate (98% - 56675) was provided by Fluka. Ethyl 3-phenylpropionate (98% - 11.885.51) and *cis*-Stilbene (97% - 13.277.85) were obtained from Janssen. 18.2 MΩ deionized water (TOC < 1 ppb), supplied by a Q20 Millipore system, was used for the preparation of aqueous solutions and washing procedures with water. Purifications by column chromatography were carried out with Macherey silica gel (Kieselgel 60). TraceMetal grade HCl 37 % (Fisher Chemical) and Rotipuran Supra HNO₃ 69 % (Roth) were used for ICP-AES analyses. Element standards were purchased from CPI international.

High-Resolution Scanning Electron Microscopy (HR-SEM) analyses were carried out on a high-resolution JEOL JSM-7900F SEM-FEG working at 2-7 kV accelerated voltage and at a distance of 6 to 10 mm. Images were obtained with a secondary electron detector. In some cases, samples were coated with a fine layer of carbon (ca. 10 nm) using a Balzer SCF004 coater to ensure a good electric conduction for EDX analyses. EDX analyses were carried out at a 7 kV accelerated voltage using a QUANTAX energy dispersive spectrometer equipped with two Bruker XFlash6-30 detectors.

X-ray Photoelectron Spectroscopy (XPS) was carried out in an ultrahigh vacuum (UHV) spectrometer equipped with a RESOLVE 120 MCD5 hemispherical electron analyzer and a dual anode Al K α X-ray source (1486.6 eV). Survey and high-resolution spectra were recorded in constant pass energy mode (100 and 20 eV, respectively). Binding energies were calibrated by referring to the C 1s peak at 284.4 eV. Shirley-type background subtraction and fitting of the spectra were done with the software package Casa XPS vs. 2.3. High resolution XPS peaks deconvolution has been accomplished with mixed Gaussian-Lorentzian curves minimizing the mean squared error. The Pd 3d peak was fitted using two doublets (*i.e.* Pd⁰ and Pd^{II}) representing metallic and oxidized Pd species. Asymmetric and symmetric peak shapes were used to fit the metallic and oxidized Pd components, respectively. For the fitting of the C 1s peaks, five components were used corresponding to the various chemical states of the C atoms in the PDA support layer.

Inductively coupled plasma-atomic emission spectrometry (ICP-AES). For Pd loading determination, Pd@PDA@PUF samples were mineralized with aqua regia (2 mL HCl, 1 mL HNO₃) at 185°C for 50 minutes under pressure (Multiwave ECO, Anton Paar). A blank test was carried out in parallel under the same conditions. Pd quantification in the clear obtained solutions was realized by ICP-AES (Varian 720ES) at two wavelengths: 340.458 nm and 360.955 nm. Measurements were performed by the Plateforme Analytique des Inorganiques of the Institut Pluridisciplinaire Hubert Curien (UMR CNRS 7178), Strasbourg, France.

Powder X-ray diffraction (PXRD) measurements were carried out on a Bruker D-8 Advance diffractometer equipped with a Vantec detector (Cu K α radiation) working at 45 kV and 40 mA. X-ray diffractograms were recorded in the 10–80° 2 θ region at room temperature in air, using step size and step time of 0.05° and 80 s, respectively.

Gas chromatographic (GC) analyses were done on a GC Agilent with FID detectors using Agilent HP1 column (30 m, 0.35 mm, 0.25 μ m), with hydrogen as gas carrier and with tetradecane as the internal standard. The retention times and GC responses in terms of area versus concentration of the reagents and products were calibrated by using pure components diluted in an acetone solution at various concentrations. The conversion and product distribution were calculated from the GC results.

NMR spectra were recorded at 298 K on a Bruker Avance III HD 400 MHz spectrometer

operating at 400.13 MHz for ^1H and at 100.61 MHz for ^{13}C . The chemical shifts are referenced to the residual deuterated or ^{13}C solvent peaks. Chemical shifts (δ) and coupling constants (J) are expressed in ppm and Hz, respectively.

IV-2) Experimental procedures

IV-2-1) Open cell polyurethane foam (PUF) coating with polydopamine (PDA)

A cubic sample of PDA@PUF of ca. 2 cm \times 2 cm \times 2 cm was coated with PDA as described in Chapter I.

IV-2-2) Functionalization of PDA@PUF with $[\text{PdCl}_2(\text{NH}_3)_4]\cdot\text{H}_2\text{O}$

A cubic sample of PDA@PUF (ca. 2 cm \times 2 cm \times 2 cm) was washed in vigorously stirred (725 rpm) $\text{H}_2\text{O}/\text{EtOH}$ (1:5) (120 mL) at room temperature for 1 h, and air-dried prior to the functionalization.

The cubic sample of PDA@PUF was then immersed in a solution of $[\text{Pd}(\text{NH}_3)_4\text{Cl}_2]\cdot\text{H}_2\text{O}$ (20 mg, 0.076 mmol) in $\text{H}_2\text{O}/\text{EtOH}$ (1:5) (120 mL) at room temperature. After 19 h of stirring at 725 rpm, the resulting Pd-functionalized foam, Pd@PDA@PUF, was removed from the reaction medium, washed in vigorously stirred water (3 \times 120 mL) and ethanol (2 \times 100 mL), and then dried in an oven at 80 $^\circ\text{C}$ for 1 h.

Pd@PDA@PUF was characterized by HR-SEM, SEM-EDX, XPS, XRD, TGA and ICP-AES revealing a mean Pd content of 2.437 ± 0.323 g/kg (0.244 ± 0.032 wt%) assessed from the analysis of six samples.

IV-2-3) General procedure for the catalytic alkyne-to-alkene hydrogenations with Pd@PDA@PUF

A stirring bar and a cubic sample of Pd@PDA@PUF of ca. 8 cm³, whose mass was adjusted in function of its Pd content established by ICP-AES to have a Pd loading of 7 μmol , were introduced in a Schlenk tube. Ethanol (20 mL) was then added to immerse totally the foam, and H_2 was bubbled through the solution at room temperature for 30 min under a constant flow rate (13 mL/min). Afterwards, the selected alkyne (1.52, 3 or 6 mmol) (Pd content: 0.46, 0.23 or 0.12 mol% vs. substrate) was added in one portion by syringe to the stirred solution (625 rpm), and T_0 reaction time was set. During the reaction course, H_2 was fed under ambient conditions (room temperature and atmospheric pressure) at a constant flow rate (2 or 13 mL/min). The reaction was kinetically monitored by sampling regularly the reaction medium, and analysing the removed aliquots (50 μL) by GC or ^1H NMR. The aliquots were diluted with acetone or ethanol (3 mL) for GC analysis or dried under high vacuum and re-dissolved in a deuterated solvent (CDCl_3 or $(\text{CD}_3)_2\text{CO}$) for ^1H NMR spectroscopy.

An aqueous solution containing $[\text{PdCl}_2(\text{NH}_3)_4] \cdot \text{H}_2\text{O}$ (with a Pd load of 1% relative to the mass of carbon) was impregnated on the carbon bulk using classical wet impregnation process and the obtained composite was dried at 110 °C for 5 h-12 h, subjected to a heat treatment between 250-350 °C under air for 2 h, and reduced under a hydrogen atmosphere (50 mL/min) at 300-450 °C for 1 h.

IV-2-4) General procedure for the Suzuki cross-couplings of phenylboronic acid and aryl bromides with Pd@PDA@PUF under aerobic conditions

A stirring bar and a cubic sample of Pd@PDA@PUF of ca. 8 cm³, whose mass was adjusted in function of its Pd content established by ICP-AES to have a Pd loading of 7 μmol, were introduced in a tube in a similar fashion to the hydrogenation experiments. Ethanol/water (1:1) (8 mL) was then added to immerse the foam. This was followed by the addition of the phenylboronic acid (0.6 or 3.6 mmol), K₂CO₃ (0.75 or 4.5 mmol), and aryl bromide (0.5 or 3 mmol) (Pd content: 1.4 or 0.23 mol% vs. aryl bromide). The reaction mixture was then heated under stirring (625 rpm) by putting the tube in an oil bath at 65 °C. After 4 h, the reaction medium was poured into water (2 mL) and the product extracted with ethyl acetate (2 × 10 mL). The combined extracts were then washed with brine (10 mL) and dried over anhydrous MgSO₄. At this point, an aliquot was removed by syringe to determine the conversion of the aryl bromide by GC analysis, and the solvent was removed under reduced pressure. The crude material was then purified by column chromatography over silica with petroleum ether/ethyl acetate (20:1) as eluent to give the desired product, whose identity was confirmed by ¹H and ¹³C NMR in CDCl₃.

IV-2-5) Pd@PDA@PUF recovery and reuse in successive semi-hydrogenation and Suzuki reactions

The above-described general procedures for the catalytic alkyne-to-alkene hydrogenations and Suzuki couplings were followed using phenylacetylene (3 mmol) and a H₂ flow rate of 13 mL/min for the semi-hydrogenations, bromobenzene (3 mmol) and phenylboronic acid (3.6 mmol) for the Suzuki couplings, and a single cubic sample of Pd@PDA@PUF of ca. 8 cm³, (270 mg, 0.276 wt% Pd, i.e.: 7.00 · 10⁻³ mmol) as catalyst for the 15 successive runs. Five initial runs of semi-hydrogenation were conducted, then five runs of Suzuki coupling, then again 5 final runs of semi-hydrogenation. After each semi-hydrogenation run, the Pd@PDA@PUF foam was washed by immersing it in EtOH (20 mL × 3) in an ultrasonic bath (80 W, 50/60 Hz) at 25 °C for 10 min, and dried under vacuum. After each Suzuki run, the Pd@PDA@PUF foam was first washed with H₂O (10 mL × 1) and ethyl acetate (10 mL × 2) (collecting all washing liquors and adding them to the reactive mixture for analysis), then washed with EtOH (10 mL × 3) in the ultrasonic bath (80 W, 50/60 Hz) at 25 °C for 10

min, and dried under vacuum.

IV-2-6) Stop-and-go experiment for the semi-hydrogenation of 4-octyne with Pd@PDA@PUF

In this control experiment conducted for highlighting the absence of Pd leaching into the liquid medium, the above-described general procedure for the catalytic alkyne-to-alkene hydrogenations was followed using 4-octyne (3 mmol) as substrate, a H₂ flow rate of 13 mL/min, and a cubic sample of Pd@PDA@PUF of ca. 8 cm³, whose mass was adjusted in function of its Pd content established by ICP-AES to have a Pd loading of 7 μmol, as catalyst, except that, after 0.5 h reaction, the Pd@PDA@PUF foam was removed from the reaction medium for 1 h. Then, Pd@PDA@PUF was reintroduced in the reacting vessel for 0.5 h, removed again for 1 h, then reintroduced a last time for 0.5 h, and finally removed definitively. During the whole process, H₂ was constantly fed into the medium as to maintain its concentration constant. The course of the reaction was monitored by sampling the reaction medium at T = 0.5, 1.5, 2, 3, 3.5 and 4.5 h, and analysing the removed aliquots (50 μL) by GC after dilution in acetone (3 mL).

IV-2-7) Alkyne vs. alkene competing hydrogenation with Pd@PDA@PUF

In this experiment conducted for highlighting the excellent selectivity in the semi-hydrogenation of 3-hexyne to (Z)-3-hexene, the above-described general procedure for the catalytic alkyne-to-alkene hydrogenations was followed using a H₂ flow rate of 13 mL/min, a cubic sample of Pd@PDA@PUF of ca. 8 cm³, whose mass was adjusted in function of its Pd content established by ICP-AES to have a Pd loading of 7 μmol, as catalyst, and a 60:40 mixture of 3-hexyne (1.8 mmol) and (Z)-2-hexene (1.2 mmol), as reagents at T₀. The course of the reaction was monitored by sampling regularly the reaction medium and analysing the removed aliquots (50 μL) by GC after dilution in acetone (3 mL).

IV-2-8) Phenylacetylene-to-styrene hydrogenation with [Pd(NH₃)₄Cl₂]·H₂O

In this experiment conducted for comparing the activity of Pd@PDA@PUF with that of the unsupported catalyst precursor, [Pd(NH₃)₄Cl₂]·H₂O (1.8 mg, 7.0 μmol) was added to ethanol (20 mL) and H₂ was bubbled at room temperature for 30 min under a flow rate of 13 mL/min. Afterwards, the phenylacetylene (3 mmol) (Pd content: 0.23 mol % vs. substrate) was added in one portion by syringe to the stirred solvent (625 rpm), and T₀ reaction time was set. During the reaction course, H₂ was fed under ambient conditions (room temperature and atmospheric pressure) at a constant flow rate (13 mL/min). The course of the reaction was monitored by sampling the reaction medium at T = 1 h and analysing the removed aliquot (50 μL) by GC after dilution in acetone (3 mL); 91% phenylacetylene conversion with 95% styrene selectivity

was observed.

V) References

1. Blaser, H. U.; Schnyder, A.; Steiner, H.; Rössler, F.; Baumeister, P., Selective hydrogenation of functionalized hydrocarbons, in *Handbook of Heterogeneous Catalysis*: ed. G. Ertl, H. Knözinger, F. Schüth and J. Weitkamp, Wiley-VCH, Weinheim, 2008, 3284-3308.
2. A. M. Kluver and C. J. Elsevier, in *Handbook of homogeneous hydrogenation*, ed. J. G. de Vries and C. J. Elsevier, Wiley-VCH, Weinheim, 2007, Vol. 3, 375-394.
3. Oger, C.; Balas, L.; Durand, T.; Galano, J.-M., Are alkyne reductions chemo-, regio-, and stereoselective enough to provide pure (Z)-olefins in polyfunctionalized bioactive molecules? *Chem. Rev.* **2013**, *113* (3), 1313-1350.
4. Teschner, D.; Vass, E.; Hävecker, M.; Zafeiratos, S.; Schnörch, P.; Sauer, H.; Knop-Gericke, A.; Schlögl, R.; Chamam, M.; Wootsch, A., Alkyne hydrogenation over Pd catalysts: A new paradigm. *J. Catal.* **2006**, *242* (1), 26-37.
5. Domínguez-Domínguez, S.; Berenguer-Murcia, Á.; Pradhan, B. K.; Linares-Solano, Á.; Cazorla-Amorós, D., Semihydrogenation of phenylacetylene catalyzed by palladium nanoparticles supported on carbon materials. *J. Phys. Chem. C* **2008**, *112* (10), 3827-3834.
6. Venkatesan, R.; Pechtl, M. H.; Scholten, J. D.; Pezzi, R. P.; Machado, G.; Dupont, J., Palladium nanoparticle catalysts in ionic liquids: synthesis, characterisation and selective partial hydrogenation of alkynes to Z-alkenes. *J. Mater. Chem.* **2011**, *21* (9), 3030-3036.
7. Uberman, P. M.; Costa, N. J.; Philippot, K.; Carmona, R. C.; Dos Santos, A. A.; Rossi, L. M., A recoverable Pd nanocatalyst for selective semi-hydrogenation of alkynes: hydrogenation of benzyl-propargylamines as a challenging model. *Green Chem.* **2014**, *16* (10), 4566-4574.
8. Delgado, J. A.; Benkirane, O.; Claver, C.; Curulla-Ferré, D.; Godard, C., Advances in the preparation of highly selective nanocatalysts for the semi-hydrogenation of alkynes using colloidal approaches. *Dalton Trans.* **2017**, *46* (37), 12381-12403.
9. Teschner, D.; Borsodi, J.; Wootsch, A.; Révay, Z.; Havecker, M.; Knop-Gericke, A.; Jackson, S. D.; Schlogl, R., The roles of subsurface carbon and hydrogen in palladium-catalyzed alkyne hydrogenation. *Science* **2008**, *320* (5872), 86-89.
10. Zhang, L.; Zhou, M.; Wang, A.; Zhang, T., Selective hydrogenation over supported metal catalysts: from nanoparticles to single atoms. *Chem. Rev.* **2019**, *120* (2), 683-733.
11. da Silva, F. P.; Fiorio, J. L.; Rossi, L. M., Tuning the catalytic activity and selectivity of

- Pd nanoparticles using ligand-modified supports and surfaces. *ACS Omega* **2017**, *2* (9), 6014-6022.
12. Zhao, Y.; Fu, G.; Zheng, N., Shaping the selectivity in heterogeneous hydrogenation by using molecular modification strategies: Experiment and theory. *Catal. Today* **2017**, *279*, 36-44.
 13. Zhao, M.; Ji, Y.; Wang, M.; Zhong, N.; Kang, Z.; Asao, N.; Jiang, W.-J.; Chen, Q., Composition-dependent morphology of bi- and trimetallic phosphides: Construction of amorphous Pd–Cu–Ni–P nanoparticles as a selective and versatile Catalyst. *ACS Appl. Mater. Interfaces* **2017**, *9* (40), 34804-34811.
 14. Markov, P. V.; Bragina, G. O.; Rassolov, A. V.; Baeva, G. N.; Mashkovsky, I. S.; Murzin, V. Y.; Zubavichus, Y. V.; Stakheev, A. Y., Pd–Cu catalyst prepared from heterobimetallic PdCu₂(OAc)₆: An XRD-EXAFS study and activity/selectivity in the liquid-phase hydrogenation of a C≡C bond. *Mendeleev Commun.* **2016**, *26* (6), 502-504.
 15. Kruppe, C. M.; Krooswyk, J. D.; Trenary, M., Selective hydrogenation of acetylene to ethylene in the presence of a carbonaceous surface layer on a Pd/Cu (111) single-atom alloy. *ACS Catal.* **2017**, *7* (12), 8042-8049.
 16. Kyriakou, G.; Boucher, M. B.; Jewell, A. D.; Lewis, E. A.; Lawton, T. J.; Baber, A. E.; Tierney, H. L.; Flytzani-Stephanopoulos, M.; Sykes, E. C. H., Isolated metal atom geometries as a strategy for selective heterogeneous hydrogenations. *Science* **2012**, *335* (6073), 1209-1212.
 17. Lu, Y.; Feng, X.; Takale, B. S.; Yamamoto, Y.; Zhang, W.; Bao, M., Highly selective semihydrogenation of alkynes to alkenes by using an unsupported nanoporous palladium catalyst: No leaching of palladium into the reaction mixture. *ACS Catal.* **2017**, *7* (12), 8296-8303.
 18. Kuwahara, Y.; Kango, H.; Yamashita, H., Pd nanoparticles and aminopolymers confined in hollow silica spheres as efficient and reusable heterogeneous catalysts for semihydrogenation of alkynes. *ACS Catal.* **2019**, *9* (3), 1993-2006.
 19. Shen, C.; Ji, Y.; Wang, P.; Bai, S.; Wang, M.; Li, Y.; Huang, X.; Shao, Q., Interface Confinement in Metal Nanosheet for High-Efficiency Semi-Hydrogenation of Alkynes. *ACS Catal.* **2021**, *11* (9), 5231-5239.
 20. Wang, Z.; Zou, Y.; Li, Y.; Cheng, Y., Metal - Containing Polydopamine Nanomaterials: Catalysis, Energy, and Theranostics. *Small* **2020**, *16* (18), 1907042.
 21. Kunfi, A.; London, G., Polydopamine: an emerging material in the catalysis of organic transformations. *Synthesis* **2019**, *51* (14), 2829-2838.
 22. Manna, J.; Akbayrak, S.; Özkar, S., Palladium (0) nanoparticles supported on polydopamine coated CoFe₂O₄ as highly active, magnetically isolable and reusable

- catalyst for hydrogen generation from the hydrolysis of ammonia borane. *Appl. Catal. B* **2017**, *208*, 104-115.
23. Li, Y.; Xu, L.; Xu, B.; Mao, Z.; Xu, H.; Zhong, Y.; Zhang, L.; Wang, B.; Sui, X., Cellulose sponge supported palladium nanoparticles as recyclable cross-coupling catalysts. *ACS Appl. Mater. Interfaces* **2017**, *9* (20), 17155-17162.
 24. Kunfi, A.; May, Z.; Németh, P.; London, G., Polydopamine supported palladium nanoparticles: Highly efficient catalysts in Suzuki cross-coupling and tandem Suzuki cross-coupling/nitroarene reductions under green reaction conditions. *J. Catal.* **2018**, *361*, 84-93.
 25. Pardieu, E.; Chau, N. T. T.; Dintzer, T.; Romero, T.; Favier, D.; Roland, T.; Edouard, D.; Jierry, L.; Ritleng, V., Polydopamine-coated open cell polyurethane foams as an inexpensive, flexible yet robust catalyst support: a proof of concept. *Chem. Commun.* **2016**, *52* (25), 4691-4693.
 26. Khouya, A. A.; Martinez, M. L. M.; Bertani, P.; Romero, T.; Favier, D.; Roland, T.; Guidal, V.; Bellière-Baca, V.; Edouard, D.; Jierry, L.; Ritleng, V., Coating of polydopamine on polyurethane open cell foams to design soft structured supports for molecular catalysts. *Chem. Commun.* **2019**, *55* (79), 11960-11963.
 27. Ahn, B. K., Perspectives on mussel-inspired wet adhesion. *J. Am. Chem. Soc.* **2017**, *139* (30), 10166-10171.
 28. Saiz - Poseu, J.; Mancebo - Aracil, J.; Nador, F.; Busqué, F.; Ruiz - Molina, D., The chemistry behind catechol - based adhesion. *Angew. Chem. Int. Ed.* **2019**, *58* (3), 696-714.
 29. Ball, V., Polydopamine films and particles with catalytic activity. *Catal. Today* **2018**, *301*, 196-203.
 30. Xi, J.; Xiao, J.; Xiao, F.; Jin, Y.; Dong, Y.; Jing, F.; Wang, S., Mussel-inspired functionalization of cotton for nano-catalyst support and its application in a fixed-bed system with high performance. *Sci. Rep.* **2016**, *6* (1), 21904.
 31. Kunfi, A.; Szabó, V.; Mastalir, Á.; Bucsi, I.; Mohai, M.; Németh, P.; Bertóti, I.; London, G., Palladium on polydopamine: its true potential in catalytic transfer hydrogenations and heck coupling reactions. *ChemCatChem* **2017**, *9* (16), 3236-3244.
 32. Huebner, S.; de Vries, J. G.; Farina, V., Why does industry not use immobilized transition metal complexes as catalysts? *Adv. Synth. Catal.* **2016**, *358* (1), 3-25.
 33. Ait Khouya, A.; Ba, H.; Baaziz, W.; Nhut, J.-M.; Rossin, A.; Zafeiratos, S.; Ersen, O.; Giambastiani, G.; Ritleng, V.; Pham-Huu, C., Palladium Nanosheet-Carbon Black Powder Composites for Selective Hydrogenation of Alkynes to Alkenes. *ACS Appl. Nano Mater.* **2021**, *4* (2), 2265-2277.

34. Lee, K. H.; Lee, B.; Lee, K. R.; Yi, M. H.; Hur, N. H., Dual Pd and CuFe₂O₄ nanoparticles encapsulated in a core/shell silica microsphere for selective hydrogenation of arylacetylenes. *Chem. Commun.* **2012**, 48 (37), 4414-4416.
35. Song, S.; Li, K.; Pan, J.; Wang, F.; Li, J.; Feng, J.; Yao, S.; Ge, X.; Wang, X.; Zhang, H., Achieving the Trade - Off between Selectivity and Activity in Semihydrogenation of Alkynes by Fabrication of (Asymmetrical Pd@Ag Core)@(CeO₂ Shell) Nanocatalysts via Autoredox Reaction. *Adv. Mater.* **2017**, 29 (8), 1605332.
36. Deng, D.; Yang, Y.; Gong, Y.; Li, Y.; Xu, X.; Wang, Y., Palladium nanoparticles supported on mpg-C₃N₄ as active catalyst for semihydrogenation of phenylacetylene under mild conditions. *Green Chem.* **2013**, 15 (9), 2525-2531.
37. Yang, S.; Cao, C.; Peng, L.; Zhang, J.; Han, B.; Song, W., A Pd-Cu₂O nanocomposite as an effective synergistic catalyst for selective semi-hydrogenation of the terminal alkynes only. *Chem. Commun.* **2016**, 52 (18), 3627-3630.
38. Yoshii, T.; Umemoto, D.; Kuwahara, Y.; Mori, K.; Yamashita, H., Engineering of Surface Environment of Pd Nanoparticle Catalysts on Carbon Support with Pyrene-Thiol Ligands for Semihydrogenation of Alkynes. *ACS Appl. Mater. Interfaces* **2019**, 11 (41), 37708-37719.
39. Yin, X.-P.; Tang, S.-F.; Zhang, C.; Wang, H.-J.; Si, R.; Lu, X.-L.; Lu, T.-B., Graphdiyne-based Pd single-atom catalyst for semihydrogenation of alkynes to alkenes with high selectivity and conversion under mild conditions. *J. Mater. Chem. A* **2020**, 8 (40), 20925-20930.
40. Boucher, M. B.; Zugic, B.; Cladaras, G.; Kammert, J.; Marcinkowski, M. D.; Lawton, T. J.; Sykes, E. C. H.; Flytzani-Stephanopoulos, M., Single atom alloy surface analogs in Pd_{0.18} Cu₁₅ nanoparticles for selective hydrogenation reactions. *PhysChemChemPhys* **2013**, 15 (29), 12187-12196.
41. Li, Z.; Ren, Q.; Wang, X.; Chen, W.; Leng, L.; Zhang, M.; Horton, J. H.; Liu, B.; Xu, Q.; Wu, W., Highly Active and Stable Palladium Single-Atom Catalyst Achieved by a Thermal Atomization Strategy on an SBA-15 Molecular Sieve for Semi-Hydrogenation Reactions. *ACS Appl. Mater. Interfaces* **2021**, 13 (2), 2530-2537.
42. Overlaps of the ¹H NMR peaks of the reaction products with those of the starting material prevented to carry out precise kinetic monitoring of the reaction.
43. Diederich, F.; Stang, P. J., *Metal-catalyzed cross-coupling reactions*. John Wiley & Sons: 2008.
44. Colacot, T. J., *New trends in cross-coupling: theory and applications*. Royal Society of Chemistry: 2015.
45. Biffis, A.; Centomo, P.; Del Zotto, A.; Zecca, M., Pd metal catalysts for cross-couplings and related reactions in the 21st century: a critical review. *Chem. Rev.* **2018**, 118 (4),

2249-2295.

46. Tao, B.; Boykin, D. W., Simple amine/Pd(OAc)₂-catalyzed Suzuki coupling reactions of aryl bromides under mild aerobic conditions. *J. Org. Chem.* **2004**, 69 (13), 4330-4335.
47. Marziale, A. N.; Faul, S. H.; Reiner, T.; Schneider, S.; Eppinger, J., Facile palladium catalyzed Suzuki–Miyaura coupling in air and water at ambient temperature. *Green Chem.* **2010**, 12 (1), 35-38.
48. Liu, C.; Rao, X.; Zhang, Y.; Li, X.; Qiu, J.; Jin, Z., An Aerobic and Very Fast Pd/C - Catalyzed Ligand - Free and Aqueous Suzuki Reaction Under Mild Conditions. *Eur. J. Org. Chem.* **2013**, 2013 (20), 4345-4350.
49. Ding, G.; Hao, L.; Xu, H.; Wang, L.; Chen, J.; Li, T.; Tu, X.; Zhang, Q., Atomically dispersed palladium catalyses Suzuki–Miyaura reactions under phosphine-free conditions. *Commun. Chem.* **2020**, 3 (1), 1-8.
50. It can however not be excluded that the low BE tale in spectrum A may also be due to differential charging.
51. D'Alterio, M. C.; Casals - Cruañas, È.; Tzouras, N. V.; Talarico, G.; Nolan, S. P.; Poater, A., Mechanistic Aspects of the Palladium - Catalyzed Suzuki - Miyaura Cross - Coupling Reaction. *Chem. Eur. J.* **2021**, 27 (54), 13481-13493.

Chapter III: Supporting information

Optimization studies for the semi-hydrogenation of phenylacetylene (PA) to styrene (ST) with Pd@PDA@PUF in EtOH at RT

S2

Figure S1. Kinetic monitoring of the optimization tests of PA semi-hydrogenation with Pd@PDA@PUF

S3

Table S1. Results of optimization tests of PA semi-hydrogenation to ST

S3

Optimization studies for the semi-hydrogenation of phenylacetylene (PA) to styrene (ST) with Pd@PDA@PUF in EtOH at RT

All successive experiments were carried out with the same Pd@PDA@PUF foam of ca. 8 cm³ whose mass was adjusted in function of its Pd content to have a Pd loading of 7 μmol. The two first trials, run with a Pd loading of 0.46 mol% and a H₂ flow of 13 mL/min, displayed similar reaction kinetics, with 98% conversion of PA and 97% selectivity to ST after 3.3 h for the 1st run (TON = 213, TOF = 65 h⁻¹), and 93% conversion and 90% ST selectivity after 3 h in the 2nd run (TON = 202, TOF = 67 h⁻¹) (Table S1, entries A and B). Once all alkyne had been consumed, the selectivity began to drop down as over-hydrogenation occurred (Fig. S6A and S6B). In view of these encouraging results, notably the little acceleration of the reaction kinetics between the two runs, we performed a third run under the same conditions. As can be seen in Figure S6C, we again observed a very selective conversion of PA to ST without any appreciable competition of further hydrogenation of the latter to give ethylbenzene (EB) until all PA had been consumed. Thus, 97% conversion was reached in 3 h with a ST selectivity of 88% (TON = 211, TOF = 70 h⁻¹) (Table S1, entry C). In the 4th run, the rate of H₂ flow was decreased from 13 to 2 mL/min in order to map out its influence on the catalytic performance. No positive effect was observed on the hydrogenation selectivity, as only 94% ST selectivity at 81% PA conversion was observed after 2 h reaction and as it dropped similarly once all PA was consumed (Figure S6D and Table S1, entry D). We thus maintained the H₂ flow rate to 13 mL/min for the next two experiments, but increased the reactant's concentration to 3 and 6 mmol, conversely decreasing the catalyst loading from 0.46 mol% to 0.23 mol% in the 5th run (Figure S6E) and to 0.11 mol% in the 6th run (Figure S6F). Remarkably, the Pd@PDA@PUF catalyst maintained a very high chemoselectivity with higher kinetics in the 5th run, achieving as high as 91% conversion with 95% selectivity to ST after 2 h (TON = 396; TOF = 197 h⁻¹) (Table S1, entry E). Again, ST hydrogenation to EB occurred appreciably only after full consumption of PA. When the substrate loading was doubled again to 6 mmol, the selectivity and the turnover frequency gratifyingly maintained to the same level, with 98% PA conversion with 94% selectivity after 4.25 h, thus giving a TON of 891 and a TOF of 210 h⁻¹ (Table S1, entry F). The latter conditions were chosen as the standard conditions.

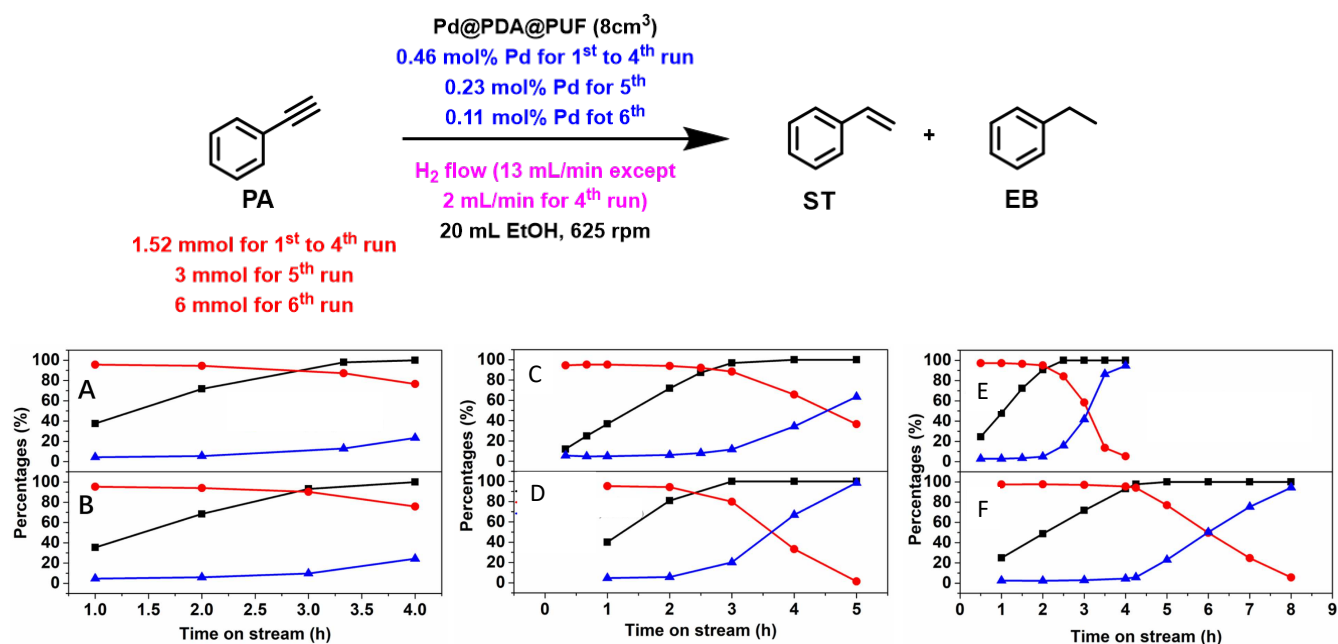


Figure S1. Kinetic monitoring of the optimization tests of PA semi-hydrogenation with Pd@PDA@PUF (ca. 8 cm³, Pd content 7.00·10⁻³ mmol) in EtOH (20 mL) at RT under 625 rpm. **A, B, C:** PA (1.52 mmol), H₂ (13 mL/min); **D:** PA (1.52 mmol), H₂ (2 mL/min); **E:** PA (3 mmol), H₂ (13 mL/min); **F:** PA (6 mmol), H₂ (13 mL/min). Black curves: PA conversion. Red curves: selectivity to ST. Blue curves: selectivity to ethylbenzene (EB).

Table S1. Results of optimization tests of PA semi-hydrogenation to ST.

Entry	Cat. loading (Pd mol%)	H ₂ flow speed	Time (h)	Conv. (%) ^a	Select. (%) ^a	TON ^b	TOF (h ⁻¹)
A	0.46	13	3.3	98	97	207	63
B	0.46	13	3	93	90	182	61
C	0.46	13	3	97	88	186	62
D	0.46	2	2	81	94	166	83
E	0.23	13	2	91	95	376	188
F	0.12	13	4.25	98	95	776	183

^a PA conversion and ST selectivity were determined by GC analysis. ^b Turnover number expressed as mol of PA converted to ST vs. the catalytic loading.

General conclusion

General conclusion

The objectives of this thesis, carried out with the support of the University of Strasbourg (IdEx Unistra 2019), concerned the use of open-cell polyurethane foams as structured catalytic supports for heterogeneous catalysis with both molecular and inorganic catalysts, in particular, with visible-light photocatalysts based on coordination complexes or organic dyes and Pd NPs-based catalysts.

To begin with, an introductory chapter presented generalities about supported catalysis, including the common forms of supports and relevant applications. Notably, this chapter also described the different types of functionalizations and applications obtained with open cell polyurethane foams coated with polydopamine, a mussel-inspired adhesive layer that allows further functionalization without altering the foams mechanic and transport properties, that have been reported in the literature up to now.

In **Chapter I**, the covalent anchoring of APTES onto PDA@PUF by condensation of the trialkoxysilane group with the catechols moieties of the PDA layer, followed by a two-step further functionalization with $\text{Ru}(\text{bpy})_3^{2+}$ was presented, as well as the characterization of the resulting material, $\text{Ru}(\text{bpy})_3\text{-APTES@PDA@PUF}$, by ^{29}Si CP-MAS NMR, ICP-AES, SEM and EDX. This heterogeneous catalyst proved applicable as a reusable photocatalyst for benzylic amine homocouplings and cross dehydrogenative couplings under visible-light irradiation and molecular oxygen as a green oxygen source. The recycling and scope experiments proved that this material was catalytically effective and versatile in both reactions. The foam could be used at least 6 times without loss of activity in a “dip-and-play” mode. Impressively, despite some catalyst leaching, an improvement of the catalytic performances of $\text{Ru}(\text{bpy})_3\text{-APTES@PDA@PUF}$ was even observed in both reactions, which most likely resulted from a modification of the uppermost layer of polydopamine that rendered the photocatalyst more accessible. Progressive color lightening, surface smoothing and XPS characterizations support this possible explanation.

In **Chapter II**, in a similar fashion to $\text{Ru}(\text{bpy})_3\text{-APTES@PDA@PUF}$, EY-APTES@PDA@PUF was prepared via covalent anchoring of APTES onto PDA@PUF and subsequent EDC-mediated coupling with EY, and characterized by ^{29}Si CP-MAS NMR, ICP-AES and SEM. The catalytic performance of EY-APTES@PDA@PUF however showed some limitations when investigating different types of photocatalytic reactions under visible light. In the initial study of oxidation of 2-methyl-5-nitroisquinolin-2-ium iodide, EY-APTES@PDA@PUF showed a stable activity in recycling tests still allowing 71% isolated yield in the sixth run. In the second model reaction, the oxidation of methyl *p*-tolyl sulfide to its

corresponding sulfoxide, severe deactivation was however observed in recycling tests, from 98% in the 1st run to 59% in the 5th run, highlighting an important leaching of eosin Y. The strategy used in **Chapter I** seems unfortunately to be not suitable for eosin Y. Alternative functionalization strategies based on (i) a one-pot protocol implying the coupling of eosin Y with APTES in the presence of COMU instead of EDC prior to the covalent anchoring procedure by condensation of the alkoxy silane groups of APTES with the catechols of PDA and (ii) a novel one-step coating-and-functionalization protocol yielded EY-APTES1@PDA@PUF and PDA-EY@PUF materials. The latter gave high conversions in the selected model reaction in their first run, but then experienced gradual deactivation in recycling tests as well. The observed leaching may originate from an important adsorption of eosin Y onto the PDA adhesive layer instead of the expected couplings.

Finally, in **Chapter III**, a versatile and highly reliable heterogeneous catalyst, Pd@PDA@PUF was prepared based on an effective and simple strategy that does not involve a reduction procedure. Specifically, after a simple dip-coating protocol of PDA@PUF in a hydro-alcoholic solution of Pd(NH₃)₄Cl₂·H₂O at room temperature, this easy-to-make composite acted as an efficient and reusable heterogeneous catalyst for the semi-hydrogenation of alkynes giving remarkably high alkene selectivity (up to 99%) at full alkyne conversion, as well as for the Suzuki coupling of aryl bromides under aerobic conditions. Moreover, the Pd@PDA@PUF catalyst showed no decay either in activity or in selectivity when running the hydrogenation and coupling reactions for 15 cycles even though washing procedures in an ultrasonic bath during each catalytic run were included. The as-recovered catalyst even displayed improved catalytic performance due to both the progressive *in situ* reduction of the Pd(II) immobilized species into Pd(0), as demonstrated by XPS studies, and to strong interaction between Pd and the PDA layer that prevented re-oxidation of the Pd active phase during the air exposure and Pd leaching into the medium. Furthermore, HR-SEM and SEM-EDX studies suggested an initial simple coordination of the Pd(II) ions by the catechol moieties of the PDA layer. The resulting “single atom”-type dispersion of the active phase is supposed to be at the origin of the very high selectivity observed in alkyne semi-hydrogenations.

We expect the facile preparation and excellent catalytic and reusable performances of this Pd@PDA@PUF structured catalyst that can be used in a “dip-and-play” mode to be of guiding significance for a wider range of applications in the future.

Résumé

Dans cette thèse, nous présentons un support catalytique structuré multifonctionnel basé sur des mousses à cellules ouvertes de polyuréthane (PUF) revêtues d'une couche de polydopamine (PDA). Basé sur le principe d'adhésion des moules, ce revêtement biomimétique de PDA permet la fonctionnalisation chimique de la surface des PUF sans altérer leurs propriétés mécaniques et de transport. Dans une première partie, l'ancrage covalent d'APTES comportant un bras trialkoxysilane sur PDA@PUF suivi d'une fonctionnalisation avec Ru(bpy)₃²⁺ ou de l'éosine Y a procuré les matériaux Ru(bpy)₃-APTES@PDA@PUF et EY-APTES@PDA@PUF. Ru(bpy)₃-APTES@PDA@PUF s'est révélé être un photocatalyseur efficace et réutilisable pour des réactions d'homocouplage d'amines benzyliques et de couplages déshydrogénés croisés sous irradiation de lumière visible. EY-APTES@PDA@PUF, en revanche, a montré des limitations lors de l'étude de différentes réactions photocatalytiques d'oxydation sous lumière visible, due à un lessivage non-négligeable de l'éosine Y. Dans une deuxième partie, un simple protocole d'enrobage par immersion de PDA@PUF dans une solution hydro-alcoolique de Pd(NH₃)₄Cl₂.H₂O à température ambiante a fourni le matériau Pd@PDA@PUF. Ce composite facile à préparer agit comme un catalyseur hétérogène efficace et hautement réutilisable, sans procédure préalable de réduction, pour la semi-hydrogénation sélective d'alcyne et le couplage de Suzuki de bromures d'aryle dans des conditions aérobies. Des caractérisations approfondies suggèrent une simple coordination initiale d'ions de Pd(II) par les unités catéchols de la couche de PDA, résultant en une dispersion de la phase active de type « atome isolé », ainsi qu'une réduction progressive du Pd(II) en Pd(0).

Mots-clés : support catalytique structuré, polydopamine, mousse de polyuréthane, photocatalyse hétérogène, semi-hydrogénation d'alcyne, couplage de Suzuki

Résumé en anglais

In this thesis, we present a multi-functional structured catalytic support based on open cell polyurethane foams (PUF) coated with polydopamine (PDA). Based on the mussels' adhesion principle, this biomimetic coating allows surface chemical functionalizations of PUF without altering their mechanical and transport properties. In a first part, the covalent anchoring of APTES bearing a trialkoxysilane arm onto PDA@PUF foam, followed by functionalization with Ru(bpy)₃²⁺ or eosin Y provided Ru(bpy)₃-APTES@PDA@PUF and EY-APTES@PDA@PUF materials. Ru(bpy)₃-APTES@PDA@PUF proved to be an efficient and reusable photocatalyst for benzylic amine homocouplings and cross dehydrogenative couplings under visible-light irradiation. EY-APTES@PDA@PUF, in contrast, showed some limitations when investigating different types of photocatalytic oxidation reactions under visible light, due to non-negligible eosin Y leaching. In a second part, a simple dip-coating protocol of PDA@PUF in a hydro-alcoholic solution of Pd(NH₃)₄Cl₂.H₂O at room temperature afforded Pd@PDA@PUF. This easy-to-make composite acted as an efficient and highly reusable heterogeneous catalyst, without prior-reduction processes, for the selective semi-hydrogenation of alkynes and for the Suzuki coupling of aryl bromides under aerobic conditions. Thorough characterizations suggest an initial simple coordination of the Pd(II) ions by the catechol moieties of the PDA layer, resulting in a single atom-type dispersion of the active phase, and a progressive reduction under catalytic conditions of Pd(II) into Pd(0).

Keywords: structured catalytic support, polydopamine, polyurethane foams, heterogeneous photocatalysis, alkyne semi-hydrogenation, Suzuki-coupling